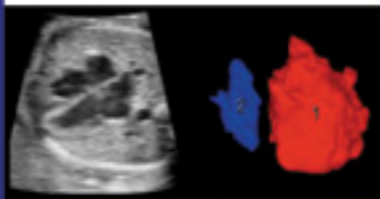


ISBN: 978-1-60805-044-4

# 4D Fetal Echocardiography



**Editor:**  
Giuseppe Ricci  
Università di Roma "Tor Vergata"  
Italy

**Co-Editor:**  
Domenico Andruzzi  
Università di Roma "Tor Vergata"  
Italy

**Bentham Books**

## FOREWORD

When Drs Rizzo and Arduini asked me to write this preface, I was honored and thrilled to have the opportunity to introduce this outstanding work!

Examining the fetal heart has always presented a huge challenge for ultrasound specialists. When I started in ultrasound 30 years ago, no one knew how to perform or even attempt the examination of the heart. Fetal echocardiography has progressed very rapidly, fueled by advances in image quality as well as increasing focus of the ultrasound community on the need for a proper examination of the heart. Even today, the detection of congenital heart defects remains at the very bottom of the list of identifiable abnormalities on a standard fetal sonogram, and well under 50% of congenital heart defects are identified by prenatally. Detection of congenital heart disease has lagged behind the successful detection of other abnormalities of the fetus despite our best attempts to teach the necessary skills. The fetal heart is a difficult organ to evaluate due its very small size, complex anatomy, dynamic blood flow physiology, as well as rapid rhythmical movement.

The importance of evaluating the heart cannot be over emphasized. Heart defects are among the most common malformations in the developing fetus and many of these anomalies are part of complex syndromes such as aneuploidies. Heart anomalies that occur as isolated defects are among the most challenging to detect, but are particularly important due to the need to prepare for a potentially sick newborn at delivery. I remember back in the early 80's when I first started in fetal ultrasound, the heart remained an enigma for many years and it was only after I missed several congenital heart defects in a row that I took on the enormous task of understanding the fetal heart and how it works. Unfortunately back then we did not have any books or educational aids such as Drs Rizzo and Arduini's wonderful e-book to guide us in learning how to evaluate the fetal heart.

I have been impressed for many years with the careers of Dr. Rizzo and Dr. Arduini who have made enormous contributions in the field of fetal imaging and in particular fetal echocardiography. They have both published extensively on this subject and are extremely well qualified to write and edit such a book. Drs Rizzo and Arduini have made significant contributions in fetal echocardiography over many years and have been instrumental in developing many of the Doppler aspects of the fetal heart evaluation. They have assembled an impressive group of authors here, and have edited a first class book on 3-D and 4-D of the fetal heart. They have understood that 3-D and 4-D volume imaging are necessary to evaluate the fetal heart due to its inherent complexity of motion, flow and anatomy.

The book is very well organized in multiple short chapters that are beautifully illustrated both with ultrasound images and diagrams. Initially, they introduce the subject with a chapter on the epidemiology of fetal heart defects and why they are important. Next are the basic chapters on screening and on normal anatomy, which are key for the beginners as well as the more seasoned examiner. The following chapters introduce 3-D and 4D ultrasound, starting with technical aspects of how to obtain a good image. Many practitioners are intimidated by the complexity of obtaining 3-D and 4-D images. The chapters that introduce the technical aspects of 3-D such as image display and manipulation of the image are all superb introductions on how to produce the best image. The book then focuses on 3-D and 4-D evaluation of blood flow using Doppler, a key subject in the evaluation of the heart. Additional chapters cover new technologies, such as the use of the matrix probe and the automated screening possibilities for the fetal heart. This volume includes the often forgotten venous anatomy of the heart and its connections, an extraordinarily valuable chapter. The chapters on anomalies are divided into septal defects, right heart, left heart, and cono truncal abnormalities and each chapter combines 2-D, 3-D/4-D and Doppler in the demonstration of these malformations. The book also describes the state of the art for 1<sup>st</sup> trimester echocardiography, followed by quantitative aspects of the function of the fetal heart including stroke volume and cardiac output. The last chapter involves other forms of imaging of the fetal heart, such as, MRI.

This book, while very comprehensive, remains simple in its approach. It makes a very complex and rather intimidating organ accessible to both the novice and the seasoned examiner. Furthermore, this book is presented as an E book which is a very innovative format, awaited with great anticipation. Such novel media will challenge the primacy of bulky printed books. Many books will soon be available as E books and carried as a small discrete thumb-drive or even down loaded perhaps on an electronic device such as a Kindle. Electronic versions of books are

the future of our industry and Drs. Rizzo and Arduini have stepped up to the plate in choosing such a modern and practical display for their book.

In conclusion, I am very excited about this E book, not only because of its superbly organized, well illustrated and presented content, but also because as an E book it can be carried and propagated throughout our community much more easily than a hard copy book would be. The authors have succeeded admirably in their endeavor to produce what promises to be a outstanding resource on the examination of the fetal heart.

**Beryl R. Benacerraf M.D.**

Clinical Professor of OB GYN and Radiology  
Harvard Medical School  
Boston Massachusetts

## PREFACE

The examination of the fetal heart is part of the comprehensive fetal scan, but this examination is still considered a challenge even for experienced sonographers. Over the years the number of ultrasound techniques used in fetal cardiology impressively increased and no other fetal organ is examined with as many modalities as the fetal heart including high resolution two dimensional (2D) imaging, M-mode examination, spectral, color, power, high-definition digital Doppler, B flow as well as tissue Doppler. It is, however, common knowledge that despite the availability of all these technologies, screening programs, especially when limited to the study of the “four chamber view”, have shown disappointing low detection rates for congenital heart disease (CHD). Although the identification of CHD can be improved by routinely visualizing the outflow tracts, their diagnosis is greatly affected by the skill of the operator as well as his ability to interpret the findings.

Very recently three- and four- dimensional (3D and 4D) technologies have been introduced in fetal cardiology and have revolutionized the way in which it is possible to study the heart. 4D ultrasonography may reduce the operator dependency of CHD diagnosis and adds the possibility to obtain offline virtual planes in cardiac examinations, views of the fetal heart difficult or impossible to obtain with conventional 2D ultrasound.

This new fetal cardiology ebook, we believe, will be of great value for all practicing clinicians wanting to start the study of the fetal heart with 4D ultrasonography. We have chosen a panel of contributors that are both leaders in this field and can represent the differences in practice between Europe and United States. This is a comprehensive guide intended for anyone interested in fetal heart scanning performing both routine screening ultrasonographic examinations and targeted heart scans. It aims to assist the reader with the following questions: how can I use this technology to acquire cardiac volumes?, how do I handle cardiac volume data sets after acquisition? , how can I improve diagnosis and definition of CHD?

It is our hope that this book will provide a bridge between scientists using and testing new technologies for research purposes and clinicians wishing to improve their daily practice.

**Domenico Arduini**

**Giuseppe Rizzo**



## CONTRIBUTORS

**Alfred Abuhamad, MD**

Department of Obstetrics and Gynecology,  
Eastern Virginia Medical School,  
Norfolk, VA, USA

**Reuven Achiron, MD**

Department of Obstetrics and Gynecology,  
The Chaim Sheba Medical Center,  
Tel Hashomer, Affiliated with the Sackler Faculty of Medicine,  
Tel Aviv University,  
Tel Aviv, Israel

**Domenico Arduini, MD**

Department of Obstetrics and Gynecology  
Università Roma Tor Vergata  
Rome Italy

**Timothy Bennett, MD**

Department of Obstetrics and Gynecology,  
University of Missouri-Kansas City School Medicine,  
Kansas City, MI, USA

**Gianluca Campobasso, MD**

Fetal Medicine Unit,  
Di Venere and Sarcone Hospitals. ASL Bari.  
Bari, Italy

**Rabih Chaoui, MD**

Prenatal Diagnosis and Human Genetics  
Berlin, Germany

**Sarah M Cohen, MD**

Department of Obstetrics and Gynecology,  
Hadassah-Hebrew University Medical Centers – Mt. Scopus,  
Jerusalem, Israel

**Valentina De Robertis, MD**

Fetal Medicine Unit,  
Di Venere and Sarcone Hospitals. ASL Bari.  
Bari, Italy

**Greggory R. De Vore, MD**

Fetal Diagnostic Center  
Pasadena, CA USA

**Marco Di Maurizio, MD**

Department of Radiology,  
Ospedale Meyer  
Florence, Italy

**Jimmy Espinoza, MD**

Department of Obstetrics and Gynecology  
William Beaumont Hospital  
Royal Oak, MI USA

**Giuliano Farina, PhD**

Department of Obstetrics and Gynecology  
Azienda Ospedaliera “C.Poma”  
Mantova, Italy

**Laura Franceschetti, MD**

Department of Obstetrics and Gynecology  
Azienda Ospedaliera “C.Poma”  
Mantova , Italy

**Michal Lipschutz, MD**

Department of Obstetrics and Gynecology,  
Hadassah-Hebrew University Medical Centers – Mt. Scopus,  
Jerusalem, Israel

**Pietro Gaglioti, MD**

Department of Obstetrics and Gynecology,  
Maternal-Fetal Medicine Unit,  
University of Turin,  
Turin Italy

**Liat Gindes, MD**

Department of Obstetrics and Gynecology,  
The Chaim Sheba Medical Center,  
Tel Hashomer, Affiliated with the Sackler Faculty of Medicine,  
Tel Aviv University,  
Tel Aviv, Israel

**Gianpaolo Grisolia, MD**

Department of Obstetrics and Gynecology  
Azienda Ospedaliera “C.Poma”  
Mantova, Italy

**Maurice Guirgis, MD**

University Paris VII  
Service Explorations Fonctionnelles  
Hôpital Robert Debré  
Paris France

**Wesley Lee, MD**

Division of Fetal Imaging,  
William Beaumont Hospital,  
Royal Oak, MI, USA

**Lucia Manganaro, MD,**

Department of Radiology,  
Università “La Sapienza”  
Rome, Italy

**Dev Maulik, MD, PhD,**

Department of Obstetrics and Gynecology,  
University of Missouri-Kansas City School Medicine,  
Kansas City, Missouri, USA

**Baruch Messing, MD**

Department of Obstetrics and Gynecology,  
Hadassah-Hebrew University Medical Centers – Mt. Scopus,  
Jerusalem, Israel

**David Mundy, MD,**

Department of Obstetrics and Gynecology,  
University of Missouri-Kansas City School Medicine,  
Kansas City, Missouri, USA

**Roberta Iacobelli, MD**

Department of Pediatric Cardiology and Cardiac Surgery  
Bambino Gesù' Hospital,  
Rome Italy

**Manuela Oberto, MD**

Department of Obstetrics and Gynecology,  
Maternal-Fetal Medicine Unit,  
University of Turin,  
Turin Italy

**Giovanna Oggè, MD**

Department of Obstetrics and Gynecology,  
Maternal-Fetal Medicine Unit,  
University of Turin,  
Turin Italy

**Dario Paladini, MD**

Fetal Medicine & Cardiology Unit,  
Department of Obstetrics and Gynecology,  
University Federico II of Naples  
Naples, Italy

**Luciano Pasquini, MD**

Department of Pediatric Cardiology and Cardiac Surgery  
Bambino Gesù' Hospital,  
Rome Italy

**Georgios Rembouskos, MD**

Fetal Medicine Unit,  
Di Venere and Sarcone Hospitals. ASL Bari.  
Bari, Italy

**Giuseppe Rizzo, MD**

Department of Obstetrics and Gynecology  
Università Roma Tor Vergata  
Rome Italy

**Roberto Romero, MD**

Department of Obstetrics and Gynecology,  
Wayne State University School of Medicine,  
Perinatology Research Branch Intramural Division, NICHD, NIH, DHHS,  
Hutzel Women's Hospital  
Detroit, MI, USA

**Sara Savelli, MD**

Department of Radiology,  
Università “La Sapienza”  
Rome, Italy

**Gabriella Sglavo, MD**

Fetal Medicine & Cardiology Unit,  
Department of Obstetrics and Gynecology,  
University Federico II of Naples  
Naples, Italy

**Elena Sinkovskaya, MD**

Department of Obstetrics and Gynecology,  
Eastern Virginia Medical School,  
Norfolk, VA USA

**Fabrizio Taddei, MD**

Department of Obstetrics and Gynecology  
Azienda Ospedaliera “C.Poma” –  
Mantova - Italy

**Tullia Todros, MD**

Department of Obstetrics and Gynecology,  
Maternal-Fetal Medicine Unit,  
University of Turin,  
Turin Italy

**Alessandra Toscano, MD**

Department of Pediatric Cardiology and Cardiac Surgery  
Bambino Gesù Hospital,  
Rome Italy

**Dan V Valsky, MD**

Department of Obstetrics and Gynecology,  
Hadassah-Hebrew University Medical Centers – Mt. Scopus,  
Jerusalem, Israel

**Nicola Volpe, MD**

Fetal Medicine Unit,  
Di Venere and Sarcone Hospitals. ASL Bari.  
Bari, Italy

**Paolo Volpe, MD**

Fetal Medicine Unit,  
Di Venere and Sarcone Hospitals. ASL Bari.  
Bari, Italy

**Alina Weissmann-Brenne, MD**

Department of Obstetrics and Gynecology,  
The Chaim Sheba Medical Center,  
Tel Hashomer, Affiliated with the Sackler Faculty of Medicine,  
Tel Aviv University,  
Tel Aviv, Israel

**Simcha Yagel, MD**

Department of Obstetrics and Gynecology,  
Hadassah-Hebrew University Medical Centers – Mt. Scopus,  
Jerusalem, Israel

**Lami Yeo, MD**

Department of Obstetrics and Gynecology,  
Wayne State University School of Medicine,  
Perinatology Research Branch Intramural Division, NICHD, NIH, DHHS,  
Hutzel Women's Hospital  
Detroit, MI, USA

---

## **Epidemiology of Congenital Heart Diseases**

**Maurice Guirgis\***

*Service Explorations Fonctionnelles Hôpital Robert Debré PARIS- FRANCE*

**Abstract:** Congenital heart defects (CHD) are among the most common birth defects, occurring in 5 to 10 per 100 live births. This substantial variation in the reported epidemiology of CHD is due to differences in applied methodologies. An increasing total prevalence of CHD has been recently reported, mainly due to increase in prevalence of small defects easily diagnosed by echocardiography, as well as an increase in prevalence of conotruncal defects and atrioventricular septal defects. In order to provide a comprehensive epidemiological overview, future studies should use international classification system as well as consistent inclusion and exclusion criteria. Further studies are also required to evaluate precisely the impact of fetal cardiac diagnosis on the prevalence and outcome of CHD. Epidemiology of CHD provides an overview of the distribution and characteristics of risk factors. Environmental potential risk factors are reviewed as they may provide an opportunity for prevention of some forms of CHD.

**Key Words:** Congenital Heart Disease, Epidemiology, Environmental Risk Factor.

### **INTRODUCTION**

Congenital heart defects (CHD) defined as “gross structural anomalies of the heart or intrathoracic vessels that are actually or potentially of functional significance”, are among the most common congenital anomalies affecting about 5 to 10 per 1000 live births and are considered as the leading cause of infant deaths resulting from congenital anomalies [1,2,3].

### **CAVEATS IN ASSESSMENT OF INCIDENCE OF CHD**

Accurate determination of the incidence of CHD is difficult and subject to great variation across different populations and registries: some mild and asymptomatic cases may not be diagnosed and consequently they are underestimated; other severe cases may die in the neonatal period without a diagnosis or autopsy done. However development of echocardiography as an accurate diagnostic tool for CHD [2], resulted in increased estimated values for incidence of CHD, secondary to improved prenatal diagnosis [4,5], as well as improved diagnosis of overlooked and mild lesions (e.g., increased diagnosis of cases with small atrial septal defects (ASD), and isolated small ventricular septal defects (VSD), which tend to resolve spontaneously).

To avoid confusion, and in order to provide a comprehensive review, epidemiological studies reporting total prevalence of CHD, should cover a geographically well defined area, and should include CHD occurring in live births, termination of pregnancy, late miscarriages and stillbirths. Cases with functional or unspecified cardiac murmur, patent ductus arteriosus (PDA) associated to prematurity, peripheral pulmonary artery stenosis (PPS), should be excluded, according to the European Surveillance of congenital anomalies EUROCAT exclusion list [6]. Furthermore, it is better to relate the absolute incidence of each specific lesion, to live births, rather than describing its incidence as a proportion of all CHD. In a recent study from Denmark, the overall CHD birth prevalence, have been reported to have increased [7] from 73 to 113 per 10.000 live births from 1977 to 2005 with stabilization of the prevalence after 1996–1997. The increased prevalence was primarily due to an increase in VSD and ASD prevalence, related to improved diagnosis by echocardiography as reported by others [8,9,10,11]. The total prevalence of conotruncal defects, atrioventricular septal defects (AVSD), and right ventricular outflow obstruction (RVOTO) increased also significantly [7, 8], probably due to changes in the pregnancy risk factors particularly the increasing incidence of type 2 diabetes among women of childbearing age [7,12].

### **IMPACT OF FETAL DIAGNOSIS OF CHD**

Fetal diagnosis of structural heart defects by ultrasound ranges from 8% in eastern Europe to 48% in France [4] due to an active policy in prenatal screening and involvement of obstetricians and sonographers in screening for cardiac

---

\*Address Correspondence to **Maurice Guirgis:** University Paris VII, Service Explorations Fonctionnelles, Hôpital Robert Debré, 48 bd Serurier 75019 Paris France; Email: guirgis1@hotmail.com

malformations during routine obstetrical ultrasounds. This may have a potential impact on the incidence of CHD if termination of pregnancy is decided [4,13, 14]. In a study including 2454 cases with CHD, collected from 20 registries of congenital malformations in 12 European countries, termination of pregnancy was performed in 293 cases [12%] varying from 0% to 49% according to the registry [4]. In a recent analysis obtained from the Paris registry of congenital malformations, Koshnood et al. [5], reported increase rate of termination of pregnancy for cases with hypoplastic left heart syndrome (HLHS) detected by fetal echocardiography, that increased from 13.6%, between 1983-1988 to 72.4% between 1989-1994, before reaching a rate of 63% between 1995- 2000. Further studies are required to assess the impact of fetal medicine in the prevalence and outcome of CHD.

## **GEOGRAPHIC, RACIAL, ETHNIC & SOCIO-ECONOMIC DISTRIBUTION OF CHD**

The reported incidence of various cardiac defects may vary according to different geographic regions [11, 15-17] probably related to genetic and racial factors. For example, studies of ethnic influence on the pattern of CHD in the United Kingdom revealed a higher incidence of left obstructive disease such as aortic stenosis (AS) and coarctation of aorta (Ao Coa) in non-Asian (9%) than Asian (3%) infants [15]. This was also reported from epidemiologic studies from Saudi Arabia [11] and Japan [16], where a low incidence of AS and Ao Coa was reported (4.8% and 3.7% respectively of all patients with CHD) contrasting with a higher incidence reported from Europe [17]. A low incidence of AVSD was also reported from Japan [16] contrasting with a higher incidence in United Kingdom [15].

Compared with black infants, white infants have been found to have an increased prevalence of Ebstein's anomaly, AS, Pulmonary atresia, AVSD, ASD, Ao Coa, Transposition of great arteries (TGA) and Tetralogy of Fallot (TOF), while less white infants were found among cases with Pulmonary stenosis (PS) and heterotaxia [18]. These results highlight racial variations in CHD and may suggest that socio-economic status (SES) account for some of this variation, as also evidenced by an increased risk for TGA reported with low SES that included mother's education, poverty, and unemployment [19].

## **SEX DISTRIBUTION**

As regards sex distribution of CHD; some lesions such as Ao Coa, AS, TGA show strong male predominance [11, 20-21]. On the other hand, female predominance is observed in PDA, ASD, AVSD and PS [20, 21]. Gensburg et al [22], classifying isolated lesions according to the time of embryonic disturbed organogenesis, found male predominance in those lesions developing in later gestation.

## **ETIOLOGY OF CHD**

Cardiovascular development involves a series of complex events precisely orchestrated and regulated by specific genes. CHD represent multiple underlying etiologies: genetic, environmental, teratogenic exposures, multifactorial and unknown mechanisms.

The precise links between genetic and environmental factors, are incompletely understood. Environmental factors may affect gene expression directly or may block the action of gene product. Some outflow tract (Truncus Arteriosus, Double outlet right ventricle) that may be associated with the DiGeorge (CATCH 22 syndrome) may result also from interfering with migration of neural crest cells by certain chemicals (bis-diamine, tran-retinoic acid), or by experimentally removal of cranial neural crest cells [23].

The current state of knowledge on genetic causes of CHD [24] is reviewed separately in another chapter. Environmental factors involved in the etiology of CHD are multiple and include maternal diseases, drug exposures, alcohol, and other environmental exposures [24,25,26]. The potential factors that might influence the risk for CHD including periconceptional folic acid intake which may reduce the risk [27-29] and those factors that increase the risk for CHD are discussed.

## **ROLE OF MULTIVITAMINS AND FOLIC ACID**

Periconceptional intake of multivitamins supplements containing folic acid [27,28] was reported to possibly reduce the risk of CHD up to 60% [27]. In a recent work [29], fortification of grain products with folic acid in Canada, was followed by a significant decrease in the birth prevalence of severe CHD strongly supporting the protective effect of Folic acid. Specifically, the birth prevalence did not change in the eight years before fortification and decreased in the seven years after fortification with a significant change in time trend between the two periods for conotruncal defects and non-conotruncal defects [29].

## MATERNAL DISEASES AND CONDITIONS

### MATERNAL DIABETES

CHD is found in 3-5% of pregnant women with maternal pregestational diabetes [30-32]. Associations of CHD with gestational diabetes are probably due to inclusion of pregnant women with previously undetected type 2 diabetes among those classified as having gestational diabetes. Almost all cardiac lesions have been reported, mainly outflow tract lesions, conotruncal anomalies, AVSD, TGA, VSD, HLHS and Ao Coa [30-32]. Cardiac malformation occurs before the seventh week of gestation possibly by abnormal glucose level affecting the expression of a regulatory gene in the embryo, leading to apoptotic cellular changes [32]. Another possible mechanism is the generation of free radicals resulting from metabolic abnormalities as suggested by prevention of diabetic embryopathy in animal studies by antioxidants [33-34].

### Phenylketonuria

Maternal phenylketonuria is associated with increased risk of heart defects through increased blood levels of phenylalanine and phenyl pyruvic acid [35,36]. The most frequent defects are TOF, Ao Coa, VSD, PDA, Single ventricle, and ASD. Diet control before conception and during pregnancy reduces the risk of CHD [36].

Rubella, Febrile Illnesses, and Influenza Maternal rubella infection during pregnancy can result in increased incidence of CHD about 35% [37-39]. Common reported defects are PS, PDA, VSD, PPS, and VSD [40,41]. Maternal febrile illnesses, influenza, during the first trimester of pregnancy, may also be associated with an increased risk for certain heart defects such as conotruncal lesions, right and left obstructive lesions, VSD and Ao Coa [42-44].

### Maternal HIV

Children infected with HIV-1 has not been reported to be associated with an increased risk of CHD. [45]. Irrespective of their HIV-1 status, infants born to women infected with HIV-1 have significantly worse cardiac function than other infants [45-46].

### Maternal Stress

Intense maternal stress (e.g. divorce, death of a relative,...) during the periconceptional period was associated with increased risk of delivering infants with certain congenital anomalies particularly with conotruncal heart defects and neural tube defects [47, 48].

## MATERNAL DRUG INTAKE

Table 1 summarizes main maternal drug exposure -during the first trimester of pregnancy and periconceptional period - associated with CHD [24-26, 48-55].

**Table 1:** MATERNAL DRUG INTAKE AND CHD . Data from references [24, 25, 26, 48-55]

DRUG	CHD
Lithium	ASEEbstein's anomaly, Mitral & tricuspid regurge
Retinoic Acid	Conotruncal malformations
Trimethadione	TOF, HLHS, TGA,
Phenytoin	Coarctation, PDA,AS, PS
Coumadin	PPS, PDA
Thalidomide	PS, TGA, *TAPVR,VSD, ASD, TA, TOF
Ibuprofen	TGA, AVSD, VSD, Bicuspid valve
Trimethoprim-Sulfonamide,	
Sulfalazine	Any defects
Angiotensin-converting	
enzyme inhibitors	ASD, VSD, PS, PDA
Metronidazole	
Valproic acid	Outflow tract, VSD TOF, others

\*TAPVR: Total Anomalous pulmonary Venous Return



Some of the drugs were reported with associated risks of CHD, but only limited information is available e.g. Angiotensin –converting enzymes [49], Trimethoprim-Sulfonamide [50-51], metronidazole [24] , fluconazole [52,53].

## **OTHER MATERNAL NON THERAPEUTIC & ENVIRONMENTAL EXPOSURE**

### **Alcohol**

Several studies have reported teratogenic effects of alcohol consumption during pregnancy, including cardiac defects [56]. A more recent case-control study that examined the risk of congenital anomalies with different sporadic and daily doses of alcohol consumption in Spain, reported an increased risk of CHD only with the highest level of maternal consumption of alcohol per day [57].

### **Cocaine and Marijuana**

Maternal cocaine ingestion was reported to induce coronary thrombosis in the developing fetal heart leading to single ventricle [58]. Association of maternal intake of cocaine with other defects was also reported : Ebstein's anomaly , VSD, heterotaxy [ 24,59, 60].

### **Cigarette Smoking**

The relationship between gestational smoking and congenital defects has been studied, however the information is inconclusive. Some studies have reported associations of maternal smoking with ASD, AVSD, TOF [61], however, no associations were found in other reports [24,62]. Further research on large population-based studies is required to clarify this relationship.

### **Organic Solvents**

Some studies reported increased risk of TGA, HLHS, Ao Coa, TOF, PS with maternal exposure to solvents and paints [24]. However the precise links are difficult to clarify, because the composition varies between different commercial preparations.

### **Pesticides & Other Toxic Substances**

In the Baltimore-Washington Infant Study (BWIS), potential exposure to herbicides and rodenticides was associated with an increased risk of TGA, while potential exposure to pesticides was associated with TAPVR and VSD [24]. A more recent case-control study of various end-product uses reported an increased risk of conotruncal defects with maternal reports of exposure to insecticides [63].

### **Air Pollution**

Gilboa et al [64], observed positive associations between carbon monoxide and isolated ASD, TOF, particulate matter <10 µm in aerodynamic diameter and isolated ASD as well as between ozone and VSD. Further studies are also required to clarify if air pollution exposure influences the risk for CHD.

### **Maternal Home Tap Water Consumption**

A positive association between a mother's consumption of home tap water during the first trimester of pregnancy and cardiac anomalies. This was unrelated to water contamination, mother's race, or her educational level [65].

### **Waste Sites and Ionizing Radiation**

Much of the recent evidence about possible increase risk of CHD in communities situated near hazardous waste sites are inconsistent [66] and may not ultimately prove to be causal. Few reports on possible associations of CHD with maternal exposure to ionizing radiation in occupational settings or as part of medical or dental evaluations, found no clear evidence of any associations [24], and further studies are also required to clarify the precise relationship between these factors and CHD.

## **CONCLUSION**

CHD is associated with a considerable disease burden at both country and individual levels. Although there is a substantial variation in the reported prevalence of CHD in the literature, due to differences in epidemiological

studies, however recent studies suggest an increased prevalence of CHD, mainly by increased incidence of small lesions easily detectable by echocardiography, as well as increased prevalence of conotruncal and atrioventricular septal defects.

Fetal diagnosis of CHD may affect the prevalence and the outcome of CHD. The impact of fetal diagnosis on prevalence, and outcome of CHD requires further investigations as there is no available uniform parental counselling and ethical guidelines.

Prevention of CHD is actually limited to our actual knowledge of the proportion of CHD attributable to non inherited potentially modifiable environmental fetal exposure, that although difficult to estimate, may account for 13.6% to 30.2% of cases [26].

Further epidemiological studies, based on large population-based studies, using more standardized case ascertainment and classification methods are required, to unmask some of the mysteries of abnormal cardiogenesis and clarify the precise links between inherited and non inherited risk factors and CHD, in order to be able to develop adequate prevention strategies.

## REFERENCES

- [1] Bosi G. Congenital heart defects and disease: an epidemiological overview. *It. J. Pediatr.* 2004;30:261-266.
- [2] Lee K, Koshnood B, Chen L et al. Infant mortality from congenital malformations in the united states, 1970- 1997. *Obstet. Gynecol.* 2001;98/620-627.
- [3] Hoffman JI, Kaplan S. The incidence of congenital heart disease. *J Am Coll Cardiol.* 2002; 39: 1890-1900.
- [4] Garne E, Stoll C, Clementi M, Euroscan group. Evaluation of prenatal diagnosis of congenital heart diseases by ultrasound: experience from 20 Europeans registries. *Ultrasound Obstet Gynecol.* 2001; 17: 386-391.
- [5] Khoshnood B, De Vigan C, Vodovar V *et al.* Trends in prenatal diagnosis, pregnancy termination, and perinatal mortality of newborns with congenital heart disease in France, 1983-2000: a population-based evaluation. *Pediatrics* 2005;115(1):95-101
- [6] Prevalence of congenital anomalies (Database). <http://eurocat.Ulster.ac.uk/pubdata:tables.html>
- [7] Oyen N, Poulsen G, Boyd HA *et al.* National time trends in congenital heart defects, Denmark, 1977-2005. *Am Heart J* 2009; 157: 467-473.
- [8] Dadvand P, Rankon J Sirley MDF *et al.* Descriptive epidemiology of congenital heart disease in Northern England. *Paediatr Perinat Epidemiol.* 2009 Jan;23(1):58-65.
- [9] Layde PM, Dooley K, Errickson JD *et al.* Is there an epidemic of ventricular septal defects in the USA. *Lancet* 1980;23:407-408.
- [10] Meberg A, Otterstad JE, Frøland G, *et al.* Increasing incidence of ventricular septal defects by improved detection rate. *Acta Paediatr.* 1994;83:653-657.
- [11] Alabdulgader AAA. Congenital heart disease in Saudi Arabia: current epidemiology and future projections. *East Medit. Heart J* 2006 Volume 12 supplement 2: S157-S167.
- [12] Mokdad AH, Bowman BA, Ford ES, *et al.* The continuing epidemics of obesity and diabetes in the United States. *JAMA.* 2001;286:1195-1200.
- [13] Stoll C, Alembik Y, Dott B, *et al.* Impact of prenatal diagnosis on live birth prevalence of children with congenital anomalies. *Ann Genet.* 2002;45:115-121.
- [14] Bull C. Current and potential impact of fetal diagnosis on prevalence and spectrum of serious congenital heart disease at term in the UK. *Lancet* 1999; 354 1242-1247.
- [15] Sadiq M, Stümper O, Wright JG, De Giovanni JV, Billingham C, Silove ED. Influence of ethnic origin on the pattern of congenital heart defects in the first year of life. *Br Heart J,* 1995,73(2):173-176.
- [16] Nakazawa M, Seguchi M, Takao A. Prevalence of congenital heart disease in Japan. In: Clark EB, Takao A, eds. *Developmental cardiology: morphogenesis and function.* Mount Kisco, New York, Futura Publishing Co., 1990, 541-548.
- [17] Meszaros M *et al.* Birth prevalence of congenital cardiovascular malformations in Hungary. *Acta paediatrica academiae scientiarum hungaricae,* 1980, 21(4):221-225.
- [18] Correa-Villasenor A, McCarter R, Downing J, Ferencz C. White-black differences in cardiovascular malformations in infancy and socioeconomic factors: the Baltimore-Washington Infant Study Group. *Am J Epidemiol.* 1991; 134: 393-402.
- [19] Carmichael SL, Nelson V, Shaw GM, Wasserman CR, Croen LA. Socio-economic status and risk of conotruncal heart defects and orofacial clefts. *Paediatr Perinat Epidemiol.* 2003; 17: 264-271.
- [20] Perry LW *et al.* Infants with congenital heart disease: the cases. In: Ferencz Carl *et al.*, eds. *Perspectives in pediatric cardiology. 4 Epidemiology of congenital heart disease: the Baltimore-Washington infant heart study, 1981-1989.* Mount Kisco, New York, Futura Publishing Co., 1993, 33-62.

- [21] Pradat P. Epidemiology of major congenital heart defects in Sweden, 1981–1986. *Journal of epidemiology and community health*, 1992, 46(3):211–215.
- [22] Gensburg LJ, Marshall EG, Druschel CM. Examining potential demographic risks factors for congenital cardiovascular malformations on a time development model. *Pediatric and perinatal epidemiology*, 1993, 7(4):434–449.
- [23] Kirby ML. Cardiac morphogenesis-recent research advances. *Pediatr Res* 1987; 21:219-224.
- [24] Ferencz C, Correa-Villasenor A, Loffredo CA, eds. *Genetic and Environmental Risk Factors of Major Cardiovascular Malformations: The Baltimore-Washington Infant Study: 1981–1989*. Armonk, NY: Futura Publishing Co; 1997.
- [25] Jenkins KJ, Correa A, Feinstein JA, *et al*. Non-inherited risk factors and congenital cardiovascular defects: Current knowledge: a scientific statement from the American Heart Association Council on Cardiovascular Disease in the Young: endorsed by the American Academy of Pediatrics. *Circulation*. 2007;15:2995–3014.
- [26] Wilson PD, Loffredo CA, Correa-Villasenor A, Ferencz C. Attributable fraction for cardiac malformations. *Am J Epidemiol*. 1998;148:414–423.
- [27] Czeizel AE. Periconceptional folic acid containing multivitamin supplementation. *Eur J Obstet Gynecol Reprod Biol*. 1998; 78:151–161.
- [28] Botto LD, Mulinare J, Erickson JD. Occurrence of congenital heart defects in relation to maternal multivitamin use. *Am J Epidemiol*. 2000; 151:878–884.
- [29] Ionescu-Ittu R, Marelli AJ, Mackie AS. Prevalence of severe congenital heart disease after folic acid fortification of grain products: time trend analysis in Quebec, Canada *BMJ* 2009; 338:1261-1263.
- [30] Wren C, Birrell G, Hawthorne G. Cardiovascular malformations in infants of diabetic mothers. *Heart*. 2003; 89: 1217–1220.
- [31] Schaefer-Graf UM, Buchanan TA, Xiang A, Songster G, Montoro M, Kjos SL. Patterns of congenital anomalies and relationship to initial maternal fasting glucose levels in pregnancies complicated by type 2 and gestational diabetes. *Am J Obstet Gynecol*. 2000; 182: 313–320.
- [32] Kousseff BG. Diabetic embryopathy. *Curr Opin Pediatr*. 1999;11:348–352.
- [33] Viana M, Herrera E, Bonet B. Teratogenic effects of diabetes mellitus in the rat: prevention by vitamin E. *Diabetologia*. 1996;39:1041–1046.
- [34] Siman CM, Gittenberger-De Groot AC, Wisse B, Eriksson UF. Malformations in offspring of diabetic rats: morphometric analysis of neural crest-derived organs and effects of maternal vitamin E treatment. *Teratology*.2000;61:355–367.
- [35] Levy HL, Guldberg P, Guttler F *et al*. Congenital heart disease in maternal phenylketonuria: report from the Maternal PKU Collaborative Study. *Pediatr Res*. 2001; 49: 636–642.
- [36] Rouse B, Azen C. Effect of high maternal blood phenylalanine on offspring congenital anomalies and developmental outcome at ages 4 and 6 years: the importance of strict dietary control preconception and throughout pregnancy. *J Pediatr*.2004; 144: 235–239.
- [37] Gregg NM, Ramsay Brevis W, Heseltine M. The occurrence of congenital defects in children following maternal rubella during pregnancy. *Med J Aust*.1945; 2:122–126.
- [38] Stuckey D. Congenital heart defects following maternal rubella during pregnancy. *Br Heart J*. 1956; 18: 519–522.
- [39] Campbell M. Place of maternal rubella in the aetiology of congenital heart disease. *BMJ*. 1961;1:691–696.
- [40] Cochi SL, Edmonds LE, Dyer K *et al*. Congenital rubella syndrome in the United States, 1970–1985: on the verge of elimination. *Am J Epidemiol*. 1989;129: 349–361.
- [41] Tikkanen J, Heinonen OP. Maternal hyperthermia during pregnancy and cardiovascular malformations in the offspring. *Eur J Epidemiol*. 1991;7: 628–635.
- [42] Zhang J, Cai WW. Association of the common cold in the first trimester of pregnancy with birth defects. *Pediatrics*. 1993; 92: 559–563.
- [43] Mirkes PE, Cornel LM, Park HW, Dunningham ML. Induction of thermotolerance in early postimplantation rat embryos is associated with increased resistance to hyperthermia-induced apoptosis. *Teratology*.1997;56:210–219.
- [44] Roulston A, Marcellus RC, Branton PE. Viruses and apoptosis. *Annu Rev Microbiol*. 1999;53:577–628.
- [45] Hornberger LK, Lipshultz SE, Easley KA, *et al*. Cardiac structure and function in fetuses of mothers infected with HIV: the prospective PCHIV multicenter study. *Am Heart J*.2000; 140: 575–584.
- [46] Starc TJ, Lipshultz SE, Kaplan S, *et al*. Cardiac complications in children with human immunodeficiency virus infection: Pediatric Pulmonary and Cardiac Complications of Vertically Transmitted HIV Infection (P2C2 HIV) Study Group, National Heart, Lung, and Blood Institute. *Pediatrics*. 1999; 104: e14.
- [47] Carmichael SL, Shaw GM. Maternal life event stress and congenital anomalies. *Epidemiology*.2000; 11: 0–35.
- [48] Adams MM, Mulinare J, Dooley K. Risk factors for conotruncal cardiac defects in Atlanta. *J Am Coll Cardiol*. 1989; 14: 432–442.
- [49] Cooper WO, Hernandez-Diaz S, Arbogast PG, *et al*. Major congenital malformations after first-trimester exposure to ACE inhibitors. *N Engl J Med*. 2006; 354: 2443–2451.
- [50] Czeizel AE, Rockenbauer M, Sorensen HT, Olsen J. The teratogenic risk of trimethoprim-sulfonamides: a population based case-control study. *Reprod Toxicol*. 2001; 15: 637–646.

- [51] Hernandez-Diaz S, Werler MM, Walker AM, Mitchell AA. Folic acid antagonists during pregnancy and the risk of birth defects. *N Engl J Med.* 2000; 343:1608–1614.
- [52] Jick SS. Pregnancy outcomes after maternal exposure to fluconazole. *Pharmacotherapy.* 1999; 19: 221–222.
- [53] Pursley TJ, Blomquist IK, Abraham J, Andersen HF, Bartley JA. Fluconazole-induced congenital anomalies in three infants. *Clin Infect Dis.* 1996; 22: 336–340.
- [54] Schardein JL. Anticonvulsants. In: *Chemically Induced Birth Defects.* 3rd ed. New York, NY: Marcel Dekker; 2000: 179–235.
- [55] Alsdorf R, Wyszyski D. Teratogenicity of sodium valproate. *Expert Opin Drug Saf.* 2005 ;4(2): 345-353.
- [56] Clarren SK, Smith DW. The fetal alcohol syndrome. *N Engl J Med.* 1978; 298: 1063–1067.
- [57] Martinez-Frias ML, Bermejo E, Rodriguez-Pinilla E, Frias JL. Risk for congenital anomalies associated with different sporadic and daily doses of alcohol consumption during pregnancy: a case-control study. *Birth Defects Res A Clin Mol Teratol.* 2004;70:194–200.
- [58] Shepard TH, Fantel AG, Kapur RP. Fetal coronary thrombosis as a cause of single ventricular heart. *Teratology.*1991;43:113–117.
- [59] Shaw GM, Malcoe LH, Lammer EJ, Swan SH. Maternal use of cocaine during pregnancy and congenital cardiac anomalies. *J Pediatr.* 1991; 118: 167–168.
- [60] Williams LJ, Correa A, Rasmussen S. Maternal lifestyle factors and risk for ventricular septal defects. *Birth Defects Res A Clin Mol Teratol.* 2004;70 :59-64.
- [61] Torfs CP, Christianson RE. Maternal risk factors and major associated defects in infants with Down syndrome. *Epidemiology.*1999;10: 64–270.
- [62] Kallen K. Maternal smoking and congenital heart defects. *Eur J Epidemiol.* 1999; 15: 731–737.
- [63] Shaw GM, Nelson V, Iovannisci DM, Finnell RH, Lammer EJ. Maternal occupational chemical exposures and biotransformation genotypes as risk factors for selected congenital anomalies. *Am J Epidemiol.* 2003;157: 75–484.
- [64] Gilboa SM, Mendola P, Olshan AF, *et al.*Relation between ambient air quality and selected birth defects, seven county study, Texas, 1997–2000. *Am J Epidemiol.* 2005; 162: 238–252.
- [65] Shaw GM, Swan SH, Harris JA, Malcoe LH. Maternal water consumption during pregnancy and congenital cardiac anomalies. *Epidemiology.*1990;1: 06–211.
- [66] Croen LA, Shaw GM, Sanbonmatsu L, Selvin S, Buffler PA. Maternal residential proximity to hazardous waste sites and risk for selected congenital malformations. *Epidemiology.*1997;8: 347–354.

## Second Trimester Screening of Congenital Heart Disease

Giovanna Oggè, Pietro Gaglioti, Manuela Oberto and Tullia Todros\*

*Department of Obstetrics and Gynecology, Maternal-Fetal Medicine Unit, University of Turin, Italy*

**Abstract:** Congenital heart diseases (CHD) are frequent fetal anomalies, with an important impact on perinatal mortality and morbidity. Prenatal diagnosis has a demonstrated effect in decreasing the overall prevalence at birth, and in improving the outcomes of specific malformations; moreover, the great majority of these malformations occurs in the absence of any risk factor. All of these features strongly evidence the need for a screening test that can be applied to the general population, to identify a selected group of fetuses for the more specific, complex, and time-consuming diagnostic test (fetal echocardiography). The systematic visualization of the four chamber view and the outflow tracts during routine anatomical scan has progressively increased the prenatal detection rate of CHD. However, a number of potentially diagnosable defects are still missed in the screening setting. Three-dimensional ultrasonography could provide a useful tool to ameliorate the current performance of CHD screening; however this possibility needs to be further explored.

**Key Words:** Congenital Heart Disease, Diagnosis, Fetal Echocardiography, Screening.

### INTRODUCTION

Congenital heart diseases (CHD) are the most common congenital anomalies, with a prevalence of around 9/1000 livebirth [1]; moreover they account for the majority of infant deaths due to congenital malformations [2, 3].

Prenatal diagnosis of CHD implies a number of potential advantages: 1) if it is early enough during gestation, it allows consideration of termination of pregnancy [4]; 2) it consents the planning and timing of delivery in a referral centre, leading to better conditions at surgery; 3) it permits *in utero* treatment, although, to date, few procedures have been performed (ballon valvuloplasty for aortic or pulmonary stenosis [5, 6], atrial septoplasty for hypoplastic left ventricle with restrictive foramen ovale [7-9], cardiocentesis for pericardial effusion [10-15]) and available data are too sparse to attest a benefit [16, 17]. In contrast, pharmacological transplacental therapy for fetal arrhythmias has become a well accepted practice, based on a consistent body of evidence [18].

Although several risk factors for the development of CHD are recognized (see Table 1), the great majority of these malformations are diagnosed in low-risk pregnancies [19]. This enhances the need for a screening test, which ideally should be simple and rapid enough to be systematically applied to the general population, to identify cases eligible for fetal echocardiography [20, 21]. The usefulness of a systematic screening program is further confirmed by the fact that the majority of prenatal diagnoses of CHD actually occur in women who have been referred to echocardiography because of a suspicion at the screening exam [22].

**Table 1:** Risk factors for CHD (indications for fetal echocardiography). Modified from [23].

<b>Family history</b>	First-degree relative of proband
<b>Maternal diseases</b>	Pregestational diabetes mellitus
	Phenylketonuria
	Autoimmune diseases: anti-Ro (SSA) and anti-La (SSB)
<b>Maternal infections</b>	Parvovirus B19
	Rubeovirus
	Coxsackie virus

\*Address correspondence to Tullia Todros: Department of Obstetrics and Gynecology, University of Turin, Ospedale S Anna Corso Spezia, 60, 10126 Torino Italy; Email: tullia.todros@unito.it

Table 1: cont....

<b>Teratogen exposure</b>	Retinoids Phenytoin Carbamazepine Valproic acid Lithium Alcohol
<b>Fetal anomalies</b>	Suspected fetal heart anomaly at screening scan Extra-cardiac anomalies Non-immune hydrops Abnormal fetal karyotype Increased nuchal translucency Persistent fetal arrhythmias

The first significant effect of prenatal diagnosis of CHD has been the reduction of the prevalence of these anomalies at birth, secondary to increased termination of affected pregnancies. The proportion of termination of pregnancies, among prenatally diagnosed CHD, is 50% [24], and an increase in the number of anomalies diagnosed *in utero* as well as an anticipation of the diagnoses is likely to augment the absolute number of terminated pregnancies.

Contrary to the expectations, a positive impact of prenatal diagnosis on the overall survival rate of neonates with CHD has not been demonstrated [25]. One explanation is that prenatally diagnosed CHD tend to be more severe than those diagnosed postnatally, and they are more frequently associated with chromosomal and extra-cardiac anomalies, that negatively influence their prognosis [26].

However, a positive impact of prenatal diagnosis on neonatal outcomes has been demonstrated for specific CHD, namely aortic coarctation [27], transposition of great arteries [28], hypoplastic left heart syndrome [29, 30].

### THE FOUR CHAMBER VIEW

A first screening test for CHD was proposed in the 80's, and it was based on the inclusion of the four chamber view in all routine ultrasound performed since 16 weeks of gestational age [31].

The main advantage of such a method is the possibility to examine several cardiac structures in one single ultrasonographic plane. Indeed, the correct visualization of the four chamber view, either from an apical or from a transverse approach, allows the evaluation of [32].

- the cardiac situs and the anatomical relationship between the heart and the abdominal organs
- the cardiac axis
- the morphology and symmetry of the ventricles and the atria
- the integrity of the ventricular septum
- the presence of the atrial septum primum
- the foramen ovale bulging toward the left atrium
- the opening of the atrioventricular valves
- the thickness of the ventricular wall
- the absence of pericardial effusion
- the cardiac rate and the regularity of the rhythm

(see Figures 1 - 4).

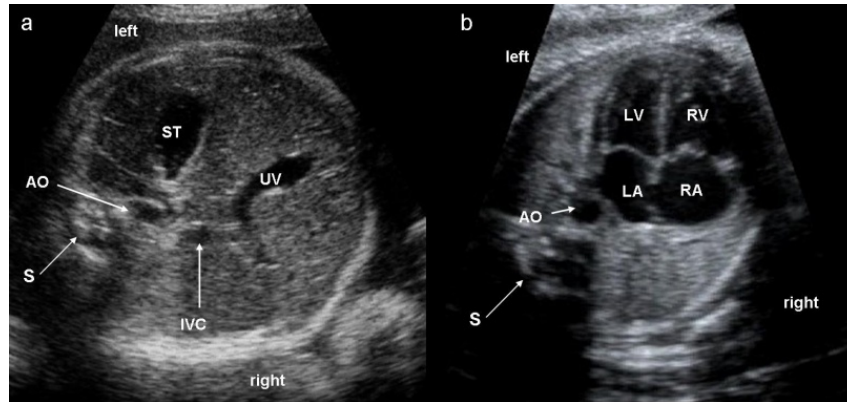


**Figure 1:** a) Transverse section of the fetal abdomen: the stomach (ST) is on the left side; the transverse sections of the descending aorta (AO) and inferior vena cava (IVC) are in front of the spine (S), at the left and at the right respectively. The intrahepatic portion of the umbilical vein (UV) is also seen in this section.

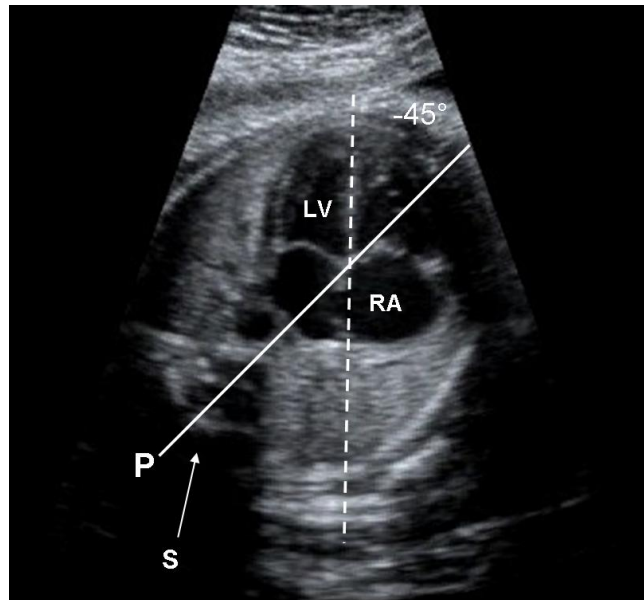


**Figure 2:** Transverse section of fetal thorax: the longitudinal axis of the heart (dashed line) forms an angle of about  $45^\circ$  with respect to the antero-posterior axis (AP) of the thorax. The apex of the heart is on the left. LV: left ventricle; RA: right atrium; S: spine.

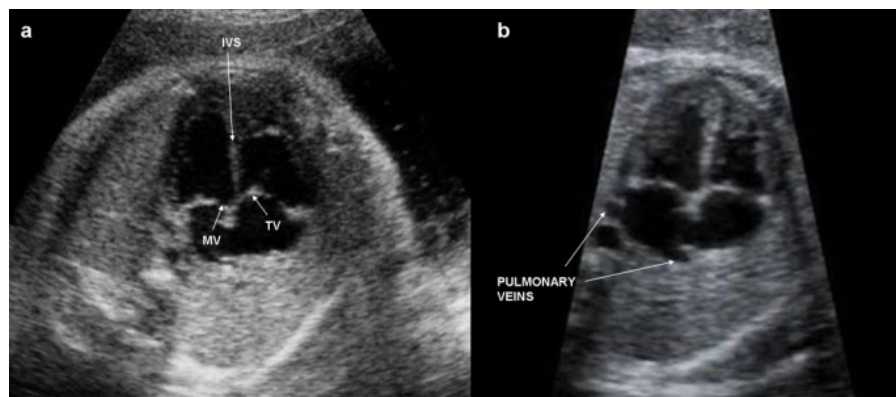


**Figure 3:** Apical four chamber view: a) the septal leaflet of the tricuspid valve (TV) has a more apical insertion on the interventricular septum (IVS) than the mitral valve (MV); b) pulmonary veins draining in left atrium.

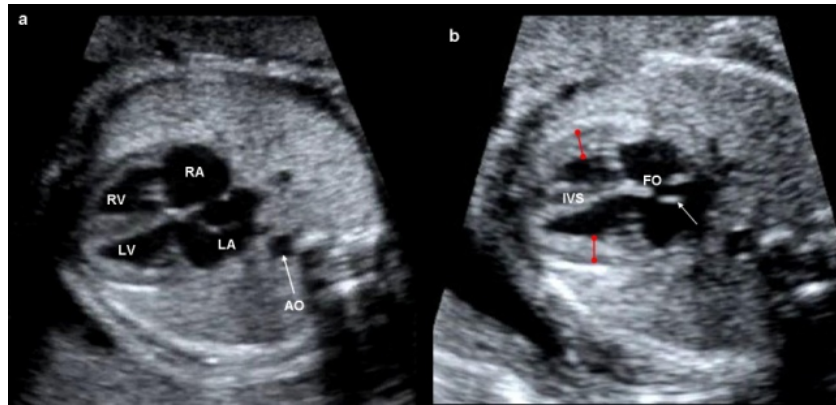


**Figure 4:** Transverse four chambers view: the apex of the heart is at the left of the fetal thorax. a) the interventricular septum and the walls of the ventricles are better visualized than in the apical view. b) the thickness of the ventricular walls (red lines) and septum (IVS) can be studied. The valve of the foramen ovale (arrow) moves toward the left atrium. LA: left atrium; LV: left ventricle; RV: right ventricle; RA: right atrium; FO: foramen ovale.

b) transverse section of the fetal thorax: transverse section of the descending aorta (AO) and apical four chamber view of the heart. LA: left atrium; LV: left ventricle; RV: right ventricle; RA:right atrium

Hence, the visualization of the four chamber view allows the detection of the wide range of CHD that directly or indirectly modify the above mentioned anatomical structures (see Table 2).

The first reports on the diagnostic accuracy of the four chamber view showed very encouraging results, with sensitivities ranging from 70 to 90%, thus promoting its wide diffusion [31-34]. However, several subsequent studies provided sensitivity values lower than 30% [35-37].

Many factors account for the discrepancies in the detection rate of the four chamber view, including:

- the experience of the operator
- the CHD prevalence in the study population, which can be high-risk, low-risk or unselected
- the operative definition of CHD, which can include or exclude minor defects that are more difficult to diagnose
- the gestational age at the time of the ultrasound, which influences both the possibility to obtain images of adequate quality and to detect progressive defects
- the study design, prospective or retrospective
- the duration and the accuracy of the neonatal follow-up.

Indeed, the first and more promising results came from studies that were performed in referral centres, on high-risk or unselected populations, and by highly specialized operators [31, 32], while the more disappointing results were from multicentric studies, on low-risk populations, and thus better reflect the efficacy on the field of the screening intervention [35, 36].

## THE OUTFLOW TRACTS VIEWS

The main limitation of the four chamber view lies in the impossibility to detect anomalies affecting the ventricle-arterial connections, unless they indirectly alter the morphology of the cardiac chambers or the cardiac axis (see Table 2). Importantly, this group of CHD includes conditions, such as transposition of the great arteries, which require early neonatal intervention, and therefore would receive the greatest advantage from accurate prenatal diagnosis. Therefore several investigators suggested to add to the four-chamber view the visualisation of the left ventricular outflow tract (five chamber view) [38, 39], or the visualisation of both outflow tracts [40-43].



The outflow tracts can be evaluated both by the left ventricle and right ventricle “long axis” views and by the “short axis” view [44] (see Figures 5–7)

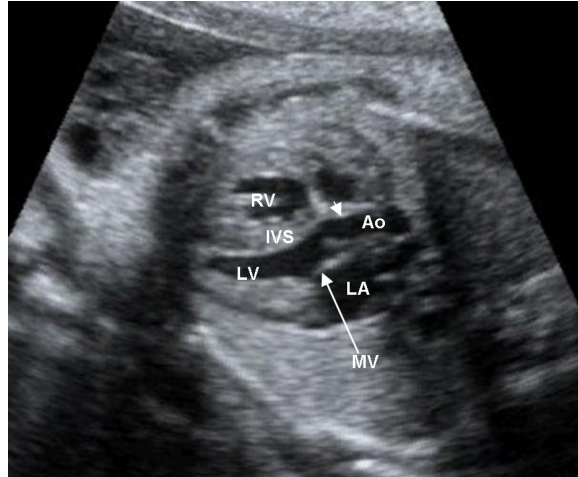


**Figure 5:** left ventricle long axis view: note the continuity of the aorta anterior wall (arrowhead) with the interventricular septum (IVS) and the continuity of the aorta posterior wall with the anterior leaflet of the mitral valve (MV) (arrow). LA: left atrium. LV: left ventricle; Ao: aorta. RV: right ventricle.

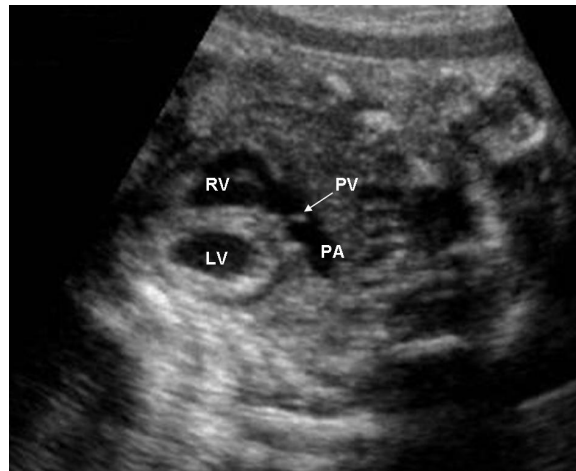


**Figure 6:** right ventricle long axis view: the pulmonary artery (PA) originates from the infundibular portion of the right ventricle (RV). PV: pulmonary valve; LV: left ventricle

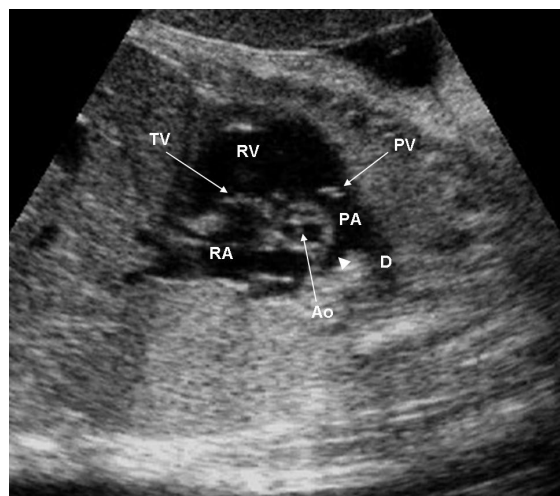


**Figure 7** Longitudinal section of the fetal thorax. Short axis view of the great vessels: the aorta (Ao) is in the centre, in transverse section, while the pulmonary artery is visualized in a longitudinal plane, arising from the right ventricle (RV) and in continuity

with the ductus arteriosus (D). The right pulmonary artery is also displayed (arrowhead). RA: right atrium; TV: tricuspid valve; PA: pulmonary artery; PV: pulmonary valve.

The long axis views allow visualizing the aorta and the pulmonary artery, with approximately equal diameters, emerging from left and right ventricle respectively, and crossing at about a 70° angle just above their origin. The aorta originates from the more posterior ventricle; its anterior wall is in continuity with the ventricular septum, while its posterior wall is in continuity with the anterior leaflet of the mitral valve. The pulmonary artery originates from the more anterior ventricle, and bifurcates into the right pulmonary artery and the ductus arteriosus.

Other authors suggested to include the “three vessels and trachea” view into the screening exam of the fetal heart (see Fig. 8).

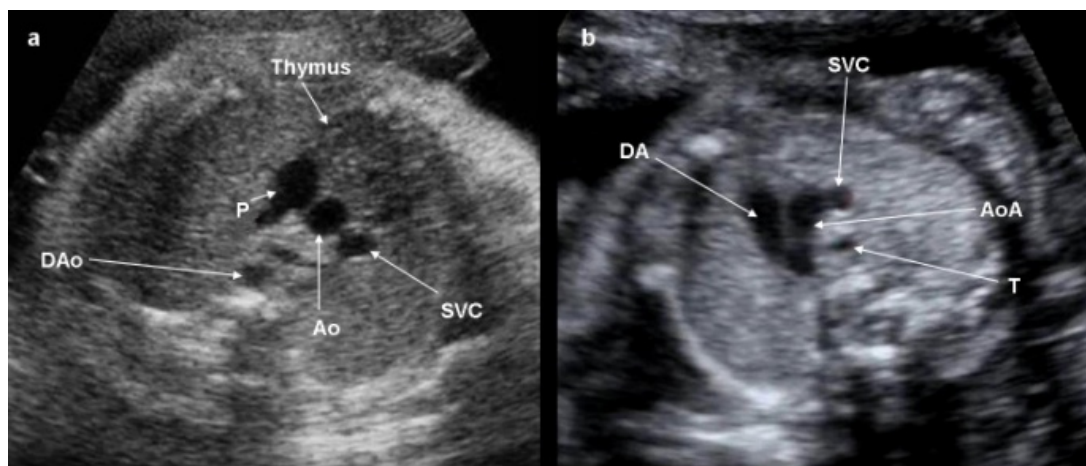


**Figure 8:** the three vessels can be seen with transverse sections of the fetal thorax above the heart. a) from left to right: pulmonary artery (P), aorta (Ao), superior vena cava (SVC). Note the thymus between the three vessels and the anterior wall of the thorax. b) Moving cranially from the three vessels view, making a slight caudal tilt of the ultrasound beam to the left, allows the aortic arch (AoA) and duct (DA) to be imaged simultaneously.

#### **DAo: Descending Aorta; T: Trachea**

This latter is a transverse thorax plane, which permits to verify the presence, position and size of the pulmonary artery, the ascending aorta and the superior vena cava [45], and is considered equally informative with regards to the anatomy of the great vessels compared with the outflow tracts, but more easy to obtain. Several studies have shown that the routine visualization of the outflow tracts – the “extended- basic” cardiac scan [22] – actually increases the sensitivity of the four chamber view. Although once again the highest detection rates come from studies conducted in referral centres and on the high-risk population [19, 45]. nonetheless even multicentric studies on the low-risk population could demonstrate a significant benefit compared with the four chamber view alone [46, 47].

**Table 2:** CHD and prenatal diagnosis

---

#### **CHD usually associated with abnormal four-chamber view**

---

- 1) *Heart abnormalities with a direct effect on the anatomy of the cardiac chambers*
  - Hypoplastic left heart syndrome
  - Hypoplastic right heart syndrome
  - Atrioventricular septal defects
  - Large ventricular septal defects
  - Atrio-ventricular valve abnormalities
  - Ebstein’s anomaly
  - Double inlet ventricle
- 2) *Abnormalities of the great vessels with an indirect effect on the symmetry of the cardiac chambers*
  - Severe aortic coarctation
  - Severe aortic stenosis
  - Severe pulmonary stenosis or pulmonary atresia with intact interventricular septum

---

3) *Abnormalities of the situs*

4) *Myocardial hypertrophy*

5) *Cardiac tumors*

6) *Pericardial effusions*

---

**CHD usually not associated with abnormal four-chamber view**

---

1) *Abnormalities of the great vessels without any effect on cardiac chamber anatomy*

Tetralogy of Fallot

Transposition of the great arteries

Double outlet ventricle

Truncus arteriosus

Mild aortic stenosis

Mild pulmonary stenosis

Pulmonary atresia with ventricular septal defect

---

**Most frequent CHD with a progressive evolution possibly not detectable during the second trimester scan**

---

Pulmonary stenosis

Aortic coarctation

Ventricular hypoplasia

---

**CHD not detectable in utero**

---

Isolated atrial septal defect

Small ventricular septal defects

Patent foramen ovale

Patent ductus arteriosus

---

## EARLY SCREENING

The fetal heart is completely formed 56 days after conception (10 weeks of postconceptional age, i.e. 8 weeks of gestational age). As a result of the rapid advances in the resolution power of ultrasound machines, a growing number of reports have gathered since the early 90's, showing the feasibility of examination of the fetal heart early in gestation [48-54].

The advantages of a reliable early test are intuitive: in high risk pregnancies, the confirmation of normal cardiac anatomy would reduce maternal anxiety, while the early recognition of a severe CHD would allow the termination of pregnancy in safer conditions, and would provide a longer temporal window for karyotyping, multidisciplinary counselling, the couple's decision-making, and the planning of the pregnancy's and neonatal care. However, although the feasibility of the echocardiographic study at 12-13 weeks of gestational age, by specialized operators and in high-risk pregnancies, is well demonstrated, there is no solid evidence to-date to support the advantage of the anticipation of the cardiac fetal screening in the low-risk population [55].

## THE ROLE OF NUCHAL TRANSLUCENCY IN PRENATAL SCREENING OF CHD

The measurement of nuchal translucency (NT) between 11 and 14 weeks of gestational age is a widely diffuse screening test for chromosomal anomalies. In addition, an association between increased NT and CHD, in the absence of chromosomal defects, has been demonstrated, suggesting a potential role for NT as an early screening test for CHD [56-68]. Several studies designed to assess the accuracy of this screening approach have reported very heterogenic results, partly due to the differences in the prospective or retrospective study design, and the extent of the postnatal follow-up (see [69] for review). However, the most recent studies tend to evidence quite a low detection rate: the adoption of a cut-off of 2.5 multiple of the median (MoM), approximately corresponding to the 99<sup>th</sup> percentile for gestational age, allows the identification of 7% of all the CHD and 13.5% of major CHD, with 1% of the population undergoing echocardiography [70]. These data, which are definitely disappointing, compared with the midtrimester "extended basic" scan, do not justify the adoption of NT as a screening test for the general population. However, the finding of increased NT ( $\geq 2.5$  MoM) during the aneuploidies screening test, should be considered as an indication for fetal echocardiography.

## IMPORTANCE OF TRAINING

There is solid evidence that the sensitivity of the prenatal screening of CHD is strongly dependent not only on the number of sonographic views, but also on the operator's experience. The systematic adoption of a training program for the visualization of the four chamber view and the outflow tracts view in Northern England, has increased the proportion of severe CHD that were diagnosed *in utero* from 17 to 30% [71]. A recent Norwegian study [72] measured the accuracy of second trimester ultrasound performed by sonographers and midwives in diagnosing CHD in an unselected population: they found that more experienced operators (who had carried more than 2000 routine scans) were more likely to obtain both four chamber view and outflow tracts view than less experienced operators (75% vs 36% of cases); as expected, this difference was associated with a significantly better detection rate of major heart defects (52% vs. 32.5%).

## ROLE OF 3D ULTRASOUND IN THE PRENATAL SCREENING OF CHD

The prenatal screening for CHD is a promising field of application for 3D ultrasound, which still needs to be adequately explored. Indeed, many of the peculiar characteristics of 3D sonography make it an ideal tool for the screening setting. The possibility to reconstruct offline virtually any different plane from a single acquired volume, makes this technology more efficient, reducing the time needed per each single exam; the advantage in term of time saved (which implies the possibility to examine a greater number of subjects) appears to be significant even after considering the additional time needed for the offline manipulation and interpretation of volumes [73-77].

A precious feature of 3D ultrasound is the feasibility to reconstruct offline planes that were not acquired during the patient examination, therefore making the sonogram less operator-dependent [73,74,75] (see Fig 9).

A further advantage of the use of 3D ultrasound as a screening tool, is the opportunity to send the acquired volumes to a referral centre for evaluation in the case of a suspicion of malformation, without any need to move the patient.

The other face of the coin, however, is the new set of skills that have to be acquired by the operator, in order to obtain good informative volumes, minimize artifacts, and interpret the reconstructed planes [58].

On the basis of these considerations, several studies have been conducted to demonstrate the feasibility of the mid-trimester anatomic screening survey, demonstrating a good degree of agreement between the 3D and the 2D sonographic examination [74, 75, 77].

The application of these concepts to the screening of CHD is partly limited by the peculiarity of the motion of this organ, which clearly increases the risk of artifacts. Moreover, the evaluation of cardiac function and rhythm relies on the assessment of real-time scans. However, the possibility to study the moving heart (but not to evaluate the heart rhythm) has been overcome, to a certain extent, by the introduction of the spatio-temporal correlation image technique (STIC).

One claimed benefit of 3D technology is that the acquisition of a single volume dataset allows the visualization of other planes that might be technically more difficult to obtain. When considering the standard exam of the fetal heart, the acquisition of a cardiac volume from the chamber view, can therefore allow the visualization of the more challenging outflow tracts views[78]. Paladini *et al* [79] have recently addressed this issue by assessing the diagnostic accuracy in the evaluation of the outflow tracts using STIC volumes acquired from the four-chamber view. In this study, a group of 14 sonologists of low-to-intermediate experience in basic cardiac scanning, were given a short training in the evaluation of the outflow tracts and volume manipulation; immediately after, they were asked to examine offline 26 volumes, acquired from the four chamber view between 19 and 23 weeks of gestational age, including 16 normal cases and 10 with conotruncal anomalies. Overall sensitivity was 83%, specificity 87% positive predictive value 80% and negative predictive value 89%; the sensitivity per each single anomaly ranged from 50% for transposition of great arteries with intact ventricular septum, to 100% for double outlet right ventricle with or without pulmonary atresia, and transposition of great arteries with ventricular septal defect. However, the study was not designed to evaluate the ability of the sonologists to acquire volumes of adequate quality, and to recognize and discard those of poor quality. Maybe more importantly, the high prevalence of CHD in the study population (38%) prevents the application of these results to the general population.

In summary, three-dimensional ultrasonography possess many characteristics to become a useful tool for the screening of CHD (as well as other malformations). However, before it can be adopted in the general practice, protocols, indications, and terminology should be further standardized and accepted. Moreover, a learning curve should be anticipated, and education and training should be systematically provided to allow the operators to achieve the new skills.

## REFERENCES

- [1] Ainsworth S, Wyllie JP, Wren C. Prevalence and clinical significance of cardiac murmurs in neonates. *Arch Dis Child Fetal Neonatal Ed* 1999; 80: F43-45
- [2] Young ID, Clarke M. Lethal malformations and perinatal mortality: a 10 year review with comparison of ethnic differences. *Br Med* 1987; 11;295: 89-91
- [3] Lee K, Khoshnood B, Chen L, Wall SN, Cromie WJ, Mittendorf RL. Infant mortality from congenital malformations in the United States, 1970-1997. *Obstet Gynecol* 2001; 98: 620-627
- [4] Neilson JP. Ultrasound for fetal assessment in early pregnancy. *The Cochrane Library*. Volume (4), 2005
- [5] Kohl T, Sharland G, Allan LD, Gembruch U, Chaoui R, Lopes LM, Zielinsky P, Huhta J, Silverman NH. World experience of percutaneous ultrasound-guided balloon valvuloplasty in human fetuses with severe aortic valve obstruction. *Am J Cardiol* 2000; 85: 1230-1233
- [6] Kobayashi T, Momoi N, Fukuda Y, Suzuki H. Percutaneous balloon valvuloplasty of both pulmonary and aortic valves in a neonate with pulmonary atresia and critical aortic stenosis. *Pediatr Cardiol* 2005; 26: 839-42
- [7] Vida VL, Bacha EA, Larrazabal A, Gauvreau K, Thiagaragan R, Fynn-Thompson F, Pigula FA, Mayer JE Jr, del Nido PJ, Tworetzky W, Lock JE, Marshall AC. Hypoplastic left heart syndrome with intact or highly restrictive atrial septum: surgical experience from a single center. *Ann Thorac Surg* 2007; 84: 581-5
- [8] Quintero RA, Huhta J, Suh E, Chmait R, Romero R, Angel J. *In-utero* cardiac fetal surgery: laser atrial septotomy in the treatment of hypoplastic left heart syndrome with intact atrial septum. *Am J Obstet Gynecol* 2005; **193**: 1424-1428
- [9] Marshall AC, van der Velde ME, Tworetzky W, Gomez CA, Wilkins-Haug L, Benson CB, Jennings RW, Lock JE. Creation of an atrial septal defect in utero for fetuses with hypoplastic left heart syndrome and intact or highly restrictive atrial septum. *Circulation* 2004; 110: 253-258
- [10] Sarno AP Junior, Wilson RD. Fetal cardiocentesis: a review of indications, risks, applications and technique. *Fetal Diagn Ther* 2008; 23: 237-44
- [11] McAuliffe FM, Hornberger LK, Johnson J, Chitayat D, Ryan G. Cardiac diverticulum with pericardial effusion: report of two new cases treated by *in-utero* pericardiocentesis and a review of the literature. *Ultrasound Obstet Gynecol* 2005; 25: 401-404
- [12] Prefumo F, Bhide A, Thilaganathan B, Carvalho JS. Fetal congenital cardiac diverticulum with pericardial effusion: two cases with different presentations in the first trimester of pregnancy. *Ultrasound Obstet Gynecol* 2005; 25: 405-408.
- [13] Johnson J-AM, Ryan G, Toy A, Smallhorn J. Prenatal diagnosis of a diverticulum associated with pericardial effusion: successful outcome following pericardiocentesis. *Prenat Diagn* 1996; 16: 954-957
- [14] Bader R, Hornberger LK, Nijmeh LJ, Al-Kazaleh F, Ryan G, Toi A, Viero S, Butany J, Chitayat D. Fetal pericardial teratoma: presentation of two cases and review of the literature. *Am J Perinatol* 2006; 23: 53-58
- [15] Benatar A, Vaughan J, Nicolini U, Trotter S, Corrin B, Lincoln C. Prenatal pericardiocentesis: its role in the management of intrapericardial teratoma. *Obstet Gynecol* 1992; 79: 856-859
- [16] Pavlovic M, Acharya G, Huhta JC. Controversies of fetal cardiac intervention. *Early Hum Dev* 2008; 84:149-53
- [17] Gardiner HM. In-utero intervention for congenital heart disease. *Best Pract Res Clin Obstet Gynaecol* 2008; 22: 49-61
- [18] Mellander M. Perinatal management, counselling and outcome of fetuses with congenital heart disease. *Semin Fetal Neonatal Med* 2005; 10: 586-593
- [19] Achiron R, Glaser J, Gelernter I, Hegesh J, Yagel S. Extended fetal echocardiographic examination for detecting cardiac malformations in low risk pregnancies. *BMJ* 1992; 304 (3828): 671-674
- [20] Robinson JN, Simpson LL, Abuhamad AZ. Screening for fetal heart disease with ultrasound. *Clin Obstet Gynecol* 2003; 46 (4): 890-896
- [21] Smythe JF, Copel JA, Kleinman CS. Outcome of prenatally detected cardiac malformations. *Am J Cardiol* 1992; 69: 1471-1474
- [22] Perri T, Cohen-Sacher B, Hod M, Berant M, Meizner I, Bar J. Risk factors for cardiac malformations detected by fetal echocardiography in a tertiary center. *J Matern Fetal Neonatal Med*. 2005;17: 123-128
- [23] The International Society of Ultrasound in Obstetrics and Gynecology. Cardiac screening examination of the fetus: guidelines for performing the 'basic' and 'extended basic' cardiac scan. *Ultrasound Obstet Gynecol* 2006; 27: 107-113.
- [24] Bull C. Current and potential impact of fetal diagnosis on prevalence and spectrum of serious congenital heart disease at term in the UK. *Lancet* 1999; 354: 1242-1247

- [25] Sullivan ID. Prenatal diagnosis of structural heart disease: does it make a difference to survival? *Arch Dis Child Fetal Neonatal Ed.* 2002;87F:19-20
- [26] Chiappa E. The impact of prenatal diagnosis of congenital heart disease on pediatric cardiology and cardiac surgery. *J Cardiovasc Med* 2007; 8:12-16
- [27] Franklin O, Burch M, Manning N, Sleeman K, Gould S, Archer N. Prenatal diagnosis of coarctation of the aorta improves survival and reduces morbidity. *Heart.* 2002; 87: 67-69
- [28] Bonnet D, Coltri A, Butera G, Fermont L, Le Bidois J, Kachaner J, Sidi D. Detection of transposition of the great arteries in fetuses reduces neonatal morbidity and mortality. *Circulation* 1999; 99 (7): 916-918
- [29] Tworetzky W, McElhinney DB, Reddy VM, Brook MM, Hanley FL, Silverman NH. Improved surgical outcome after fetal diagnosis of hypoplastic left heart syndrome. *Circulation.* 2001; 103: 1269-1273
- [30] Mahle WT, Clancy RR, McGaurn SP, Goin JE, Clark BJ. Impact of prenatal diagnosis on survival and early neurologic morbidity in neonates with the hypoplastic left heart syndrome. *Pediatrics* 2001; 107: 1277-1282
- [31] Allan LD, Crawford DC, Chita Sk, et al. Prenatal screening for congenital heart disease. *BMJ* 1986; 292:1717-1719
- [32] Copel JA, Pilu G, Green J, Hobbins JC, Kleinman CS. Fetal echocardiographic screening for congenital heart disease: the importance of the four-chamber view. *Am J Obstet Gynecol* 1987; 157: 648-655
- [33] Sharland GK, Allan LD. Screening for congenital heart disease prenatally. Results of a 2 1/2-year study in the South East Thames Region. *Br J Obstet Gynaecol* 1992; 99: 220-225
- [34] Luck CA. Value of routine ultrasound scanning at 19 weeks: a four year study of 8849 deliveries. *BMJ* 1992; 304: 1474-1478
- [35] Tegnander E, Eik-Nes SH, Johansen OJ, Linker DT. Prenatal detection of heart defects at the routine fetal examination at 18 weeks in a non-selected population. *Ultrasound Obstet Gynecol* 1995; 5: 372-380
- [36] Buskens E, Grobbee DE, Frohn-Mulder IM, Stewart PA, Juttman RE, Wladimiroff JW, Hess J. Efficacy of routine fetal ultrasound screening for congenital heart disease in normal pregnancy. *Circulation* 1996; 94: 67-72
- [37] Todros T, Faggiano F, Chiappa E, Gaglioti P, Mitola B, Sciarrone A, and the Gruppo Piemontese for Prenatal Screening of Congenital Heart Disease. Accuracy of routine ultrasonography in screening heart disease prenatally. *Prenat Diagn* 1997; 17: 901-906
- [38] Kirk JS, Riggs TW, Comstock CH, Lee W, Yang SS, Weinhouse E. Prenatal screening for cardiac anomalies: the value of routine addition of the aortic root to the four chamber view. *Obstet Gynecol* 1994, 84: 427-431
- [39] Comstock CH. What to expect from routine midtrimester screening for congenital heart disease. *Semin Perinatol* 2000; 24: 331-342
- [40] DeVore GR. The aortic and pulmonary outflow tract screening in the human fetus. *J Ultrasound Med* 1992, 11: 345-348
- [41] Bromley B, Estroff JA, Sanders SP, Parad R, Roberts D, Frigoletto FD Jr, Benacerraf BR. Fetal echocardiography: accuracy and limitations in a population at high and low risk for heart defects. *Am J Obstet Gynecol* 1992; 166:1473-1481
- [42] Kirk JS, Comstock CH, Lee W, Smith RS, Riggs TW, Weinhouse E. Sonographic screening to detect fetal cardiac anomalies: a 5-year experience with 111 abnormal cases. *Obstet Gynecol* 1997; 89(2): 227-232
- [43] Stoll C, Dott B, Alembick Y, De Geeter B. Evaluation and evolution during time of prenatal diagnosis of congenital heart diseases by routine fetal ultrasonographic examination. *Ann Genet* 2002; 45: 21-27
- [44] Naderi S, McGahan P. A primer for fetal cardiac imaging. A stepwise approach for 2-dimensional imaging. *Ultrasound Quarterly* 2008; 24: 195-206
- [45] Yagel S, Arbel R, Anteby EY, Raveh D, Achiron R. The three vessels and trachea view (3VT) in fetal cardiac scanning. *Ultrasound Obstet Gynecol* 2002; 20: 340-345
- [46] Oggè G, Gaglioti P, Maccanti S, Faggiano F, Todros T. Prenatal screening for congenital heart disease with four-chamber and outflow-tract views: a multicenter study. *Ultrasound Obstet Gynecol* 2006; 28: 779-784
- [47] Tegnander E, Williams W, Johansen OJ, Blaas HG, Eik-Nes SH. Prenatal detection of heart defects in a non-selected population of 30,149 fetuses--detection rates and outcome. *Ultrasound Obstet Gynecol* 2006; 27: 252-265
- [48] Gembruch U, Knöpfle G, Chatterjee M, Bald R, Hansmann M. First-trimester diagnosis of fetal congenital heart disease by transvaginal two-dimensional and Doppler echocardiography. *Obstet Gynecol* 1990;75: 496-498
- [49] Bronshtein M, Zimmer EZ, Milo S, Ho SY, Lorber A, Gerlis LM. Fetal cardiac abnormalities detected by transvaginal sonography at 12-16 weeks' gestation. *Obstet Gynecol.* 1991; 78: 374-378
- [50] Gembruch U, Knöpfle G, Bald R, Hansmann M. Early diagnosis of fetal congenital heart disease by transvaginal echocardiography. *Ultrasound Obstet Gynecol.* 1993;3: 310-317
- [51] Bronshtein M, Zimmer EZ, Gerlis LM, Lorber A, Drugan A. Early ultrasound diagnosis of fetal congenital heart defects in high-risk and low-risk pregnancies. *Obstet Gynecol.* 1993; 82: 225-229
- [52] Achiron R, Rotstein Z, Lipitz S, Mashiach S, Hegesh J. First-trimester diagnosis of fetal congenital heart disease by transvaginal ultrasonography. *Obstet Gynecol.* 1994; 84: 69-72
- [53] Achiron R, Weissman A, Rotstein Z, Lipitz S, Mashiach S, Hegesh J. Transvaginal echocardiographic examination of the fetal heart between 13 and 15 weeks' gestation in a low-risk population. *J Ultrasound Med* 1994;13: 783-789

- [54] Yagel S, Cohen SM, Messing B. First and early second trimester fetal heart screening. *Curr Opin Obstet Gynecol* 2007; 19: 183-190
- [55] Rustico MA, Benettoni A, D'Ottavio G, Fischer-Tamaro L, Conoscenti GC, Meir Y, Natale R, Bussani R, Mandruzzato GP. Early screening for fetal cardiac anomalies by transvaginal echocardiography in an unselected population: the role of operator experience. *Ultrasound Obstet Gynecol*. 2000;16: 614-619
- [56] Hyett J, Moscoso G, Papapanagiotou G, Perdu M, Nicolaides KH. Abnormalities of the heart and great arteries in chromosomally normal fetuses with increased nuchal translucency thickness at 11-13 weeks of gestation. *Ultrasound Obstet Gynecol* 1996; 4: 245-250
- [57] Bilardo CM, Pajkrt E, de Graaf I, Mol BW, Bleker OP. Outcome of fetuses with enlarged nuchal translucency and normal karyotype. *Ultrasound Obstet Gynecol* 1998; 11: 401-406
- [58] Hafner E, Schuchter K, Liebhart E, Philipp K. Results of routine fetal nuchal translucency measurements at weeks 10-13 in 4233 unselected pregnant women. *Prenat Diagn* 1998; 18: 29-34
- [59] Souka AP, Snijders RJ, Novakov A, Soares W, Nicolaides KH. Defects and syndromes in chromosomally normal fetuses with increased nuchal translucency thickness at 10-14 weeks of gestation. *Ultrasound Obstet Gynecol* 1998; 11: 391-400
- [60] Souka AP, Krampfl E, Bakalis S, Heath V, Nicolaides KH. Outcome of pregnancy in chromosomally normal fetuses with increased nuchal translucency in the first trimester. *Ultrasound Obstet Gynecol* 2001; 18: 9-17
- [61] Souka AP, Von Kaisenberg CS, Hyett JA, Sonek JD, Nicolaides KH. Increased nuchal translucency with normal karyotype. *Am J Obstet Gynecol* 2005; 192: 1005-1021
- [62] Ghi T, Huggon IC, Zosmer N, Nicolaides KH. Incidence of major structural cardiac defects associated with increased nuchal translucency but normal karyotype. *Ultrasound Obstet Gynecol* 2001; 18: 610-614
- [63] Michailidis GD, Economides DL. Nuchal translucency measurement and pregnancy outcome in karyotypically normal fetuses. *Ultrasound Obstet Gynecol* 2001; 17: 102-105
- [64] Orvos H, Wayda K, Kozinszky Z, Katona M, Pál A, Szabó J. Increased nuchal translucency and congenital heart defects in euploid fetuses. The Szeged experience. *Eur J Obstet Gynecol Reprod Biol* 2002; 101: 124-128
- [65] Makrydimas G, Sotiriadis A, Ioannidis JP. Screening performance of first-trimester nuchal translucency for major cardiac defects: a meta-analysis. *Am J Obstet Gynecol* 2003; 189: 1330-1335
- [66] Makrydimas G, Sotiriadis A, Huggon IC, Simpson J, Sharland G, Carvalho JS, Daubeney PE, Ioannidis JP. Nuchal translucency and fetal cardiac defects: a pooled analysis of major fetal echocardiography centers. *Am J Obstet Gynecol* 2005; 192: 89-95
- [67] Westin M, Saltvedt S, Bergman G, Almström H, Grunewald C, Valentin L. Is measurement of nuchal translucency thickness a useful screening tool for heart defects? A study of 16,383 fetuses. *Ultrasound Obstet Gynecol* 2006; 27: 632-9
- [68] Westin M, Saltvedt S, Almström H, Grunewald C, Valentin L. By how much does increased nuchal translucency increase the risk of adverse pregnancy outcome in chromosomally normal fetuses? A study of 16,260 fetuses derived from an unselected pregnant population. *Ultrasound Obstet Gynecol* 2007; 29: 150-158
- [69] Clur SA, Otenkamp J, Bilardo CM. The nuchal translucency and the fetal heart: a literature review. *Prenat Diagn*. 2009 Apr 27. [Epub ahead of print]
- [70] Simpson LL, Malone FD, Bianchi DW, Ball RH, Nyberg DA, Comstock CH, Saade G, Eddleman K, Gross SJ, Dugoff L, Craigo SD, Timor-Tritsch IE, Carr SR, Wolfe HM, Tripp T, D'Alton ME, for the First and Second Trimester Evaluation of Risk (FASTER) Research Consortium. Nuchal translucency and the risk of congenital heart disease. *Obstet Gynecol* 2007; 109: 376-383
- [71] Hunter S, Heads A, Wyllie J, Robson S. Prenatal diagnosis of congenital heart disease in the northern region of England: benefits of a training programme for obstetric ultrasonographers. *Heart* 2000; 84: 294-298
- [72] Tegnander E, Eik-Nes SH. The examiner's ultrasound experience has a significant impact on the detection rate of congenital heart defects at the second-trimester fetal examination. *Ultrasound Obstet Gynecol* 2006; 28: 8-14
- [73] Benacerraf BR, Benson CB, Abuhamad AZ, Copel JA, Abramowicz JS, DeVore GR, Doubilet PM, Lee W, Lev-Toaff A, Merz E, Nelson TR, O'Neill MJ, Parsons AK, Platt LD, Pretorius DH, Timor-Tritsch E. Three- and 4- dimensional ultrasound in obstetrics and gynecology. Proceedings of the American Institute of Ultrasound in Medicine Consensus Conference. *J Ultrasound Med* 2005; 24:1587-1597
- [74] Benacerraf BR, Shipp TD, Bromley B. How sonographic tomography will change the face of obstetric sonography. A pilot study. *J Ultrasound Med* 2005; 24: 371-378
- [75] Benacerraf BR, Shipp TD, Bromley B. Three-dimensional US of the fetus: volume imaging. *Radiology* 2006; 238 (3): 988-996
- [76] Benacerraf BR. Tomographic sonography of the fetus. Is it accurate enough to be a frontline screen for fetal malformation? *J Ultrasound Med* 2006; 25: 687-689
- [77] Gonçalves LF, Nien JK, Espinoza J, Kusanovic JP, Lee W, Swope B, Soto E, Treadwell MC, Romero R. What does 2-dimensional imaging add to 3- and 4-dimensional obstetric ultrasonography? *J Ultrasound Med*. 2006 Jun; 25: 691-699

- [78] Gonçalves LF, Espinoza J, Romero R, Lee W, Treadwell MC, Huang R, Devore G, Chaiworapongsa T, Schoen ML, Beyer B. Four-dimensional fetal echocardiography with spatiotemporal image correlation (STIC): a systematic study of standard cardiac views assessed by different observers. *J Matern Fetal Neonatal Med.* 2005;17: 323-331
- [79] Paladini D, Sglavo G, Greco E, Nappi C. Cardiac screening by STIC: can sonologist performing the 20-week anomaly scan pick up outflow tract abnormalities by scrolling the A-plane of STIC volumes? *Ultrasound Obstet Gynecol* 2008; 32: 865-870



## The Examination of the Normal Fetal Heart

Alessandra Toscano, Luciano Pasquini\* and Roberta Iacobelli

*Department of Pediatric Cardiology and Cardiac Surgery, Bambino Gesù' Hospital, Rome, Italy*

**Abstract:** The heart, anatomically and embryologically, is a segmented structure. The atria, the ventricles and the great arteries are the three major fundamental components. The heart should be examined echocardiographically by Sequential Segmental Analysis from the venous to the arterial poles following the blood flow. Each segment is evaluated independently considering not only the segmental situs (or location into the body) but also the connections of each heart segment to the others. A systematic approach by Sequential Segmental Analysis is a cornerstone of fetal cardiac study. First step is the identification of fetal heart position followed by the identification of position of the heart in relation to the body and the anatomic study of each cardiac chamber, and finally, the study of cardiac rhythms and function. The heart can be observed in infinity of planes, but few sections are the basis of fetal cardiac study. The examination starts with abdominal cross-sectional view for the identification of the viscero-atrial situs. Then the transthoracic four-chamber view should be obtained. This view allows to obtain a large amount of information specially regarding the atria and ventricles, atrioventricular valves, interatrial and interventricular septum. Ventriculo-arterial connections are well identified by a gentle sweep towards the fetal neck, left ventricular outflow tract and ascending aorta are first visualized and, by further sweeping, also right ventricular outflow tract, branch pulmonary arteries and ductus arteriosus are correctly identified. The three vessel view give us information regarding left or right location of aortic arch. Short axis of the heart is evaluated from the cavo-atrial and ventricular segments to the ductal and aortic arches. Finally the study of heart rate and rhythm and of myocardial function ends the fetal heart examination.

**Key Words:** Fetal Heart, Ultrasound, Diagnostic Planes, Segmental Analysis

### FETAL CARDIAC ANATOMY

The heart should be examined ultrasonographically by sequential segmental analysis starting from the venous and finishing at the arterial poles [1]. It is helpful to consider the heart as a segmented structure represented by three regions: atria, ventricles, and great arteries [2]. The two connecting cardiac segments are the atrioventricular canal or junction and the infundibulum or conus arteriosus. Each region, in turn, is partitioned into two components, usually right-sided and left-sided. There are only a limited number of possible connections between the three major regions, regardless of their spatial orientations. In practice, each region is evaluated independently, following the direction of blood flow: systemic and pulmonary veins, atria, atrioventricular valves, ventricles and right ventricular outflow tract, semilunar valves, and great arteries. In a systematic manner, right-sided and left-sided structures at each level are evaluated according to their morphology, their positions and connections to segments. The diagnostic problem generated by congenital heart disease is that the morphologically or anatomically right atrium, left atrium, right ventricle, and left ventricle can from the positional standpoint be “anywhere”. Morphologic anatomic identification is the cornerstone of accurate diagnosis. It starts with the identification of readily recognizable landmarks and progresses to more subtle findings. The step-by-step approach that we use includes: the identification of the fetal position, the position of the heart in relation to the body, the number of chambers and their connections, and finally, the rhythm.

### POSITION OF THE FETUS IN THE UTERUS

Correct prenatal determination of the fetal right/left axis is essential for the diagnosis of fetal malformations, in particular congenital heart anomalies. To assess the cardiac position in the uterus, observe the fetal position: is it cephalic or breech? Then identify the position of the spine and of the cardiac apex ([Clip 1](#)).

### LOCATION IN THE CHEST

With regard to the position of the heart in the chest, two questions arise that can be answered: where is the heart

\*Address correspondence to Luciano Pasquini: Department of Pediatric Cardiology and Cardiac Surgery, Bambino Gesù' Hospital, Piazza S. Onofrio, 4 - 00165 Rome Italy; Email: pasquini@opbg.net

located, and what is the direction of the cardiac apex? Within the thorax, the heart can be described as left-sided (normal), right-sided, or in a midline position. The position of the heart in the mediastinum is affected not only by underlying cardiac malformations but also by abnormalities in adjacent structures. Some hearts are abnormally displaced from their usual position in the anterior left central chest. This abnormal cardiac position can be caused by a diaphragmatic hernia or space-occupying lesion, such as cystic adenomatoid malformation. Position abnormalities can also be secondary to fetal lung hypoplasia or agenesis. Rightward displacement of the heart constitutes dextroposition, a leftward shift represents levoposition, and shifts toward the midline are called mesoposition.

## **ORIENTATION IN THE CHEST**

The left-right orientation of the abdominal organs and of the heart in vertebrate is a non random and highly conserved phenomenon [3], probably controlled by several genes [4,5,6,7]. Levocardia is the normal state and is characterized by a ventricular apex that is directed leftward, anteriorly and somewhat inferiorly. In Dextrocardia, the apex is directed to the right of midline [8-11]. Mesocardia is the location of the heart with the cardiac base-apex axis directed to the midline of the thorax [12].

## **THE ATRIA**

There are two main type of visceratrial situs (situs meaning location). Situs solitus, the normal pattern of anatomic organization in which the right atrium is right -sided and the left atrium is left-sided,. In situs inversus is present an inverted or mirror image pattern where the right atrium is left- sided and the left atrium is right- sided. Situs “ambiguus” indicates that the type of visceratrial situs is anatomically uncertain or indeterminated, and it occurs in the heterotaxy syndrome with asplenia or polysplenia [13-15].

## **THE VENTRICLES**

There are two types of ventricular situs: D-loop ventricles, in which the morphologically right ventricle is typically right-sided, and the morphologically left ventricle is left-sided. L-loop ventricles, that is, inverted or mirror image ventricles in which the right ventricle is typically left-sided and left ventricle is right-sided [16].

## **THE GREAT ARTERIES**

Solitus Normally Related (the usual normal), Inverted Normally Related (mirror image), Malposition of the Aorta (anterior to the pulmonary artery): D (anterior and right), L (anterior and left), A (just anterior) [17].

## **FETAL ECHOCARDIOGRAPHIC PROJECTIONS**

The heart can be observed in infinity of planes, but few sections are the basis on which most of the diagnoses are made [18]. The basic cardiac screening examination relies on at least five transverse images of the heart and vasculature and three sagittal images [19,20].

## **ABDOMINAL CROSS-SECTIONAL VIEW**

The stomach should be seen on the left side of the fetus and just below the heart and diaphragm. It is important to localize the spine and the transverse descending aorta, which is a circle laying anterior to the spine. Usually in a normal fetus the descending aorta is in the left side and points to the left atrium ([Clip 2](#)).

## **TRANSTHORACIC FOUR CHAMBER VIEW**

The four-chamber view is generally easy to achieve and is useful for identifying the atria, ventricles, and respective septae [21]. A normal heart is usually no larger than one-third the area of the chest ([Clip 3](#)). The majority of the heart is in left chest. The heart is normally deviated about  $45 \pm 20^\circ$  (2 standard deviations) toward the left side of the fetus (Fig. 1). Situs abnormalities should be suspected when the fetal heart and/or stomach is/are not found on the left side as well. The atria should have equal size and thickness. From the standard 4-chamber view, one should

sweep posteriorly to demonstrate the coronary sinus ([Clip 4](#)). The right atrium is anterior and the left posterior. The left atrium is related to the descending aorta posteriorly. The morphologic features of the atrial appendages are usually appreciable only when the atria are outlined by excessive pericardial fluid. The interatrial septum is open at the level of the *foramen ovale*. The *foramen ovale* flap is visible in the left atrium, beating toward the left side [22]. The *foramen ovale* occupies about one third of the atrial septum. The flap valve has a biphasic motion during the cardiac cycle, partially closing at end systole and during atrial contraction end diastole. In the right atrium, two thin lines distinct from the interatrial septum can occasionally be seen. The Eustachian valve, a crest between the inferior vena cava and the wall of the right atrium, is located close to the inferior vena cava. The Chiari network is composed of abnormal lacelike strands that attach to the Eustachian\_valve and the *crista terminalis*. It results from the incomplete reabsorption of the *septum spurium*, which should be completed by the 3rd month and persists in about 1% of patients. The confluence of the pulmonary venous connections to the back of the left atrium should be identified. Exception: anomalous venous return. In the four-chamber view the most anterior vein is the inferior pulmonary vein; the most posterior is the superior pulmonary vein. To confirm an apparently normal pulmonary venous connection to the left atrium, forward flow from the vein in the pulmonary parenchyma into the atrium should be documented on color flow mapping ([Clip 5](#)), and ideally adding pulsed wave doppler. The normal pulmonary venous pulsed Doppler tracing shows forward flow throughout systole and early diastole with occasionally reversal of flow in late diastole. The flow pattern reflects left atrial events, the “suction” effect of atrial relaxation, followed by descent of the mitral valve orifice, late systole, passive opening of the mitral valve, early diastole, and atrial contraction that may cause minimal flow reversal in late ventricular diastole.

In the second trimester, the ventricles should be approximately equal in size, however, it is important to note that in later gestation, the right ventricle becomes slightly larger than left and should not be confused with pathologic right ventricular dilation [23, 24]. The right ventricle is the most anterior structure and closest to the anterior chest wall. The insertion of the tricuspid valve along the interventricular septum is more apical than the insertion of the mitral valve. The right ventricular apex should contain the moderator band, causing the apex to appear “filled in” ([Clip 6](#)). In favorable cases one can note the difference in lining of the two ventricles: the right ventricle has a more coarse lining than the left due to a coarser trabeculation. The left side of the interventricular septum is free of papillary muscle while a papillary muscle, implants on the septum in the right ventricle (i.e. the muscle of the septal leaflet of the tricuspid valve). In the left ventricle there are two papillary muscles in the left ventricle, while in the right ventricle three papillary muscles are present. The valve follows the ventricle, thus a bicuspid valve is an indicator of left ventricle, while a tricuspid valve marks a right ventricle. In a normal fetus, there is no atrioventricular valve regurgitation.

Doppler echocardiography may prove to be useful as an adjunct to imaging echocardiography for evaluation of fetal cardiac anatomy and function.

Doppler velocity measurements were obtained by placing the Doppler sample volume immediately distal to the valve leaflets in the ventricle. Using pulsed Doppler, there is a typical biphasic shape of the diastolic flow velocity waveform with an early peak diastolic velocity (E) and a second peak during atrial contraction (A-wave); E is smaller than A, and the E : A ratio increases during pregnancy toward 1, to be inverted after birth. Fetal cardiac blood flow patterns differ from those in the neonate and the adult. Flow in the fetus results from simultaneous ejection from both right and left ventricles into the systemic circulation.

The diameters of the mitral and tricuspid valve annuli can be evaluated as well as the lengths of the left and right ventricles. Several reference limits for dimensional measures based on gestational age have been published [25, 26].

The ventricular septum should appear intact. The ventricular septum will appear thin and an area of dropout may be seen just below the atrioventricular valves when imaged from the apex ([Clip 7](#), Fig. 2). In an apical four-chamber view, caution should be taken not to confuse this artifact with a ventricular septal defect. Imaging from a lateral view perpendicular to the septum will better demonstrate its thickness and continuity. Small septal defects can be very difficult to confirm if the ultrasound imaging system fails to provide a sufficient degree of lateral resolution, especially if fetal size and position are unfavorable.

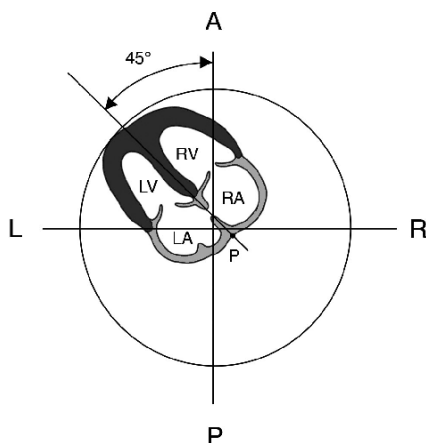


**Figure 1:** Fetal cardiac axis and position. LA, left atrium, LV, left ventricle, RA, right atrium, RV, right ventricle. The cardiac axis can be measured from a four-chamber view of the fetal heart.

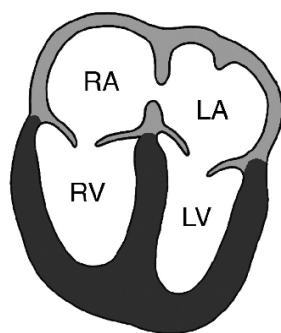


**Figure 2:** Four-Chamber view of the fetal heart. LA, left atrium, LV, left ventricle, RA, right atrium, RV, right ventricle.

### CARDIAC LONG-AXIS VIEW

The long-axis view is aligned with the left ventricular outflow tract ([Clip 8](#), [Fig. 3](#)). Evaluation of outflow tracts can increase the detection rates for major cardiac malformations above those achievable by the four-chamber view alone [27,28]. The four chamber view is inadequate for determining the conotruncus anomaly and in particular Transposition of the Great Arteries, Tetralogy of Fallot, Subaortic Ventricular Septal Defect, Double Outlet Right Ventricle, and Truncus Arteriosus. From the four-chamber view a slight cranial angulation of the transducer should reveal the left ventricular outflow tract the aortic valve and proximal ascending aorta, (also called the five-chamber view) ([Clip 9](#)). The left ventricular outflow tract view confirms the presence of a great vessel originating from the left ventricle. The continuity between the mitral and aortic valves and the absence of sub-aortic conus should be noted. The size of the ascending aorta can be measured. The anterior leaflet is in continuity with the posterior wall of the aorta. The anterior wall of the aorta is in continuity with the interventricular septum. The aortic valve and ascending aorta are seen arising centrally from the four-chamber view with the ascending aorta directed toward the right shoulder. The aortic valve moves freely and should not be thickened. For the arterial Doppler studies, the transducer must be positioned so that the sample volume is placed parallel to the flow. With pulsed Doppler, a single peak flow velocity waveform for the aortic valve should be demonstrated. The peak systolic velocity increases from 50 to 110 cm/s during the second half of pregnancy and it is higher across the aortic than the pulmonary valve. Time to peak velocity in the aorta is longer than in the pulmonary trunk. The ventricular output can be calculated by using the product of the valve area and mean velocity of flow, When the left ventricular outflow tract is truly the aorta, it should even be possible to trace the vessel into its arch, from which three arteries originate into the neck. The ventricular septum should appear intact from the apex to crux and from the apex to the anterior wall of the aorta.

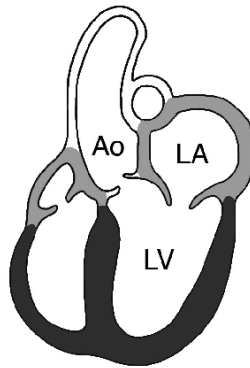


**Figure 3:** Left ventricular outflow tract. LA, left atrium, LV, left ventricle, Ao, ascending aorta.

#### **FOUR-CHAMBER SWEEP TO THE RIGHT VENTRICULAR OUTFLOW TRACT VIEW**

Continuing the sweep toward the fetal neck, a view of the right ventricular outflow tract documents the presence of a great vessel starting from a morphologic right ventricle. The pulmonary artery normally arises from the right ventricle and courses toward the left of the more posterior ascending aorta ([Clip 10](#), Fig. 4).

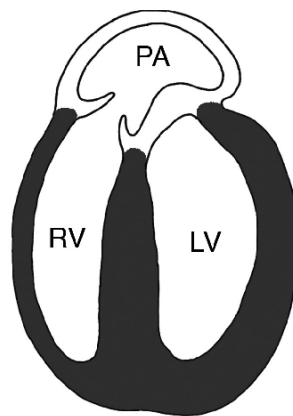


**Figure 4:** Right ventricular outflow tract. LV, left ventricle, RV, right ventricle. PA, pulmonary artery.

The bifurcation of the pulmonary artery and ductus arteriosus completes this view. The right ventricular outflow tract can be confirmed as a pulmonary artery only if its distal end appears bifurcated. The distal pulmonary artery normally divides toward the left side into a ductus arteriosus that continues into the descending aorta. The right side branch into the right pulmonary artery. The great arteries are similar in size, but the pulmonary artery at the valve ring may be slightly bigger than the aorta. The pulmonary valve is anterior and cranial to the aortic valve. The great arteries cross over at their origin.

#### **THE THREE-VESSEL VIEW**

Demonstrates the long axis views of the tranverse aortic arch and ductus arteriosus and the short axis views of the superior vena cava and trachea ([Clip 11](#)) [29-33].

#### **THE SHORT AXIS VIEW / THE RIGHT HEART VIEWS**

This section demonstrates the right ventricle and the ventricular outflow tract. The main pulmonary artery originates from the anterior ventricle and trifurcates into a large vessel, the ductus going into the descending aorta, and two small vessels, the pulmonary arteries. The pulmonary valve is anterior and cranial to the aortic valve. This is the best section to demonstrate the pulmonary valve ([Clip 12](#), Fig. 5).

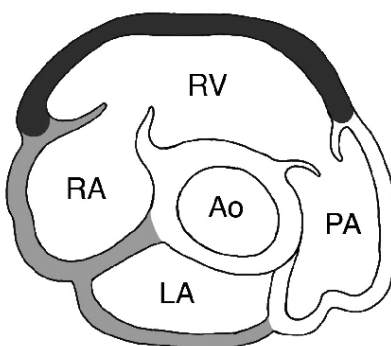


**Figure 5:** Short-axis view. LA, left atrium, RA, right atrium, RV, right ventricle, PA, pulmonary artery, Ao, aorta.

### DUCTAL AND AORTIC ARCH VIEW

In a normal fetus, the aortic arch can be evaluated in both transverse and longitudinal views. The transverse view is more useful because the distal arch can be followed to its connection to the duct, and the two vessels can be directly compared in size, they should be equal in diameter. The longitudinal view shows the tight “hook” shape of the normal arch ([Clip 13](#), Fig. 6) [34-36]. The aortic arch is obtained with the beam aligned from anterior right of the fetal chest to posterior left of the fetal chest. The side of the aortic arch can be readily shown in fetal life, using the orizzontal view of the arch. The ductal view is obtained when the imaging plane is aligned with the right ventricular outflow tract and main pulmonary artery. In the ductal view, the main pulmonary artery, and ductal arch are well seen and main pulmonary artery size can be easily measured. The ductal arch is formed by the communication of the ductus arteriosus with the descending aorta, appears more flattened than the aortic arch and will have no head and neck vessels arising from it. Note laminar flow, direction, and velocity with color flow and spectral (pulsed wave) Doppler. Normal ductal velocities in 20- to 39-week fetuses range from 50 to 140 cm/sec in peak systole and 6 to 30 cm/sec in peak diastole. Premature ductal constriction is distinguished by either an increase in peak systolic and end diastolic velocities or absolute absence of flow in case of premature closure. Severe constriction leads to progressive right ventricular pressure overload, hydrops, and fetal death. Retrograde flow in the ductus arteriosus should prompt investigation for an right ventricular outflow tract obstruction.

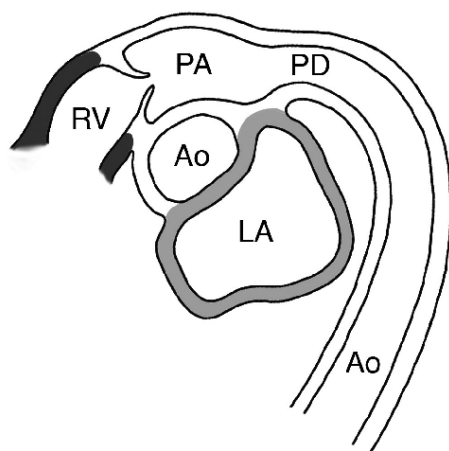


**Figure 6:** Ductal view and aortic arch view. RV, right ventricle, PA, pulmonary artery, PD, ductus arteriosus, Ao, aortic arch, LA, left atrium.

### CAVAL LONG-AXIS VIEW

The caval long-axis view is obtained with the imaging plane parallel to the caval connections to the right atrium. The superior vena cava and the inferior vena cava drain from a posterior position to a medial connection to the right atrium ([Clip 14](#), Fig. 7).

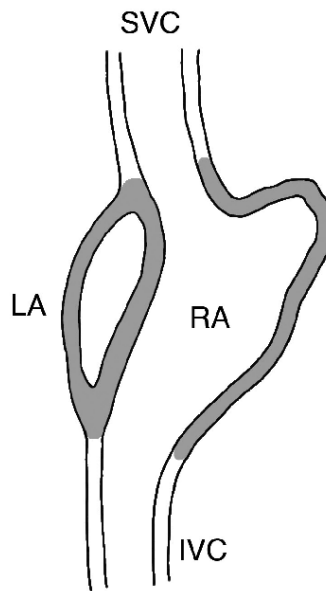


**Figure 7:** Caval long-axis view. LA, left atrium, SVC, superior vena cava, IVC, inferior vena cava, RA, right atrium.

## MYOCARDIAL FUNCTION

An assessment of fetal cardiac function can be made using traditional M mode to provide information on wall thickness and ventricular shortening fraction. An m-mode set of measurements can be made with the beam set perpendicular to the lower half of the interventricular septum [37,38]. The function can be measured as a shortening fraction  $> 30\%$  (diastole-systole/diastole). Diastolic function is impaired when a fetal and a fully developed myocardium are compared, indicating that fetal myocardium is less compliant. Observations on the diastolic function of the human fetal myocardium are made by Doppler echocardiographic blood flow velocity profiles. In the human fetus, peak blood flow velocity is greater during active filling (atrial contraction) than during the rapid filling phase, because of the atriosystolic function. This finding indicates diminished ventricular compliance in the fetal heart [39]. The fetus has a limited range of heart rates over which cardiac outputs can be maintained. Prolonged extreme bradycardia (heart rate less than 50 beats/min) or tachycardia (heart rate higher than 200) is known to cause congestive heart failure and hydrops. Some investigators have stated that alterations in heart rate are the major determinants of cardiac output. The relationship between cardiac cycle length and stroke volume indicates that the major regulator of cardiac output in the human fetus is the Frank-Starling mechanism.

## HEART RATE

Cardiac rate and regular rhythm should be confirmed. Fetal cardiac activity is detectable from 6 weeks on by suprapubic ultrasound and about one week earlier by transvaginal ultrasound. The normal fetal heart rate varies with gestational age. It is around 100 beats per minute (bpm) at 8 weeks, reaches 175 bpm by 10 weeks, 150 at 15 weeks and slows further to about  $140 \pm 20$  bpm at 20 weeks and  $130 \pm 20$  bpm at term. Mild bradycardia is transiently observed in normal second-trimester fetuses. Fixed bradycardia, especially heart rates that remain below 110 beats per minute, requires timely evaluation for possible heart block. Mild tachycardia ( $>160$  beats per minute) can occur as a normal variant during fetal movement. Persistent tachycardia, however, should be further evaluated for possible fetal distress or more serious tachydysrhythmias [40,41].

## REFERENCES

- [1] Van Praagh R. The segmental approach to diagnosis in congenital heart disease. The cardiovascular system. Birth Defect : Original article Series 1972; 8: 4-23.
- [2] Van Praagh R, Weinberg PM, Matsuoka R, Van Praagh S: Malposition of the heart. In : Adams FH, Emmanouilides GC (eds) : Moss'Heart Disease in Infants, Children and Adolescents, 3rd ed. Baltimore, Williams e Wilkins. 1983; pp. 422-458.
- [3] Brown Na, Wolpert J: The development of handedness in left/right asymmetry. Development 1990; 109: 1.

- [4] Casey B, Devoto M, Jones KL, Ballabio A. Mapping a gene for familial situs abnormalities to human chromosome Xq2 q27.1. *Nat Genet* 1993; 5: 403–7.
- [5] Ferrero GB, Gebbia M, Pilia G *et al.* A submicroscopic deletion in Xq26 associated with familial situs ambiguus. *Am J Hum Genet* 1997; 61: 395–401
- [6] Ware SM, Peng J, Zhu L *et al.* Identification and functional analysis of ZIC3 mutations in heterotaxy and related congenital heart defects. *Am J Hum Genet* 2004; 74: 93–105.
- [7] Casey B, Devoto M, Jones KL, Ballabio A: Mapping a gene for familiar situs abnormalities to human chromosome Xq24-q27.1 *Nature* 1993; 5: 403.
- [8] Van Praagh R, Van Praagh S, Vlad P, Keith JD: Anatomic types of congenital Dextrocardia. Diagnostic and Embryologic implications. *Am J Cardiol* 1964; 13: 510-31.
- [9] Comstock CH: “Normal fetal heart axis and position.” *Obstet Gynecol* 1987; 70:255-9.
- [10] Shipp TD, Bromley BB, Hornberger LK, Nadel A, Benacerraf BR. Levorotation of the fetal cardiac axis: a clue for the presence of congenital heart disease. *Obstet Gynecol* 1995, 85: 97-102.
- [11] Smith RS, Comstock CH, Kirk JS, Lee W. Ultrasonographic left cardiac axis deviation: a marker for fetal anomalies. *Obstet Gynecol* 1995; 85: 187-91.
- [12] Lev M, Liberthson RR, Golden JG, Eckner FA, Arcilla RA. The pathologic anatomy of mesocardia. *Am J Cardiol* 1971; 28 : 428-35.
- [13] Macartney FJ, Zuberbuhler JR, Anderson RH. Morphological considerations pertaining to recognition of atrial isomerism. Consequences for sequential chamber localisation. *Br Heart J* 1980; 44: 657.
- [14] Lin JH, Chang CI, Wang JK *et al.* Intrauterine diagnosis of heterotaxy syndrome. *Am Heart J* 2002; 143: 1002–8.
- [15] De Araujo LML, Silverman NH, Filly RA, Golbu MS, Finkbeiner WE, Schmidt KG. Prenatal detection of left atrial isomerism by ultrasound. *J Ultrasound Med* 1987; 6: 667-70.
- [16] Pasquini L, Sanders SP, Parness I, *et al.* Echocardiographic and anatomic findings in atrioventricular discordance with ventriculoarterial concordance. *Am J Cardiol* 1988 1;62(17):1256-62.
- [17] Pasquini L, Sanders SP, Parness IA, Colan SD, Van Praagh S, Mayer JE Jr *et al.* Conal anatomy in 119 patients with d-loop transposition of the great arteries and ventricular septal defect: an echocardiographic and pathologic study. *J Am Coll Cardiol* 1993; 21(7): 1712-21.
- [18] Rychik J, Ayres N, Cuneo B, *et al.* American Society of Echocardiography guidelines and standards for performance of the fetal echocardiogram. *J Am Soc Echocardiogr* 2004; 17: 803–10.
- [19] Wood D, Respondek-Liberska M, Puerto B, Weiner S Perinatal echocardiography: protocols for evaluating the fetal and neonatal heart. World Association of Perinatal Medicine Ultrasonography Working Group. *J Perinat Med.* 2009; 37(1): 5-11.
- [20] Cardiac screening examination of the fetus: guidelines for performing the 'basic' and 'extended basic' cardiac scan. *Ultrasound Obstet Gynecol.* 2006; 27(1): 107-13.
- [21] Copel JA, Pihu G, Green J, Hobbins JC, Kleinman CS. Fetal echocardiographic screening for congenital heart disease: the importance of the four-chamber view. *Am J Obstet Gynecol* 1987; 157: 648–55.
- [22] Berning RA, Silverman NH, Villegas M, Sahn DJ, Martin GR, Rice MJ. Reversed shunting across the ductus arteriosus or atrial septum in utero heralds severe congenital heart disease. *J Am Coll Cardiol* 1996; 27: 481-6.
- [23] Sharland GK, Chan KY, Allan LD. Coarctation of the aorta: difficulties in prenatal diagnosis. *Br Heart J* 1994; 71: 70–5.
- [24] Kirk JS, Comstock CH, Lee W, Smith RS, Riggs TW, Weinhouse E. Fetal cardiac asymmetry: a marker for congenital heart disease. *Obstet Gynecol* 1999; 93: 189–92
- [25] Sharland GK, Allan LD. Normal fetal cardiac measurements derived by cross-sectional echocardiography. *Ultrasound Obstet Gynecol* 1992; 2: 175-81.
- [26] Tan J, Silverman NH, Hoffman JIE, Villegas M, Schmidt KG. Cardiac dimensions determined by cross-sectional echocardiography in the normal human fetus from 18 weeks to term. *Am J Cardiol* 1992; 70: 1459-67.
- [27] Wigton TR, Sabbagha RE, Tamura RK, Cohen L, Minogue JP, Strasburger JF. Sonographic diagnosis of congenital heart disease: comparison between the four-chamber view and multiple cardiac views. *Obstet Gynecol* 1993; 82: 219– 24.
- [28] Kirk JS, Riggs TW, Comstock CH, Lee W, Yang SS, Weinhouse E. Prenatal screening for cardiac anomalies: the value of routine addition of the aortic root to the four-chamber view. *Obstet Gynecol* 1994; 84: 427–31.
- [29] Yoo S-J, Lee Y-H, Cho KS. Abnormal three-vessel view on sonography: a clue to the diagnosis of congenital heart disease in the fetus. *AJR Am J Roentgenol* 1999; 172: 825– 30.
- [30] Kirk JS, Riggs TW, Comstock CH, Lee W, Yang SS, Weinhouse E. Prenatal screening for cardiac anomalies: the value of routine addition of the aortic root to the four-chamber view. *Obstet Gynecol* 1994; 84: 427–31.
- [31] DeVore G. The aortic and pulmonary outflow tract screening examination in the human fetus. *J Ultrasound Med* 1992; 11: 345–8.
- [32] Vinals F, Heredia F, Giuliano A. The role of the three vessels and trachea view (3VT) in the diagnosis of congenital heart defects. *Ultrasound Obstet Gynecol* 2003; 22: 358–67.



- [33] Yagel S, Arbel R, Anteby EY, Raveh D, Achiron R. The three vessels and trachea view (3VT) in fetal cardiac scanning. *Ultrasound Obstet Gynecol* 2002; 20: 340–5.
- [34] Allan LD, Tynan MJ, Campbell S, Wilkinson JL, Anderson RH. Echocardiographic and anatomical correlates in the fetus. *Br Heart J* 1980; 44: 444–51.
- [35] Nomiya M, Ueda Y, Toyota Y, Kawano H. Fetal aortic isthmus growth and morphology in late gestation. *Ultrasound Obstet Gynecol.* 2002; 19(2): 153-7.
- [36] Pasquini L, Mellander M, Seale A, et al. Z-scores of the fetal aortic isthmus and duct: an aid to assessing arch hypoplasia. *Ultrasound Obstet Gynecol.* 2007; 29: 628–33.
- [37] DeVore GR, Siassi B, Platt LD. Fetal Echocardiography. IV. M-mode assessment of ventricular size and contractility during the second and third trimesters of pregnancy in the normal fetus. *Am J Obstet Gynecol* 1984; 150: 981–8.
- [38] Simpson J. Echocardiographic evaluation of cardiac function in the fetus. *Prenatal Diagn* 2004; 24: 1081-91.
- [39] Reed KL, Sahn DJ, Scagnelli S, Anderson CF, Shenker L. Doppler echocardiographic studies of diastolic function in the human fetal heart: changes during gestation. *J Am Coll Cardiol* 1986b; 8: 391–5.
- [40] Kleinman C, Donnerstein R, Jaffe C, et al. Fetal echocardiography. A tool for evaluation of in utero cardiac arrhythmias and monitoring of in utero therapy. *Am J Cardiol* 1983; 51:237-43.
- [41] Copel JA, Liang RI, Demasio K, Ozeren S, Kleinman CS The clinical significance of the irregular fetal heart rhythm. *Am J Obstet Gynecol* 2000; 182: 813–17.

## Real Time Three Dimensional Fetal Echocardiography Using Two Dimensional Array Technology.

Dev Maulik\*, MD, PhD, David Mundy, MD and Timothy Bennett, MD

*Department of Obstetrics and Gynecology, University of Missouri-Kansas City School Medicine, Kansas City, Missouri, USA*

**Abstract:** Three dimensional (3D) echocardiography represents a major paradigm shift in medical ultrasound imaging. As opposed to reconstructed 3D echocardiography which is based on a series of two dimensional images, the revolutionary development of the two dimensional (2D) matrix phased array transducer permits true real time live 3D imaging of the fetal heart. Preliminary experience has demonstrated that real time/live 3D echocardiography is not only feasible in assessing the fetal cardiac anomalies, it also permits unique comprehensive views of the fetal heart that are unattainable with 2D echocardiography. With further evolution of the technology, and appropriate education and training RT3D echocardiography may evolve as a powerful supplement to conventional 2D echocardiography.

**Key Words:** Real time three dimensional, Fetal echocardiography, Live 3D, Two dimensional matrix transducer.

### INTRODUCTION

Congenital heart disease (CHD) continues to be a significant contributor to adverse perinatal outcomes and its prenatal recognition significantly improves the perinatal outcome [1]. Prenatal diagnosis of CHD has been possible only because of the advances in fetal echocardiography over the last three decades (Table 1). Recent advances in three dimensional (3D) ultrasound imaging represent one of the most important technological innovations in this field. Even in 2D echocardiography, the operator conceptually recreates the spatial 3D reality of the fetal heart out of the 2D sonographic images. Although the current approach continues to function well, the advantages of 3D imaging are potentially significant revealing anatomical and functional complexities of the heart.

Currently there are two approaches to 3D sonography: (a) real time 3D (RT3D) echocardiography which generates and displays 3D images in real time, and (b) reconstructed 3D echocardiography which displays 3D images synthesized from sequential 2D images [2]. Real time 3D echocardiography is also known as live 3D echocardiography. The term four dimensional echocardiography is used to denote 3D images in motion, time being the fourth dimension. However, this may not distinguish between real time and reconstructed images. The technology of real time 3D echocardiography is still evolving and this review critically appraises this emerging technology in relation to fetal applications. The use of real time 3D in adult cardiac imaging [3] and in fetal cardiac assessment have been reported [4].

**Table 1:** Developmental History of Fetal Echocardiography

Echo Mode	First Author	Journal
M-mode	Winsberg	Invest Radiol, 1972
2D Echo	Allan et al	Br Heart J, 1980
	Kleinman et al	Pediatrics, 1980
Duplex M-mode	DeVore et al	Am J Ob Gyn, 1980
Duplex PW Doppler	Maulik et al	Am J Cardiol, 1982
Color Flow Doppler	Maulik et al	Am J Cardiol, 1985(Ab)
		Angiology, 1986

\*Address correspondence to Dev Maulik MD: Department of Obstetrics and Gynecology, University of Missouri Kansas City School Medicine, 2411 Holmes Street Kansas City, MO 64108-2792 USA Email: umkc\_som\_journal@umkc.edu

## DEVELOPMENT OF THREE DIMENSIONAL ECHOCARDIOGRAPHY

The innovation of 3D medical imaging can be traced to computed tomography (CT) and magnetic resonance imaging (MRI) technologies and essentially where the 2D tomographic image slices generated by these modalities are digitally reconstructed to produce 3D images. These developments have revolutionized medical imaging and diagnostics. However, even with the continuing advances in technology, CT and MRI are not useful for diagnostic imaging of the fetal heart.

Over the past decades, pioneering investigators utilized various experimental approaches involving offline reconstruction of 2D images [5-7]. The mode of image acquisition required locating the position of the transducer so that images could be collated in 3D spatial orientation. The method of tracking the transducer location included mechanical acoustic and magnetic devices. One of the most frequently utilized techniques in adult echocardiography employed a rotational transesophageal transducer with reconstruction of the 3D images with on or offline computers. However, these 3D methods could not perform in real time because of technological limitations.

Similar technical solutions evolved for creating of 3D echocardiographic images in the fetus [8, 9]. These approaches were based on postimaging reconstruction of fetal cardiac anatomy out of stored scanned volume data acquired by automatic or freehand techniques. These techniques produced fetal cardiac images that were not amenable to any useful interpretation because of the image quality and a lack of coherence between cardiac anatomical imaging and cardiac activity. These limitations, however, were substantially rectified through the innovation of gating techniques such as spatio-temporal image correlation (STIC) combined with a motorized rotating transducer head [10]. The method was innovated in Kretztechnik of Austria which is now a subsidiary of GE Healthcare. This approach is currently available in various ultrasound devices and is used to produce surface rendered images of the fetus (Figure ). There are numerous reports on fetal echocardiography using reconstructed approach with STIC. However, this approach does not offer true real time 3D cardiac imaging and has several limitations including high susceptibility to motion artifacts.

Two dimensional phased array technology for true RT3D ultrasound imaging was developed at the Duke University by von Ramm and associates [11]. Apparently the idea was first conceived for potential use as a sonar camera for underwater search and rescue. Because of its diagnostic potentials, the concept led to the development of medical imaging transducers with 2D array of numerous piezoelectric elements. and sparse phased array technology. In this array system, only a limited set of the elements of the array are used for transmission and reception of echoes. The image resolution of the sparse array technology was not adequate and the device as produced commercially (Volumetrics Ultrasound, North Carolina, USA) was not widely used. The next significant advances occurred in the Andover facility of the Agilent Technologies Healthcare Solutions Group, now a part of the Philips Medical System (Andover, Massachusetts, US) leading to the development of second generation two dimensional phased array technology. More recently, Siemens has also developed its own brand of real time 3D imaging technology. However, this is not available for fetal application at the time of writing this review.

The developmental milestones of 3D echocardiography of the fetus are summarized in Table 2.

**Table 2:** Developmental History of Three Dimensional Fetal Echocardiography

Echo Mode	First Author	Journal
3D Fetal Echo – 2D image integration	Sklansky et al	J Ultrasound Med, 1999
Reconstructed 3D Fetal Echo – STIC	DeVore et al	Ultrasound Ob Gyn, 2003
Real time 3D	Maulik et al	Echocardiography, 2003

## BASIC PRINCIPLES OF REAL TIME THREE DIMENSIONAL SONOGRAPHY

There are three fundamental steps of 3D sonography: (a) image acquisition, (b) image processing and (c) image display. These steps are sequential. Contemporaneous implementation of these processes during scanning constitutes RT3D ultrasound (Fig. 1).

## IMAGE ACQUISITION AND PROCESSING

### Two Dimensional Matrix Transducer

The 2D matrix transducer is a phased array device comprised of approximately two to three thousand piezoelectric elements distributed in a two dimensional matrix array. All the elements transmit and receive unlike the sparse array system. The system steers the acoustic beam both in the azimuth and elevation producing a 3D pyramidal volume image data set in real time. The enormous volume of data thus generated offer a formidable challenge for real time processing. However, this issue was resolved by organizing the elements in groups known as subarrays with each subarray having its own beamformer. The subarray beam forming provides front end processing of the ultrasound signals, reduces the enormous computing burden, and facilitates RT3D image generation and display. Multiple miniaturized computer processor boards embedded inside the transducer handle perform this task.

### Image Data Processing

The 3D image data are then transmitted to the ultrasound device's main computer system which handles simultaneously multiple streams of digital image data. Utilizing advanced data processing, the system generates a three dimensional pyramid shaped digital image data set (Fig. 1).

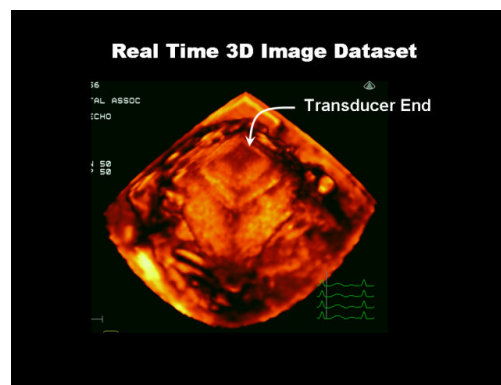


**Figure 1:** Real time 3D image data set is displayed. The upper end of the pyramid indicates the two dimensional transducer footprint (arrow).

No gating is needed for this acquisition. This is known as the live 3D volume acquisition. A wider pyramidal volume known as the full volume measuring can also be imaged by swift automatic real time acquisition and integration of subvolumes. Generation of the full volume, however, requires some form of cardiac gating. In the adult or pediatric patient this is provided by the electrocardiogram of the patient. Obviously this is not feasible in the fetus. We have successfully simulated cardiac gating with an external electronic pulse generator trigger enabling us to acquire full volume data set of the fetal heart without any recognizable artifacts. The gating function is now integrated in the device.

## THREE DIMENSIONAL IMAGE DISPLAY AND ANALYSES

The final critical component in 3D imaging is the analyses and display of the volume data set. This can be performed on the machine or offline using a proprietary software program (QLab, Philips Medical Systems) (Fig. 2).

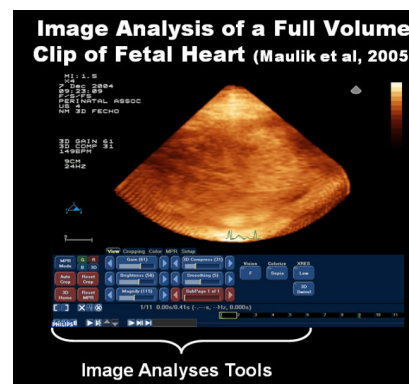


**Figure 2:** Real time 3D fetal echocardiography: A full volume 3D image data clip of the fetal heart and software image analysis tools are displayed in this illustration.

Three dimensional images can be displayed by (a) surface rendering with identification of various structures, or (b) volume rendering which creates a texture mapped block such as a pyramidal 3D object which can be rotated and cropped to reveal internal structures or flow (Fig. 3).

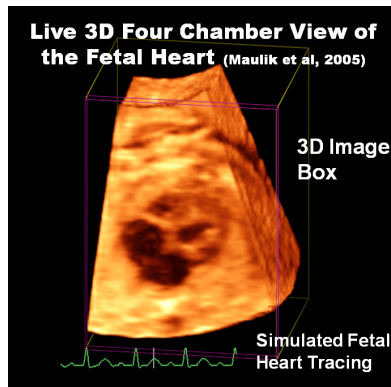


**Figure 3:** Live 3D echocardiogram showing a four chamber view of the fetal heart. Fine line box depicts 3D orientation of the image data. The electrocardiogram in the lower part of the figure is actually simulated fetal heart tracing.

In addition to the structural evaluation, assessment of several cardiac functional parameters such as the ventricular volume and the ejection fraction can be determined. The software also allows optimization of the image attributes such as brightness and contrast. Fetal applications of these echocardiographic techniques are further discussed below.

The 3D image processing and display require defining the spatial location of a point in 3D space from the image data. The unit of 3D spatial graphic information is known as a voxel. The term stands for volume pixel and constitutes the smallest definable unit of a 3D image. A voxel is the 3D counterpart of a pixel which defines location in a 2D plane. Geometrically, the relative spatial locations of a voxel are represented by the Cartesian coordinates  $x$ ,  $y$  and  $z$  (Fig. 4).

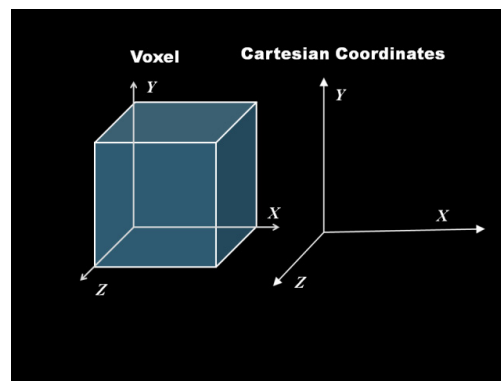


**Figure 4:** Graphic illustration of the concept of a voxel which forms the units of the 3D image data. X, Y and Z represents the orthogonal coordinates (Cartesian) for the 3D space.

The location is defined by the point's distances from three orthogonal planes determined by these coordinates. This is a fundamental concept for 3D image processing and interpretation. Each voxel can be digitally quantified to represent objective properties such as opacity, density, color, velocity, or even time.

## VOLUME RENDERED VIEWS

The volume rendered moving image clips are reanalyzed with the software. This includes cropping image volume along the Cartesian orthogonal co-ordinates, X, Y, Z (Fig. 5). Additional intracardiac anatomical views can be revealed by rotating the cropped 3D volume. Cropping can also be performed in variable inclined or oblique planes also known as adjustable planes.

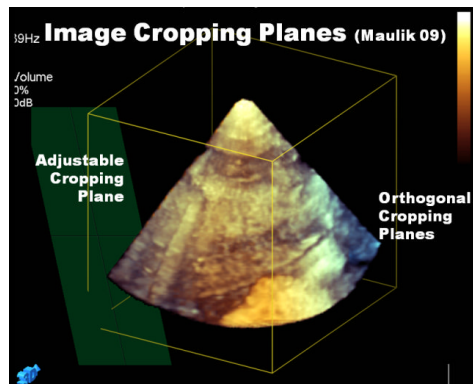


**Figure 5:** Real time 3D fetal echocardiography. Fetal cardiac 3D image volume data is shown with the orthogonal (line box around the volume) and adjustable (green panel) cropping planes.

This technique permits a systematic examination of the cardiac chambers, the atrioventricular connections, the mitral and tricuspid valves, the interventricular and interatrial septa, and the outflow tracts and their interrelationship (Fig. 6).

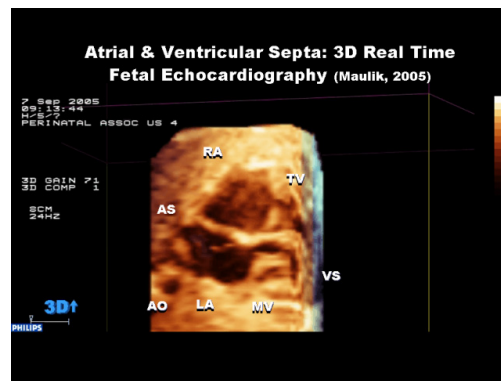


**Figure 6:** Real time 3D fetal echocardiogram showing cardiac structures following cropping in two orthogonal planes and rotating the image data set.

Moreover, it enables visualization of surface or “en face” views of intracardiac structures. Such anatomical views and details could be of great value for prenatal diagnosis and prognostication.

## TWO DIMENSIONAL VIEWS OF THREE DIMENSIONAL IMAGE DATA: MULTIPLANAR AND TOMOGRAPHIC VIEWS

Multipanar viewing using orthogonal and inclined planes can also be performed revealing display of 2D cardiac images in three separate planes simultaneously (Fig. 7).

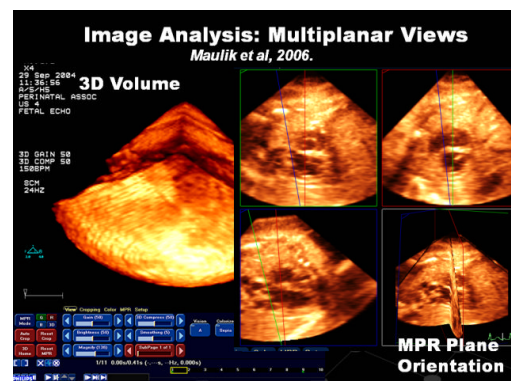


**Figure 7:** Real time 3D fetal echocardiography. The left panel shows the 3D image data volume and the software analytic tools. The right panel shows multiplanar views of the fetal heart. The lower right subpanel shows the image planes (MPR) of the other three 2D cardiac images.

Similarly, tomographic 2D image slices of the heart can be generated with control over the region of interest, the number of slices and the thickness of a slice (Fig. 8)

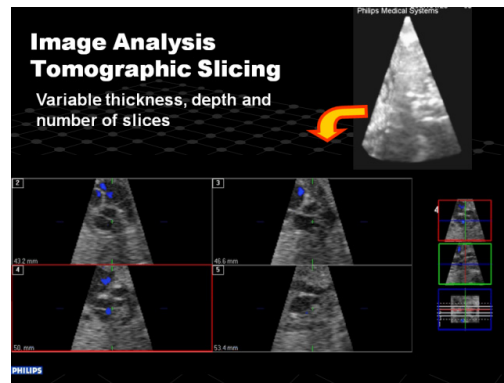


**Figure 8:** Real time 3D fetal echocardiogram showing the tomographic slicing of the 3D cardiac image volume (upper right panel). The lower most right panels show the orientation, thickness and number of image slices.

### THREE DIMENSIONAL REAL TIME COLOR DOPPLER ECHOCARDIOGRAPHY

Three dimensional color Doppler imaging of the intracardiac flow can be acquired with 2D matrix array technology (Fig. 9). However, the inherent limitations of Doppler sonography such as angle dependence are also applicable in these modalities.

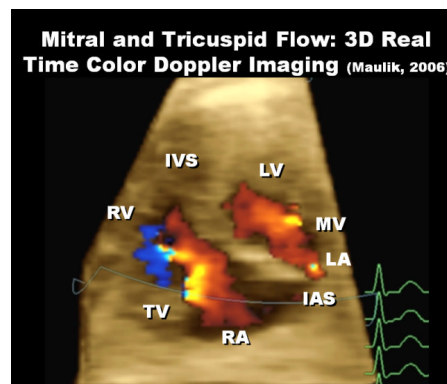


**Figure 9:** Real time 3D color Doppler fetal echocardiogram showing atrioventricular flow. LA = left atrium; LV = left ventricle; RA = right atrium; RV = right ventricle; MV = mitral valve; TV = tricuspid valve; IAS = interatrial septum; IVS = interventricular septum; S = ventricular septum

Three dimensional color Doppler flow depiction can be used to quantify abnormal flow conditions such as regurgitant jets and turbulent flow (Fig. 10). Potential also exists to quantify volumetric flow using this approach.

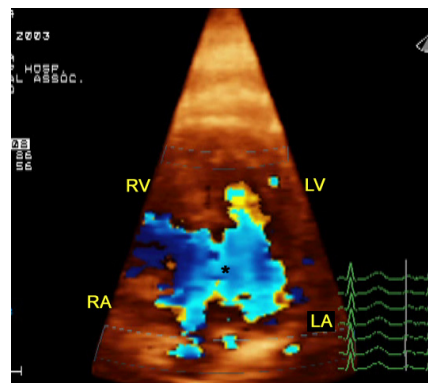


**Figure 10:** Live 3D echocardiography in 36 week old fetus with complete atrioventricular septal defect. Four chamber views cropped to show the abnormal atrioventricular hemodynamics. (Modified with permission from reference 4)

## FUNCTIONAL ASSESSMENT OF THE HEART

An additional innovative aspect of the image analytic software is the ability to perform dynamic cardiac quantification such as the ventricular volume through the cardiac cycle and the ejection fraction. The distinct advantage of RT3D approach over traditional echocardiography is that it is not subject to assumptions regarding the volume and the shape. The current RT3D technology allows fast creation of a full 3D wire-mesh endocardial volume that is sensitive to the annulus and apex motions. Detailed analysis of the left regional and global ventricular function can be performed using RT3D technology.

## FETAL APPLICATION OF RT3D ECHOCARDIOGRAPHY

The feasibility of using RT3D fetal echocardiography was demonstrated by Maulik and colleagues in 2003. The study demonstrated the unique capabilities of the technique in clarifying the complex structural and hemodynamic abnormalities of congenital heart defects of the fetus. Specifically, the en face views of cardiac lesions such as common atrio-ventricular valves or a ventricular septal defect provide anatomical perspectives beyond the scope of the existing two dimensional echocardiography technology (Figs. 11, 12 and 13) [4].

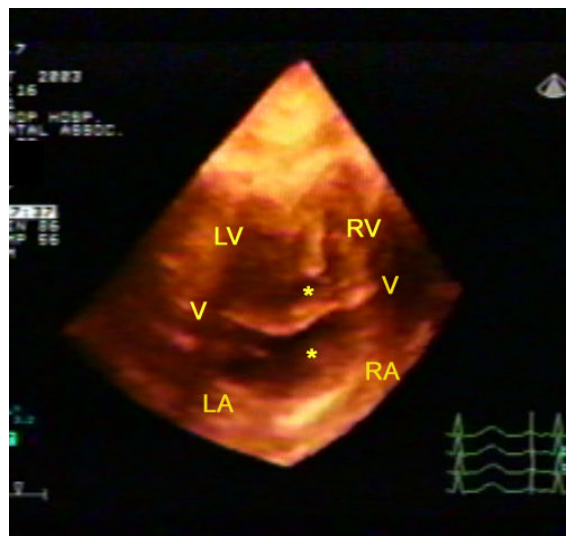


**Figure 11:** Live 3D echocardiography in 36 week old fetus with complete atrioventricular septal defect. Four chamber views cropped to show the common atrioventricular valve (v) and the defect (asterisk). (Modified with permission from reference 4)

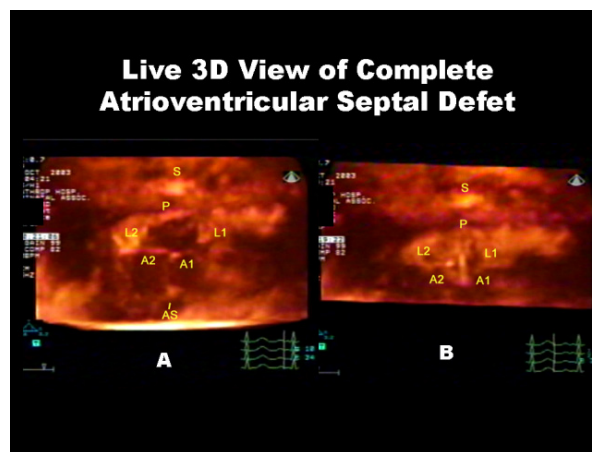


**Figure 12:** Live 3D echocardiography in 36 week old fetus with complete atrioventricular septal defect. The pyramidal section has been cropped from the top and rotated toward the examiner to display all five leaflets of the common atrioventricular valve (V); posterior (P), left lateral (L1), left anterior (A1), right anterior (A2), and right lateral (L2). Small portion of the ventricular septum (S) and atrial septum (AS) have been retained to show their relationship to V. V is open in A and closed in B (Modified with permission from reference 4)



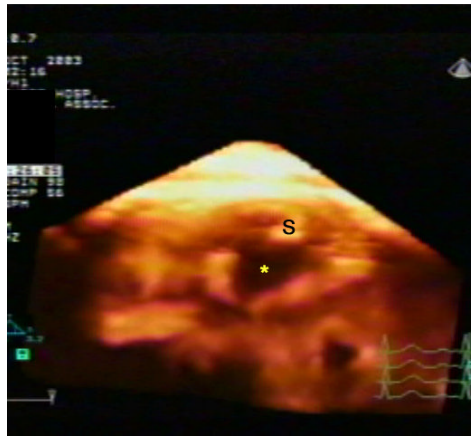


**Figure 13:** Live 3D echocardiography in 36 week old fetus with complete atrioventricular septal defect. En face viewing of the defect (asterisk) from the inferior aspect. (Modified with permission from reference 4)

Subsequent publications have further confirmed this [12]. Acar and colleagues used RT3D echocardiography using the matrix probe in 60 fetuses 16 of whom had congenital cardiac defects or myocardial dysfunction. The procedure was successful in 93%. The investigators found the technique helpful allowing a multiplanar and novel inside 3D views of the fetal heart. Chen and co-workers compared diagnostic efficacy of RT3D echocardiography with 2D echocardiography in 30 patients with complex defects. [13]. Receiver operating characteristic (ROC) analysis showed that when in predicting the surgical findings, RT3D echocardiography was correct in 75.6% and 2D echocardiography was correct in 64.4% of the cases.

#### CHALLENGES FOR REAL TIME 3D ECHOCARDIOGRAPHY OF THE FETUS

The major challenge for the current stage of the technology is the natural resistance to adopting apparently complex new technology. This is partly related to the fact the value of real time 3D echocardiography in prenatal diagnosis of complex cardiac defects remains underestimated. There are also technological issues related to fetal application of the technology. This technology is developed primarily for adult and pediatric cardiac diagnosis and therefore is not optimized for fetal application. Specifically the currently available 3 Mz adult transducer may not provide optimal resolution for prenatal diagnosis. The current 7 MHz pediatric transducer provides significantly improved image resolution but may not always provide enough depth penetration. The newer generation transducers with pure crystal technology may improve this situation.

The software tools for image analysis are highly sophisticated but may offer a steep learning curve for many. A recent study demonstrated the benefits of intensive education and training on the diagnostic efficacy. Jenkins and associates [14] investigated the impact of an intensive interactive training course on the efficacy of RT3D echocardiography in adult patients and found that training significantly improved the correct diagnosis rate of the new technique. However, there was no additional value of the technique over traditional 2D technology without such training although most participants had access to the RT3D method. This would be even more relevant for fetal application of the technology. Emergence of automation in image analysis may also significantly enhance its adoption for the main stream practice. Finally there is a great need for further research and education in this field.

#### REFERENCE

- [1] Tworetzky W, McElhinney DB, Reddy VM, Brook MM, Hanley FL, Silverman NH Improved surgical outcome after fetal diagnosis of hypoplastic left heart syndrome. *Circulation*. 2001;103:1269-73.
- [2] Maulik D. "Four Dimensional B Mode and Color Doppler Echocardiography of the Human Fetus." In Maulik, D (ed) *Principles and Practice of Doppler Sonography in Obstetrics and Gynecology*, 2nd Edition; Springer-Verlag, NY. 2005.
- [3] Singh V, Nanda NC, Agrawal G, Vengala S, Dod HS, Misra V, Narayan V. Live three-dimensional echocardiographic assessment of mitral stenosis. *Echocardiography*. 2003;20:743-50.
- [4] Maulik D, Nanda NC, Singh V, *et al* Live three-dimensional echocardiography of the human fetus. *Echocardiography*. 2003;20:715-21.
- [5] Dekker DL, Piziali RL and Dong E Jr. A system for ultrasonically imaging the human heart in three dimensions. *Computer Biomed Research*. 1974; 7:544-553.

- [6] Ghosh A, Nanda NC, Maurer G. Three-dimensional reconstruction of echo-cardiographic images using the rotation method. *Ultrasound Med Biol.* 1982;8:655-61.
- [7] Matsumoto M, Inoue M, Tamura S, Tanaka K, Abe H. Three-dimensional echocardiography for spatial visualization and volume calculation of cardiac structures. *J Clin Ultrasound.* 1981;9:157-65.
- [8] Sklansky MS, Nelson TR, Pretorius DH. Three-dimensional fetal echocardiography: gated versus nongated techniques. *J Ultrasound Med.* 1998;17:451-7.
- [9] Falkensammer P, Brandl H. *Ultrasound Technology Update: 4D fetal echocardiography; Spatio-temporal image correlation.* GE Medical Systems, Kretz Ultrasound 2003; <http://www.gemedicalsystems.com>.
- [10] DeVore GR, Polanco B, Sklansky MS, Platt LD. The 'spin' technique: a new method for examination of the fetal outflow tracts using three-dimensional ultrasound. *Ultrasound Obstet Gynecol.* 2004;24:72-82.
- [11] Von Ramm OT, Smith SW, Pavy HG Jr. High speed ultrasound volumetric imaging system. Part II. Parallel processing and image display. *IEEE Trans Ultrason Ferroelec Ferq Contr.* 1991; 38:109-115.
- [12] Acar P, Dulac Y, Taktak A, Abadir S. Real-time three-dimensional fetal echocardiography using matrix probe. *Prenat Diagn.* 2005;25:370-5.
- [13] Chen GZ, Huang GY, Tao ZY, Liu XQ, Lin QS. Value of real-time 3-dimensional echocardiography sectional diagnosis in complex congenital heart disease evaluated by receiver operating characteristic analysis. *J Am Soc Echocardiogr.* 2008;21:458-63.
- [14] Jenkins C, Monaghan M, Shirali G, Guraraja R, and Marwick TH. An intensive interactive course for 3D echocardiography: is 'crop till you drop' an effective learning strategy? *Eur J Echocar* (2008) 9, 373–380.

## Rendering Cardiac Volumes in Three and Four-Dimensional Ultrasonography

**Jimmy Espinoza\***

*Department of Obstetrics and Gynecology, William Beaumont Hospital Royal Oak, MI USA*

**Abstract:** This chapter summarizes different approaches currently used to examine the fetal heart using three and four-dimensional ultrasonography with a particular emphasis on multiplanar display and novel rendering modalities. These new imaging modalities provide important insight into the normal and abnormal fetal cardiac anatomy and function and have the potential to reduce the operator dependency that characterizes two-dimensional ultrasound.

**Key Words:** Fetal Echocardiography, 4D Fetal Echocardiography, Volume Rendering.

### INTRODUCTION

A growing body of evidence indicates that four-dimensional (4D) ultrasound imaging with spatiotemporal image correlation (STIC) facilitates examination of the fetal heart [1-45]. Thus, 4D fetal echocardiography have the potential to reduce the operator dependency that characterize two-dimensional ultrasonography and may increase the detection rate of congenital heart defects (CHDs). Volume datasets obtained with 4D sonography can be compared with blocks of pathological specimens, where all the anatomical information is contained in the block and the information displayed depends on the level at which the block is cut, with the additional advantages that these planes can be assessed in a virtual beating heart and that rendering techniques can be used to gain additional insight into the structure and function of the fetal heart. Prenatal diagnosis of congenital heart defects is challenging because of the structural complexity of the heart and the expertise required to master the use of standard planes for fetal echocardiography. In addition fetal and/or maternal motion, maternal body mass index, gestational age, adequacy of the amniotic fluid volume and fetal position are important factors that can affect image quality. Prenatal diagnosis of CHDs is desirable because unrecognized congenital heart defects may be associated with worse neonatal outcome. 4D ultrasonography with spatiotemporal image correlation (STIC) allows the acquisition and storage of volume data sets of the fetal heart using which can be resliced to obtain the standard planes for fetal echocardiography, as well as novel planes. In addition to this anatomic information, functional information of the fetal heart can also be obtained including the direction of blood flow if the volume dataset was obtained color Doppler or high dimensional (HD) power Doppler

The image quality contained in a STIC volume dataset can be substantially improved by optimizing the settings before acquisition. This can be achieved by adjusting the two-dimensional grayscale and color Doppler parameters. Our preference is to use low persistence, high contrast, and high frame rate settings. Typical acquisition time ranges from 5 to 15 seconds. Shorter acquisition times can be used to minimize motion artifacts but this reduces the image spatial resolution. At the time of volume acquisition, transverse sweeps of the fetal thorax can yield better images of four-chamber, five-chamber, and three-vessel and trachea views. In contrast, sagittal sweeps through the fetal thorax can yield better images of the aortic and ductal arches as well as the venous connections to the fetal heart

### Evaluation of the Fetal Heart Using 3D and 4D Ultrasonography

Two-dimensional (2D) ultrasonography relies on standard anatomic planes for the examination of the fetal heart, including the four-chamber view, three-vessel and trachea view, the left and right outflow tracts [46-51]. However, visualization of vascular connections to the fetal heart with two-dimensional (2D) ultrasonography requires the examiner to scan these vascular structures in multiple scanning planes to obtain a mental reconstruction of their spatial relationships. This process can be facilitated using different display modalities used in 3D and 4D ultrasonography including power Doppler reconstruction 3D and 4D volume datasets, [52-56] minimum projection mode, [39] inversion mode, [40, 42, 57] and B-flow. [58-60]

\*Address correspondence to Jimmy Espinoza MD: Department of Obstetrics and Gynecology William Beaumont Hospital Royal Oak, MI USA; E-mail: Jimmy.Espinoza@beaumont.edu

## Multiplanar Display

Multiplanar display is a unique modality available in 3D and 4D ultrasonography that allows for the simultaneous visualization of three anatomic planes which are orthogonal to each other: the transverse, sagittal and coronal planes (Fig. 1).

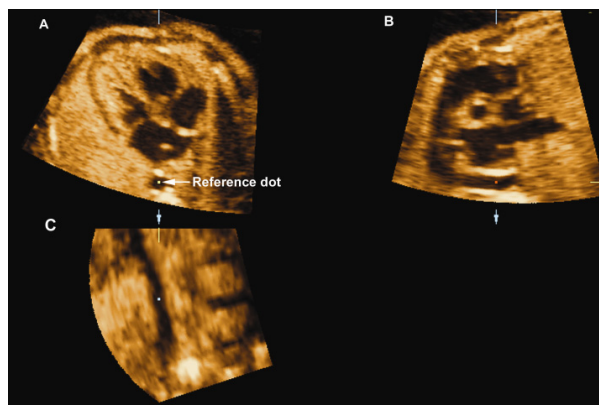


**Figure 1:** Volume datasets were adjusted to display the four chamber view in panel A, where the fetal aorta was aligned with the crux of the heart in the vertical plane. The reference dot was positioned in the aorta allowing the visualization of the coronal view of the descending aorta in panel C.

Moreover, an imaging tool referred as the reference dot allows for the identification of anatomic structures in these three orthogonal planes. This display modality can also be used to scroll through the volume data set to visualize the transverse view of the upper abdomen, four-chamber view, five-chamber view and the three-vessel view.

A central feature of this display modality is the ability to focus on a specific anatomic structure in panel A by placing the reference dot in the structure and visualizing the same structure in two perpendicular planes displayed in panels B and C (Fig. 1). Using this approach we demonstrated that the simultaneous display of orthogonal planes of abnormal vascular connections to the fetal heart facilitated the identification of the nature of the abnormal vessel and the visualization of its spatial relationships with other vascular structures. Indeed, the multiplanar view allowed for the visualization of the drainage of a dilated azygos/vein into the SVC (Fig. 2) in a fetus with interrupted IVC with hemiazygos vein continuation.

This technique involves the visualization of standard views used in fetal echocardiography in panel A and the subsequent placement of the reference dot in the abnormal vascular structure to identify the nature of the vessel and its connections which were displayed using the sagittal and coronal planes in panels B and C, respectively. This technique can be improved by adding the spin technique [61] (see below).

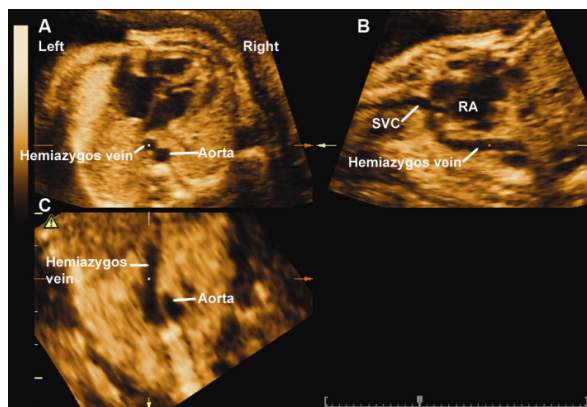


**Figure 2:** Multiplanar display of a dilated hemiazygos vein in a fetus with interrupted inferior vena cava and dextrocardia. The reference dot was placed in the dilated hemiazygos vein in the four chamber view of the heart in panel A. This allowed for both the visualization of the sagittal view of the hemiazygos vein in panel B and the coronal view of the dilated hemiazygos vein in panel C. The rotation of the coronal view to a vertical position on panel C allowed for the visualization of the dilated hemiazygos vein draining into the SVC. SVC: superior vena cava; RA: right atrium

Several algorithms using the multiplanar display have been proposed for simultaneous display of both outflow tracts [25], to visualize the aortic and ductal arches [62], ([Video 1](#)) and to determine the nature of vascular connections to the fetal heart using the spin technique [38]. The later involves positioning the reference dot in the center of the structure and ‘spinning’ the volume data set around the  $y$  axis to determine its spatial relationship with the heart and other vascular structures and to identify its nature

A detailed examination of the fetal heart has been proposed to include a long-axis view of the arterial duct [51] (sagittal view of the ductal arch). This sonographic plane allows visualization of the right ventricle in continuity with the main pulmonary artery, pulmonary valve, ductus arteriosus, and descending aorta, as well as a transverse view of the ascending aorta (Fig. 3).

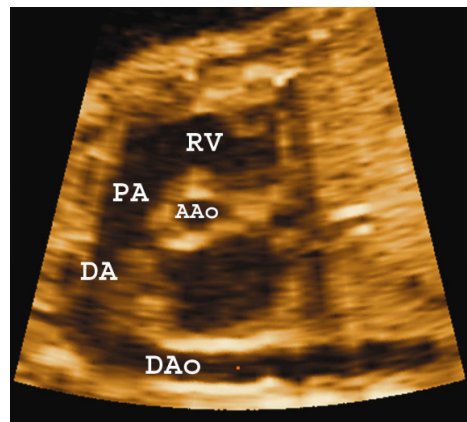


**Figure 3:** The components of the sagittal view of the ductal arch (Fig. 1a) as determined by the multiplanar display are displayed in Fig. 1b, including: right ventricular outlet (RV), main pulmonary artery (PA), ductus arteriosus (DA), descending aorta (DAo), and a cross-section of the ascending aorta (AAo).

The sagittal view of the ductal arch can be easily obtained using 4D volume datasets of the fetal heart acquired with STIC by following the first two steps of a reported algorithm [63]. Briefly:

1. The volume datasets are adjusted to display the four-chamber view in panel A, where the fetal aorta was aligned with the crux of the heart in the vertical plane. The reference dot is positioned in the aorta, allowing the visualization of the coronal view of the descending aorta in panel C (Fig. 1).
2. In panel C, the image is rotated to display the aorta in a vertical position. This allowed for the visualization of the sagittal view of the ductal arch in panel B and the four chamber view in panel A (Fig. 4).

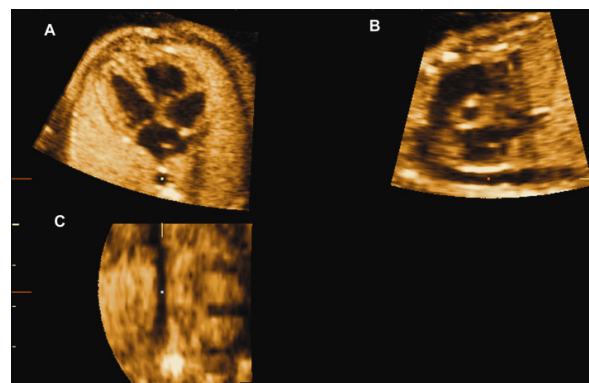


**Figure 4:** In panel C, the image was rotated to display the aorta in a vertical position, when necessary. This allowed for the visualization of the longitudinal view of the ductal arch in panel B.

[Video 2](#) illustrates the simplicity of these steps. A retrospective study using this approach [63] reported that the visualization rate of the sagittal view of the ductal arch was significantly lower in fetuses with conotruncal anomalies 5.6% (1/18), than among normal fetuses [93.1% (108/116)] and those with other CHDs [79.4% (27/34);  $p < 0.01$ ]. The authors concluded that the inability to visualize the ductal arch using the proposed algorithm should raise the possibility of conotruncal anomalies because it is associated with a nine-fold increase in the risk for a

conotruncal anomaly [64]. However, prospective studies are required to determine the value of the proposed approach in the screening for conotruncal anomalies

Rendering techniques can also be applied to the visualization of vascular connections to the fetal heart to obtain a depth perspective using a “thick slice”.<sup>64</sup> (Fig. 5)

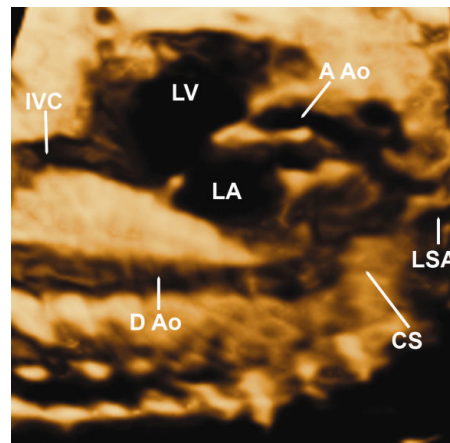


**Figure 5:** “thick slice” rendering of an aortic arch in a patient with aortic coarctation. Contraductal shelf (CS), descending aorta (D Ao), inferior vena cava (IVC), left ventricle (LV), left atrium (LA), ascending aorta (A Ao), left subclavian artery (LSA)

### Automated Display of Multiple Slices

Several ultrasound manufacturers provide software to automatically slice 3D and 4D volume data sets (Multislice View™ ; Accuvix, Medison, Seoul, Korea; Tomographic Ultrasound Imaging; GE Healthcare, Milwaukee, WI; iSlice; Philips Medical Systems, Bothell, WA; Multi-Slice View; Siemens Medical Solutions, Malvern, PA). This technology allows an examiner to automatically display several slices that are parallel to each other on a single screen

TUI has been introduced as a new display technology for 3DUS and 4DUS. This modality allows for the simultaneous display of up to eight parallel planes whose distance can be adjusted for a better visualization of anatomic planes. Thus, TUI allows the visualization of multiple sections of a beating heart at the same time. An “overview image” is shown on the upper left corner. This view shows a plane orthogonal to the slices, and parallel lines demarcate the position of the slices within the volume dataset (Fig. 6).

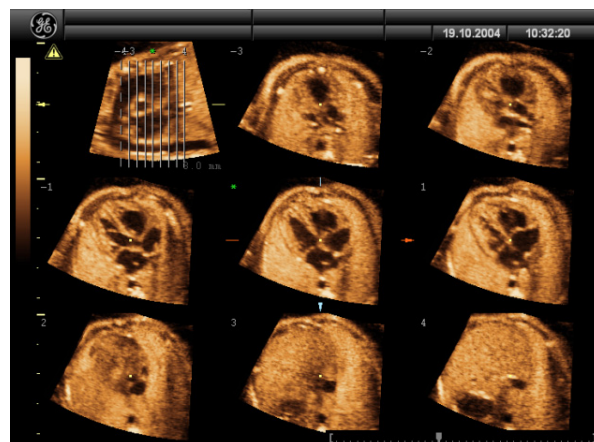


**Figure 6:** An “overview image” is shown on the upper left corner. The parallel lines determine the position of the eight orthogonal planes to the plane containing the “overview image”

The user can adjust the number and position of the slices with specific software controls. TUI has been used for the examination of the fetal heart [65-68]. and other fetal organs [69]. However, the simple use of parallel planes to the four-chamber view of the heart does not allow for the visualization of the long axis view of the left outflow tract and the short axis view of the aorta, which are considered part of an integral examination of the fetal heart [49-51, 70].



Moreover, the untargeted use of TUI allows for the simultaneous display of anatomic planes with and without diagnostic value. In order to determine the minimum number of images required for a comprehensive examination of the fetal heart we developed an algorithm using TUI and STIC [71]. This algorithm allows for the simultaneous visualization of the standard planes for fetal echocardiography including the four-chamber view, three-vessel view, left outflow tract and short axis (right outflow tract), in most fetuses without CHDs [71]. With the use of this algorithm a normal four-chamber view, five-chamber view, longitudinal view of the ductal arch, three-vessel and trachea view, left outflow tract and short axis were visualized in 99%, 96.9%, 98.5%, 88.2%, 93.3%, and 87.2% of the volume datasets, respectively.

Similar results were recently reported by Rizzo et al [72]. using STIC and a simplified method referred to as the “three-steps technique.”

The former algorithm involves the steps that are displayed in [Video 3](#) and include:

**Step 1:** Placement of the reference dot in the crux of the heart and alignment of the aorta in the midline on panel A (Fig. 7)

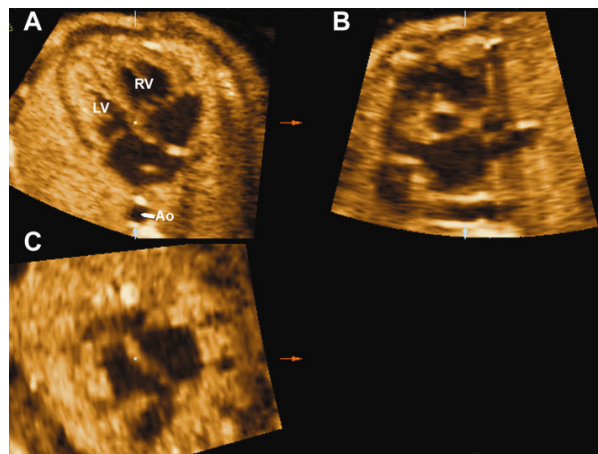


**Figure 7:** Volume datasets were adjusted to display the four chamber view in panel A, where the fetal aorta was aligned with the crux of the heart in the vertical plane. RV: right ventricle; LV: left ventricle; Ao: aorta

**Step 2:** Placement of the reference dot on the aorta in panel A to visualize the coronal view of the aorta in Panel C (Fig. 8)

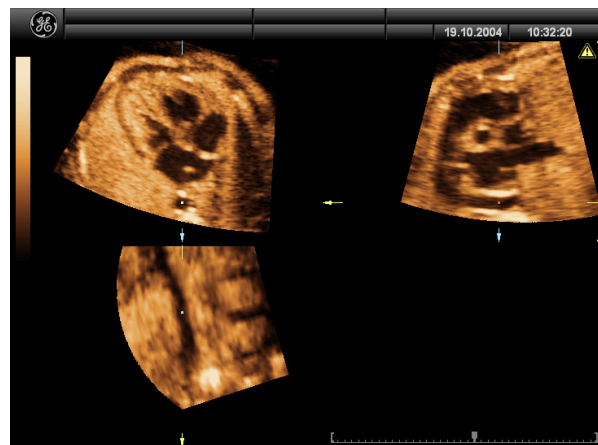


**Figure 8:** The reference dot was positioned on the aorta in panel A allowing the visualization of the coronal view of the descending aorta in panel C.

**Step 3:** On panel C, rotate the aorta until it is in a vertical position. This allows the visualization of the sagittal view of the ductal arch in panel B (Fig. 9)

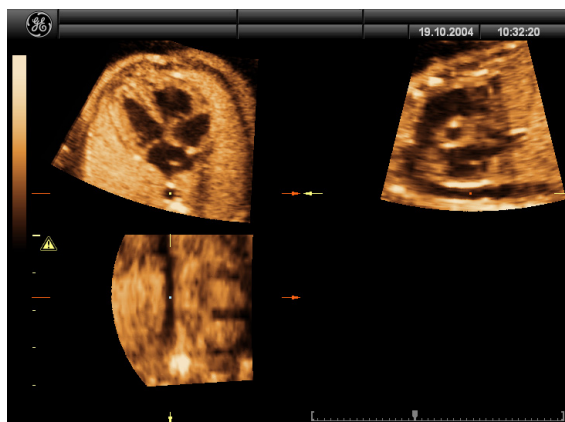


**Figure 9:** In panel C the image was rotated to display the aorta in a vertical position. This allowed for the visualization

Step 4: Move the reference dot back to crux of the heart in panel A, in preparation for TUI activation

Step 5: Activate Tomographic Ultrasound Imaging

Step 6: Reduce the number of slices to 3 and change the display format to four planes. This will automatically enlarge the images displayed (Fig. 10)

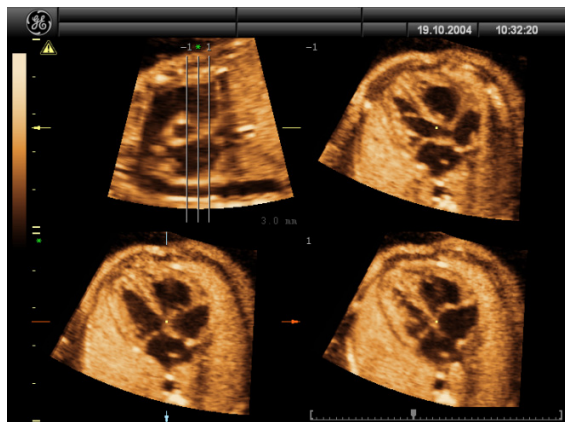


**Fig 10:** see text

Step 7: Right click on panel A and move the image to place reference dot in the aorta. This step allowed the visualization of the five-chamber view on panel C which corresponds to the slice marked with an asterisk in the “overview image” (Fig. 11)

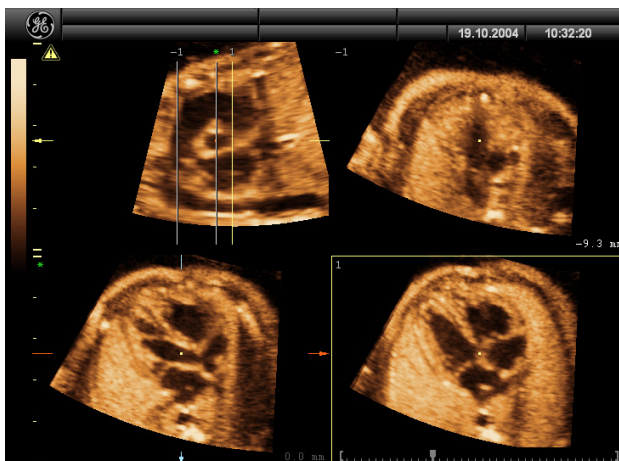


**Figure 11:** see text



**Step 8:** Click on the “adjust” option and right click on panel B to display a horizontal arrow. Move this arrow to the left until the upper line (-1) on panel A coincides with the ductal arch. (Fig. 11)

**Step 9:** Right click on panel D to display the horizontal arrow. Move this arrow to the left until the lower line (1) on panel A coincides with the edge of the aorta. This allowed the visualization of the four-chamber view on panel D in 99% (193/195) of fetuses without heart defects (Fig. 11)

**Step 10:** Left click on panel C and on “Rotation Y”. Scroll the bar on the “Rotation Y” to the right until the left outflow tract is visualized on panel C. This is generally accomplished with a right sided rotation between 8 to 22 degrees depending on the gestational age at which the volume dataset was obtained. This step allows the visualization of the left outflow tract in panel C and the short axis of the aorta in panel A. In about one third of fetuses the reference dot in panel C need to be placed above the aortic valve to visualize the short axis of the aorta in panel A. (Fig. 12)

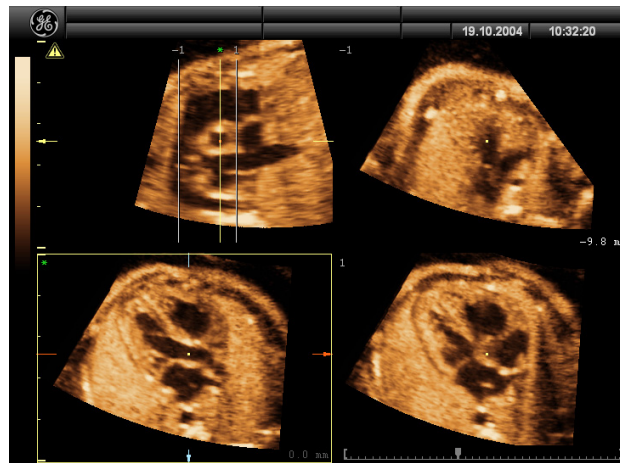


**Figure 12:** see text

### Rendering Techniques

Several rendering algorithms have been described for visualization of the three-dimensional structure and spatial relationships of great vessels and venous return to the heart. These images can be obtained by acquiring volume data sets with gray-scale, color Doppler, power Doppler or B-flow imaging

### Inversion Mode

The “inversion mode” is a new rendering algorithm that transforms echolucent structures into solid vowels. Thus, anechoic structures such as the heart chambers, lumen of the great vessels, stomach and bladder appear echogenic on the rendered image, whereas structures that are normally echogenic prior to gray-scale inversion become anechoic. Post processing adjustments are performed as necessary, including adjustments of the gamma curve, threshold and transparency to improve image quality. The technique allows examiners to obtain 4D rendered images of cardiovascular structures from volume data sets acquired with gray-scale only, without the need for color Doppler, power Doppler, or B-flow imaging. We have previously demonstrated the value of the display technique in the visualization of dilated azygos or hemiazygos veins and their spatial relationships with the descending aorta, the aortic arch, the SVC, the right atrium, and the fetal spine in cases of interrupted IVC associated with and without heterodox syndromes (Fig. 13).

As mentioned above, volume datasets obtained with a sagittal sweep of the fetal chest are preferred over those obtained using a transverse sweep when evaluating the normal or abnormal vascular connection to the fetal heart. Once a sagittal view of the heart is visualized in Panel A, the region of interest was selected in panel B, reducing the rendering box height and width to display only the fetal spine, fetal heart and its vascular connections. Next the direction of view (green dotted line) was set to display the sagittal view of the heart in the anteroposterior projection and finally the “inversion mode” rendering algorithm was selected in the ultrasound equipment with the threshold filter set between 70 and 90.

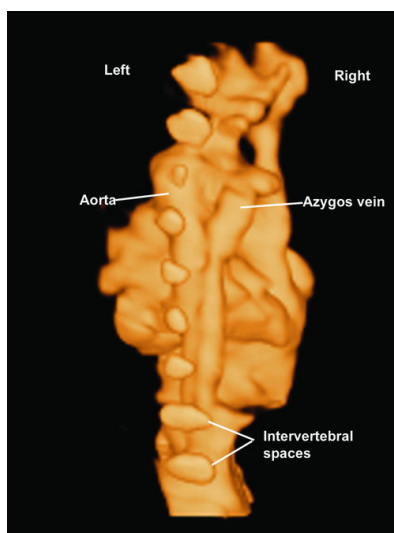


**Figure 13:** Three-dimensional images of a fetal heart rendered with the “inversion mode” in case of interrupted IVC with azygos vein continuation. RA: right atrium; SVC: superior vena cava. A posterior view of the fetal heart shows a dilated azygos vein located to the right of the descending aorta. The arch of this vein forms a Y image with the aortic arch before joining the SVC

### Transparence Modes

The minimum projection mode (MPM) is another volume-rendering tool that allows preferential display of minimum gray values within a volume dataset. This algorithm can be useful for displaying vascular structures and fluid-filled organs [73-74]. The MPM can provide important insight into the spatial relationships of abnormal vascular connections to the fetal heart in the upper mediastinum and could potentially be useful in the determination of atria morphology in cases of left and right isomerism.<sup>39</sup> (Fig. 14)

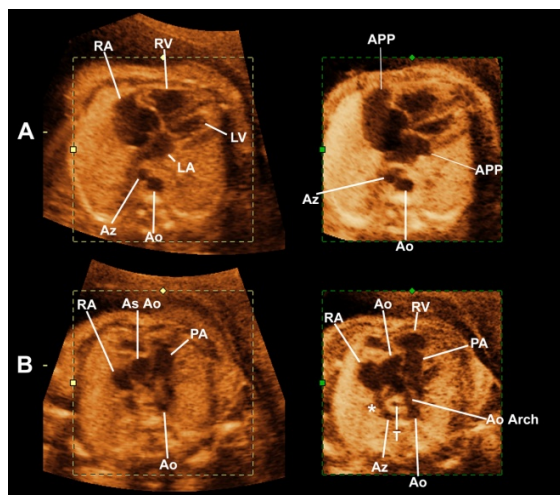


**Figure 14:** Comparison of minimum projection mode (MPM) images, on the right, with their corresponding two-dimensional images, on the left, in a case of left isomerism with interrupted IVC and azygos continuation. A) The four-chamber view shows a two-vessel sign; the MPM image shows that both atria appendages (APP) are morphologically left; B) Three-vessel view. In the MPM image, the azygos vein drains into the superior vena cava (SVC) and the right atrium, whereas the two-dimensional ultrasound image shows only the ascending aorta, the pulmonary artery and the dilated right atrium. RA: right atrium, RV: right ventricle; LV: left ventricle; LA left atrium, Ao: aorta; AZ: Azygos vein; PA: pulmonary artery; Ao Arch: aortic arch, T: trachea, \*: Azygos' arch

### B-flow

B-flow is a new display modality in 4D ultrasound that digitally enhances signals from weak blood reflectors from vessels and, at the same time, suppresses strong signals from surrounding tissues [75-77]. Because this technology does not rely on Doppler methods to display blood flow, it is angle-independent and does not interfere with the frame rate. This is potentially advantageous over color or power Doppler imaging when used in conjunction with

STIC for the evaluation of the fetal vasculature. In B-flow imaging the echoes from the tissue and that of the blood flow can be displayed with high resolution and without the overlay that characterizes color Doppler imaging. Moreover, B-flow may have less signal drop out when the ultrasound beam is perpendicular to the vessel. The use of B-flow in the case presented herein demonstrates that this imaging modality provides important insight into the location and nature of arch abnormalities in fetuses with coarctation of aorta. Indeed, B-flow allowed for a clear visualization of a thin and tortuous aortic arch as well as its spatial relationships with the fetal heart and other vascular structures (Fig 15).

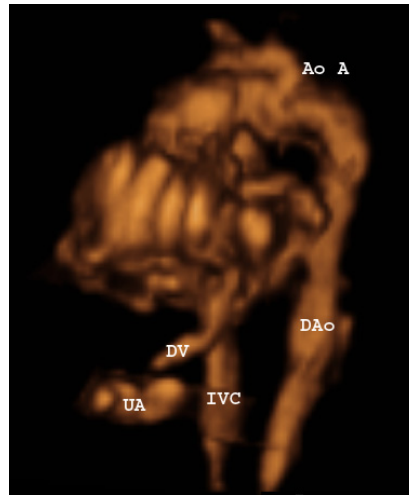


**Figure 15:** B-flow imaging of a narrow and tortuous aortic arch and its relationship with the heart and other vascular structures: aortic arch (Ao A), descending aorta (DAo), ductus venosus (DV), inferior vena cava (IVC), umbilical artery (UA)

## REFERENCES

- [1] Deng J, Gardener JE, Rodeck CH, Lees WR. Fetal echocardiography in three and four dimensions. *Ultrasound Med.Biol.* 1996;22:979-86
- [2] Meyer-Wittkopf M, Cook A, McLennan A, Summers P, Sharland GK, Maxwell DJ. Evaluation of three-dimensional ultrasonography and magnetic resonance imaging in assessment of congenital heart anomalies in fetal cardiac specimens. *Ultrasound Obstet.Gynecol.* 1996;8:303-08.
- [3] Nelson TR, Pretorius DH, Sklansky M, Hagen-Ansert S. Three-dimensional echocardiographic evaluation of fetal heart anatomy and function: acquisition, analysis, and display. *J.Ultrasound Med.* 1996;15:1-9.
- [4] Zosmer N, Jurkovic D, Jauniaux E, Gruboeck K, Lees C, Campbell S. Selection and identification of standard cardiac views from three-dimensional volume scans of the fetal thorax. *J.Ultrasound Med.* 1996;15:25-32.
- [5] Chang FM, Hsu KF, Ko HC, Yao BL, Chang CH, Yu CH et al. Fetal heart volume assessment by three-dimensional ultrasound. *Ultrasound Obstet.Gynecol.* 1997;9:42-48.
- [6] Sklansky MS, Nelson TR, Pretorius DH. Usefulness of gated three-dimensional fetal echocardiography to reconstruct and display structures not visualized with two-dimensional imaging. *Am.J.Cardiol.* 1997;80:665-68.
- [7] Levental M, Pretorius DH, Sklansky MS, Budorick NE, Nelson TR, Lou K. Three-dimensional ultrasonography of normal fetal heart: comparison with two-dimensional imaging. *J.Ultrasound Med.* 1998;17:341-48.
- [8] Nelson TR. Three-dimensional fetal echocardiography. *Prog.Biophys.Mol.Biol.* 1998;69:257-72.
- [9] Sklansky MS, Nelson TR, Pretorius DH. Three-dimensional fetal echocardiography: gated versus nongated techniques. *J.Ultrasound Med.* 1998;17:451-57.
- [10] Sklansky MS, Nelson T, Strachan M, Pretorius D. Real-time three-dimensional fetal echocardiography: initial feasibility study. *J.Ultrasound Med.* 1999;18:745-52.
- [11] Guerra FA, Isla AI, Aguilar RC, Fritz EG. Use of free-hand three-dimensional ultrasound software in the study of the fetal heart. *Ultrasound Obstet.Gynecol.* 2000;16:329-34.
- [12] Levi S, Cos-Sanchez T. [Fetal echocardiography volume mode (3 dimensions)]. *J.Gynecol.Obstet.Biol.Reprod.(Paris)* 2000;29:261-63.
- [13] Meyer-Wittkopf M, Rappe N, Sierra F, Barth H, Schmidt S. Three-dimensional (3-D) ultrasonography for obtaining the four and five-chamber view: comparison with cross-sectional (2-D) fetal sonographic screening. *Ultrasound Obstet.Gynecol.* 2000;15:397-402.
- [14] Scharf A, Geka F, Steinborn A, Frey H, Schlemmer A, Sohn C. 3D real-time imaging of the fetal heart. *Fetal Diagn.Ther.* 2000;15:267-74.

- [15] Bega G, Kuhlman K, Lev-Toaff A, Kurtz A, Wapner R. Application of three-dimensional ultrasonography in the evaluation of the fetal heart. *J.Ultrasound Med.* 2001;20:307-13.
- [16] Deng J, Yates R, Birkett AG, Ruff CF, Linney AD, Lees WR et al. Online motion-gated dynamic three-dimensional echocardiography in the fetus--preliminary results. *Ultrasound Med.Biol.* 2001;27:43-50.
- [17] Meyer-Wittkopf M, Cooper S, Vaughan J, Sholler G. Three-dimensional (3D) echocardiographic analysis of congenital heart disease in the fetus: comparison with cross-sectional (2D) fetal echocardiography. *Ultrasound Obstet.Gynecol.* 2001;17:485-92.
- [18] Meyer-Wittkopf M, Cole A, Cooper SG, Schmidt S, Sholler GF. Three-dimensional quantitative echocardiographic assessment of ventricular volume in healthy human fetuses and in fetuses with congenital heart disease. *J.Ultrasound Med.* 2001;20:317-27.
- [19] Michailidis GD, Simpson JM, Karidas C, Economides DL. Detailed three-dimensional fetal echocardiography facilitated by an Internet link. *Ultrasound Obstet.Gynecol.* 2001;18:325-28.
- [20] Arzt W, Tulzer G, Aigner M. [Real time 3D sonography of the normal fetal heart--clinical evaluation]. *Ultraschall Med.* 2002;23:388-91.
- [21] Deng J, Yates R, Sullivan ID, Mcdonald D, Linney AD, Lees WR et al. Dynamic three-dimensional color Doppler ultrasound of human fetal intracardiac flow. *Ultrasound Obstet.Gynecol.* 2002;20:131-36.
- [22] Deng J, Sullivan ID, Yates R, Vogel M, Mcdonald D, Linney AD et al. Real-time three-dimensional fetal echocardiography--optimal imaging windows. *Ultrasound Med.Biol.* 2002;28:1099-105.
- [23] Deng J, Richards R. Dynamic three-dimensional gray-scale and color Doppler ultrasound of the fetal heart for dynamic diagnosis. *Ultrasound Obstet.Gynecol.* 2002;20:209.
- [24] DeVore GR, Falkensammer P, Sklansky MS, Platt LD. Spatio-temporal image correlation (STIC): new technology for evaluation of the fetal heart. *Ultrasound Obstet.Gynecol.* 2003;22:380-87.
- [25] Goncalves LF, Lee W, Chaiworapongsa T, Espinoza J, Schoen ML, Falkensammer P et al. Four-dimensional ultrasonography of the fetal heart with spatiotemporal image correlation. *Am.J.Obstet.Gynecol.* 2003;189:1792-802.
- [26] Herberg U, Goldberg H, Breuer J. Dynamic free-hand three-dimensional fetal echocardiography gated by cardiotocography. *Ultrasound Obstet.Gynecol.* 2003;22:493-502.
- [27] Jurgens J, Chaoui R. Three-dimensional multiplanar time-motion ultrasound or anatomical M-mode of the fetal heart: a new technique in fetal echocardiography. *Ultrasound Obstet.Gynecol.* 2003;21:119-23.
- [28] Maulik D, Nanda NC, Singh V, Dod H, Vengala S, Sinha A et al. Live three-dimensional echocardiography of the human fetus. *Echocardiography.* 2003;20:715-21.
- [29] Meyer-Wittkopf M, Hofbeck M. [Two- and three-dimensional echocardiographic analysis of congenital heart disease in the fetus]. *Herz* 2003;28:240-49.
- [30] Sklansky M. New dimensions and directions in fetal cardiology. *Curr.Opin.Pediatr.* 2003;15:463-71.
- [31] Vinals F, Poblete P, Giuliano A. Spatio-temporal image correlation (STIC): a new tool for the prenatal screening of congenital heart defects. *Ultrasound Obstet.Gynecol.* 2003;22:388-94.
- [32] Abuhamad A. Automated multiplanar imaging: a novel approach to ultrasonography. *J.Ultrasound Med.* 2004;23:573-76.
- [33] Acar P, Dulac Y, Taktak A, Villaceque M. [Real time 3D echocardiography in congenital heart disease]. *Arch.Mal Coeur Vaiss.* 2004;97:472-78.
- [34] Bhat AH, Corbett VN, Liu R, Carpenter ND, Liu NW, Wu AM et al. Validation of volume and mass assessments for human fetal heart imaging by 4-dimensional spatiotemporal image correlation echocardiography: in vitro balloon model experiments. *J.Ultrasound Med.* 2004;23:1151-59.
- [35] Bhat AH, Corbett V, Carpenter N, Liu N, Liu R, Wu A et al. Fetal ventricular mass determination on three-dimensional echocardiography: studies in normal fetuses and validation experiments. *Circulation* 2004;110:1054-60.
- [36] Brekke S, Tegnander E, Torp HG, Eik-Nes SH. Tissue Doppler gated (TDOG) dynamic three-dimensional ultrasound imaging of the fetal heart. *Ultrasound Obstet.Gynecol.* 2004;24:192-98.
- [37] Chaoui R, Hoffmann J, Heling KS. Three-dimensional (3D) and 4D color Doppler fetal echocardiography using spatio-temporal image correlation (STIC). *Ultrasound Obstet.Gynecol.* 2004;23:535-45.
- [38] DeVore GR, Polanco B, Sklansky MS, Platt LD. The 'spin' technique: a new method for examination of the fetal outflow tracts using three-dimensional ultrasound. *Ultrasound Obstet.Gynecol.* 2004;24:72-82.
- [39] Espinoza J, Goncalves LF, Lee W, Chaiworapongsa T, Treadwell MC, Stites S et al. The use of the minimum projection mode in 4-dimensional examination of the fetal heart with spatiotemporal image correlation. *J.Ultrasound Med.* 2004;23:1337-48.
- [40] Goncalves LF, Espinoza J, Lee W, Mazor M, Romero R. Three- and four-dimensional reconstruction of the aortic and ductal arches using inversion mode: a new rendering algorithm for visualization of fluid-filled anatomical structures. *Ultrasound Obstet.Gynecol.* 2004;24:696-98.
- [41] Sklansky MS, DeVore GR, Wong PC. Real-time 3-dimensional fetal echocardiography with an instantaneous volume-rendered display: early description and pictorial essay. *J.Ultrasound Med.* 2004;23:283-89.

- [42] Espinoza J, Goncalves LF, Lee W, Mazor M, Romero R. A novel method to improve prenatal diagnosis of abnormal systemic venous connections using three- and four-dimensional ultrasonography and 'inversion mode'. *Ultrasound Obstet.Gynecol.* 2005;25:428-34.
- [43] Herberg U, Goldberg H, Breuer J. Three- and four-dimensional freehand fetal echocardiography: a feasibility study using a hand-held Doppler probe for cardiac gating. *Ultrasound Obstet.Gynecol.* 2005;25:362-71.
- [44] Vinals F, Mandujano L, Vargas G, Giuliano A. Prenatal diagnosis of congenital heart disease using four-dimensional spatio-temporal image correlation (STIC) telemedicine via an Internet link: a pilot study. *Ultrasound Obstet.Gynecol.* 2005;25:25-31.
- [45] Yagel S, Valsky DV, Messing B. Detailed assessment of fetal ventricular septal defect with 4D color Doppler ultrasound using spatio-temporal image correlation technology. *Ultrasound Obstet.Gynecol.* 2005;25:97-98.
- [46] Bromley B, Estroff JA, Sanders SP, Parad R, Roberts D, Frigoletto FD, Jr. et al. Fetal echocardiography: accuracy and limitations in a population at high and low risk for heart defects. *Am.J Obstet Gynecol.* 1992;166:1473-81.
- [47] Benacerraf BR. Sonographic detection of fetal anomalies of the aortic and pulmonary arteries: value of four-chamber view vs direct images. *AJR Am.J Roentgenol.* 1994;163:1483-89.
- [48] Comstock CH. What to expect from routine midtrimester screening for congenital heart disease. *Semin.Perinatol.* 2000;24:331-42.
- [49] Carvalho JS, Mavrides E, Shinebourne EA, Campbell S, Thilaganathan B. Improving the effectiveness of routine prenatal screening for major congenital heart defects. *Heart* 2002;88:387-91.
- [50] Chaoui R. The examination of the normal fetal heart using two-dimensional fetal echocardiography. In: Yagel S, Silverman NH, Gembruch U, editors. *Fetal Cardiology*. London: Martin Dunitz; 2003. p. 141-49.
- [51] Allan L. Technique of fetal echocardiography. *Pediatr Cardiol* 2004;25:223-33.
- [52] Kalache K, Romero R, Goncalves LF, Chaiworapongsa T, Espinoza J, Schoen ML et al. Three-dimensional color power imaging of the fetal hepatic circulation. *Am.J.Obstet.Gynecol.* 2003;189:1401-06.
- [53] Ruano R, Benachi A, Aubry MC, Brunelle F, Dumez Y, Dommergues M. Perinatal three-dimensional color power Doppler ultrasonography of vein of Galen aneurysms. *J.Ultrasound Med.* 2003;22:1357-62.
- [54] Lee W, Kalache KD, Chaiworapongsa T, Londono J, Treadwell MC, Johnson A et al. Three-dimensional power Doppler ultrasonography during pregnancy. *J.Ultrasound Med.* 2003;22:91-97.
- [55] Chaoui R, Schneider MB, Kalache KD. Right aortic arch with vascular ring and aberrant left subclavian artery: prenatal diagnosis assisted by three-dimensional power Doppler ultrasound. *Ultrasound Obstet.Gynecol.* 2003;22:661-63.
- [56] Goncalves LF, Romero R, Espinoza J, Lee W, Treadwell M, Chintala K et al. Four-dimensional ultrasonography of the fetal heart using color Doppler spatiotemporal image correlation. *J.Ultrasound Med.* 2004;23:473-81.
- [57] Benacerraf BR. Inversion mode display of 3D sonography: applications in obstetric and gynecologic imaging. *AJR Am J Roentgenol.* 2006;187:965-71.
- [58] Deng J, Rodeck CH. New fetal cardiac imaging techniques. *Prenat.Diagn.* 2004;24:1092-103.
- [59] Goncalves LF, Espinoza J, Lee W, Nien JK, Hong JS, Santolaya-Forgas J et al. A new approach to fetal echocardiography: digital casts of the fetal cardiac chambers and great vessels for detection of congenital heart disease. *J Ultrasound Med.* 2005;24:415-24.
- [60] Volpe P, Campobasso G, Stanziano A, De R, V, Di Paolo S, Caruso G et al. Novel application of 4D sonography with B-flow imaging and spatio-temporal image correlation (STIC) in the assessment of the anatomy of pulmonary arteries in fetuses with pulmonary atresia and ventricular septal defect. *Ultrasound Obstet Gynecol* 2006;28:40-46.
- [61] Rizzo G, Arduini D, Capponi A. Use of the multiplanar display in evaluation of a persistent left superior vena cava in the fetal heart using 4-dimensional ultrasonography: advantage of adding the spin technique. *J Ultrasound Med* 2008;27:497-98.
- [62] Bega G, Lev-Toaff A, Kuhlman K, Kurtz A, Goldberg B, Wapner R. Three-dimensional ultrasonographic imaging in obstetrics: present and future applications. *J.Ultrasound Med.* 2001;20:391-408.
- [63] Espinoza J, Romero R, Kusanovic JP, Gotsch F, Erez O, Lee W et al. The role of the sagittal view of the ductal arch in identification of fetuses with conotruncal anomalies using 4-dimensional ultrasonography. *J Ultrasound Med* 2007;26:1181-88.
- [64] Goncalves LF, Lee W, Espinoza J, Romero R. Examination of the fetal heart by four-dimensional (4D) ultrasound with spatio-temporal image correlation (STIC). *Ultrasound Obstet Gynecol* 2006;27:336-48.
- [65] DeVore GR, Polanko B. Tomographic ultrasound imaging of the fetal heart: a new technique for identifying normal and abnormal cardiac anatomy. *J Ultrasound Med.* 2005;24:1685-96.
- [66] Goncalves LF, Espinoza J, Romero R, Kusanovic J, Swope B, Nien JK et al. Four-dimensional ultrasonography of the fetal heart using a novel Tomographic Ultrasound Imaging display. *J.Perinat.Med.* 2006;34:39-55.
- [67] Rizzo G, Capponi A, Cavicchioni O, Vendola M, Pietrolucci ME, Arduini D. Application of automated sonography on 4-dimensional volumes of fetuses with transposition of the great arteries. *J Ultrasound Med* 2008;27:771-76.

- [68] Rizzo G, Capponi A, Vendola M, Pietrolucci ME, Arduini D. Role of tomographic ultrasound imaging with spatiotemporal image correlation for identifying fetal ventricular septal defects. *J Ultrasound Med* 2008;27:1071-75.
- [69] Leung KY, Ngai CS, Chan BC, Leung WC, Lee CP, Tang MH. Three-dimensional extended imaging: a new display modality for three-dimensional ultrasound examination. *Ultrasound Obstet.Gynecol.* 2005;26:244-51.
- [70] Bromley B, Estroff JA, Sanders SP, Parad R, Roberts D, Frigoletto FD, Jr. et al. Fetal echocardiography: accuracy and limitations in a population at high and low risk for heart defects. *Am J Obstet Gynecol* 1992;166:1473-81.
- [71] Espinoza J, Kusanovic JP, Goncalves LF, Nien JK, Hassan S, Lee W et al. A novel algorithm for comprehensive fetal echocardiography using 4-dimensional ultrasonography and tomographic imaging. *J Ultrasound Med* 2006;25:947-56.
- [72] Rizzo G, Capponi A, Muscatello A, Cavicchioni O, Vendola M, Arduini D. Examination of the fetal heart by four-dimensional ultrasound with spatiotemporal image correlation during routine second-trimester examination: the 'three-steps technique'. *Fetal Diagn.Ther.* 2008;24:126-31.
- [73] Baba K, Okai T. Basis and principles of three-dimensional ultrasound. In: Baba K, Jurkovic D, editors. *Three-dimensional ultrasound in obstetrics and gynecology*. New York: Parthenon Publishing Group; 1997. p. 1-21.
- [74] Kettl K, Gritzky A. Introduction to three-dimensional ultrasound technology and future aspects. In: Kurjak A, editor. *Three-Dimensional Power Doppler in Obstetrics and Gynecology*. New York: Parthenon Publishing Group; 2000. p. 1-7.
- [75] Pooh RK. New application of B-flow sono-angiography in perinatology. *Ultrasound Obstet.Gynecol.* 2000;15:163.
- [76] Deane C. Extended field-of-view and B-flow ultrasound: fashion or future? *Ultrasound Obstet.Gynecol.* 2000;15:96-97.
- [77] Devore GR. Three-dimensional and four-dimensional fetal echocardiography: a new frontier. *Curr.Opin.Pediatr.* 2005;17:592-604.

## Analysis of Acquired Volumes: Methodological Approach

Greggory R DeVore

Fetal Diagnostic Center Pasadena, CA, USA

**Abstract:** The purpose of this paper is to review how 3D/4D echocardiographic images can be manipulated to maximize the information regarding cardiac structure to improve the diagnostic yield of congenital heart defects. The following topics are discussed: (1) the differences between 3D and 4D ultrasound; (2) basic imaging principles of four-dimensional ultrasound when using spatial-temporal image correlation, real-time volume display, and matrix array technology; (3) analysis of acquired volumes using X,Y and Z rotation, the transverse sweep, the spin technique, tomographic imaging, rendering, inversion, and B-flow. The conclusion is that while the 3D and 4D volumes are easy to acquire, the user must understand the number of tools available to enhance the examination of the fetal heart.

**Key Words:** 4D ultrasound, Fetal echocardiography, Cardiac volumes, Methodology.

### INTRODUCTION

Fetal echocardiography was introduced to clinical medicine in the early 1980's when the first studies reported its use for evaluation of cardiac arrhythmias as well as basic cardiac anatomy using M-mode, M-Mode-directed real-time, and real-time ultrasound [1-21]. In the late 1980's color and pulsed Doppler ultrasound were added to the armamentarium so that blood flow could be evaluated. [22-29]. These diagnostic tools allowed the fetal examiner utilize tools that were the standard for pediatric and adult echocardiography [30].

During the past seven years a new imaging modality, 3D/4D ultrasound, has emerged as an important adjunct to cardiac imaging [31-72]. This modality has allowed the examiner to review cardiac anatomical relationships in a manner that has not been available in the past. After acquiring 3D/4D fetal cardiac volume datasets the examiner must use sophisticated online and/or offline computer programs to analyze the fetal heart. For many physicians who are only familiar with acquiring and interpreting 2D images (B-mode, color Doppler, pulsed Doppler) the concept of manipulating a 3D/4D dataset may be a daunting task. The purpose of this paper is to review how 3D/4D echocardiographic images can be manipulated to maximize the information regarding cardiac structure for improved diagnostic yield. This paper will include a description of each technique, a cine clip illustrating the technique, a link to a free downloadable program used for volume manipulation, and sample volumes the user can download and evaluate.

### DIFFERENCES BETWEEN 3D AND 4D ULTRASOUND

When three-dimensional (3D) ultrasound was introduced to the imaging community as a commercial product it consisted of multiple 2D images that were stacked one behind another during a manual or automated sweep of the transducer beam through an area of interest (Fig. 1).

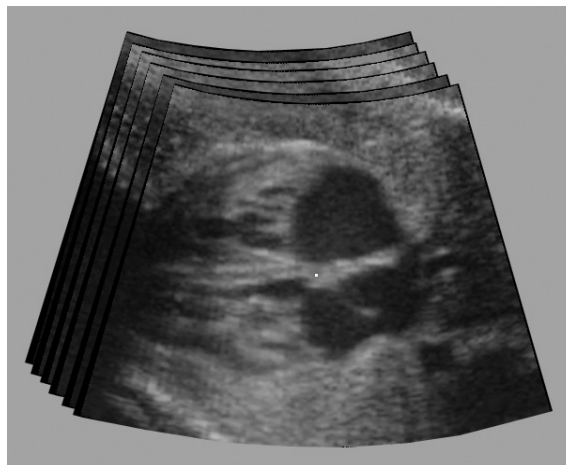


**Figure 1:** This illustrates the acquisition of multiple 2D images obtained during the sweep of the transducer beam through the

\*Address correspondence to Greggory R DeVore: Feala Diagnostic Center Pasadena CA, USA; E-mail: fetelecho@fetelecho.com



fetal chest. These images are used to create a dataset of voxels that are used to reconstruct 3D and 4D images of the fetal heart. This technique is used with mechanical transducers in non-pediatric 3D and 4D ultrasound machines.

Imaging of the heart proceeded without regard to changes in diastolic and systolic cardiac configuration that occur during the cardiac cycle. The “non-gated” approach to reconstructive 3D imaging results in a “static” image display of non-cardiovascular and cardiovascular anatomy that can be examined simultaneously in three planes (X, Y and Z) that are perpendicular to each other (Fig. 2).

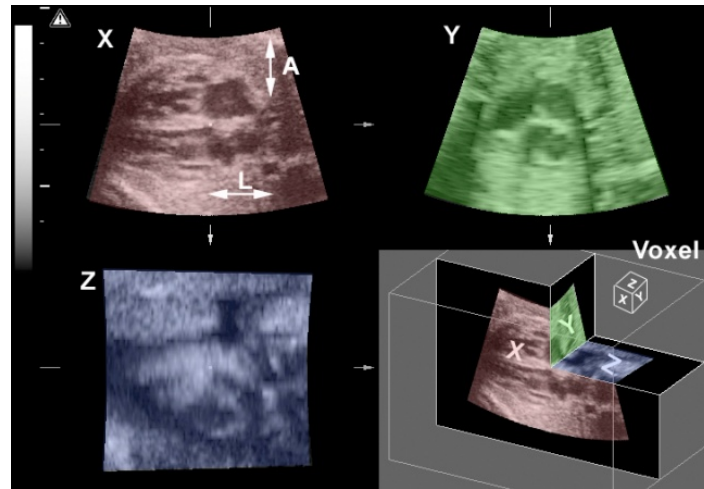


**Figure 2:** Following the acquisition of sequential, parallel 2D images, the volume dataset is created containing voxels. Each voxel consists of a volume of image pixels that have an X, Y, and Z component. The X plane image is obtained during the initial acquisition and has the characteristics of axial (A) and lateral (L) resolution of the 2D image which is a function of the characteristics of the transducer beam. The Y and Z planes also have axial and lateral resolution. However, the resolution in these planes is a function of the transducer beam as well as the size of the voxel that is created from the original volume dataset. For this reason, the Y and Z images are of lower resolution than the image in the X plane.

The X plane image has the highest resolution and is equivalent to the 2D image displayed during the 3D volume acquisition (Fig. 2). The X plane image consists of pixels that have the properties of axial and lateral resolution, identical to a typical 2D image. Axial resolution provides the greatest detail for imaging tissue structures in the plane of the ultrasound beam, while lateral resolution provides less detail because it displays structures lateral to the ultrasound beam (Fig. 2). Therefore, the X plane image would be equivalent to a 2D image displayed during a non-3D examination of the fetus. As the two-dimensional images acquired during the 3D volume acquisition are stacked one behind another, a voxel is created which has X, Y, and Z components (Fig. 2). The size of the voxel determines the resolution of the images in the Y and Z planes (Fig. 2). The 3D Y plane displays an image perpendicular to the X plane, in a vertical orientation (Fig. 2). This image has less detail than the X plane image because it is reconstructed from voxels within the volume dataset. Although the Y plane image has less detail than the X plane image, it has more detail than the Z plane image. The Z plane image is perpendicular and horizontal to the X plane (Fig. 2).

While the ability to examine cardiac structures in three perpendicular planes is a new approach not available with conventional 2D imaging, there are two limitations when comparing this to a 2D real-time image display of the fetal heart. The first is that the image is “static”, thus not displaying a real-time image of cardiac structures, i.e. wall motion and opening and closing of valves. This would be equivalent to a freeze frame image obtained by pausing a video tape player, or freezing a still image while performing a live 2D real-time examination. The second limitation is the speed at which the volume dataset is acquired. All 3D ultrasound machines allow the examiner to control the sweep speed during image acquisition. The slower the sweep speed, the higher the resolution of the images displayed in the Y and Z planes. However, at slower sweep speeds artifact is introduced in the Y and Z planes as the result of fetal somatic and cardiac motion (Fig. 3), thus negating the benefit of the 3D volume dataset. Conversely, the faster the sweep speed the lower the resolution in the Y and Z planes. However, with a faster sweep speed there is less of a chance of artifact introduced from cardiac motion (Fig. 3).



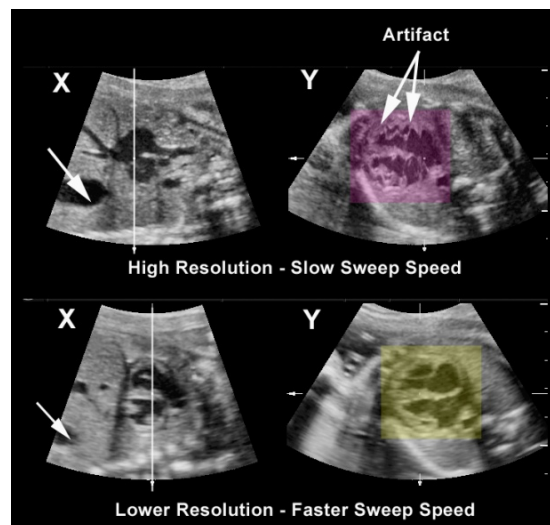


**Figure 3:** This is a static 3D sweep through the fetal chest containing cardiac structures. This image acquisition was sagittal, from left to right. The Y plane illustrates the reconstructed four-chamber view of the heart. The upper panel demonstrates the X and Y planes in which the sweep speed is set at a slow rate to acquire a greater number of 2D images to construct the 3D dataset. Using this technique increases the image resolution in the X plane. However, because of the decreased sweep speed, there is artifact in the Y plane resulting from contraction of the fetal heart during the image acquisition. The lower panel demonstrates a similar sweep at a lower speed. The Y plane does not demonstrate artifact, however, the image resolution of the four-chamber view is less.

Because the 3D static sweep captures cardiac structures randomly within the cardiac cycle, measurements of chamber and outflow tract dimensions at end-diastole or end-systole cannot be made. Therefore, when the examiner acquires a 3D static volume dataset of the fetal heart it is desirable to determine the transducer sweep speed that optimizes image resolution without introducing movement artifact in the Y and Z planes.

### Basic Imaging Principles of Four-Dimensional Ultrasound

The question often asked is “what is four-dimensional (4D) ultrasound?” The fourth dimension is time, i.e. rapidly displaying 3D datasets so that the structures displayed on the screen appear to be moving. This gives the impression of motion such as a smiling face, movement of extremities, and contraction of the heart. This is similar to real-time ultrasound in which static 2D images are displayed on the screen at a rapid rate (frequency) giving the illusion of movement. Currently, there are several 4D technologies that are commercially available that will be discussed in this section.

### Spatial–Temporal Image Correlation (STIC)

Initially the reconstruction of image datasets was time consuming and could only be performed with computerized offline data analysis and rendering. This prevented the clinical use of this technology on a widespread basis. In 2002 GE-Kretz (Voluson 730 Expert, Zipf, Austria) introduced the first clinical ultrasound machine that reconstructed 3-dimensional datasets of the fetal heart and displayed a cine loop of a single cardiac cycle [48]. The technology that was used is called spatial–temporal image correlation (STIC). After the introduction of B-mode STIC in 2002, STIC color and power Doppler were introduced in 2003 [44]. Since the first introduction of STIC, additional manufacturers have introduced similar technologies. The STIC volume display consists of thousands of 2D images acquired through the area of interest during a single sweep that lasts between 7.5 and 15 seconds. The images are then analyzed and multiple volumes are correlated with end-systole and end-diastole to create a cine loop of a single cardiac cycle. This allows the examiner to evaluate the volume dataset, identical to what is accomplished with the 3D static volume, with the only difference being that cardiac structures are viewed as a cine loop of a single cardiac cycle. STIC technology can display the data as either a B-mode image, B-mode with color Doppler, B-mode with Power Doppler, color Doppler, power Doppler, and B-flow (Fig. 4).

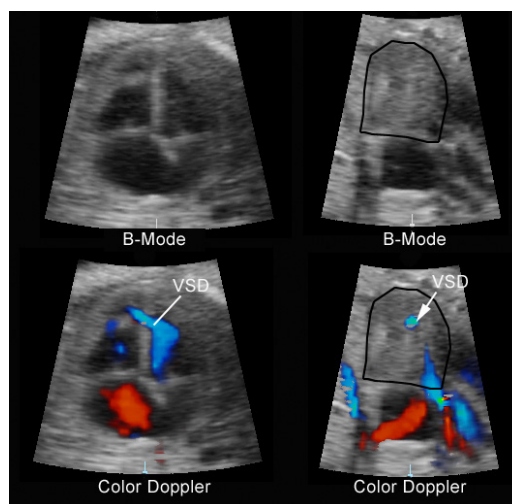


**Figure 4:** This is a STIC acquisition of the four-chamber view. The upper and lower panels are identical images, except for display of the color Doppler in the lower panel. The upper panel demonstrates the four-chamber view in the X plane and an “enface” view (outlined by black line) of the ventricular septum in the Y plane. Careful examination does not suggest any pathology of the interventricular septum. The lower panel, with color Doppler activated, demonstrates a shunting ventricular septal defect near the apex in the X plane. The size and location of the septal defect is clearly identified in the “enface” view of the Y plane.

The only limitation of the STIC volume data acquisition is that fetal movement may occur during the volume acquisition. Depending upon the type of movement (fetal breathing, gross body movement, maternal breathing) the images in the X, Y and Z planes may be minimally altered, or may become non-interpretable. Like the static 3D volume data acquisition, the resolution of the images in the X, Y, and Z planes are a function of how the user acquires the volume dataset. The volume sweep speed can be selected between 7.5 and 15 seconds and the angle of the sweep between 15 and 40 degrees. The angle of the sweep is equivalent to the distance covered during the sweep; a shorter distance is equivalent to a smaller angle; a larger distance is equivalent to a larger angle

For example, if the selected time is 7.5 seconds, a fixed number of images will be acquired whether the angle is 15 or 40 degrees. Therefore, the image resolution will be higher when the angle is 15 degrees than if it were 40 degrees. The reason for this is that although the same number of images are acquired during the 7.5 seconds, there is a greater distance between the images than when the angle is smaller. This results in lower resolution images in the Y and Z planes in the 40 degree sweep than in the 15 degree sweep. The advantages of STIC technology are the following: (1) looped cardiac cycle that simultaneously displays cardiac anatomy in the X, Y and Z planes (Fig. 5),

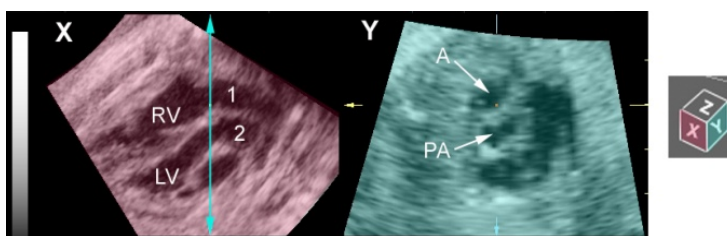


**Figure 5:** Using STIC technology, the outflow tracts are imaged cephalad to the four-chamber view demonstrating two outflow tracts (1 and 2) parallel to each other as they exit their respective ventricles. By rotating the image so that the outflow tracts are perpendicular to a horizontal plane, the outflow tracts are viewed in the short axis in the Y plane, demonstrating both to be adjacent to each other. This fetus had d-transposition of the great arteries.

(2) depending upon the settings selected (maximal time acquisition, minimal angle volume to image the cardiac structures) the image resolution is improved when compared to the 3D static volume sweep, (3) a single cardiac cycle is displayed allowing the examiner to examine cardiac anatomy frame-by-frame or in the cine-loop mode, (4) color Doppler and power Doppler flow dynamics can be examined simultaneously in the X, Y and Z planes (Fig. 4), (5) end-diastole and end-systole can be determined and cardiac measurements can be made from the B-mode images in the X, Y and Z planes. (Fig. 6).

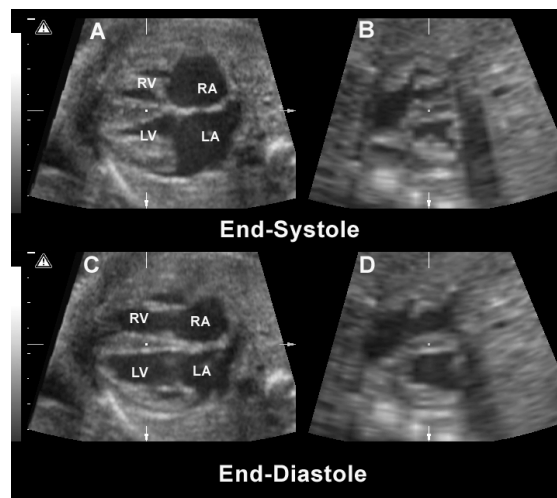


**Figure 6:** Isolation of end-systole and end-diastole from a STIC volume from which measurements of atrial and ventricular chambers can be made from the four-chamber view (A and C). Using this approach facilitates cardiac measurements because the examiner can align the heart in the short axis view (B and D) so that the widest and smallest dimension of the ventricular or atrial chambers are measured accurately. RA=right atrium, LA=left atrium, RV=right ventricle, LV=left ventricle.

### Real-Time Volume Display

Using a mechanical array probe (GE-Kretz Voluson 730 Expert, Zipf, Austria; Philips HD 11, Bothel, WA, USA) multiple sequential volumes are acquired and displayed continuously on the screen. This results in an image sequence similar to 2D real-time imaging. Because of limitations of computer processing of volume datasets, the quality of the image is markedly decreased when compared to a 2D real-time image, static 3D image, or a 4D STIC image (Fig. 7).

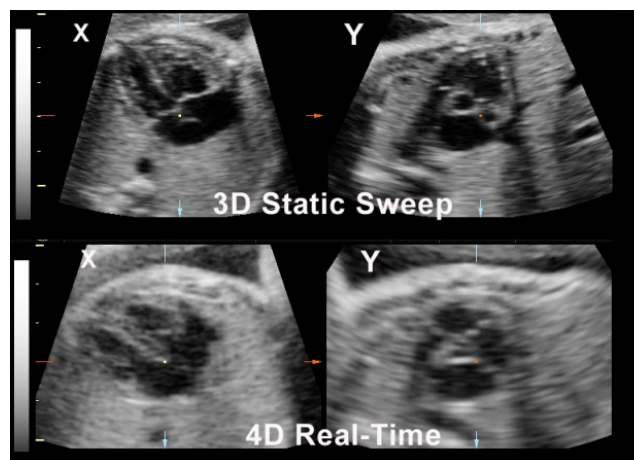


**Figure 7:** This compares images acquired using the 3D static sweep and the 4D real-time obtained with a mechanical array probe. The 4D real-time image was acquired at a volume rate of 6 Hz. To accomplish this requires a rapid sweep speed, thus resulting in a lower resolution image compared to the 3D static sweep in the upper panel. The only benefit of the 4D real-time display is that the examiner can visualize the contracting heart, although the frame rate is 6 Hz.

However, if the examiner is desirous of evaluating the heart in the Y and Z planes, this can be accomplished without introducing artifact, as is the case with the static or STIC acquisition, described above.

In 2002 Philips Ultrasound (Bothel, WA, USA) introduced the matrix array probe to adult cardiology in which all elements of the probe are fired simultaneously in a 3-dimensional matrix, generating a truncated pyramidal volume of ultrasound virtually instantaneously. This is in contrast to 3D/4D imaging described above which reconstructs volumes from a series of 2D images acquired over time. For this reason, “real-time” 3D technology, unlike reconstructive 3D technology, does not require cardiac gating to capture cardiac motion. Because of the faster frame

rate achieved with this technology than with the mechanical array probe, there is no movement artifact introduced into the Y and Z planes of the volume dataset (Fig. 8).

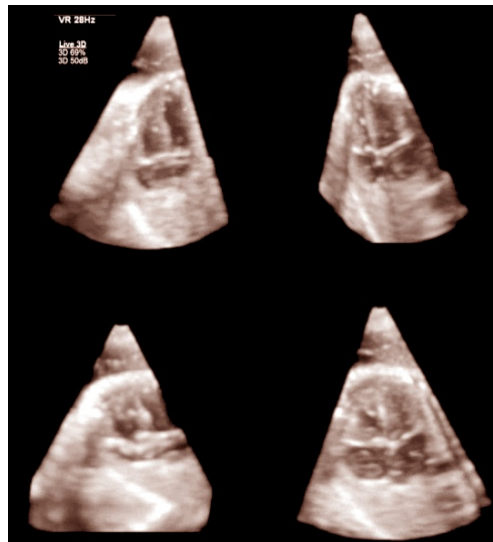


**Figure 8:** This is a real-time 4D volume examination of the fetal heart using the maxtrix array 4D probe. The images are of the fetal heart taken using different orientations of the cut plane as it passes through the four-chamber view. Because the ultrasound volume dataset is acquired simultaneously in all planes (X, Y, and Z), the volume rate is higher (28 volumes/second) than when using the mechanical array probe (6 volumes/second).

One of the limitations of the current technology is that the size of the acquired volume dataset is smaller than what can be acquired using STIC technology, which limits its use in the third trimester of pregnancy. However, a novel approach has recently been described to address this problem [66]. Because of lower transmitted ultrasound frequencies using the matrix array, the volume dataset acquired with the STIC technique provides the highest image resolution.

## ANALYSIS OF THE ACQUIRED VOLUMES

Although we have reviewed the different image acquisition techniques, the analysis of acquired volumes will focus on 3D and 4D STIC volume datasets. To illustrate the principles for each of the following topics a descriptive cine clip can be viewed that illustrates each step-by-step technique. A free copy of 4D View (GE-Kretz Voluson 730 Expert, Zipf, Austria) can be downloaded from the following Internet link: <http://www.volusonclub.net/4dview>. After downloading this program select the *Free Unlimited De-Featured Version* during the installation process. This will provide you with the basic elements for our discussion. Download two volume datasets that can be opened and analyzed with 4D View. The first volume is a B-Mode volume from a normal fetal heart.. The second is a normal color Doppler volume from a normal fetal heart.

### Rotating the XYZ Planes

Once the 3D/4D volume has been acquired, the examiner often chooses to rotate the XYZ planes to view cardiac anatomy from the A, B, or C reference images. To accomplish this there are two approaches. The rotation buttons can be used for each of the XYZ planes. However, this may be confusing to the examiner, depending upon which reference image is selected, A, B or C. The approach that I prefer uses the right and left buttons of the mouse. Click the following link to review the instructional cine entitled, "[ROTATION](#)"

### Transverse Sweep

The transverse sweep is a technique that has been used to evaluate the four-chamber, five-chamber, three-vessel and the tracheal views. If the examiner can demonstrate these views to be normal, then major structural abnormalities of the fetal heart can be excluded (Fig. 9). (74-76)

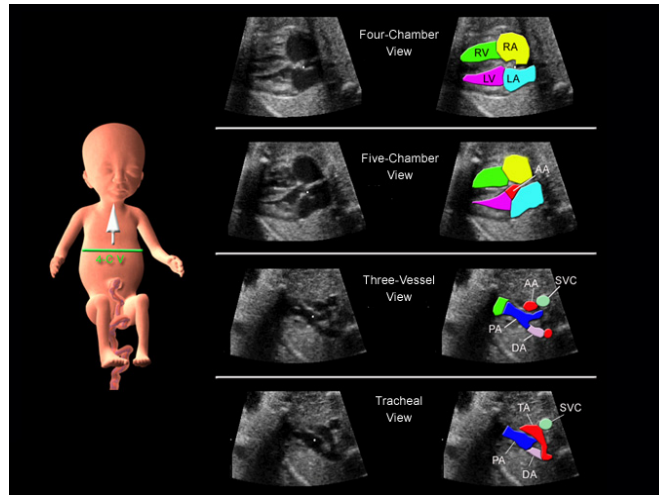


**Figure 9:** The views can be obtained by directing the ultrasound beam from the four-chamber view to the upper thorax in a transverse plane. The views that are observed in sequential order are the four-chamber view, the five-chamber view, the three-vessel view, and the tracheal view. If all of these views are normal, then major congenital heart defects can be eliminated. RA=right atrium, LA=left atrium, RV=right ventricle, LV=left ventricle, AA=ascending aorta, PA=pulmonary artery, SVC=superior vena cava, DA=ductus arteriosus, TA=transverse aortic arch.

These views can be examined from the 3D/4D volume by a simple technique of moving the reference dot through the B reference image, resulting in imaging of the above views in reference image A. Click the following link to review the instructional cine entitled, “[SWEEP.](#)”

### Spin Technique

This technique utilizes the concept of rotation, described above, to systematically identify the left outflow tract, the aortic arch, and the main pulmonary artery and its bifurcation (Fig. 10) [47].

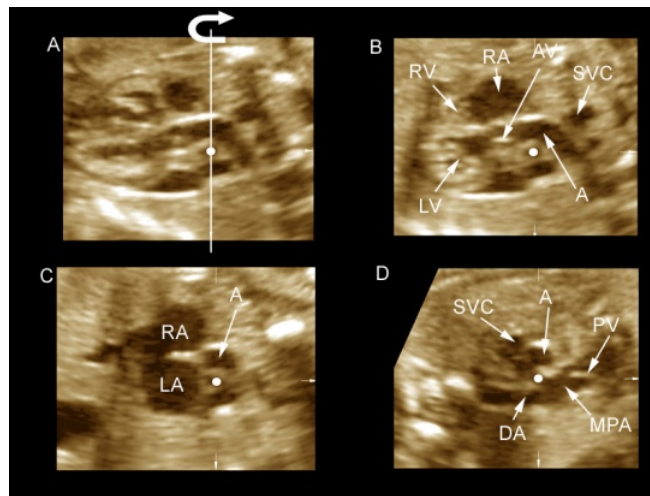


**Figure 10:** Panel A is the five-chamber view. The reference dot (white circle) is placed within the vessel inferior to the ascending aorta which should be the right pulmonary artery (A). The volume dataset is then turned around the Y axis (Panels B, C, and D) until the right pulmonary artery is elongated and demonstrated to exit the main pulmonary artery (Panel D). The “spin technique” can be used to identify any vessel in the cardiovascular system. These views are complimentary and additive to the transverse sweep, described above. Click the following link to review the instructional cine entitled, “[SPIN.](#)”

### Tomographic Imaging

Tomographic imaging displays multiple, simultaneous views of the heart from either a static or STIC volume [77] (Fig. 11).



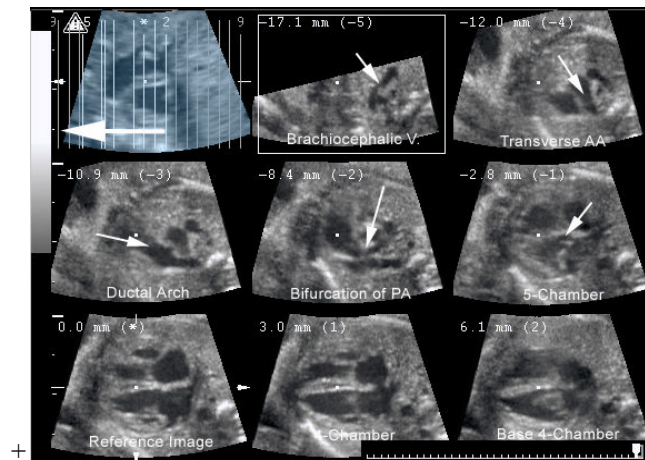


**Figure 11:** These images are from a STIC acquisition. The panel of 9 images are displayed at exactly the same point in the cardiac cycle. The upper left image has parallel lines that represent the labeled images that are perpendicular to this image. The reference image is indicated by an \*. From this point images to the right are indicated by + mm, while images to the left are indicated by – mm. For identification purposes, the + and – millimeters indicators are not useful, but the absolute value is. For example, the base of the four-chamber view is 6.1 mm below the reference image, the five-chamber view is 2.8 mm above the reference image, the bifurcation of the pulmonary artery is 8.4 mm above the reference image, and the transverse aortic arch is 12 mm above the reference image.

The benefit of this technique is that the examiner can view the necessary transverse views (4-chamber, 5-chamber, 3-vessel, and tracheal) used to screen for congenital heart defects. Click the link to review the instructional cine entitled, “[TUI.](#)”

### Rendering

Another benefit of static and STIC volume acquisitions is that the 2D images contained within each volume can be compiled to create a 3-dimensional model of the heart. For example, the typical 2-dimensional four-chamber view can be rendered to provide a 3-dimensional structure that demonstrates depth. Fig. 12 illustrates a 3-dimensional rendered image that demonstrates and inferior vena cava in the back wall of the right atrium.

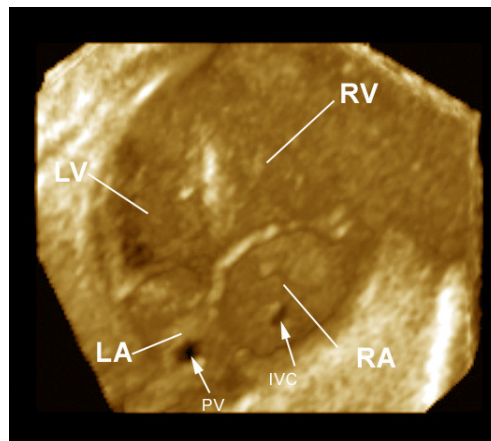


**Figure 12:** This is a 3D rendered four-chamber view of the fetal heart. While the image has the appearance of a 2D image, the rendering provides depth so that the back walls of the atrial and ventricular chambers can be identified. The right atrium demonstrates the opening of the inferior vena cava (IVC) and the left atrium the opening of one of the pulmonary veins (PV). RA=right atrium, LA=left atrium, RV=right ventricle, LV=left ventricle.

Click the link to review the instructional cine entitled, “[RENDERING.](#)”

### Invert

Another method utilized for creating a 3-dimensional image of the heart is the inversion mode. This technique requires the examiner to render the 3-dimensional heart (see above, Rendering) and then invert the colors. This

creates an image that has the appearance of a mold of the heart (Fig. 13). Click the link to review the instructional cine entitled, [“INVERT”](#)

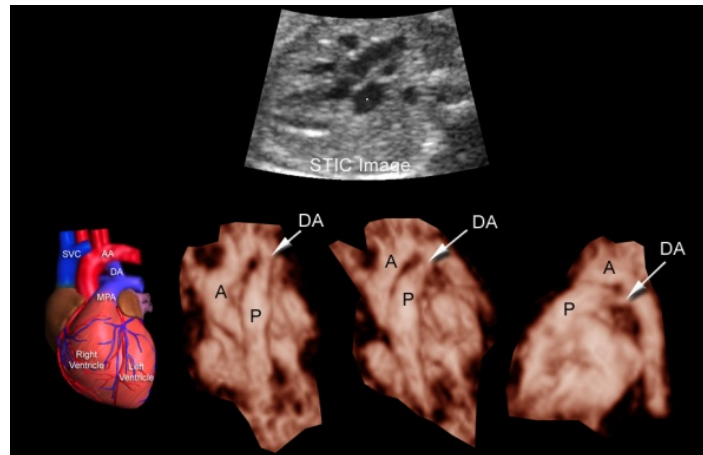


**Figure 13:** The STIC B-mode image is of the left outflow tract as it exits the left ventricle. The rendered inverted images demonstrate the crossing of the main pulmonary artery (P) and the aorta (A) as well as the ductus arteriosus (DA).

### Examination of the Interventricular Septum

Evaluation of the ventricular septum is usually performed at the level of the four-chamber view. Unfortunately, this view represents only a portion of the septum. Using 3D/4D STIC acquisitions the entire septum can be examined for evidence of defects that are not in plane of the four-chamber view [18] (Fig. 4). Click the link to review the instructional cine entitled, [“SEPTUM.”](#)

### Identification of the Aortic and Ductal Arches

Many examiners have difficulty identifying the aortic and ductal arches without using a systematic approach (Fig. 14).

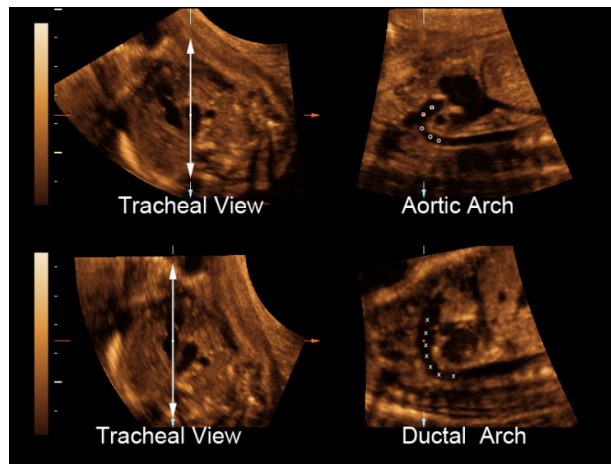


**Figure 14:** The aortic and ductal arches can be identified by aligning their respective vessels at the level of the tracheal view. After aligning each vessel in the vertical plane, the perpendicular image reveals the aortic and ductal arches, respectively.

Using 3D/4D STIC acquisitions, a systematic approach can be used to identify these vessels. The cine clip entitled “ARCHES” will illustrate two techniques for identification of the aortic arch and one technique for identification of the ductal arch. Click the link [“ARCHES”](#) to review the instructional cine.

### Rendered B-Flow

B-mode ultrasound identifies soft tissue and the blood pool when examining fetal cardiovascular structures. However, it does not identify the flow of blood. In order for most examiners to identify blood flow color Doppler or

Power Doppler is used. One of the problems with the rendered color Doppler image is that the borders are not as well defined between the blood pool and the chamber walls. However, B-flow is a technique in which moving red blood cells are identified from the B-mode image (Fig. 15).

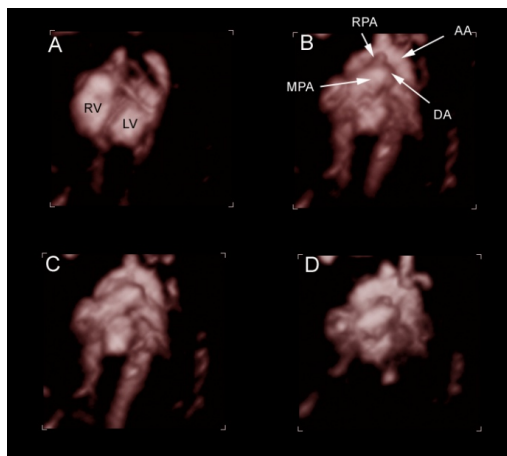


**Figure 15:** This is a B-flow image sequence from a 17 week fetus. Panel A represents filling of the right (RV) and left (LV) ventricular chambers during diastole. Panel B demonstrates ventricular systole after the ventricles have emptied. This image demonstrates the relationships of the main pulmonary artery (MPA), right pulmonary artery going beneath the aortic arch (AA) and the ductus arteriosus (DA) emptying into the thoracic aorta. Panel C is similar to panel B except later in the systolic cycle. Panel D is the same image as panel C except the volume has been rotated to show the perpendicular relationship of the MPA and the AA.

This technology does not utilize Doppler principles to display blood flow. Once the B-flow image is acquired, it can be rendered to provide a 3-dimensional structure of the fetal cardiovascular system that resembles an angiogram. Click the link to view the instructional cine entitled, "[BFLOW](#)."

### Color Doppler

When a STIC acquisition includes color Doppler, the examiner can adjust the color settings so that the color does not override the vessel or chamber walls. Click the link to view the instructional cine entitled "[COLOR](#)".

### CONCLUSION

This communication has attempted to provide an overview of 3D/4D examination of the fetal heart. Although the 3D static and 4D STIC volume datasets are easy to acquire, the difficulty occurs when the volumes are analyzed. As this paper illustrates, there are a number of tools the examiner can use to evaluate acquired volumes of the fetal heart. Understanding how to use the tools enhances the evaluation of the fetal heart, especially when pathology is suspected.

### REFERENCES

- [1] Esh-Broder E, Ushakov FB, Imbar T, Yagel S. Application of free-hand three-dimensional echocardiography in the evaluation of fetal cardiac ejection fraction: a preliminary study. *Ultrasound Obstet Gynecol* 2004; 23(6): 546-51.
- [2] Simpson JM, Cook A. Repeatability of echocardiographic measurements in the human fetus. *Ultrasound Obstet Gynecol* 2002; 20(4):332-9.
- [3] Teichholz LE, Kreulen T, Herman MV, Gorlin R. Problems in echocardiographic volume determinations: echocardiographic-angiographic correlations in the presence or absence of asynergy. *Am J Cardiol* 1976; 37(1):7-11.
- [4] Bhat AH, Corbett V, Carpenter N, *et al.* Fetal ventricular mass determination on three-dimensional echocardiography: studies in normal fetuses and validation experiments. *Circulation* 2004; 110(9):1054-60.
- [5] Wyatt HL, Meerbaum S, Heng MK, Gueret P, Corday E. Cross-sectional echocardiography. III. Analysis of mathematic models for quantifying volume of symmetric and asymmetric left ventricles. *Am Heart J* 1980; 100(6 Pt 1):821-8.
- [6] Sedmera D, Pexieder T, Vuillemin M, Thompson RP, Anderson RH. Developmental patterning of the myocardium. *Anat Rec* 2000; 258(4): 319-337.
- [7] Simpson J. Echocardiographic evaluation of cardiac function in the fetus. *Prenat Diagn* 2004; 24 (13): 1081-91.



- [8] Bhat AH, Corbett VN, Liu R, *et al.* Validation of volume and mass assessments for human fetal heart imaging by 4-dimensional spatiotemporal image correlation echocardiography: in vitro balloon model experiments. *J Ultrasound Med* 2004; 23(9):1151-
- [9] Espinoza J, Gotsch F, Kusanovic, JP, *et al.* Changes in fetal cardiac geometry with gestation: implications for 3- and 4-dimensional fetal echocardiography. *J Ultrasound Med* 2007; 26(4): 427-43.
- [10] Levental M, Pretorius DH, Sklansky MS, Budorick NE, Nelson TR, Lou K. Three-dimensional ultrasonography of normal fetal heart: comparison with two-dimensional imaging. *J Ultrasound Med* 1998; 17(6):341-8.
- [11] Meyer-Wittkopf M, Cole A, Cooper SG, Schmidt S, Sholler GF. Three-dimensional quantitative echocardiographic assessment of ventricular volume in healthy human fetuses and in fetuses with congenital heart disease. *J Ultrasound Med* 2001; 20(4):317-27.
- [12] Tutschek B, Sahn DJ. Semi-automatic segmentation of fetal cardiac cavities: progress towards an automated fetal echocardiogram. *Ultrasound Obstet Gynecol* 2008; 32(2):176-80.
- [13] Uittenbogaard LB, Haak MC, Spreuwenberg MD, VanVugt JMG. A systematic analysis of the feasibility of four-dimensional ultrasound imaging using spatiotemporal image correlation in routine fetal echocardiography. *Ultrasound Obstet Gynecol* 2008; 31(6): 625- 32.
- [14] Huhta J. Congestive heart failure in the fetus. In *Fetal Cardiology* (2<sup>nd</sup> edition), Yagel S, Silverman NH, Gembruch U (eds.). Informa Healthcare USA, Inc: New York, NY, 2009; 561-78.
- [15] Messing B, Cohen SM, Valsky DV, *et al.* Fetal cardiac ventricle volumetry in the second half of gestation assessed by 4D ultrasound using STIC combined with inversion mode. *Ultrasound Obstet Gynecol* 2007; 30(2):142-51.
- [16] Molina FS, Faro C, Sotiriadis A, Dagklis T, Nicolaidis KH. Heart stroke volume and cardiac output by four-dimensional ultrasound in normal fetuses. *Ultrasound Obstet Gynecol* 2008; 32(2):181-7.
- [17] Rizzo G, Capponi A, Cavicchioni O, Vendola M, Arduini D. Fetal cardiac stroke volume determination by four-dimensional ultrasound with spatio-temporal image correlation compared with two-dimensional and Doppler ultrasonography. *Prenat Diagn* 2007; 27(12): 1147-50.
- [18] Uittenbogaard LB, Haak MC, Spreuwenberg MD, VanVugt JMG. Fetal cardiac function assessed with four-dimensional ultrasound imaging using spatiotemporal image correlation. *Ultrasound Obstet Gynecol* 2009; 33(3):272-81.
- [19] DeVore GR, Falkensammer P, Sklansky MS, Platt LD. Spatio-temporal image correlation (STIC): new technology for evaluation of the fetal heart. *Ultrasound Obstet Gynecol* 2003; 22(4):380-7.
- [20] Gonçalves LF, Lee W, Espinoza J, Romero R. Examination of the fetal heart by four-dimensional (4D) ultrasound with spatio-temporal image correlation (STIC). *Ultrasound Obstet Gynecol* 2006; 27(3):336-48.
- [21] Nelson TR, Pretorius DH, Sklansky M, Hagen-Ansert S. Three-dimensional echocardiographic evaluation of fetal heart anatomy and function: acquisition, analysis, and display. *J Ultrasound Med* 1996; 15(1):1-9.
- [22] Gonçalves LF, Espinoza J, Lee W, Mazor M, Romero R. Three- and four-dimensional reconstruction of the aortic and ductal arches using inversion mode: a new rendering algorithm for visualization of fluid-filled anatomical structures. *Ultrasound Obstet Gynecol* 2004; 24(6):696-98.
- [23] National Institute of Standards and Technology. Guidelines for Evaluating and Expressing the Uncertainty of NIST Measurement Results. <http://emtoolbox.nist.gov/Publications/NISTTechnicalNote1297s.pdf> (July 13 2009).
- [24] Bartlett JW, Frost C. Reliability, repeatability and reproducibility: analysis of measurement errors in continuous variables. *Ultrasound Obstet Gynecol* 2008; 31(4): 466-75.
- [25] Hamill N, Romero R, Hassan S, *et al.* The repeatability and reproducibility of fetal cardiac ventricular volume calculations utilizing Spatio-Temporal Image Correlation (STIC) and Virtual Organ Computer-aided AnaLysis (VOCAL™). *J Ultrasound Med*, in press.
- [26] Mielke G, Benda N. Cardiac output and central distribution of blood flow in the human fetus. *Circulation* 2001; 103(12):1662-8.
- [27] Stewart WJ, Jiang L, Mich R, Pandian N, Guerrero JL, Weyman AE. Variable effects of changes in flow rate through the aortic, pulmonary and mitral valves on valve area and flow velocity: impact on quantitative Doppler flow calculations. *J Am Coll Cardiol* 1985; 6(3):653-62.
- [28] Eik-Nes S, Marsal K, Kristofferson K. Methodology and basic problems related to blood flow studies in the human fetus. *Ultrasound Med Biol* 1984; 10(3):329-37.
- [29] Chaoui R, Heling KS, Taddei F, Bollmann R. Doppler echocardiographic analysis of blood flow through the fetal aorta and pulmonary valve in the second half of pregnancy. *Geburtshilfe Fraunheilkd* 1995; 55(4): 207-17.
- [30] Rasanen J, Wood DC, Weiner S, Ludomirski A, Huhta JC. Role of the pulmonary circulation in the distribution of human fetal cardiac output during the second half of pregnancy. *Circulation* 1996; 94(5): 1068-1073.
- [31] Thornburg KL, Reller MD. Coronary flow regulation in the fetal sheep. *Am J Physiol* 1999; 277(5 Pt 2): R1249-60.
- [32] Schmidt KG, Silverman NH, Hoffman JIE. Determination of ventricular volumes in human fetal hearts by two-dimensional echocardiography. *Am J Cardiol* 1995; 76(17):1313-16.

- [33] Allan LD, Chita SK, Al-Ghazali W, Crawford DC, Tynan M. Doppler echocardiographic evaluation of the normal human fetal heart. *Br Heart J* 1987; 57(6):528-33.
- [34] De Smedt MC, Visser GH, Meijboom EJ. Fetal cardiac output estimated by Doppler echocardiography during mid- and late gestation. *Am J Cardiol* 1987; 60(4):338-42.
- [35] Kenny JF, Plappert T, Doubilet P, *et al.* Changes in intracardiac blood flow velocities and right and left ventricular stroke volumes with gestational age in the normal human fetus: a prospective Doppler echocardiographic study. *Circulation* 1986; 74(6):1208-16.
- [36] Veille JC, Sivakoff M, Nemeth M. Evaluation of the human fetal cardiac size and function. *Am J Perinatol* 1990; 7(1):54-9.
- [37] Anderson PAW. Myocardial development. In *Fetal and Neonatal Cardiology*, Long W (ed.). W.B. Saunders: Philadelphia, PA, 1990; 17-38.
- [38] Teitel DF. Physiologic Development of the Cardiovascular System in the Fetus. In *Fetal and Neonatal Physiology* (3<sup>rd</sup> edition), Polin RA, Fox WW, Abman H (eds.). W.B. Saunders: Philadelphia, PA, 2003; 609-19.
- [39] Winberg P, Jansson M, Marions L, Lundell BP. Left ventricular output during postnatal circulatory adaptation in healthy infants born at full term. *Arch Dis Child* 1989; 64:1374-78.
- [40] Pemberton J, Li X, Kenny A, Davies CH, Minette MS, Sahn DJ. Real-time 3-dimensional Doppler echocardiography for the assessment of stroke volume: an in vivo human study compared with standard 2-dimensional echocardiography. *J Am Soc Echocardiogr* 2005; 18(10):1030-36.

## The Applications of HD and B Flow in 4D Echocardiography

Simcha Yagel, Sarah M Cohen, Dan V Valsky, Michal Lipscheutz and Baruch Messing

*Department of Obstetrics and Gynecology, Hadassah-Hebrew University Medical Centers-Mt. Scopus, Jerusalem, Israel*

**Abstract:** High Definition Power Flow Doppler (HDPD) is a bi-directional power Doppler imaging mode. B-flow is a direct-volume non-gated scanning tool that images blood flow in real-time. These ultrasound modalities have improved images of the fetal cardiovascular system to near-angiographic quality. Each has its particular advantages, which are illustrated with examples of fetal cardiovascular malformations obtained with these tools. HDPD and B-flow provide images not available to practitioners even five years ago.

### INTRODUCTION

3D and 4D ultrasound (3D/4D US) modalities have provided new ways to look at fetal echocardiographic examination [1]. These modalities are the result of impressive technological advances in motion-gated scanning and in faster frame rates and computer processors. Near real-time 3D scanning is now a reality in the clinical setting and its application to fetal echocardiography continues to enrich our understanding of the fetal cardiovascular system. Two acquisition modes, B-flow and High Definition Power Flow Doppler (HDPD) each have unique capabilities that allow greater sensitivity in imaging fetal blood flow in the heart and vessels.

### HIGH DEFINITION POWER FLOW DOPPLER

High definition power flow Doppler (HDPD) is a bi-directional power Doppler mode that depicts flow at a lower velocity than color or power Doppler. It can be combined with STIC [2] or static 3D acquisition. HDPD uses small sample volume and higher resolution to achieve images with two color directional information while avoiding overwriting vascular walls. The result is a more accurate picture of vessel contours. This modality depicts blood flow at a lower velocity than color or power Doppler, making for a bidirectional and anatomically accurate depiction of blood flow. The sensitivity of HDPD results in imaging of systolic and diastolic blood flow at the same time: for example, when HDPD is combined with STIC acquisition the ductus venosus is shown to remain filled both in systole and diastole. Figure 1 shows the normal heart and vessels extracted from a STIC acquisition with high definition Doppler.

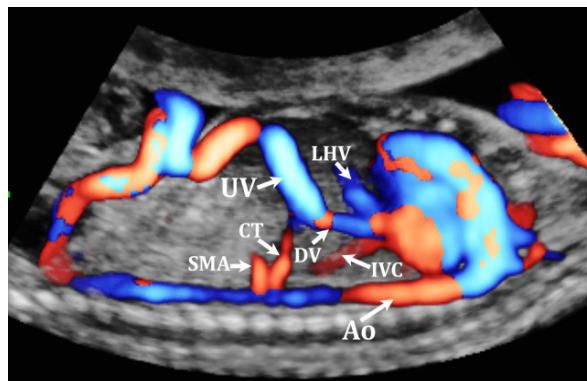


**Figure 1:** Normal heart and vasculature imaged in HDPD modality. UV, umbilical vein; LHV, left hepatic vein; SMA, superior mesenteric artery; CT, celiac trunk; DV, ductus venosus; IVC, inferior vena cava; Ao, aorta.

The caveats associated with 3D/4D technology and Doppler based images apply to HDPD as well: care must be taken when the volume is rotated, to avoid confusion of flow direction. The operator must be vigilant in confirming suspected pathology by verifying the original scanning angle, and whether flow was toward or away from the transducer.

### B-FLOW

B-flow is a newer technology in fetal cardiac studies. It is a direct-volume non-gated scanning tool that displays blood flow in real time. It is based on B-mode imaging for direct depiction of blood cell reflectors. That is to say, B-flow does not rely on Doppler shift to produce an “indirect” image of blood flow, thus it avoids some of the drawbacks of Doppler imaging such as aliasing and signal dropout at orthogonal scanning angles. B-flow results in

faster frame rates by using digital encoding of one US beam into two separate sub-beams before transmittance. Echoes from the two sub-beams are decoded differently. One sub-beam serves for conventional gray-scale myocardial imaging while the other is enhanced to provide gray-scale blood-flow imaging [3, 4]. B-flow provides sensitive ‘digital casts’ [5] of blood flowing in its vessels and the cardiac chambers. This makes it an invaluable tool in fetal echocardiography in both normal and anomalous cases. It is particularly valuable as a teaching tool, as well as in multi-disciplinary consultation and in counseling parents, when complex anatomy must be elucidated. Figure 2 shows a normal fetal heart and great vessels acquired with B-flow combined with spatio-temporal imaging correlation (STIC).

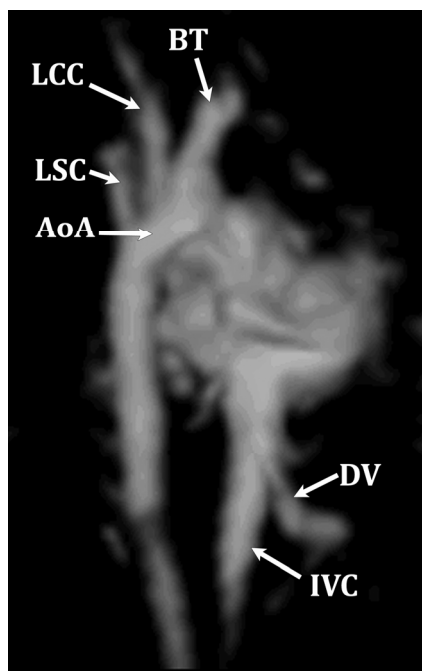


**Figure 2:** Normal heart and vasculature imaged in B-flow modality. AoA, aortic arch; LSC, left subclavian artery; LCC, left common carotid; BT, brachio-cephalic trunk; DV, ductus venosus; IVC, inferior vena cava.

As the figures below (Figures 3-20) show through various examples of cardiovascular malformations imaged in HDPD and B-flow, these new modalities provide practitioners with near-angiographic images of the fetal heart and vessels.

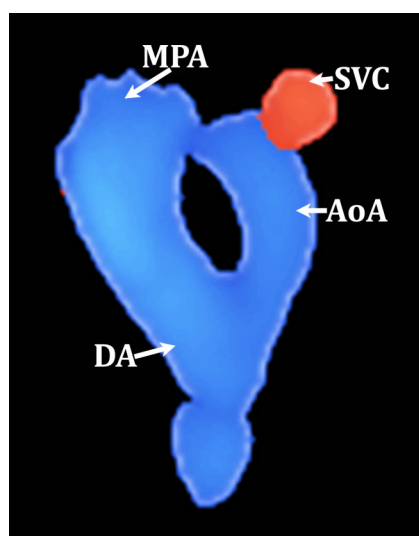


**Figure 3:** Right aortic arch anomaly, three-vessels and trachea (3VT) view, imaged in HDPD. MPA, main pulmonary artery; SVC, superior vena cava, AoA, transverse plane of the aortic arch; DA, ductus arteriosus. The ellipse in the center is the space occupied by the esophagus and trachea.

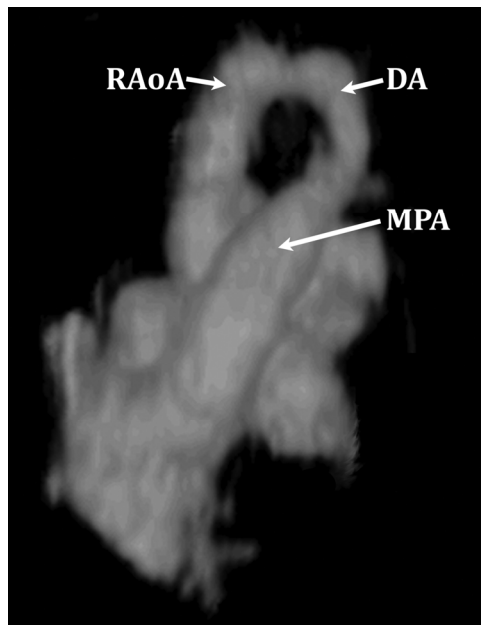


**Figure 4:** Another case of right aortic arch anomaly in the 3VT plane, imaged with B-flow. RAoA, right aortic arch; DA, ductus arteriosus; MPA, main pulmonary artery.

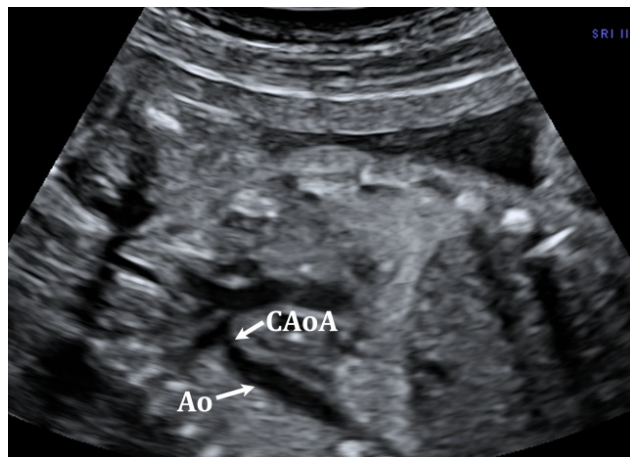


**Figure 5:** Segmental coarctation of the aorta in grayscale imaging of the long axis view aortic arch. Ao, descending aorta; CAoA, the coarctated aortic arch.

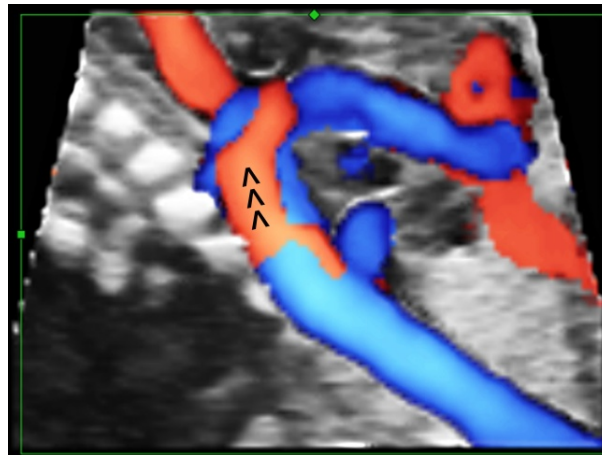


**Figure 6:** The same patient as figure 5: HDPD depicts reverse flow in the coarctation, however it does not demonstrate the narrowing of the vessel. Carets indicate the coarctation and the direction of flow.

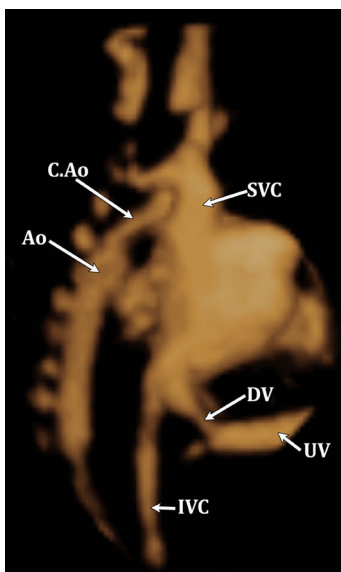


**Figure 7:** The same patient as figures 5 and 6, imaged in B-flow in right lateral view. Note that the narrowing of the aorta is clearly depicted. Ao, aorta; C.Ao, coarctation; SVC, superior vena cava; DV, ductus venosus; UV, umbilical vein; IVC, inferior vena cava.

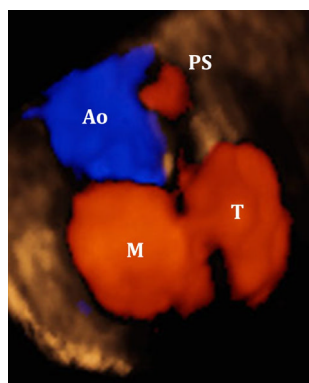


**Figure 8:** HDPD imaging with virtual planes [6] in a case of severe pulmonic stenosis. The coronal atrio-ventricular valves (CAV) plane shows the flow across the mitral (M) and tricuspid (T) valves and the aortic valve (Ao). Note the severe narrowing of the pulmonic valve annulus and reversed flow across the valve (PS).



**Figure 9:** A complicated case of transposition of the great arteries (TGA). B-flow shows that the aorta (Ao) is anterior and to the right of the pulmonary artery (PA).

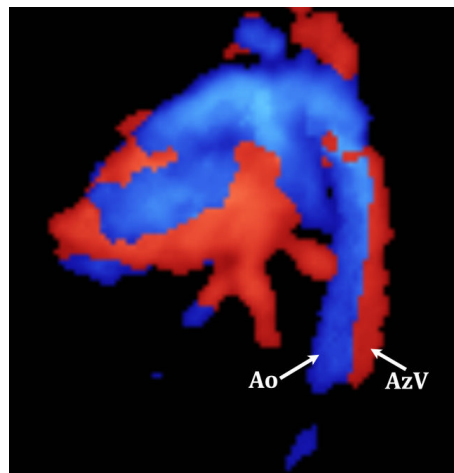


**Figure 10:** Azygos vein (AzV) flow is opposite the flow in the aorta (Ao) in this case of interrupted IVC with azygos continuation imaged in HDPD.



**Figure 11:** The vertical vein in a case of total anomalous pulmonary venous connections (TAPVC). The vertical vein (VV) is seen to cross the diaphragm (small arrows) and drains into the hepatic vessels. Note the presence of two left liver lobes and hepatic veins (HV) in this case of left isomerism.

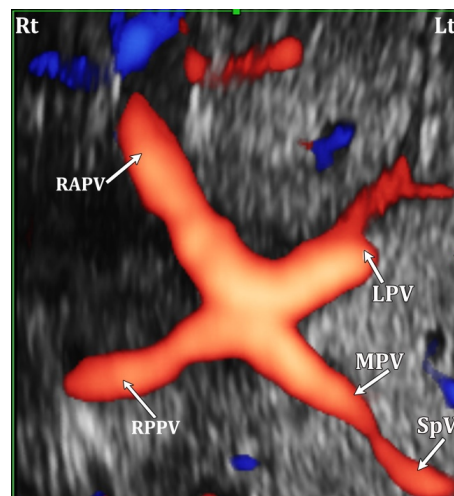


**Figure 12:** The great sensitivity of HDPD is demonstrated by this image of the normal fetal portal system, including the splenic vein. RAPV, right anterior portal vein; RPPV, right posterior portal vein; LPV, left portal vein; MPV, main portal vein; SpV, splenic vein (Rt, Lt: right and left).



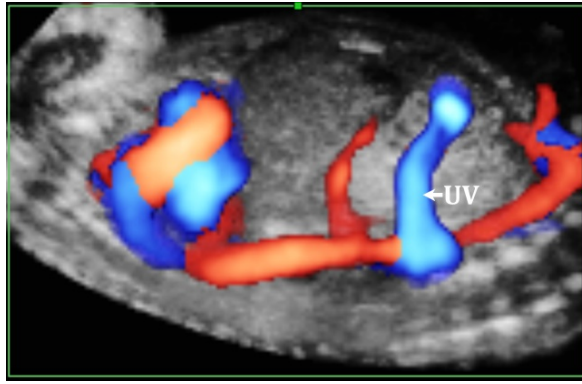


**Figure 13:** A case of agenesis of the ductus venosus (ADV) with a wide connection of the umbilical vein (UV) to the azygos-IVC shunt, and abnormal portal system.

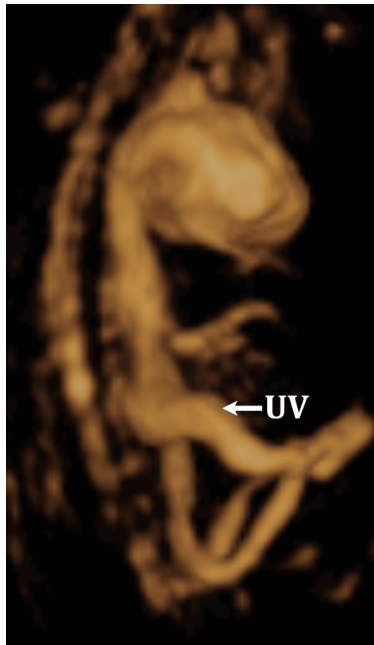


**Figure 14:** The same case as pictured in figure 13, imaged in B-flow. Note the wide connection of the UV to the azygos-IVC shunt and abnormal portal system.

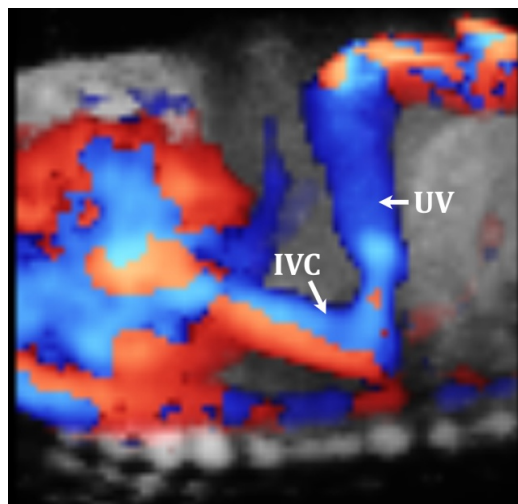


**Figure 15:** HDPD image of ADV to the IVC with a narrow shunt. The portal system (not shown) developed normally. UV, umbilical vein.



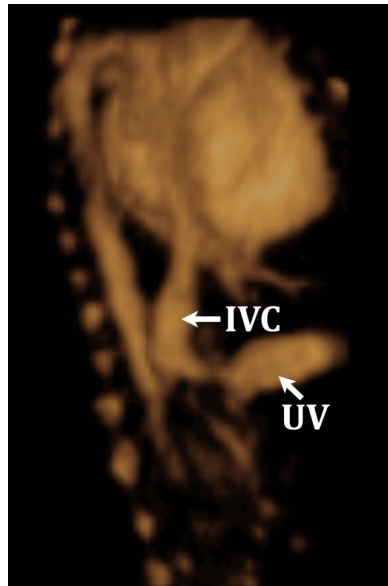


**Figure 16:** The same case imaged in B-flow as pictured in figure 15, showing the narrow shunt between the UV and IVC, which may account for the normal development of the portal system (not shown).

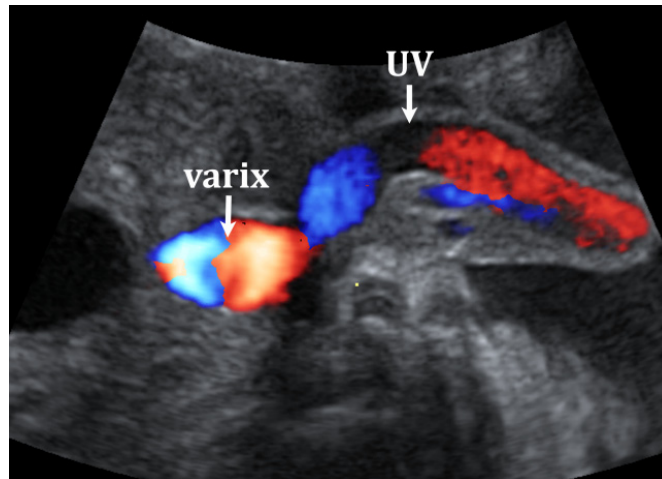


**Figure 17:** Fetal abdominal umbilical vein (FIUV) varix imaged in HDPD. Note the diameter of the varix is more than 1.5 times that of the umbilical vein (UV).

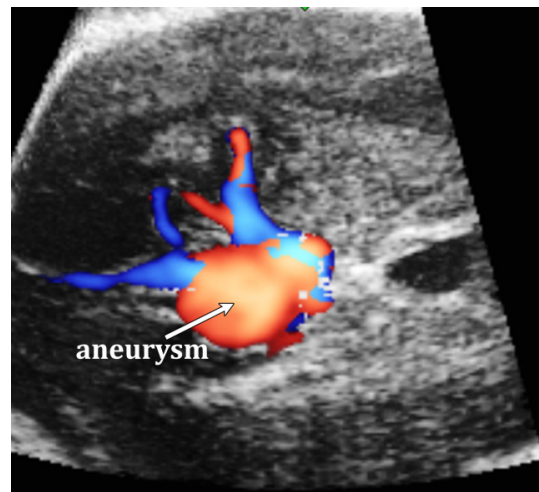


**Figure 18:** HDPD scan of aneurysm of the vein of Galen defect with surrounding tissue.

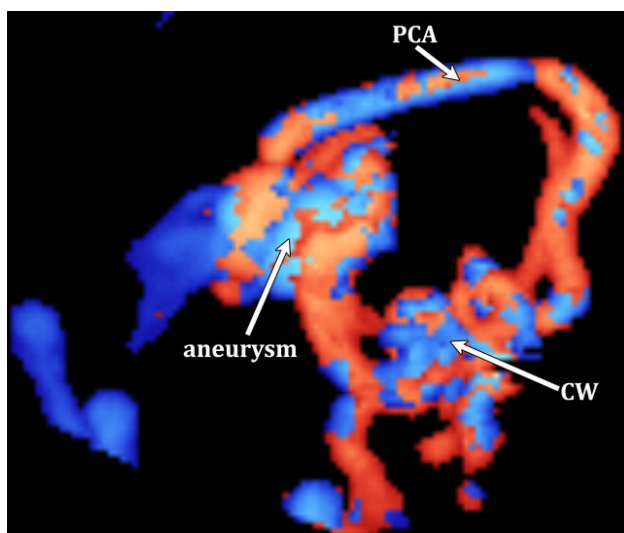


**Figure 19:** The same case as figure 18, showing the widened pericolossal artery (PCA) associated with this malformation, and the tortuous circle of Willis (CW).

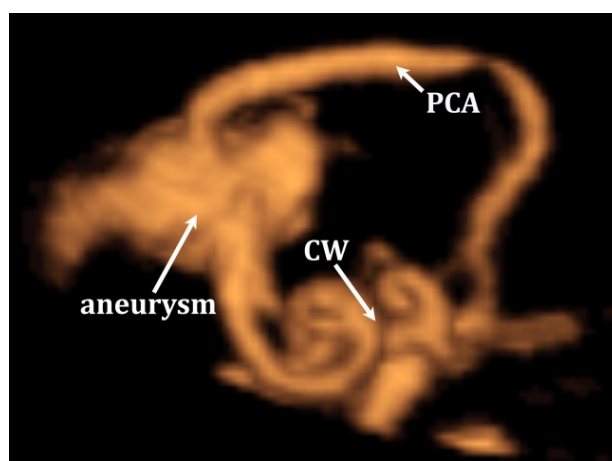


**Figure 20:** The same case of vein of Galen defect as shown in figures 18 and 19, imaged in B-flow. CW, the tortuous circle of Willis; PCA, the widened pericolossal artery.

## CONCLUSIONS

The HDPD and B-flow modalities impart enormous advantages in fetal cardiovascular scanning, improving image clarity and thereby our understanding of the normal and anomalous fetal heart and vasculature.

## REFERENCES

- [1] Yagel S, Cohen SM, Shapiro I, Valsky DV. 3D and 4D ultrasound in fetal cardiac scanning: a new look at the fetal heart. *Ultrasound Obstet Gynecol.* 2007; 29: 81-95.
- [2] DeVore GR, Falkensammer P, Sklansky MS, Platt LD. Spatio-temporal image correlation (STIC): new technology for evaluation of the fetal heart. *Ultrasound Obstet Gynecol.* 2003; 22: 380-7.
- [3] Deng J, Rodeck CH. Current applications of fetal cardiac imaging technology. *Curr Opin Obstet Gynecol.* 2006; 18: 177-84.
- [4] Pooh RK. New application of B-flow sono-angiography in perinatology. *Ultrasound Obstet Gynecol.* 2000; 15: 163.
- [5] Goncalves LF, Espinoza J, Lee W *et al.* A new approach to fetal echocardiography: digital casts of the fetal cardiac chambers and great vessels for detection of congenital heart disease. *J Ultrasound Med.* 2005; 24: 415-24.
- [6] Yagel S, Benachi A, Bonnet D *et al.* Rendering in fetal cardiac scanning: the intracardiac septa and the coronal atrioventricular valve planes. *Ultrasound Obstet Gynecol.* 2006; 28: 266-74.

## 3D Live Echocardiography with Matrix Probes

Fabrizio Taddei\*, Laura Franceschetti, Giuliano Farina and Gianpaolo Grisolia

*Department of Obstetrics and Gynecology Azienda Ospedaliera "C.Poma" - Mantova - Italy*

**Abstract:** Real-time four-dimensional (4D) echocardiography is the examination of the fetal heart in the three spatial dimensions plus motion. The matrix probe's technology allows direct volume scanning by electronically interrogation of a region of interest and acquisition of a pyramidal volume of ultrasonographic data. This technology has the potential to minimize motion artifacts associated with 3D/4D ultrasonography with a satisfactory spatial resolution. The system allows beam steering and focusing in the 3D volume dataset, making it possible to simultaneously examine two different planes of section of the same structure, in real-time, without resolution loss (*Live xPlane imaging*). The system achieves a pyramidal volume of data, creating a new real-time 3D moving imaging mode called *Live 3D Volume Imaging*, without the use of software-reconstructed section planes. Combination with Doppler techniques creates a new imaging option: *Full Volume 3D imaging*. The technique of *Thick Slice Live Volume Imaging* allows high resolution and contrast-enhanced images. The strength of this technology is the easiness in obtaining real-time images of the heart, the high volumetric frame rate and the opportunity to obtain scanning planes with the same axial and lateral resolution. These features improve the overall understanding of anatomical structure arrangement. Matrix technology could be very useful in congenital cardiac clinical applications: real-time 3D echocardiography shows instantaneous rendered images of the beating fetal heart with complex pathologies in one complete heart cycle, and application of this modality allows its spatial location in the heart and its temporal location in the cardiac cycle.

**Key Words:** 3D Ultrasound, Fetal Echocardiography, Live Echocardiography, Matrix Probes.

### INTRODUCTION

Real-time four-dimensional (4D) echocardiography is the examination of the fetal heart in the three spatial dimensions plus motion. In order to produce real-time 4D ultrasonographic images, volume datasets need to be acquired and displayed faster than the capacity of the human eye to retain a visual impression, which is estimated as one tenth to one thirtieth of a second. However, because of the difficulty in obtaining a fetal electrocardiogram to gate the heart, real time fetal echocardiography has been limited [1-14]. Different 3D echocardiographic methods have been employed in fetal echocardiography, including multiplanar, surface rendering, power and color Doppler methods or spatiotemporal image correlation. These techniques are limited by the use of off-line system, increasing reconstruction-time. With the advent of a new matrix array probe that allows real-time 4D data acquisition and image rendering, many of the above limitations could be circumvented.

The matrix probe's technology is capable of direct volume scanning. Direct volume scanning is a term proposed by Deng in 2003, to describe 3D/4D systems capable of scanning a volume of interest (1) in its totality, (2) within a time in which movement is negligible (in an instant), and (3) with sufficient spatial resolution. Since in the case of mechanical transducers the totality of the volume of interest is not scanned in an instant, the term "indirect volume scanning" applies to 3D/4D ultrasound systems that employ this technology. This has considerable implications for the examination of the moving fetus and, specially, the fetal heart, since motion artifacts can easily interfere with the quality of the images obtained if the structure of interest moves faster than the speed at which the volume dataset is being acquired. In contrast, matrix array transducers allow direct volume scanning by electronically interrogation of a region of interest and acquisition of a pyramidal volume of ultrasonographic data. This technology has the potential to minimize motion artifacts associated with 3D/4D ultrasonography and, giving a satisfactory spatial resolution, has become an attractive alternative to examine fetal heart.

### THE TECHNOLOGY

xMATRIX transducers are made by a double array of piezoelectrics elements that creates a matrix area of pulsing. This transducer's technology is based on a special laser used to cut the piezoelectric crystal into many equal-sized square elements, forming an xMATRIX element (Fig. 1).

\*Address correspondence to Fabrizio Taddei: Dept. Obstet. Gynecol. Azienda Ospedaliera "C.Poma" -Mantova-Italy; E-mail: taddei.fabrizio@tiscali.it

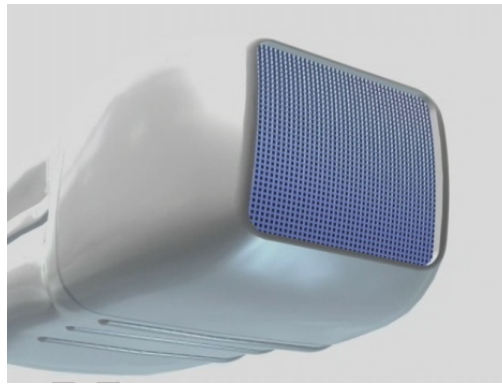


**Figure 1:** Surface of xMatrix probe.

These elements are directly connected with the beamformer in one way and with the surface of the transducer on the other hand. The beamformer permits to electronically drive these elements to fire the ultrasound beam in any direction in the space. The xMATRIX array transducer produces pyramidal volumetric ultrasound beam, composed by the beams emitted by each single element (Fig. 2).

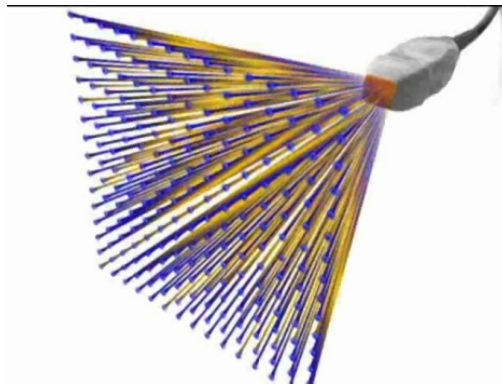


**Figure 2:** Pyramidal ultrasound beam electronically produced by xMatrix transducer.

This pulsing technique permits to create new imaging modes, other than standard 2D ultrasound image obtained by arranging the pulsing elements in a linear way.

The system allows beam steering and focusing in the 3D volume dataset, making it possible to simultaneously examine two different planes of section of the same structure, in real-time, without resolution loss (Live xPlane imaging). In this modality, images are shown on a screen divided into two parts: the original plane is on the left-hand side, while the right-hand side shows one of the different scanning planes that the sonographer can visualize using a different orientation of the ultrasound beam in the space.

This second plane can be perpendicular to the main scanning plane, but it can also be parallel or oblique. In this way, starting, for example, from an axial view of the fetal thorax showing the four chambers, and orientating the second plane (simultaneously shown on the right-hand side of the screen) in different directions, the main structures of the fetal heart can be visualized

The strength of the xMATRIX array approach for examination of fetal structures lies in the possibility of directly acquiring a pyramidal volume of ultrasonographic data, creating a new imaging mode called Live 3D Volume Imaging. By appropriately defining the ultrasound beam for each single element, it is possible to build up a pyramidal volumetric ultrasound beam, with an opening angle between 6 and 110 degrees). This volumetric ultrasound beam allows a real-time three-dimensional moving imaging (live volume imaging) without the use of software-reconstructed section planes. In other words, the volume is not created from single planes, but from a number of planes simultaneously close one to each other. This makes the voxels to have the same resolution along all the three directions of the beam (isovoxel resolution). Two orthogonal reference planes are used to localize the structures within the volume. This kind of imaging can give us the classic multiplanar view with visualization of the

three orthogonal planes in the same time, or the rendering view. Rendering is subjected to all the parameters that allow this algorithm to selectively display surface of the structures, hyperechoic or hypoechoic structures. These parameters should be set-up every time in order to create a good visualization of the rendered image.

By acquiring a high-resolution volume image even combined with Doppler techniques (color or power) a new imaging option is obtained from the xMATRIX technology: Full Volume 3D imaging. This acquisition mode gives both functional and structural data for a complete analysis (Fig. 3).

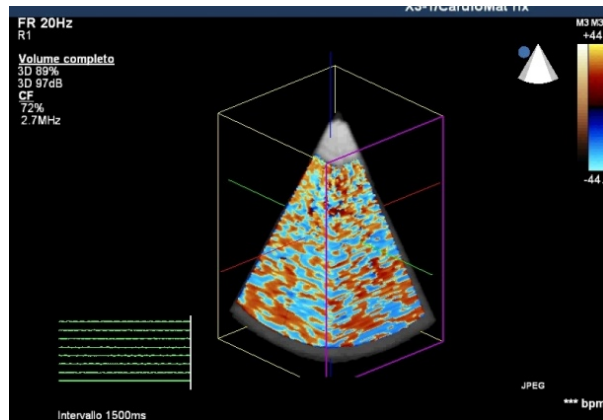


**Figure 3:** Full Volume 3D Imaging combined with Color-Doppler. This technique gives both structural and functional data for exhaustive analysis of fetal heart.

A brand new imaging modality is the Thick Slice Live Volume Imaging: the beamformer sets the acquisition angle into a low value (6-20 degrees) and increases the line density to the maximum. In this way, the image produced by thousand elements is condensed into a “thick” slice and visualized using the rendering modes. This kind of technique allows high resolution and contrast-enhanced images (Fig. 4).

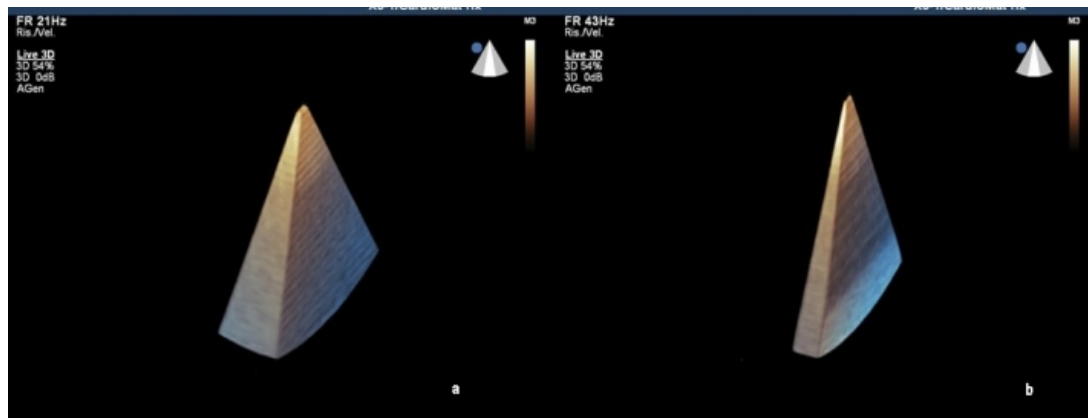


**Figure 4:** Comparison between Live 3D Imaging (a) and Thick Slice Imaging (b). Thick slice imaging has lower acquisition angle and more line density, allowing higher frame rates and better resolution.

## THE CLINICAL APPLICATION.

Two-dimensional (2D) echocardiography is an accurate and reliable technique used to evaluate normal fetal heart and congenital heart diseases. Since 2D echocardiography approaches the heart from multiple orthogonal planes, it requires the user to form a mental anatomic reconstruction to comprehend the relationship between the cardiac structural defects and the surrounding rims.

Three-dimensional echocardiography offers new insights into the anatomy of the heart valves and the septa. A complete evaluation of fetal heart in real time (three spatial dimensions plus temporal dimension) is offered by matrix arrays, that have been extensively used in clinical practice for the examination of adult and pediatric heart and, more recently, for fetal echocardiography.

### Assessment of Normal Fetal Heart Anatomy

In the Live 3D Volume imaging, the system acquires the volume dataset using a pyramidal imaging volume. Two orthogonal reference planes are used to localize cardiac structure in the volume (Fig. 5).

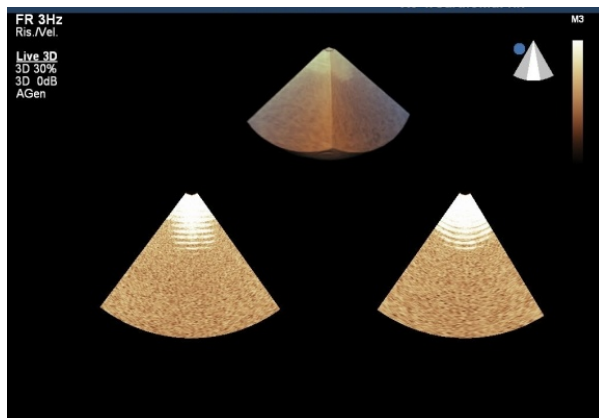


**Figure 5:** Live 3D Volume Imaging: in the lower part of the image the two reference planes used to localize the region of interest displayed by a surface rendering mode in the upper part of the image.

The software is used for navigation and cropping, and for calculation and visualization of 3D structures. For example, in fetal cardiac application navigation by cropping the volume allows surface rendered views of the intracardiac structures (en face views of the valves (Fig. 6, [Video 1](#)) and entire structure of the septa (Fig. 7).

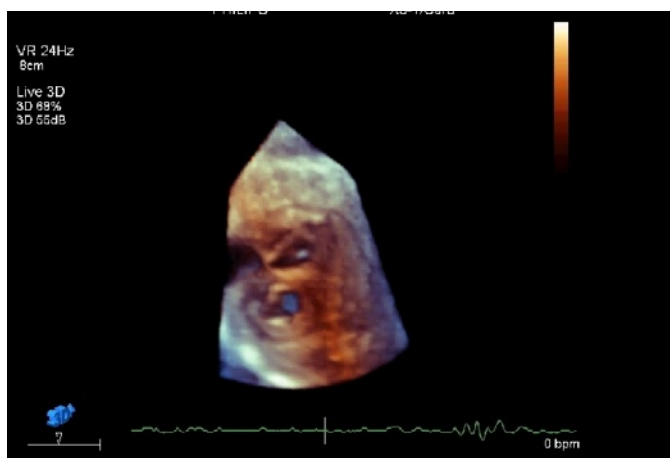


**Figure 6:** En-face surface rendering view of the atrio-ventricular valves.

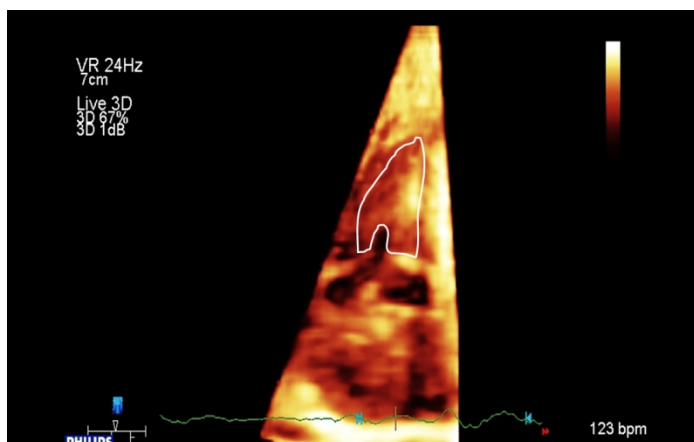


**Figure 7:** Surface rendering of the entire inter-ventricular septum and the left ventricular outflow tract.



Moreover, by using a systematic method of manipulation (cropping and rotation) of the three-dimensional pyramid it is possible to visualize, from a single volume dataset, the ascending aorta and the pulmonary trunk (Fig. 8).

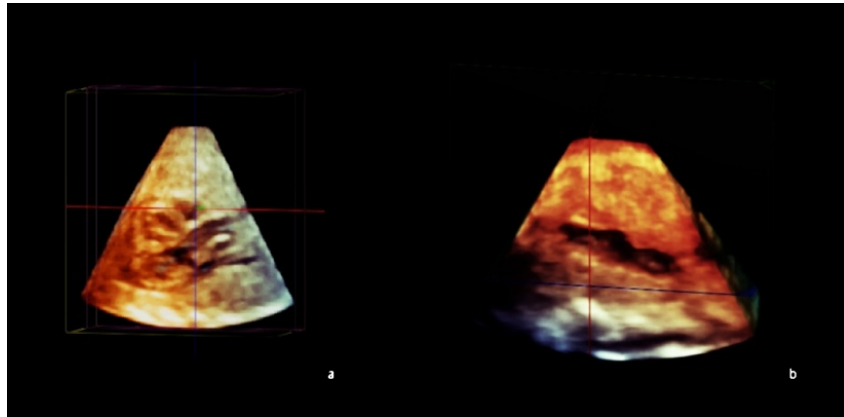


**Figure 8:** Imaging of rendered ascending aorta (a) and pulmonary trunk (b) obtained by cropping and rotating a 3D Full Volume Dataset.

Using this system, it's possible to perform real time 4D observations of the fetal heart, and to obtain instantaneous rendered 3D images of the beating fetal heart. Rendered displays of volume data allow surgeon's eye views of important and unique fetal cardiac anatomic structures, not easily visualized or understood on conventional two-dimensional (2D) imaging ([Video 2](#)).

X-plane imaging allows the scanning of two image planes of the fetal heart at different angles. Situs visceralis, four-chambers, great vessels, three vessels and arches views are obtained simultaneously without moving the transducer (Fig. 9).

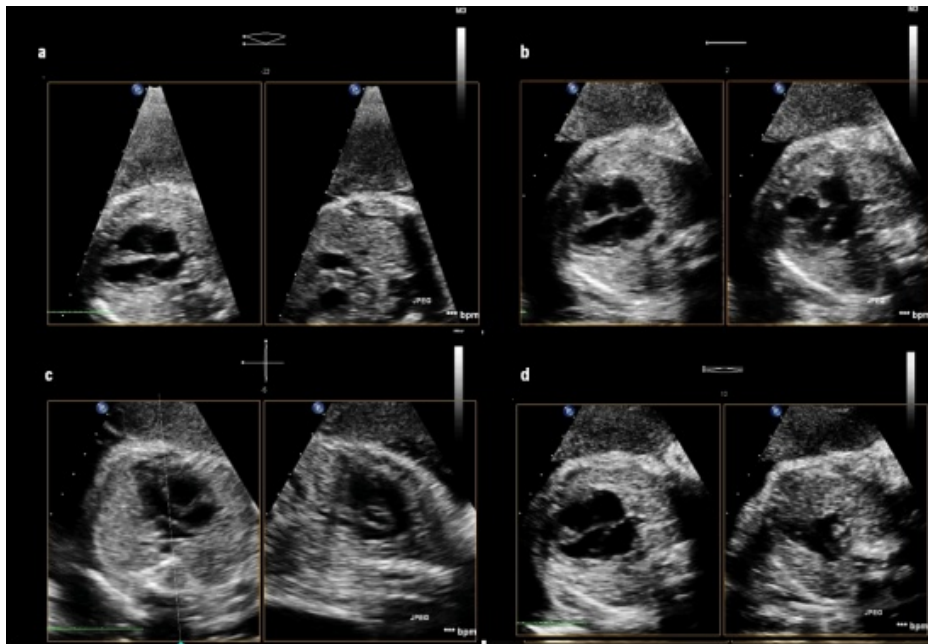


**Figure 9:** X-planes imaging displaying standard views of fetal heart examination: each image shows 4 chamber view simultaneously with stomach (a), aorta (b), pulmonary trunk (c) and three vessel view (d).

Using rotation, lateral and vertical tilts, all normal cardiac structures are identified from a unique reference image plane: atrial cavity and septum, atrioventricular valves, ventricular cavity and septum, left and right ventricular outflow tracts, ascending aorta and main pulmonary artery and its bifurcation.

In order to increase temporal resolution, thick slice volume imaging can be used (Fig. 10, [Video 3](#)).

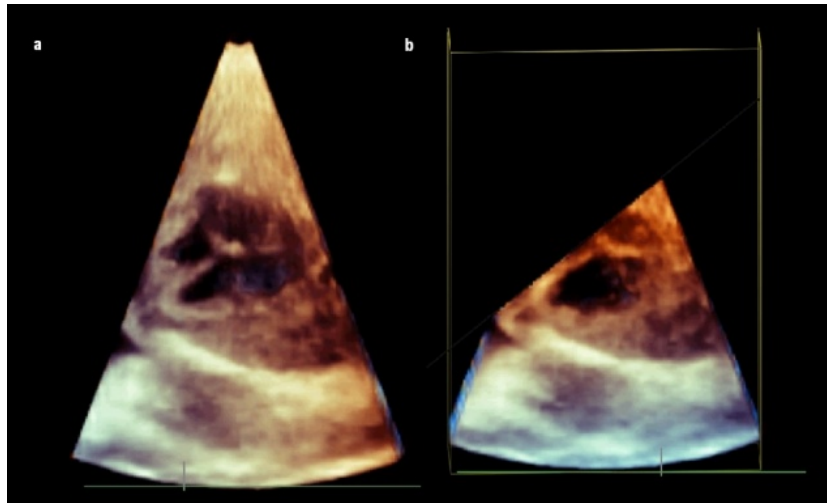


**Figure 10:** Thick Slice imaging showing the cropping technique applied for inter-ventricular septum visualization.

### Diagnosis of Congenital Heart Defects

Real time echocardiography can enable improved understanding of congenital heart disease anatomy.

Several reports have been published describing the feasibility and clinical utility of this modality in prenatal diagnosis of congenital heart defects.

In 1999, Sklansky *et al* reported preliminary observations on real-time examination of the fetal heart in 10 fetuses between 21 and 36 weeks of gestation, four of which had congenital heart disease diagnosed by 2D ultrasonography. Fair to good image quality was achieved in 11 of 12 examinations and, in 70% of the cases basic cardiac views could be adequately visualized. In 2000, Scharf *et al*. obtained images of at least satisfactory quality in 13 fetuses examined with a 2D matrix array transducer between 20 and 24 weeks of gestation. Deng *et al*. described optimal imaging windows to examine the fetal heart using this technology. Maulik *et al*. [8] reported that a comprehensive assessment of cardiac valves, atrial and ventricular chambers, and outflow tracts was possible in a group of 12 fetuses examined between 16 and 37 weeks of gestation by either real-time direct 4D ultrasonography or full volume 4D ultrasonography acquisitions triggered by an external ECG simulator device. Sklansky *et al* [11] used full volume 3D acquisitions to image fetal cardiac structures, and were able to successfully visualize a wide range of cardiac anomalies (hypoplastic left heart syndrome, atrioventricular canal, double inlet single ventricle, double outlet right ventricle and transposition of the great arteries) but not small ventricular septal defects. More recently, Acar *et al*. [1-2] reported successful visualization of fetal cardiac structures in 56 of 60 fetuses examined with either real-time direct 4D ultrasonography or live xPlane imaging.

This novel imaging technology could be very useful in a wide variety of congenital cardiac clinical applications. In fact, real-time 3D fetal echocardiography shows instantaneous rendered images of the beating fetal heart with complex pathologies in one complete heart cycle, and application of this modality allows its spatial location in the heart and its temporal location in the cardiac cycle. These observations can be made from any direction. It's also possible to navigate through the volume of data containing images of the heart in order to find the abnormal structures of interest.

The en face imaging of the septa allow for views of atrial and ventricular septal defects and their relation with both ventricles and with adjacent structures. The size of a defect and its position are crucial parameters when counseling about associated chromosomal abnormalities and evaluating postnatal follow up, whether to pursue and planning transcatheter closure treatment.

Real time imaging also enhances the comprehension of valve anatomy. Precise description of the valve anatomy can be difficult from 2D planes alone, and the surface of the leaflets and commissures are better rendered by live imaging. Additionally, congenital valve diseases are precisely revealed by 3D views, which depict the mechanism of regurgitation or obstruction. Thus, real time 3DE offers improves insight for diagnosing valve defects and predicting the success of surgical valve repair.



The real-time fetal echocardiography provides excellent depiction of pathologies such as ventricular outflow tracts in the case of double-outlet right ventricle (DORV) (Fig. 11, [Video 4](#)), transposition of the great arteries (TGA) (Fig. 12, [Video 5](#)) or tetralogy of Fallot (TOF) ([Video 6](#)). In these cases real time 4D echocardiography may assist in the evaluation of fetal cardiac anatomy and hemodynamics, and offer potential advantages relative to conventional 2D fetal echocardiography.

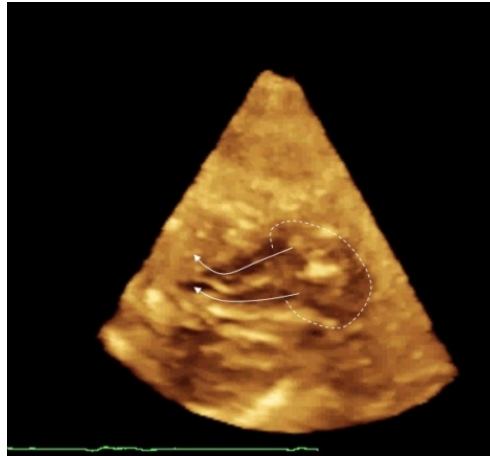


**Figure 11:** Surface rendering view from a Live 3D image of outflow tracts (arrows) in double outlet right ventricle (DORV).

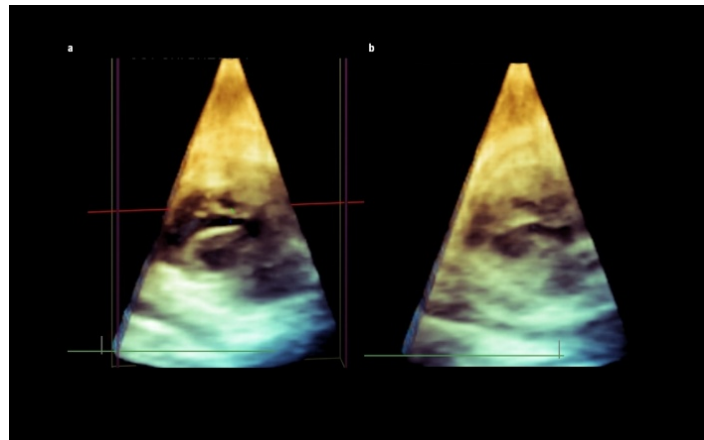


**Figure 12:** Visualization of the discordant origin of the outflow tracts from each ventricle in TGA, using planes obtained by a Live Thick Slice Live Volume dataset

In a case of congenital absence of ductus venosus [14] it has been described the usefulness of biplane and real time imaging: these imaging modalities depicted the anatomy of the systemic venous return, displaying the abnormal connection of the umbilical vein to the right atrium and the features of the systemic venous drainage. ([Video 7](#), [Video 8](#)).

There have been a few reports on real-time 3D color Doppler echocardiographic imaging of the fetal heart in the normal fetus and congenital heart disease during pregnancy. This technology allows for the depiction of the shape, direction and propagation of color flow jets in three-dimensions for analysis of ventricular septal defects, valvar and subvalvar stenosis, regurgitant jets and so forth. In certain cases real-time 3D color Doppler echocardiography also provides additional useful information to conventional 2D and 2D color flow Doppler for the correct prenatal diagnosis.

## CONCLUSIONS

Several studies have shown the feasibility of examining fetal structures, including the fetal heart, by 2D matrix array technology. However, substantial obstacles still remain and 2D matrix array transducers are not yet widely accepted in clinical practice.

One of the current limitations for fetal heart volumetric imaging includes lower image resolution, due to lower transducer frequencies in the 2D matrix array probe (1 to 7 MHz) when compared to commercially available mechanical volumetric transducers. Lower image resolution may result in distortion of fetal heart anatomy when compared to images obtained by the latest generation of mechanical volumetric transducers.

Another limitation is the low lateral resolution, in particular at deepest planes.

Practical clinical applications will depend on several technical factors, including the development of satisfactory image resolution and reliable maintenance of fast volume data acquisition rates.

The strength of this technology is the easiness in obtaining real-time images of the heart, the high volumetric frame rate and the opportunity to obtain scanning planes with the same axial and lateral resolution. These features improve the overall understanding of anatomical structure arrangement. Moreover, the cropping software gives a “cutting” plane that can be easily moved and placed in the volume, even on live imaging, in order to visualize planes not obtainable with conventional 2D, and with a better resolution than the classic 3D/4D imaging.

The present and future application of real-time 4D fetal echocardiography to the prenatal diagnosis of fetuses with congenital heart disease might be promising. However, this is not to imply that real-time 4D fetal echocardiography will replace conventional 2D fetal echocardiography. This novel technique may assist in the prenatal diagnosis of fetal cardiac anomalies, and offer the potential advantages relative to conventional 2D fetal echocardiography and color Doppler flow mapping. Moreover, the correct prenatal diagnosis of congenital heart disease may improve the prognosis of the infant after birth.

## REFERENCES

- [1] Acar P, Dulac Y, Taktak A, Abadir S. Real-time three-dimensional fetal echocardiography using matrix probe. *Prenat Diagn* 2005;25:370-5.
- [2] Acar P, Abadir S, Paranon S, Latcu G, Grosjean J, Dulac Y. Live 3D Echocardiography with the Pediatric Matrix Probe. *Echocardiography* 2007;24:750-755.
- [3] Baker GH, Shirali G, Ringewald JM, Hsia TY, Bandisode V. Usefulness of live three-dimensional transesophageal echocardiography in a congenital heart disease center. *Am J Cardiol* 2009;103:1025–1028.
- [4] Deng J, Sullivan ID, Yates R, Vogel M, McDonald D, Linney AD, Rodeck CH, Anderson RH. Real-time three-dimensional fetal echocardiography—optimal imaging windows. *Ultrasound Med Biol* 2002;28:1099-105.
- [5] Deng J. Terminology of three-dimensional and four-dimensional ultrasound imaging of the fetal heart and other moving body parts. *Ultrasound Obstet Gynecol*. 2003 Oct; 22(4):336-44.
- [6] Goncalves LF, Espinoza J, Kusanovic JP, Lee W, Nien JK, Santolaya-Forgas J, Mari G, Treadwell MC, Romero R. Applications of 2-dimensional matrix array for 3- and 4-dimensional examination of the fetus: a pictorial essay. *J Ultrasound Med* 2006;25:745-55.
- [7] Hata T, Dai S, Inubashiri E, Kanenishi K, Tanaka H, Yanagihara T, Nukazawa T. Real-time three-dimensional color Doppler fetal echocardiographic features of congenital heart disease. *J. Obstet. Gynaecol. Res.* 2008;34, 670–76
- [8] Maulik D, Nanda NC, Singh V, Dod H, Vengala S, Sinha A, Sidhu MS, Khanna D, Lysikiewicz A, Sicuranza G, Modh N. Live three-dimensional echocardiography of the human fetus. *Echocardiography* 2003;20:715-21.
- [9] Scharf A, Geka F, Steinborn A, Frey H, Schlemmer A, Sohn C. 3D real-time imaging of the fetal heart. *Fetal Diagn Ther* 2000;15:267-74.
- [10] Sklansky MS, Nelson T, Strachan M, Pretorius D. Real-time three-dimensional fetal echocardiography: initial feasibility study. *J Ultrasound Med* 1999;18:745-52.
- [11] Sklansky MS, DeVore GR, Wong PC. Real-time 3-dimensional fetal echocardiography with an instantaneous volume-rendered display: early description and pictorial essay. *J Ultrasound Med* 2004;23:283-9.
- [12] Sklansky M, Miller D, Devore G, Kung G, Pretorius D, Wong P, Chang RK. Prenatal screening for congenital heart disease using real-time three-dimensional echocardiography and a novel ‘sweep volume’ acquisition technique. *Ultrasound Obstet Gynecol* 2005;25:435-43.
- [13] Taddei F, Franceschetti L, Farina G, Prefumo F, Signorelli M, Fratelli N, Groli C. Matrix array transducers in fetal heart imaging. *Donald School J Ultrasound Obstet Gynecol*, July-Sept. 2007; 1(3):45-48.
- [14] Taddei F, Signorelli M, Prefumo F, Franceschetti L, Marasini M, Groli C. Prenatal imaging of ductus venosus agenesis using 4D ultrasound with a matrix array transducer. *Ultrasound Obstet Gynecol* 2008; 31: 476 – 477.

## Automated Echocardiography

Elena Sinkovskaya and Alfred Abuhamad

*Department of Obstetrics and Gynecology, Eastern Virginia Medical School, Norfolk, United States*

**Abstract:** The recent introduction of 3D/4D ultrasonography to clinical practice presents an important milestone in imaging technology. In this chapter, we will present the basic principles of 3D automated sonography as it relates to the examination of the fetal heart. This approach holds great promise for simplifying the fetal cardiac examination that may translate to increased prenatal detection of congenital heart disease.

**Key Words:** 3D Sonography, Fetal Echocardiography, Automated Multiplanar Imaging, Diagnostic Cardiac Planes.

### THE MAIN CONCEPT OF 3D-AUTOMATED FETAL ECHOCARDIOGRAPHY

Mounting evidence suggests that the performance of obstetric sonography with regard to the detection of fetal abnormalities has been suboptimal [1-4]. A study addressing the value of ultrasound accreditation noted that more than 40% of practices seeking accreditation by the American Institute of Ultrasound in Medicine were operating below the minimum established professional standards for the performance of obstetric sonography [5]. Several studies have documented that the efficacy of obstetric sonography is dependent on the expertise of the operator, and a significant difference has been reported between tertiary and nontertiary centers in the detection of fetal abnormalities [1-4]. Probably because of the difficulty inherent in the anatomical evaluation of the fetal heart, population-based studies have confirmed low detection rates, with more than 50% of congenital heart abnormalities remaining undetected on routine second-trimester fetal ultrasound examination [6-8]. Enhancing the detection of fetal congenital heart abnormalities, especially ductal-dependent lesions, should result in reduced morbidity and mortality of affected neonates [9-11].

One of the reasons for the suboptimal performance of obstetric sonography is related to the inherent limitations of ultrasound technology, which is operator-dependent and therefore lacking in consistency, standardization and reproducibility, especially when compared with other imaging modalities, such as computed tomography and magnetic resonance imaging. This limitation of ultrasound technology is compounded by a constantly moving target, the fetus, which adds technical difficulty to the examination.

The recent introduction of 3-dimensional (3D) ultrasonography to clinical practice provided an important advance in imaging technology. With 3D ultrasonography, an infinite number of 2D planes of a target volume are acquired. The volume acquired by 3D ultrasonography can be displayed on a monitor in 3 orthogonal planes, representing the sagittal, transverse, and coronal planes of a representative 2D plane within this volume. Such a display of 3 orthogonal planes from a 3D volume acquisition is termed a *multiplanar display*. The multiplanar display of 3D ultrasonographic volumes enables an operator to manipulate the acquired target volume to create and display reconstructed planes within this volume. Despite these recent advances in ultrasonographic imaging, the acquisition, display, and manipulation of 3D volumes is a technique that requires a substantial learning curve. Even for well-trained personnel, 3D volume manipulation can be difficult to perform, particularly when the volume involves relatively complex anatomic organs such as the fetal heart. On the other hand, these manual rotations are still dependent on the operator expertise and due to several inherent variations, like fetal position and orientation, are extremely difficult to reproduce.

Two important concepts of 3D multiplanar display need to be highlighted given its relevance to the discussion at hand. First, the acquired volume of a particular anatomic structure by 3D ultrasonography, such as a volume of the fetal heart, contains all the anatomic 2D planes for a complete anatomic evaluation of this structure. Second, for every human organ, these 2D planes that are required for a complete anatomic evaluation of that particular organ are organized in a constant anatomic relationship to each other. It is therefore theoretically possible to obtain a volume of a specific organ, such as the fetal heart, and to allow an automated program to display out of this volume all the 2D planes that are required for a complete anatomic evaluation of this organ. We termed this concept *automated multiplanar imaging* (AMI) [12].

\*Address correspondence to Dr. Elena S. Sinkovskaya: Department of Obstetrics and Gynecology, Division of Maternal-Fetal Medicine – 825 Fairfax Avenue, Suite 310, Norfolk, VA 23507, USA; Tel: +1-757-446.79.00; Email: sinkove@evms.edu

Automated sonography is based on a software program that, for various organs, relates all the standardized planes that are required for a complete anatomic evaluation of a particular organ based on the respective spatial relationship of these planes within a 3D volume. This spatial relationship between standardized planes, which can be mathematically defined by the x-, y-, and z-axis, is constant for each organ. In practical terms, the spatial relationships of the standardized 2D planes of the fetal heart are predetermined, and their respective formulas are entered into a software program. Once a 3D volume of the fetal heart is obtained from the level of a standardized plane, such as the 4-chamber view, for instance, AMI will automatically generate all other standardized planes from the acquired volume in an operator-independent method. The constant anatomic relationship of these standardized planes to each other will allow an excellent reproducibility of AMI-generated ultrasonographic images. Automated multiplanar imaging will thus allow a complete evaluation of anatomically complex organs with a standardized and operator-independent approach.

## VOLUME STANDARDIZATION

3D sonography needs to be applied at the level of volume *acquisition* and *display*. These are required first steps in the automated process [13]. Standardized acquisition parameters for specific anatomic regions will ensure that the fastest and most uniform acquisition is obtained, thus minimizing artifacts especially when dealing with fetal movement or motion within an organ such as the fetal heart. Standardization in acquisition of volumes should address the reference plane of acquisition, the size of the acquisition box, and the angle of acquisition of a specific target anatomic region. For instance, the acquisition of a volume of the fetal chest can be standardized if the acquisition reference plane is set at the level of the 4-chamber view, the borders of the acquisition box placed just outside the fetal skin and the angle of acquisition wide enough to ensure inclusion of the stomach inferiorly and the lower neck superiorly. In the mid second trimester the acquisition angle should be 35-45 degrees (Fig. 1).

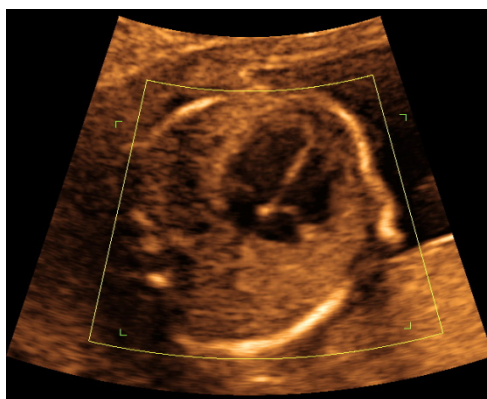


**Figure 1:** Standardization of volumes acquisition.

To standardize the display of 3D volumes, volumes need to be displayed in the multiplanar format. The multiplanar display of 3D volumes will show the reference plane (plane of acquisition) in the left upper plane (plane A) and the 2 orthogonal planes to the reference plane in the right upper plane (plane B) and left lower plane (plane C), respectively (Fig. 2).

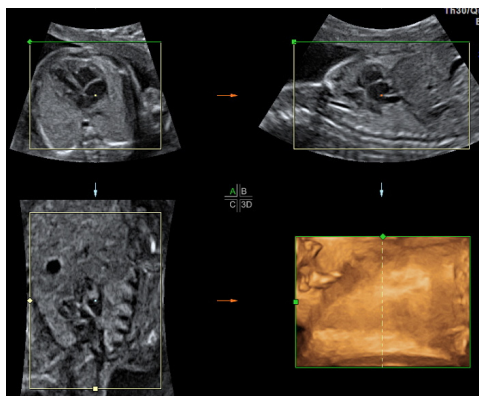


**Figure 2:** Initial multiplanar view of a 3-D sonographic volume of the fetal chest.

Standardization of display of 3D volumes needs to be applied in the A, B, and C planes to ensure uniformity of orientation in 3 dimensions. For volumes involving the chest of the fetus, standardization is best achieved by

ensuring a uniform orientation of the spine in planes A, B, and C, respectively. For fetuses in cephalic presentations, this is accomplished by rotating plane A along the z-axis (z rotation) to place the spine at the 6-o'clock position and the apex of the heart in the left upper chest (Fig. 3).

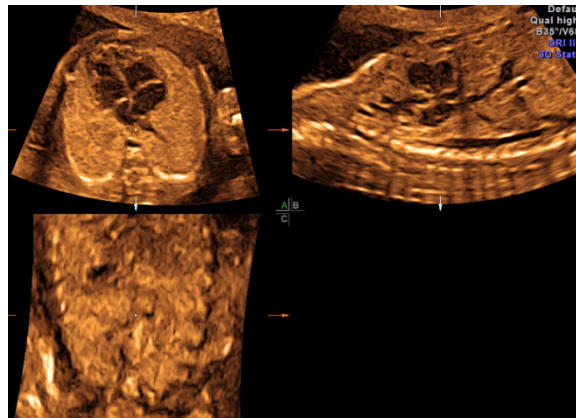


**Figure 3:** Standardization of volumes display. Plane A is rotated (four-chamber view) along the z-axis until the spine was at the 6-o'clock position.

When the reference point is placed on the fetal spine in plane A, a longitudinal view of the spine is displayed in planes B and C (Fig. 4).

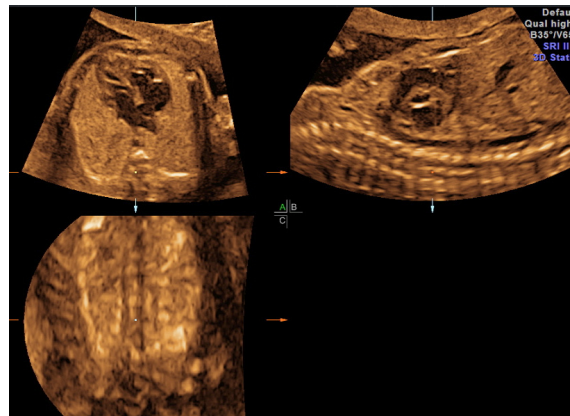


**Figure 4:** Standardization of volumes display. Reference/rotational point is placed in the fetal spine in plane A.

Standardization in planes B and C is achieved when the spine is aligned horizontally and vertically in planes B and C, respectively (z rotation in each plane). To complete the standardization, the reference point is then placed at the crux of the heart in plane A for volumes of the fetal chest (Fig. 5). For breech presentations, start by rotating the 3D volumes 180° along the y-axis, and then follow the steps above. Table 1 details standardization steps for 3D volumes obtained at the level of the fetal chest. Achieving standardization in fetal 3D imaging will result in uniformity in retrieval of diagnostic 2D planes out of 3D volumes and a simplified approach to training. Finally, with standardization, the diagnostic capabilities of volume sonography in obstetrics are enhanced.

**Table 1:** Standardization of 3D Volumes of the Fetal Chest (Cephalic Presentations\*)

Volume acquisition	
	Obtain an axial view of the chest at the level of the 4-chamber view; ensure that you have 1 full rib on each side
	Open the acquisition box wide enough to ensure that the fetal chest is contained within the box; the box boundaries should be placed just outside the fetal skin
	Use an acquisition angle that is wide enough to include the stomach inferiorly and the lower neck superiorly

**Table 1: cont....**

<b>Volume display</b>	
	Rotate image in plane A (4-chamber view) along the z-axis until the spine is at the 6-o'clock position and the apex of the heart is in the left upper chest
	Move the reference point in plane A to the spine (body of vertebra); this will bring a longitudinal view of the spine in planes B and C.
	Rotate image in plane C (coronal view) along the z-axis until the section of the midthoracic spine is aligned vertically
	Rotate image in plane B (sagittal view) along the z-axis until the section of the midthoracic spine (posterior to the heart) is aligned horizontally
	Place the reference point in plane A at the crux of the heart, at the level of the insertion of the medial leaflet of the tricuspid valve into the septum

### **Spatial Relationships of the Standard Diagnostic Fetal Cardiac Planes**

The initial required step in the automation process is to define the spatial relationships of the standard diagnostic 2D planes to a reference plane of the target organ [14]. More recently the spatial relationships to the 4-chamber view plane of 6 diagnostic cardiac planes in the second trimester of pregnancy (between 18 and 23 weeks' gestation) has been identified [15-17]. Based upon these data special software was developed. The six standard diagnostic cardiac planes include the left ventricular outflow plane (Cardiac plane 1: five-chamber view, aorta), the right ventricular outflow plane (Cardiac plane 2: pulmonary artery), the abdominal circumference plane (Cardiac plane 3: abdominal circumference, stomach), the ductal arch (Cardiac plane 4), the right atria inflow (Cardiac plane 5: vena cava inferior and superior to the right atrium) and the aortic arch (Cardiac plane 6) – Figs 6-11. In order to enhance the accuracy of the software and to account for gestational age and individual variations between fetuses, tomographic ultrasound imaging (TUI) was added to the display of each diagnostic plane. TUI was set to display seven images for each diagnostic plane. Characteristics of software and the TUI image-to-image distances are reported in Table 2.

**Table 2:** Software characteristics: spatial relationship of Cardiac planes 1-6 to the four-chamber view (4CV) reference plane and tomographic ultrasound imaging (TUI) display

<b>Cardiac plane</b>	<b>Spatial relationship to 4CV</b>	<b>TUI image-to-image distance (mm)</b>
1	<i>Parallel shift: -3.84 mm; Y rotation: 26.5</i>	0.56
2	<i>Parallel shift: -9.00 mm</i>	1
3	<i>Parallel shift: +14.0 mm</i>	2
4	<i>Y rotation: 90</i>	0.66
5	<i>Parallel shift: +5.98 mm; Y rotation: 90</i>	0.80
6	<i>Parallel shift: +3 mm; X rotation: 14; Y rotation: -2; Z rotation: -6</i>	1

### **Automated Retrieval of Standard Diagnostic Cardiac Planes**

Prospective studies were done to evaluate the ability of software to retrieve six diagnostic cardiac planes from static 3D-volumes of the normal fetal heart, in the 2<sup>nd</sup> trimester of pregnancy [15-17]. It has been reported that this software demonstrated an excellent display of all six cardiac views with appropriate quality of images in most cases. Each target cardiac plane was displayed in at least one TUI image in more than 90% of volumes. Therefore all 6 diagnostic planes were retrieved from a single 3D volume in more than 75% of cases. The software performed equally well at each gestational age between 18 and 23 weeks.

The potential clinical usefulness of automated multiplanar echocardiography was recently proved a study by Rizzo *et. al* [18]. This technique allowed successfully retrieve of outflow tracts planes from 4D volumes obtained at the level of four-chamber view and confirm discordant ventricular-arterial connection in fetuses with complete transposition of great arteries as well as with corrected TGA.

### **Limitations of the Technique**

The detailed analysis of the impact of different factors on the ability of the automated software to retrieve diagnostic planes, from 3D cardiac volume datasets has showed that besides artifacts, which are typical for 3D volume

acquisition such as fetal activity (body or breathing movements), there are limitations typical for AMI technology only. The quality of 3D volume plays a critical role in the resolution of the retrieved planes. Given that the software is dependent, for its optimum performance, on adequate 3D volumes, its performance in difficult-to-image patients remains to be determined. Therefore it was reported if the initial acquisition of the 4-chamber view required z-rotation more than 90 degrees, the ability of software to display diagnostic cardiac plane 4-6 was affected. To avoid this problem the examiner should angle the transducer to obtain a better cardiac plane.

The main limitation specifically related to the performance of the software and may be difficult to avoid, is a heart position in the chest. It was demonstrated that cardiac axis less than 35 or greater than 55 degrees caused the inability to obtain left and right ventricular outflow planes [19]. This aspect should be considered in future studies. We hope that future improvement in AMI technology will help to minimize this effect.

Furthermore, most studies focused on gestational ages of 18–23 weeks, because most fetal anatomical surveys and echocardiograms are performed within this window. The performance of this software in fetuses at other gestational ages and in those with different congenital heart disease remains to be determined.

## CONCLUSION

Our results validate the concept of automated sonography and its clinical applicability. By standardizing the approach to image acquisition and display and by substantially reducing the possibility of human error, automated sonography will improve the diagnostic acumen of ultrasound imaging and thus prove advantageous to clinical practice. Automated sonography also has the potential for improving the efficiency of ultrasound imaging by reducing the time needed to complete an ultrasound examination, thereby resulting in increased throughput of ultrasound laboratories.

## REFERENCES

- [1] Ewigman BG, Crane JP, Frigoletto FD, LeFerve ML, Bain RP, McNellis D. Effect of prenatal ultrasound screening on perinatal outcome: the RADIUS Study Group. *N Engl J Med* 1993; 171: 821–827.
- [2] Chitty LS. Ultrasound screening for fetal abnormalities. *Prenat Diagn* 1995; 15: 1241–1257.
- [3] Crane JP, LeFerve ML, Winbron RC *et al.* A randomized trial of prenatal ultrasonographic screening: impact on the detection, management, and outcome of anomalous fetuses. The RADIUS Study Group. *Am J Obstet Gynecol* 1994; 171: 392–399.
- [4] Grandjean H, Larroque D, Levi S, and the Eurofetus Study Group. The performance of routine ultrasonographic screening of pregnancies in the Eurofetus Study. *Am J Obstet Gynecol* 1999; 181: 446–454.
- [5] Abuhamad AZ, Benacerraf BR, Wolatz P, Burke BL. The accreditation of ultrasound practices: impact on compliance with minimum performance guidelines. *J Ultrasound Med* 2004; 23: 1023–1029.
- [6] Todros T, Faggiano F, Chiappa E, Gaglioti P, Mitola B, Sciarrone A, and the gruppo piemontese for prenatal screening of congenital heart disease. Accuracy of routine ultrasonography in screening for heart disease prenatally. *Prenat Diagn* 1997; 17: 901–906.
- [7] Buskens E, Grobbee DE, Frohn-Mulder IME, Stewart PA, Juttmann RE, Wladimiroff JW, Hess J. Efficacy of routine fetal ultrasound screening for congenital heart disease in normal pregnancy. *Circulation* 1996; 94: 67–72.
- [8] Tegnander E, Eik-Nes SH. The examiner's ultrasound experience has a significant impact on the detection rate of congenital heart defects at the second-trimester fetal examination. *Ultrasound Obstet Gynecol* 2006; 28: 8–14.
- [9] Chang AC, Huhta JC, Yoon GY, Wood DC, Tulzer G, Cohen A, Mennuti M, Norwood WI. Diagnosis, transport and outcome in fetuses with left ventricular outflow obstruction. *J Thorac Cardiovasc Surg* 1991; 102: 841–848.
- [10] Eapen RS, Rowland DG, Franklin WH. Effect of prenatal diagnosis of critical left heart obstruction on perinatal morbidity and mortality. *Am J Perinatol* 1998; 15: 237–242.
- [11] Santomi G, Yasukochi S, Shimuzu T, Takigiku K, Ishii T. Has fetal echocardiography improved the prognosis of congenital heart disease? Comparison of patients with hypoplastic left heart syndrome with and without prenatal diagnosis. *Pediatr Int* 1999; 41: 728–732.
- [12] Abuhamad A. Automated multiplanar imaging, a novel approach to ultrasonography. *J Ultrasound Med* 2004; 23: 573–576.
- [13] Abuhamad A. Standardization of 3-dimensional volumes in obstetric sonography, a required step for training and automation. *J Ultrasound Med* 2005; 24: 397–401.
- [14] Abuhamad A, Falkensammer P, Zaho Y. Automated sonography: defining the spatial relationship of standard diagnostic fetal cardiac planes in the second trimester of pregnancy. *J Ultrasound Med* 2007; 26: 501–507.

- [15] Abuhamad A., Falkensammer P., Reichartseder F., Zaho Y. Automated retrieval of standard diagnostic fetal cardiac ultrasound planes in the second trimester of pregnancy: a prospective evaluation of software. *Ultrasound Obstet Gynecol* 2007; 31: 30-36
- [16] Sinkovskaya E., Berkley E., Falkensammer P., Stoeckl C., Abuhamad A. Prospective evaluation of automated sonography in comprehensive fetal cardiac imaging in the second trimester of pregnancy. Abstracts of the 19<sup>th</sup> World Congress on Ultrasound in Obstetrics and Gynecology, Hamburg, Germany, September 13-17, 2009.
- [17] Sinkovskaya E., Berkley E., Falkensammer P., Stoeckl C., Abuhamad A. Automated sonography: the best fit formula for the display of the aortic arch in the second trimester of pregnancy. Abstracts of the 19<sup>th</sup> World Congress on Ultrasound in Obstetrics and Gynecology, Hamburg, Germany, September 13-17, 2009.
- [18] Rizzo G., Capponi A., Cavicchioni O., Vendola M., Pietrolucci M., Arduini D. Application of automated sonography on 4-dimensional volumes of fetuses with transposition of the great arteries. *J Ultrasound Med* 2008; 27: 771–776.
- [19] Sinkovskaya E., Berkley E., Falkensammer P., Stoeckl C., Abuhamad A. Limiting factors for performance of the automated sonography in fetal cardiac imaging in the second trimester of pregnancy. Abstracts of the 19<sup>th</sup> World Congress on Ultrasound in Obstetrics and Gynecology, Hamburg, Germany, September 13-17, 2009.



## **Four D and 2D Echocardiographic Evaluation of Anomalies of the Venous Connections**

**Paolo Volpe, Valentina De Robertis, Campobasso Gianluca, Nicola Volpe and Georgios Rembouskos**

*Fetal Medicine Unit, Di Venere and Sarcone Hospitals. ASL Bari. Italy.*

**Abstract:** Abnormalities of systemic and pulmonary venous connections are among the most frequently missed congenital heart disease (CHD) in prenatal ultrasound studies. In fact their prenatal US detection is difficult and requires adequate image resolution and attention to detail.

Recently, three-four D US has been suggested to provide a significant contribution to our understanding of the developing heart in both normal and anomalous cases. In particular “B-flow-STIC imaging” and “inversion mode” have been demonstrated to supply additional information over that provided by 2D US in the prenatal diagnosis of some congenital heart defects, including abnormalities of the venous connections.

In this chapter we report the 2D prenatal characterization of the most common anomalies of the venous connections, and describe the application and added value of 4D echocardiography with B-flow-STIC imaging or with inversion mode in the prenatal diagnosis of total anomalous pulmonary venous connections and abnormal systemic venous connections respectively

**Key Words:** 4D Sonography, Fetal Echocardiography, Venous Connection.

### **INTRODUCTION**

Abnormalities of systemic and pulmonary venous connections are often associated with additional heart defects which may be simple or complex, such as those associated with a heterotaxy syndrome [1]. Their prenatal detection is difficult and requires adequate image resolution and attention to detail.

Abnormal systemic venous connections (ASVC) include anomalies of the left and right superior vena cava and coronary sinus, and anomalies of the inferior vena cava.

Anomalous pulmonary venous connections can be partial (PAPVC) or total (TAPVC). TAPVC is characterized by the anomalous drainage of all the pulmonary veins, whereas PAPVC is characterized by the anomalous drainage of one, two, or three of the four pulmonary veins.

Three-four D US has been suggested to provide a significant contribution to our understanding of the developing heart in both normal and anomalous cases [2-8]. In particular “B-flow-STIC imaging” and “inversion mode” have been demonstrated to supply additional information over that provided by 2D US in the prenatal diagnosis of some congenital heart defects (CHD) due to the ability to trace the spatial course of the vessels involved in the anomaly [3, 5, 8,-10], and to facilitate the identification of small vessels [8-10]. In-fact B-flow – STIC imaging seems to improve the accuracy of prenatal diagnosis either of TAPVC [8-10] and of ASVC whereas inversion mode has been used only in the cases of ASVC [5]. In this chapter we report the 2D prenatal characterization of the most common anomalies of the venous connections, namely total anomalous pulmonary veins connection, persistent left superior vena cava (LSVC) with dilation of the coronary sinus (CS), interrupted inferior vena cava (IVC) with azygos continuation and describe the application and added value of 4D echocardiography with B-flow-STIC imaging or with inversion mode in the prenatal diagnosis of TAPVC and ASVC respectively.

### **B-FLOW TECHNOLOGY**

B-flow is a technique that uses digitally encoded sonographic technology to provide direct visualization of blood echoes in gray-scale [11]. It simultaneously displays both tissue morphology and blood flow using the same gray-scale schemes (unlike color Doppler flow, in which the color signals are superimposed onto structural gray-scale images). The B-flow image does not interfere with the information produced by B-mode because both utilize the same spatial resolution and frame rate.

When compared with color and power Doppler US, B-flow sonography has a higher frame rate and better spatial

\*Address correspondence to Paolo Volpe: Via Ferrannini 10, 70125, Bari Italy; Email paolo-volpe@libero.it

resolution. It allows angle independent detection of weak blood reflectors from vessels. In fact, the peripheral small blood vessels with low flow velocity can be demonstrated, because of direct visualization of blood reflectors.

The resulting image is a live gray-scale depiction of blood flow and part of the surrounding lumen. Since B-flow is one of the options of gray-scale mode a swift-switching between conventional 2D imaging and B-flow imaging can be easily obtained.

B-flow technology can be also combined with STIC (spatio temporal image correlation) (General Electrics, Kretztechnik, Zipf, Austria). STIC is an acquisition modality of fetal heart volume allowing the visualization of cardiac structures as a 4Dcine sequence, that can be combined with other applications by selecting the appropriate setting before acquisition (B-flow, color and power Doppler, ecc) or with post-processing visualization modalities (inversion mode, tomographic ultrasound imaging etc) [6].

As detailed above, B-flow with STIC allows to make precise evaluations of spatially complex vascular anomalies and to improve the visualization of very low flow and tiny vessels, which is of major interest in the definition of complex CHD including TAPVC.

The following descriptions and procedures are referred to B-flow combined with STIC.

### Volume Acquisition

Before acquiring heart volume, B-flow sensitivity and persistence need to be set accordingly: the evaluation of arterial flow requires high sensitivity and low persistence, whereas the examination of venous flow with low velocity is achieved with a higher persistence and lower sensitivity.

The acquisition technique has been described elsewhere [6]. Briefly, once the sagittal and transverse view of the fetal heart is visualized, heart volume datasets are acquired with B-flow imaging and STIC using automatic sweeps through the fetal thorax. If the operator is interested in the evaluation of the 4D reconstruction of the heart or the outflow tracts, optimal volume datasets of the 4-chamber view using transverse sweeps through the fetal thorax need to be acquired. If the operator wants to review the aortic and ductal arches, high-quality volume datasets are best acquired using sagittal sweeps through the fetal thorax. A detailed study of pulmonary venous connections requires the use of either transverse and sagittal sweeps through the fetal thorax whereas only sagittal sweeps through the fetal thorax are required for the study of systemic venous connections. The volume of interest is acquired with a sweep angle of approximately 20–40° (depending on the size of the fetus) that is usually sufficient to include the stomach, the heart, its vascular connections, including the venous ones, and the neck vessels. The size of the acquisition box is adjusted by placing its borders just outside the skin of the fetal chest. The acquisition time can be selected between 7.5 and 15 seconds.

### Multiplanar Display

Once a volume is successfully obtained, it is displayed on the screen in a multiplanar image format, demonstrating one cardiac cycle beating in the three orthogonal planes (Fig. 1).

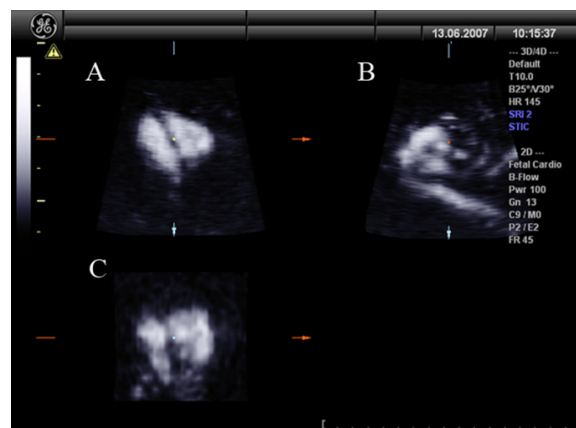


**Figure 1:** Multiplanar display of a volume dataset acquired using transverse sweep through the fetal thorax with B-flow and STIC. The A-plane is the acquisition plane and has the best image quality (upper left). The plane perpendicular to A but parallel to the ultrasound beam is identified with the letter B (upper right). The plane that is both perpendicular to A and to the ultrasound beam is defined as C (lower left) and is commonly referred to as the coronal plane. The B and C planes are the orthogonal planes

which have been reconstructed by the system. Therefore, the quality of the acquired volume can be estimated online by directly analyzing the B-plane.

The display and manipulation of volumes acquired by STIC and B-flow require a substantial learning curve. Spatial orientation may be difficult to determine and, in particular, the accurate anatomical identification of left/right and dorsal/ventral sides may be confusing after several rotations and changes of plane. These difficulties hold true for 3D volumes involving anatomically complex organs such as the fetal heart, but they are most true for a new technique of flow display such as B-flow technology. For these reasons, a standardization of the orientation of the fetal heart on-screen prior to the storage of dynamic volume datasets is a required initial step. A standardization of the modalities of display of heart volumes needs to be applied in the A, B, and C planes to ensure uniformity of orientation in the 3 dimensions. Each volume should be initially standardized in plane A (reference plane, 4-chamber view); the volume should be rotated so that the heart can be visualized at all times in a known anatomical position as if the fetus is always in vertex presentation with the apex of the heart on the left part of the panel A and the spine positioned at 6-o'clock.

In this position, on the panel B, a sagittal view of the fetal thorax is displayed with the fetal head on the left side, the fetal breech on the right side of the screen and the dorsal portion of the fetus at the bottom of the image. In this case, on the panel C, a coronal view of the fetal thorax is obtained (Fig. 2).

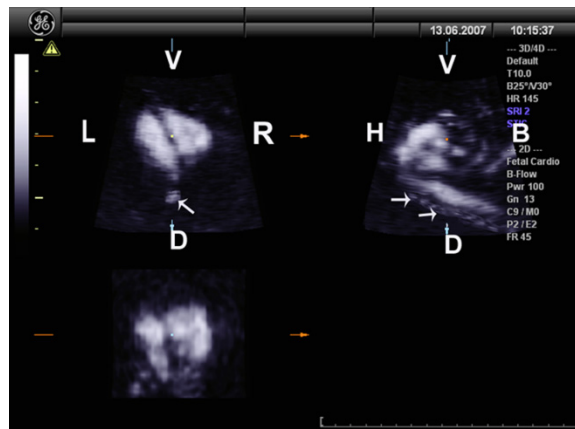


**Figure 2:** Multiplanar display of the B-flow-STIC volume in a fetus in a cephalic presentation. On panel A, the apex of the heart is positioned on the left part of the image (L); the spine (arrows) is at 6 o'clock position. On panel B, a longitudinal view of the fetal thorax is displayed with fetal head (H) on the left side of the image and fetal breech on the right side (B). R, right; V, ventral; D, dorsal.

If the fetus is lying in breech presentation with the heart apex on the right side of the panel A and with the fetal head on the right of the panel B (Fig. 3), an image rotation by 180° on the y-axis is required. In this way, the final appearance will be that shown in Fig. 2.

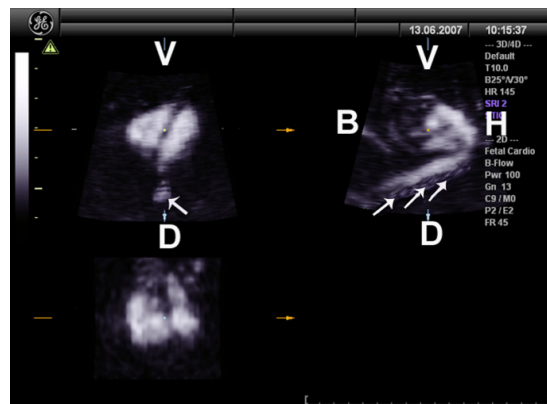


**Figure 3:** Multiplanar display of the B-flow-STIC volume in a fetus in a breech presentation. On panel A, the apex of the heart is positioned on the right side of the image; the spine (arrows) is at 6 o'clock position. On panel B, a longitudinal view of the fetal thorax is displayed with fetal head (H) on the right side of the image and fetal breech (B) on the left side. V, ventral; D, dorsal.

The use of this view will ensure that the spatial orientation of the fetus will always be the same, by simple manipulations of the volumes.

### Rendering Mode

Rendering mode allows to obtain realistic images of structures of interest that may be difficult to obtain by B-flow alone. Once the volume rendering is applied to the dataset, 3D image is displayed in the right lower panel of the screen (panel D). When the render option is activated on the 4D-viewer software, the operator should change the direction of the region of interest (ROI) and he should select one among 6 options. A craniocaudal direction of the ROI (green line on the left side of the panel B) must be selected to obtain a 3D image with the same orientation as in panel A (Fig. 4).

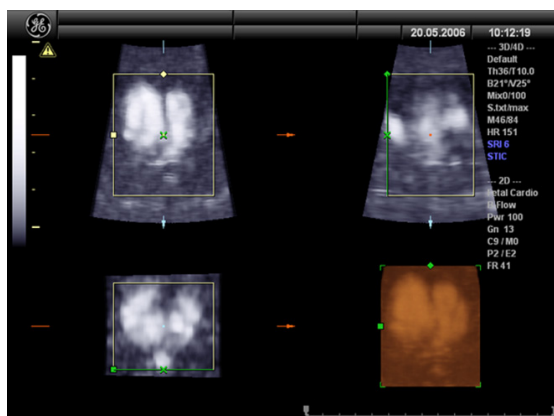


**Figure 4:** B-flow-STIC volume. When the render option is activated, a 3D rendered image is shown on panel D (lower right). Note that green line is on the left side of panel B to obtain a 3D rendered image with the same orientation as in panel A.

The thickness of the ROI may be adjusted in an attempt to display a thick-slice rendering comprising the fetal heart and its vascular connections, according to the endpoint of the rendering. Surface rendering mode may also be modified and a mixture of gradient light plus surface algorithms is selected ([Video 1](#)).

Post processing adjustments in image quality must be also performed as necessary and include: (1) gamma curve correction to optimize tissue contrast resolution, and (2) gray scale threshold and transparency to improve border recognition of surface-rendered volumes. Generally, the transparency level must be set to 20, and the threshold level between 70 and 80 (both scales range from 0 to 250). Finally, a rotation of the 3D image along the x- z- and y-axis may be needed to improve the visualization of the structures of interest.

### INVERSION MODE

The “inversion mode” is a rendering algorithm that transforms echolucent structures into echogenic voxels. Thus, anechoic structures such as the heart chambers, lumen of the great vessels, stomach and bladder appear echogenic on the rendered image, whereas structures that are normally echogenic prior to gray-scale inversion become anechoic.

Since this technique, such as B-flow, does not use color or power Doppler sonography, it does not interfere with the frame rate and it does not have the inherent limitations to image reconstruction related to the angle of insonation, temporal resolution, or intensity of the Doppler signal.

The inversion mode has been proposed as a technique capable of producing digital casts of the aortic and ductal arches and as a useful method to improve prenatal diagnosis of abnormal systemic venous connections. Therefore, the relationships between the fetal heart and great vessels and other fluid-filled non-vascular structures such as the esophagus and stomach can be visualized in a single volume dataset. Limitations of inversion mode are the absence of information regarding the velocity or direction of blood flow and it does not differentiate blood vessels from other hollow structures.

### Volume Acquisition

The inversion mode is applied to the volume data sets acquired with B-mode imaging. To obtain a high-quality volume dataset of the systemic venous connections, once the sagittal view of the heart is observed, the acquisition

should be performed with sagittal sweeps through the fetal chest and abdomen using the spatio-temporal image correlation (STIC) technique. The time of acquisition should be lasted between 7.5 and 12.5 s, and the acquisition angles should be varied from 15° to 35°.

### Volume Rendering

Volume dataset is initially displayed using multiplanar slicing. Once the volume rendering is applied to the dataset and a 3D image with the same orientation as in Panel A is displayed in the right lower panel of the screen, the inversion mode should be then applied to the volume dataset.

A thick-slice rendered image of the volume dataset should be done showing the fetal heart and its connections. Surface rendering mode can be improved if a mixture of ‘gradient light’ and ‘surface’ algorithms is selected. Post processing adjustments should be performed as necessary, including gamma curve correction to optimize tissue contrast resolution and gray scale threshold, and transparency to improve image quality. Usually low threshold and transparency levels should be adjusted until the structures of interest are visualized.

TAPVC is a multifaceted group of malformations affecting the pulmonary veins (PVs). The essential feature of these anomalies is that all the PVs drain into a site other than the morphological left atrium [10], ([Video 2](#); Fig. 5A, B).

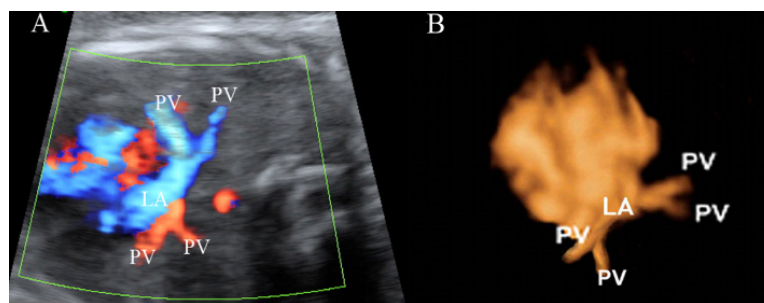


**Figure 5:** A. Two-dimensional ultrasound image. Color Doppler allows to visualize the four pulmonary veins entering the left atrium (LA). B. B-flow-STIC imaging. Normal connection of all four pulmonary veins (PV) to the left atrium (LA).

Usually, all PVs drain to the same site; however, in a few patients, different PVs are connected to separate anomalous sites. It can be categorized by the site of drainage in supracardiac, cardiac, infracardiac and mixed.

Supracardiac connection can be to the innominate vein, or directly to the right superior caval vein, to the azygos system of veins or to the left caval vein. In the most common pattern, all the 4 PVs join into a venous channel, traditionally termed the confluence, located behind the left atrium (Fig. 6A, B).

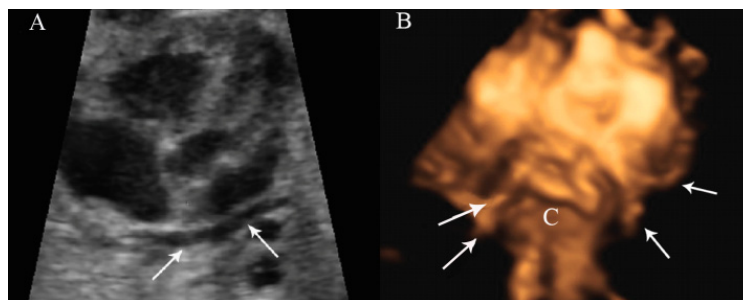


**Figure 6:** A. Two-dimensional ultrasound image showing the confluence (arrows) of pulmonary veins, posterior to the left atrium. B. B-flow-STIC imaging showing the drainage of each PV (arrow) into the confluence (C), which appears large and tortuous

From this horizontal channel, an ascending vertical vein (Fig. 7) runs up to join with the innominate vein, which then terminates in the right superior caval vein.

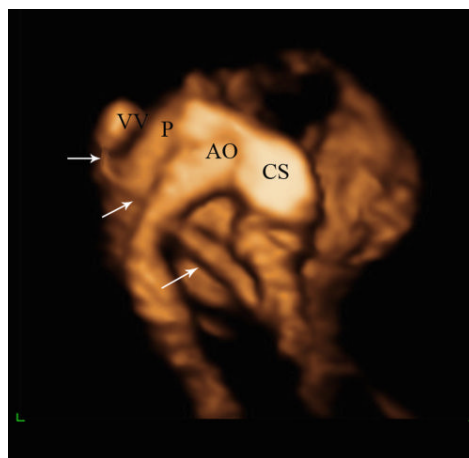


**Figure 7:** Supracardiac total anomalous pulmonary venous connection. B-flow-STIC imaging showing the ascending vertical vein (VV) and the spatial relationship between the confluence and the great vessels. The arrows indicate the entire course of the confluence. It is anterior to the thoracic aorta and drains into the ascending vertical vein. AO, thoracic aorta; C, superior vena cava; P, pulmonary artery.

The chance of obstruction of the vertical vein is crucially related to its course and is highest when the vein passes between the left pulmonary artery and the left bronchus, which thereby forms a vice constricting the anomalous vessel. Albeit less frequently, an obstruction can also occur at the opening of the innominate vein into the superior vena cava.

When TAPVC occurs through the coronary sinus (CS) it is defined as cardiac connection ([Video 3](#)). The enlarged CS could then function as an horizontal collecting venous channel. In this pattern of TAPVC, an obstruction to the venous return is rare. A direct connection of the PVs to the morphologically right atrium is seen most frequently in the setting of right isomerism. In this case both atria are of right morphology and the CS is absent. In the infracardiac pattern, PVs join together and enter a descending vertical vein that passes into the abdomen through the oesophageal orifice of the diaphragm ([Fig. 8A, B](#)).

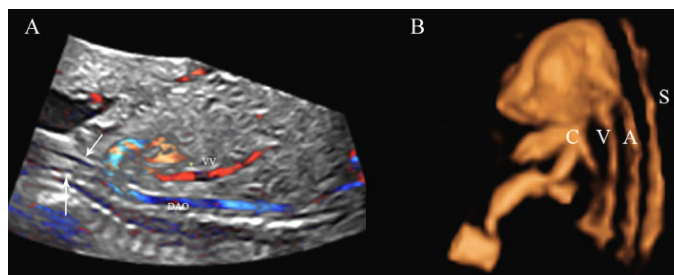


**Figure 8:** Infracardiac total anomalous pulmonary venous connection. A. Two-dimensional ultrasound image showing the descending vertical vein (VV) anterior to the descending aorta (DAO). The arrows indicate 2 neck vessels. B. B-flow-STIC imaging showing the descending vertical vein (V) which courses between the inferior vena cava (C) and the descending aorta (A); S, spine.

It then usually drains to the portal vein or to one of its tributaries and rarely to the inferior caval vein. In the former event, an obstruction is almost always present following the closure of the venous duct, because the blood must pass through the hepatic tissue to reach the systemic veins. Additionally, discrete stenoses can be found as the vertical vein passes through the diaphragm. The PVs confluence often tends to have a vertical course. Of note, it usually appears as a discrete chamber, but at times it is rather small behind the left atrium in its sopradiaphragmatic portion, and can be hardly appreciated by conventional 2D US. In the mixed pattern, the PVs drain separately to different anomalous sites.

## **2D Echocardiography**

Anomalous connection of the pulmonary veins is notoriously misdiagnosed prenatally, especially when isolated. In the few cases described prenatally, TAPVC is often associated with other cardiac anomalies in the context of heterotaxy syndromes. The diagnosis can be suspected on the 4-chamber view. Indirect signs of TAPVC are:

- 1) moderate atrioventricular disproportion, with the right sections larger than the left ones (in supradiaphragmatic forms).
- 2) a pulmonary artery significantly larger than the ascending aorta.

The fetal echocardiographic clues to the diagnosis of TAPVC include failure to demonstrate a direct pulmonary venous connection to the left atrium, the detection of a venous confluence behind the left atrium (Fig. 6A), and the visualization of an ascending or descending vertical vein (Fig. 8A). Color Doppler (with low PRF to detect the extremely low-velocity pulmonary venous flow) may be used to confirm the vascular nature of the sonolucent area behind the left atrium (differentiating it from the esophagus). Spectral Doppler assessment can then be used to detect the typical pulmonary velocity waveform.

#### **4D Echocardiography**

B-flow imaging and STIC can be advantageously used to locate normal (Fig. 5B) and abnormal pulmonary venous returns. It enables to clearly visualize the confluence of PVs (Fig. 6B), and the vertical vein departing from it (Fig. 7, 8 B). In addition, B-flow STIC imaging supplies a detailed view of the course and size of each PV, thereby allowing to reliably rule out the existence of single PV hypoplasia or atresia

#### **Interrupted Inferior Vena Cava with Azygos Continuation**

The prevalence of abnormal systemic venous return to the heart in children with congenital heart disease is 6.6%, and can reach as much as 70% in complex heart defects such as heterotaxic syndromes[5]. A frequent venous anomaly associated with these syndromes is the absence of the IVC between the renal veins and the hepatic veins. The right supracardinal vein persists to connect the caudal IVC to the azygos vein. This form of abnormal venous return is the result of connection failure between the right subcardinal vein and hepatic veins, and is present in most of cases with left isomerism (80-90% of cases); however its association with right isomerism (2,5% of cases) or with usual atrial arrangements has been reported. When there is interruption of the inferior vena cava with azygos continuation, the venous blood from the lower part of the body is usually drained into a dilated azygos or hemiazygos vein and reaches the right atrium through a superior vena cava. Usually, with azygos continuation, this is the right superior vena cava, whereas with hemiazygos continuation, the blood often reaches the right atrium through a persistent left superior vena cava and dilated CS. The azygos or hemiazygos veins ascend in parallel to the right or the left of the descending aorta respectively, before joining their corresponding superior vena cava.

#### **Persistent Left Superior Vena Cava with Dilation of the Coronary Sinus**

A persistent left superior vena cava (PLSVC) is due to the persistence of a vessel that commonly obliterates in the first trimester of gestation. There are two types of PLSVC. PLSVC connecting to the right atrium via a dilated coronary sinus forms 90% of the anomalies of the superior vena cava. In the remaining 10%, PLSVC connects to the left atrium. It is estimated that PLSVC occurs in 0.3–0.5% of the general population and up to 10% of cases in patients with CHD [12-13]. Commonly, a normal right superior vena cava (RSVC) is associated. Less frequently, however, the RSVC is absent and the PLSVC represents the only systemic vein draining blood from the upper part of the body back to the heart [13].

During the sixth week of development the cardinal veins constitute the main systemic venous drainage of the embryo [12- 14]. In fact the primary atrium receives venous tributaries from both sides of the embryo through the common cardinal (caval) vein, which connects the paired superior (which drain the cranial parts) and inferior caval veins (which drain the caudal parts). At 8 weeks, the innominate vein forms between the 2 SVCs. At 9 weeks, the left SVC is normally obliterated and only the right SVC remains [12]. The presence of a persistent LSVC can be attributed to the persistence of the proximal part of the left anterior cardinal vein [13,14]. The coronary sinus, which collects myocardial venous blood, develops from the left common caval vein, initially connected to the left superior and inferior vena cava. This explains why the vein is connected to the coronary sinus in most cases of persistent left SVC [12].

A persistent LSVC, if isolated, usually is an asymptomatic condition of no haemodynamic significance [13,14]. However, due to its significant association with other heart defects and extra cardiac anomalies, the recognition of a PLSVC should prompt a detailed cardiac and extra cardiac examination [13,14].



## 2D Echocardiography

When **interruption of the inferior vena cava with azygos continuation** is present, on the axial view of the abdomen, the azygos is close and lateral to the abdominal aorta ([Video 4](#)) and not anterior as with the inferior vena cava ([Video 5](#)). In addition on the four chamber view behind the left atrium 2 vessels rather than one of similar size but different pulsatility are identified ([Video 6](#), [Video 7](#)). The presence of two vessels behind the fetal heart has been described as the “two vessels sign”. This sonographic sign represents the descending aorta and a dilated azygos/hemiazygos vein. The connection of the azygos to the superior vena cava can be demonstrated in longitudinal view of thorax.

The echocardiographic feature of a dilated coronary sinus is easily recognized in cases of **left superior vena cava with connection to a coronary sinus**. In fact it appears prominent in a basal four-chamber view of the heart ([Fig. 9](#), [Video 8](#)).

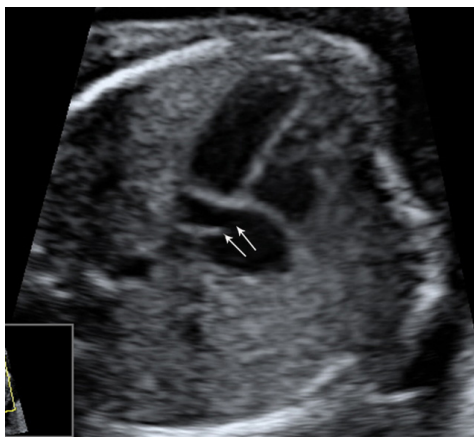


**Figure 9:** Persistent left superior vena cava. Two-dimensional ultrasound image. Axial view through the lower part of the 4-chamber view showing the dilated coronary sinus (arrows) posterior to the mitral valve.

The increased caliber of the CS is an important indirect marker of central venous drainage abnormalities [10]: in most cases it is associated with persistence of left SVC drainage into the CS, but, less frequently, it may be associated with the presence of cardiac TAPVC. The diagnosis of left superior vena cava is confirmed on the “three vessel view” ([Fig. 10](#)) where PLSVC can be identified to the left of the pulmonary trunk. If RSVC is also present, four instead of three vessels are seen ([Video 9](#)).

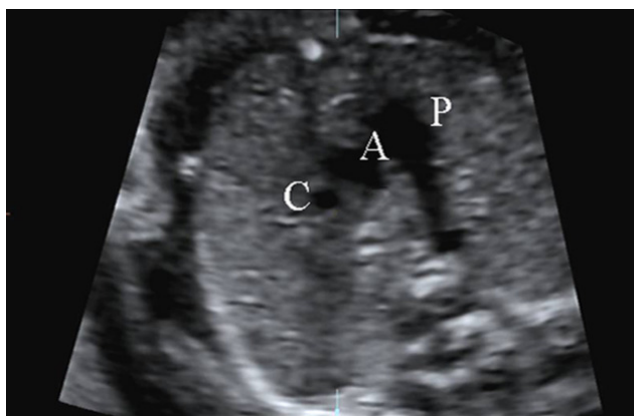


**Figure 10:** Three-vessel view of a normal fetus. The three vessels are (from right to left) the superior vena cava (C), the ascending aorta (A), and the pulmonary trunk (P). The pulmonary trunk is the largest vessel and most anterior; the superior vena cava is the smallest vessel and most posterior; the ascending aorta is in between.

When the RSVC is absent there are only three vessels: LSVC, pulmonary trunk and ascending aorta ([video 10](#)). Sagittal view of the heart, demonstrates indirect drainage of PLSVC via the coronary sinus into the right atrium ([Fig. 11](#)).



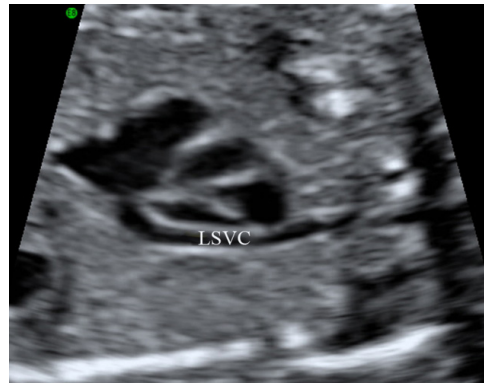


**Figure 11:** Persistent left superior vena cava. Two-dimensional ultrasound image. Sagittal view of the fetal thorax showing the persistent left superior vena cava (LSVC) and coronary sinus forming a J-shaped channel.

#### **4D Echocardiography**

4D with inversion mode clearly shows the dilated azygos vein which ascends parallel, and to the right of the descending aorta before joining the SVC (Fig. 12).

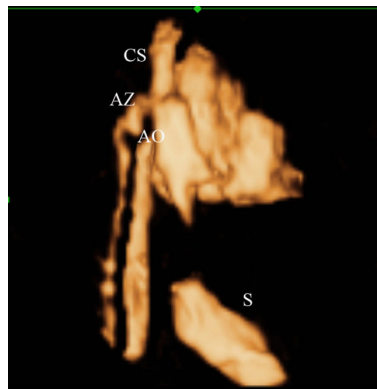


**Figure 12:** Interrupted inferior vena cava with azygos vein continuation. Three-dimensional image of a fetal heart rendered with inversion mode showing the arch of the azygos vein (AZ) joining the superior vena cava (SVC) before entering the right atrium. The parallel course of the dilated azygos vein and aorta (AO) can be seen.

In addition inversion mode improves prenatal visualization of spatial relationship of the azygos vein with the surrounding cardiovascular structures including the descending aorta.

A persistent left SVC and its spatial relationship with the surrounding cardiac structures is clearly visualized with 4D with inversion mode (Fig. 13).

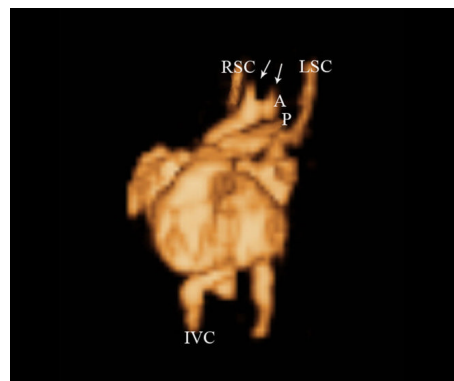


**Figure 13:** Persistent left superior vena cava. Three-dimensional image of a fetal heart rendered with inversion mode showing a persistent left SVC and its spatial relationship with the surrounding great vessels. The arrows indicate 2 neck vessels. RSC, right superior vena cava; P, pulmonary artery; A, aortic arch; IVC, inferior vena cava.

## REFERENCES

- [1] Hornberger LK. Abnormalities of systemic and pulmonary venous connection. In *Textbook of Fetal Cardiology*, Allan L, Hornberger L, Sharland G (eds). Greenwich Medical Media: London, 2000; 103–114.
- [2] Chaoui R, Hoffmann J, Heling KS. 3D and 4D color Doppler fetal echocardiography using spatio-temporal image correlation (STIC). *Ultrasound Obstet Gynecol* 2004; 23: 535–545.
- [3] Goncalves LF, Espinoza J, Lee W, Mazor M, Romero R. Three and four-dimensional reconstruction of the aortic and ductal arches using inversion mode: a new rendering algorithm for visualization of fluid-filled anatomical structures. *Ultrasound Obstet Gynecol* 2004; 24: 696–698.
- [4] DeVore GR, Polanko B. Tomographic ultrasound imaging of the fetal heart. A new technique for identifying normal and abnormal cardiac anatomy. *J Ultrasound Med*. 2005; 24: 1685–1696.
- [5] Espinoza J, Goncalves LF, Lee W, Mazor M, Romero R. A novel method to improve prenatal diagnosis of abnormal systemic venous connections using three- and four-dimensional. ultrasonography and ‘inversion mode’. *Ultrasound Obstet Gynecol* 2005; 25: 428–434.
- [6] Yagel S, Cohen SM, Shapiro I, Valsky DV. 3D and 4D ultrasound in fetal cardiac scanning: a new look at the fetal heart. *Ultrasound Obstet Gynecol* 2007; 29:81-95.
- [7] Paladini D, Volpe P, Sglavo G, Vassallo M, De Robertis V, Marasini M, Russo MG. Transposition of the great arteries in the fetus: assessment of the spatial relationships of the arterial trunks by four-dimensional echocardiography. *Ultrasound Obstet Gynecol* 2008; 31:271-6
- [8] Volpe P, Campobasso G, Stanziano A, De Robertis V, Di Paolo S, Caruso G, Volpe N, Gentile M. Novel application of 4D sonography with B-flow imaging and spatio-temporal image correlation (STIC) in the assessment of the anatomy of pulmonary arteries in fetuses with pulmonary atresia and ventricular septal defect. *Ultrasound Obstet Gynecol* 2006; 28: 40–46.
- [9] Pooh RK, Korai A. B-flow and B-flow spatio-temporal image correlation in visualizing fetal cardiac blood flow. *Croat Med J* 2005; 46: 808–811.
- [10] Volpe P, Campobasso G, De Robertis V, Di Paolo S, Caruso G, Stanziano A, Volpe N, Gentile M. Two- and four-dimensional echocardiography with B-flow imaging and spatiotemporal image correlation in prenatal diagnosis of isolated total anomalous pulmonary venous connection. *Ultrasound Obstet Gynecol* 2007; 30: 830–837.
- [11] Pooh RK. New application of B-flow sonoangiography in perinatology. *Ultrasound Obstet Gynecol* 2000; 15:163
- [12] Marcu CB, Beek AM, van Rossum AC. Unusual variation in upper-body venous anatomy found with cardiovascular MRI. *CMAJ*. 2006; 4; 175 (1): 27.
- [13] Pasquini L, Belmar C, Seale A, Gardiner HM. Prenatal diagnosis of absent right and persistent left superior vena cava. *Prenat Diagn* 2006; 26: 700–702.
- [14] Galindo A, Gutierrez-Larraya F, Escribano D, Arbues J, Velasco JM. Clinical significance of persistent left superior vena cava diagnosed in fetal life. *Ultrasound Obstet Gynecol* 2007; 30: 152–161.

## Three-Dimensional Ultrasound in Fetal Atrial, Ventricular and Atrioventricular Septal Defects

**Rabih Chaoui\***

*Prenatal Diagnosis and Human Genetics, Berlin, Germany*

**Abstract:** Atrial, ventricular and atrioventricular septal defects are the most common cardiac anomalies in the humans and occur isolated or as part of other malformations in more than the half of children with a congenital cardiac anomaly. Whereas atrial defects are difficult to detect antenatally, ventricular and atrioventricular defects are detectable on two-dimensional and color Doppler ultrasound. Three-dimensional ultrasound as STIC technology allows in fetal septal defects on one hand a safe description and documentation of the finding and on the other hand a spatial demonstration of the defect with the possibility of getting new views into the heart. The choice of the ideal plane from a 3D volume enables to get the in-line visualization of the interventricular septum with the septal defect. Orthogonal views help to visualize the defect in the different planes. Tomographic imaging aids in getting the upper abdomen and the great vessels information in addition to the septal defect view, in order to rule out a complex malformation. Rendering mode with the enface view can be used to visualize the septum from a lateral view and the common atrioventricular valve in atrioventricular septal defects. The combination with color Doppler helps to get the spatial demonstration of the defect within the heart and provide in addition information on flow events during the cardiac cycle in septal defects.

**Key Words:** Atrial septal defect, ventricular septal defect, atrioventricular septal defect, Fetal echocardiography, Spatial Temporal Image Correlation, Three-dimensional ultrasound.

### DEFINITION

#### Septal Defects:

A septal defect is an opening of the septum causing communication between the two corresponding chambers, an atrial septal defect (ASD) being a communication between both atria and a ventricular septal defect (VSD) between both ventricles. An atrioventricular septal defect combines a ventricular septal defect with an atrial septum primum defect [1].

#### Atrial Septal Defects (ASD):

According to its location an ASD is classified into septum primum, septum secundum, sinus venosus and coronary sinus defect, but the most common is in 80% the septum secundum defect also called ASD II.

#### Ventricular Septal Defects (VSD):

Similarly ventricular septal defects (VSD) are classified according to their location and there are 4 types of VSD: perimembranous, muscular, inlet and outlet. Ventricular septal defects can be isolated or associated with other cardiac defects. Ventricular septal defects associated with conotruncal defects are outlet in location

#### Atrioventricular Septal Defects (AVSD):

AVSD are classified into partial AVSD which is a synonym of septum primum ASD and into a complete AVSD. In partial AVSD, two distinct mitral and tricuspid valve annuli exist whereas in complete AVSD there is typically an abnormal common atrioventricular valve which connects to the right and left ventricle. The common atrioventricular valve usually has 5 leaflets. Complete AVSD can in addition be classified as balanced or unbalanced. In unbalanced AVSD the atrioventricular connection predominantly drains to one of the two ventricles resulting in ventricular size disproportion.

### FETAL SEPTAL DEFECTS ON 2D- AND COLOR DOPPLER ULTRASOUND

#### Atrial Septal Defect:

It is practically impossible to diagnose reliably an isolated atrial septal defect in the fetus. ASD II is located in the foramen ovale region and it is not possible to predict whether a large foramen ovale will close postnatally or not.

\*Address correspondence to **Riabih Chaoui**: Prenatal Diagnosis and Human Genetics Friedrichstraße 147; D-10117 Berlin; E-mail: chaoui@feindiagnostik.de

ASD I however can be identified in the fetus by the gap in the septum primum region which is generally accompanied with a linear insertion of both atrioventricular valves (Fig. 1). When combined with other cardiac anomalies the ASD can be suspected.

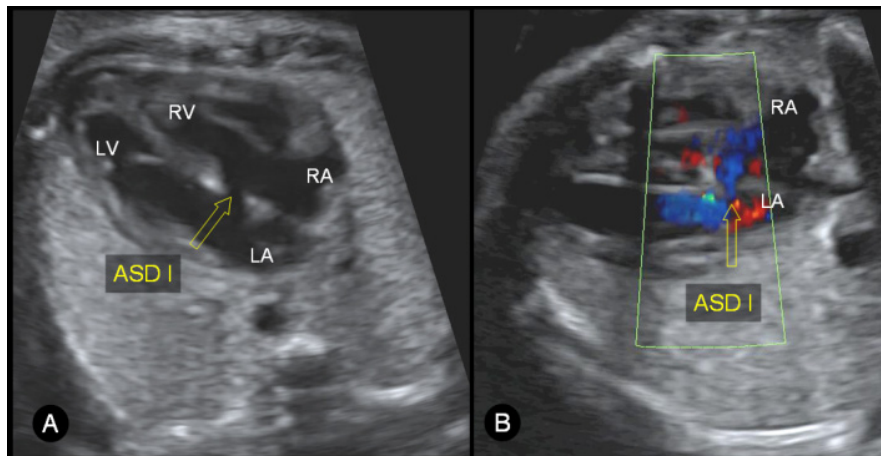


**Figure 1:** A) Atrial Septum primum defect (ASD I) with the typical gap in the septum primum region (open arrow), B) Color Doppler shows the typical right-to-left shunting (blue) across the ASD-I. LA-left atrium, LV-left ventricle, RA-Right atrium, RV-right ventricle

Color Doppler shows in ASD I a right to left shunt across the defect (Fig. 1) and blood flow direction is parallel to the alignment of the atrioventricular valves. A left superior vena cava draining into an enlarged coronary sinus may mimic the presence of a ASD I, but in color Doppler the flow in coronary sinus will be opposite.

The detection of an ASD I should alert the examiner to seek for additional cardiac and extracardiac anomalies, especially chromosomal anomalies as trisomy 21 and others.

### VENTRICULAR SEPTAL DEFECT (VSD)

This defect can be easily detected on 2D ultrasound when its size is large enough, e.g. larger than 3mm (Fig. 2).

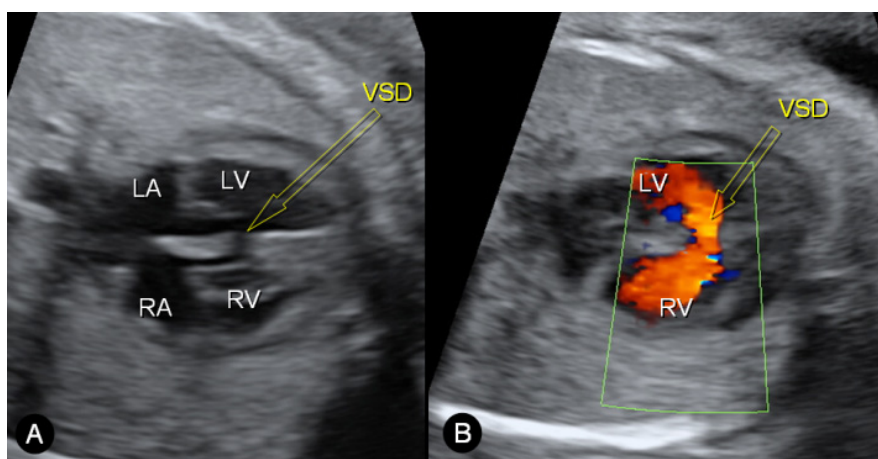


**Figure 2:** Lateral view of a four-chamber views showing large (>2mm) muscular ventricular septal defect (VSD) in the middle of the septum on 2D (A) and on color Doppler ultrasound (B). LA-left atrium, LV-left ventricle, RA-Right atrium, RV-right ventricle

Smaller VSD need either a targeted examination of the heart or the additional targeted use of color Doppler (Fig. 2). Most VSD detected prenatally are detected either in a high-risk patient with a positive family history or due to the detection of associated extracardiac anomalies.

An **inlet VSD** is found at the level of the atrioventricular valves in the four-chamber

A **muscular VSD** is generally detected on color Doppler ultrasound and is often found in the apical region of the heart with bidirectional shunt.

A **perimembranous VSD** is detected in the five chamber plane when the continuity between the ventricular septum and the ascending aorta is evaluated. It can be detected on 2D from a lateral view when its size is larger than 2-3 mm but should be confirmed by the presence of bidirectional shunt on color Doppler.

### ATRIOVENTRICULAR SEPTAL DEFECT (AVSD)

This anomaly is best detected in the apical four-chamber view either in diastole when the common valve is open presenting the defect in the center of the heart (Fig. 3) or in systole when the atrioventricular valve is closed presenting the typical linear insertion of both valves. In general a septum primum defect and an inlet ventricular septal defect are recognized in these planes. If the ventricles are of different sizes an unbalanced AVSD should be suspected.

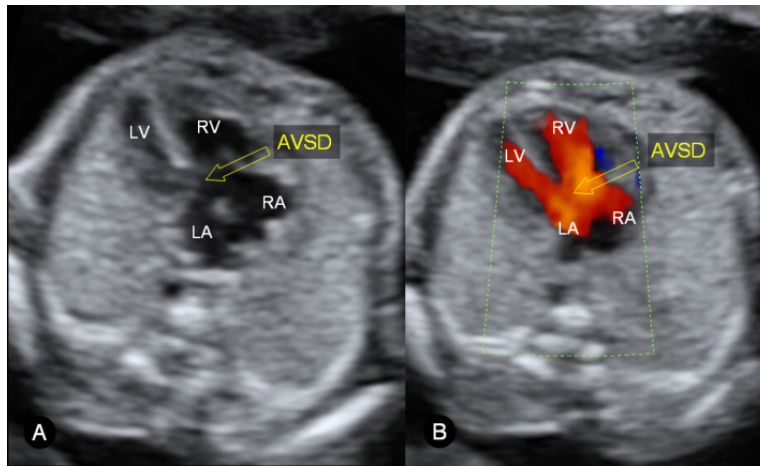


**Figure 3:** Four-chamber plane in a fetus with complete atrioventricular septal defect (AVSD) visualized during diastole. In A) the arrow points to the gap in the center of the heart. In B) color Doppler shows in diastole how blood flows typically from both atria into both ventricles crossing the midline. LA-left atrium, LV-left ventricle, RA-Right atrium, RV-right ventricle

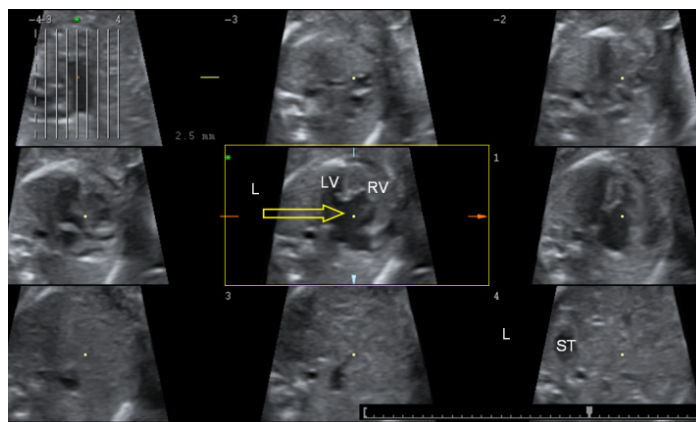
Color helps to confirm the diagnosis of AVSD showing in diastole blood flow over atrioventricular junction with a mixture of blood of all 4 cavities (Fig. 3) [2]. In diastole when the valve is closed regurgitation of the common (often dysplastic) atrioventricular valve is found [2].

AVSD is considered as the major cardiac defect found in chromosomal aberrations as trisomy 21, 18 and others. It is also very common in fetuses with heterotaxy syndrome, but in these cases it is not combined with aneuploidies [1]. Once an AVSD is detected the upper abdomen should be carefully examined and the presence of signs of heterotaxy reduce the risk of aneuploidy on one hand but increase the risk of a complex cardiac malformation as part of heterotaxy syndrome on the other.

An easy hint to facilitate detection of an AVSD is the observation of a ratio of atrial-to-ventricular length being more than 0.6 in the majority of cases conversely to a ratio of 0.5 in normal fetuses [3].

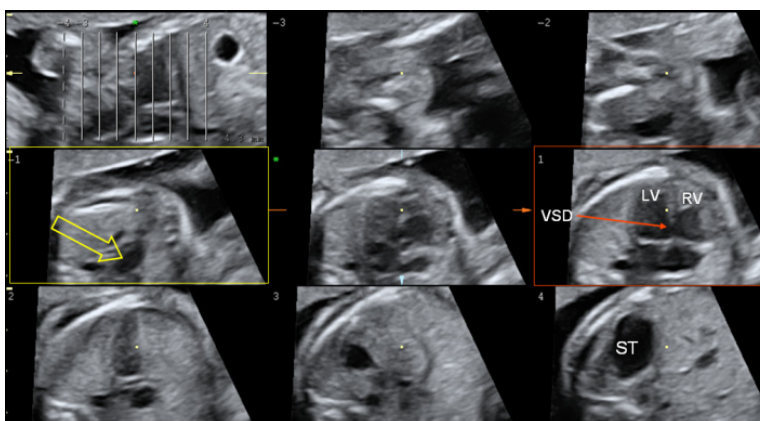
### THREE-DIMENSIONAL ULTRASOUND IN SEPTAL DEFECTS ORTHOGONAL PLANES AND TOMOGRAPHIC IMAGING

Septal defects are generally small and the information provided by a volume acquired as spatio-temporal image correlation (STIC) is generally superior to a static 3D volume in reliably demonstrating the defect. The demonstration of specific planes of a fetal heart with a septal defect either using 3D orthogonal or tomographic mode, facilitates the visualization of the lesion in addition to its adjacent planes. This visualization provides more information than on conventional 2D sonography. Ventricular and atrioventricular septal defect can be an isolated lesion but can also be a part of a complex cardiac and extracardiac malformation and tomographic ultrasound imaging has been shown to provide a better complete picture of the underlying anomaly in such cases (Figs. 4, 5) [4].



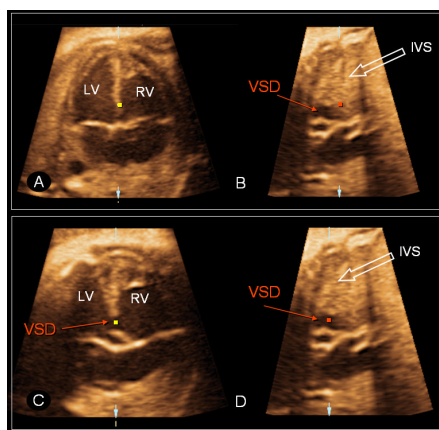
**Figure 4:** Three dimensional tomographic imaging in a fetus with a detected atrioventricular septal defect (arrow in the middle image). Tomography provides the complete image showing a normal abdominal situs with the stomach (=St) left sided). L-Left. LV-left ventricle, RV-right ventricle

Fig. 4 shows that the AVSD is not associated with heterotaxy, since the stomach is on the left side, whereas Fig. 5 shows the suspected VSD is not an isolated finding but a part of a common arterial trunk.



**Figure 5:** Three dimensional tomographic imaging in a fetus with a detected ventricular septal defect (solid arrow in red box plane). Tomographic imaging provides the additional information of abnormal great vessels (Yellow box). The yellow arrow shows that only one vessel is present. This is not an isolated VSD, but combined with a common arterial trunk. LV-left ventricle, RV-right ventricle

The orthogonal 3D display can be used in gray scale (Fig. 6) or in combination with color Doppler to demonstrate the presence of a VSD in all three planes, by placing the intersection dot on the shunting VSD (Fig. 6 [video 1](#)) [5-6].



**Figure 6:** Three-dimensional STIC volume of a heart with a ventricular septal defect (VSD), in orthogonal planes display. In the upper panels A) and B), the apical view A) is shown without the VSD visualized. B) is the orthogonal plane to A) and is the in-



line visualization of the interventricular septum (IVS). In this plane the VSD is recognized red arrow in the perimembranous part of the septum. In C) and D) the intersection dot was moved to be placed in the VSD region in D) and the VSD is also recognized in the apical view in C) as well. RV- right ventricle, LV left ventricle

For AVSD the diagnostic information in small defects is related to the demonstration of diastolic and systolic views, which is facilitated by scrolling through the volume along the time axis of the cardiac cycle (Fig. 7).

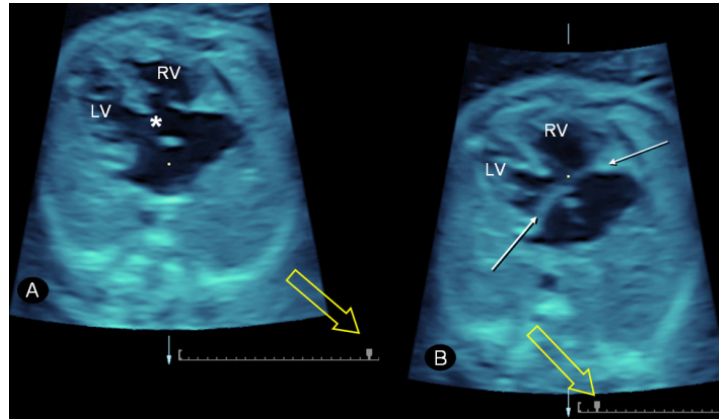


**Figure 7:** Fetus with atrioventricular (AV) septal defect. Spatio-temporal image correlation allows in addition to the choice of a selective plane (here the apical four-chamber view, the choice of the time within the cardiac cycle (opened arrows on the time axis): In A) diastolic phase with opened AV valve showing the gap in the center of the heart (Asterisk) and in B) systolic phase with closed common AV valve, both valves showing a linear insertion (white arrows). RV- right ventricle, LV left ventricle.

Volume information provides in addition the possibility of getting “ideal planes” or “anyplane” out of a volume [5-6] and the proposed “in-plane” view to demonstrate a septal defect [6], which is a plane along the interventricular septum (see Fig. 6B and D) can be easily retrieved from a STIC volume as shown in Fig. 6.

### SURFACE RENDERING MODE

Surface mode used on gray scale STIC or combined with color Doppler STIC can be used to improve the visualization of septal defects not only in the usual four-chamber view, but also by getting new planes. One of these is the “en face” view of the ventricular septum as shown for the VSD in Fig. 8 and 9. The study of the ventricular septal defect in this “en-face” view enables for large defects to be better localized on the septum (Fig. 8 perimembranous, and Fig. 9 midmuscular).

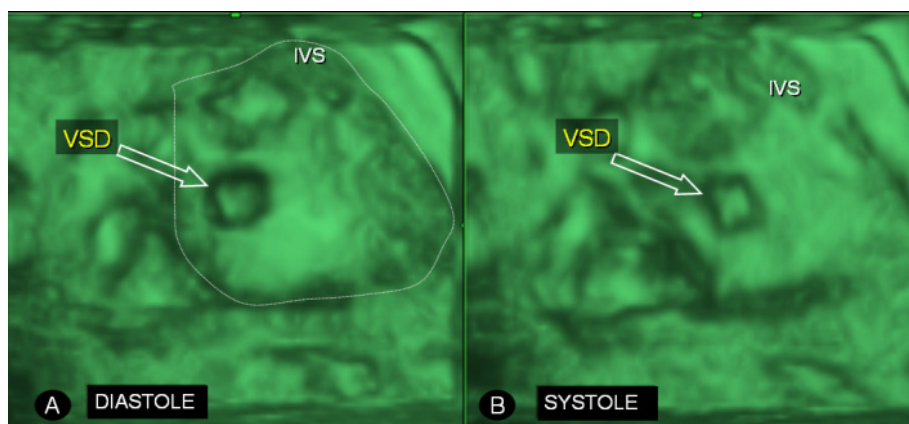


**Figure 8:** En face view of the interventricular septum (IVS) in a fetus with a large ventricular septal defect (VSD). Both images show clearly how size and shape of the VSD change during the cardiac cycle. In diastole (A) at the maximum of chamber filling the shape is circular and the size is large, whereas in systole when the chamber size is smaller the septum is „squeezed“ and the VSD is smaller and the shape not circular anymore.

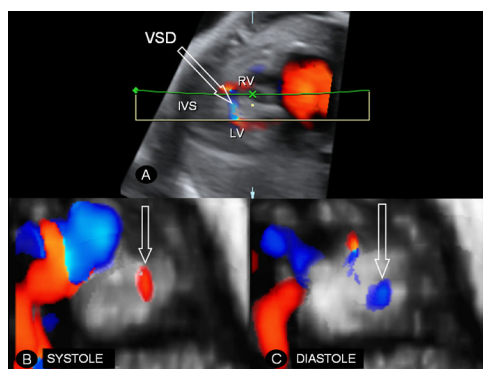


**Figure 9:** In this fetus with muscular ventricular septal defect (VSD, open arrow) color Doppler STIC acquisition allows the demonstration of flow events across the VSD during the cardiac cycle by using glass-body mode rendering. The rendering box is placed over the interventricular septum (IVS) allowing a view from the right side. During systole (A) blood flow is from left to right (red) and the VSD size appears smaller (compare with previous case). In diastole (B) blood flow is from right to left and the VSD size is larger. RV- right ventricle, LV left ventricle

In addition it demonstrates the changes of the size of the defect being large and circular in diastole when chambers are maximally filled with blood and smaller and “squeezed” in systole (Fig. 8 and 9). The addition of color or power Doppler can be combined with glass body mode to demonstrate either the en-face view on the septum (Fig. 9) or the anterior view of the heart showing both ventricles connected by the ventricular septal defect and the crossing of great vessels (Fig. 10).

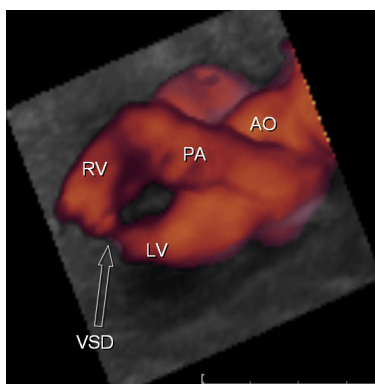


**Figure 10:** Fetus with a ventricular septal defect (VSD) shown in power Doppler STIC acquisition demonstrating in glass-body mode an anterior view to the heart. Both blood flow in right (RV) and left (LV) ventricles is demonstrated and the crossing of aorta (AO) and main pulmonary artery (PA) are clearly recognized

In atrioventricular septal defects surface rendering at the four-chamber view level may emphasize the size of the gap in the crux of the heart (Fig. 11. [video 2](#))



**Figure 11:** Four-chamber plane of a fetus with atrioventricular septal defect, showing in surface mode rendering of a STIC volume the linear insertion of the common AV valve in systole and the atrial and ventricular septal defects (Asterisks) LA-left atrium, LV-left ventricle, RA-Right atrium, RV-right ventricle



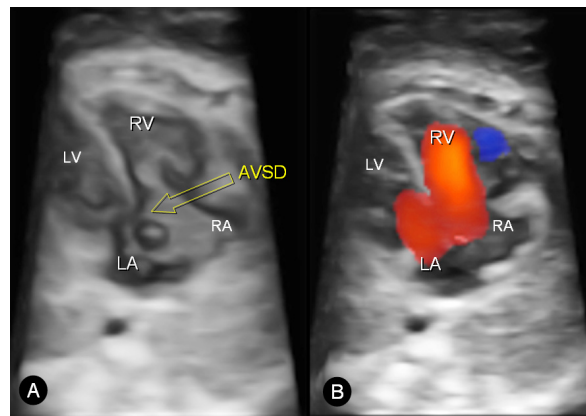


**Figure 12:** In this fetus with atrioventricular septal defect (AVSD, open arrow) color Doppler STIC acquisition allows the demonstration of flow events across the defect with 3D glass-body mode display A) shows the surface mode rendering during diastole with the opened common valve and B) shows the diastolic filling across the defect (compare with systole in next figure) LA-left atrium, LV-left ventricle, RA-Right atrium, RV-right ventricle

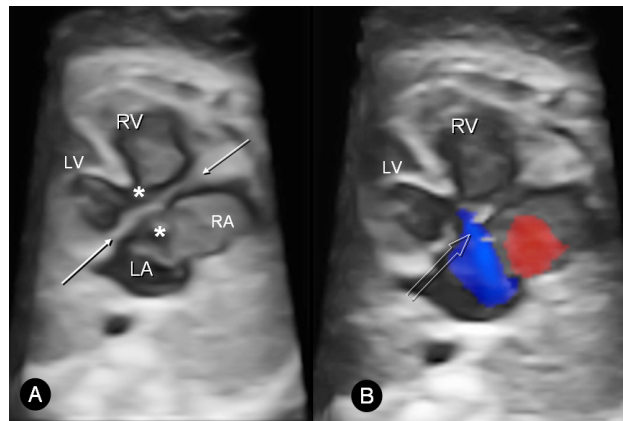


**Figure 13:** 3D glass-body mode display in a fetus with atrioventricular septal defect showing the four-chamber view during systole. A) surface mode alone shows the defect (asterisks) and the linear insertion of the common AV valve. B) color Doppler added to the surface mode shows the valve regurgitation (open arrow) with blue flow from the ventricle into the atrium. LA-left atrium, LV-left ventricle, RA-Right atrium, RV-right ventricle

The combination of STIC with color Doppler and glass body mode display allows the demonstration of the cardiac cycle related events, namely the mixture of blood flow across the defect during diastole (Fig. 12) and the valve regurgitation of the common atrioventricular valve during systole (Fig. 13).

Another approach was proposed to visualize anomalies affecting the atrioventricular valves or the arrangement of the great vessels called the “basic cardiac view” (9) (Fig. 14 [video 3](#))

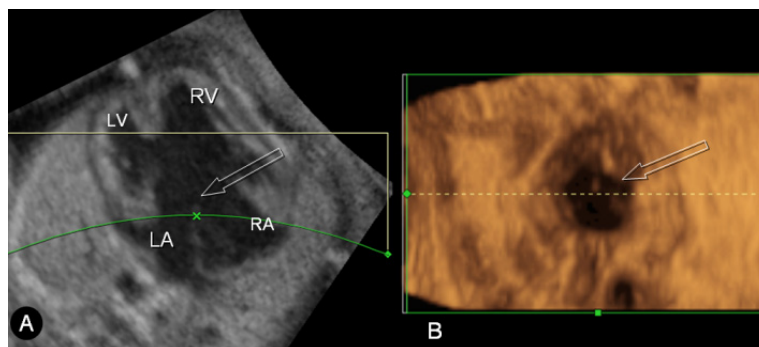


**Figure 14:** Atrioventricular septal defect (open arrow) with three dimensional surface rendering of STIC volume. The color box is placed in the atria and allows an „en face surface view“ on the common valve. In diastole the common valve orifice (B) is demonstrated clearly (open arrow)

When the 3D box is placed within the atria, the en face view on the atrioventricular valves, shows instead of two valves a single opening of the common valve (Fig. 14). The en-face view of the common AV valve can also be visualized from the ventricles which has in addition the advantage of providing valuable information on the anatomy of the valve apparatus [10].

### **COLOR DOPPLER, HIGH DEFINITION POWER DOPPLER, INVERSION MODE, B-FLOW RENDERING**

The combination of these features with STIC permits the demonstration of flow events across the septal defects as shown before and the rendering mode should be chosen accordingly to the underlying defect and the information wished. The demonstration of flow across a small VSD can for example be shown by combining B-flow or High definition power Doppler with STIC technique both enabling the detection of small defects. The use of inversion mode however, is preferably used for larger defects already recognizable on 2D [11].

### **CONCLUSIONS**

Septal defects in the fetus may be detected on two-dimensional ultrasound but are always confirmed by the use of color Doppler ultrasound. The use of three-dimensional ultrasound in fetal septal defects will preferably use spatio-temporal image correlation (STIC) acquisition. According to the wished information, orthogonal or tomography display modes can provide a better complete picture of the defect with neighbouring structures visualized, as well as an ideal demonstration of site and the range of the defect. Surface mode allows different views either the commonly used transverse views (four-chamber e.g.) or new “en face” views directly on the septum or on the atrioventricular valves. The additional combination of STIC with color Doppler, or other acquisition tools may add the spatial information of flow events in septal defects.

### **REFERENCES**

- [1] Esh-Broder E, Ushakov FB, Imbar T, Yagel S. Application of free-hand three-dimensional echocardiography in the evaluation of fetal cardiac ejection fraction: a preliminary study. *Ultrasound Obstet Gynecol* 2004; 23(6): 546-51.
- [2] Simpson JM, Cook A. Repeatability of echocardiographic measurements in the human fetus. *Ultrasound Obstet Gynecol* 2002; 20(4):332-9.
- [3] Teichholz LE, Kreulen T, Herman MV, Gorlin R. Problems in echocardiographic volume determinations: echocardiographic-angiographic correlations in the presence or absence of asynergy. *Am J Cardiol* 1976; 37(1):7-11.
- [4] Bhat AH, Corbett V, Carpenter N, *et al.* Fetal ventricular mass determination on three-dimensional echocardiography: studies in normal fetuses and validation experiments. *Circulation* 2004; 110(9):1054-60.
- [5] Wyatt HL, Meerbaum S, Heng MK, Gueret P, Corday E. Cross-sectional echocardiography. III. Analysis of mathematic models for quantifying volume of symmetric and asymmetric left ventricles. *Am Heart J* 1980; 100(6 Pt 1):821-8.
- [6] Sedmera D, Pexieder T, Vuillemin M, Thompson RP, Anderson RH. Developmental patterning of the myocardium. *Anat Rec* 2000; 258(4): 319-337.
- [7] Simpson J. Echocardiographic evaluation of cardiac function in the fetus. *Prenat Diagn* 2004; 24 (13): 1081-91.
- [8] Bhat AH, Corbett VN, Liu R, *et al.* Validation of volume and mass assessments for human fetal heart imaging by 4-dimensional spatiotemporal image correlation echocardiography: in vitro balloon model experiments. *J Ultrasound Med* 2004; 23(9):1151-
- [9] Espinoza J, Gotsch F, Kusanovic, JP, *et al.* Changes in fetal cardiac geometry with gestation: implications for 3- and 4-dimensional fetal echocardiography. *J Ultrasound Med* 2007; 26(4): 427-43.
- [10] Levental M, Pretorius DH, Sklansky MS, Budorick NE, Nelson TR, Lou K. Three-dimensional ultrasonography of normal fetal heart: comparison with two-dimensional imaging. *J Ultrasound Med* 1998; 17(6):341-8.
- [11] Meyer-Wittkopf M, Cole A, Cooper SG, Schmidt S, Sholler GF. Three-dimensional quantitative echocardiographic assessment of ventricular volume in healthy human fetuses and in fetuses with congenital heart disease. *J Ultrasound Med* 2001; 20(4):317-27.
- [12] Tutschek B, Sahn DJ. Semi-automatic segmentation of fetal cardiac cavities: progress towards an automated fetal echocardiogram. *Ultrasound Obstet Gynecol* 2008; 32(2):176-80.
- [13] Uittenbogaard LB, Haak MC, Spreuwenberg MD, VanVugt JMG. A systematic analysis of the feasibility of four-dimensional ultrasound imaging using spatiotemporal image correlation in routine fetal echocardiography. *Ultrasound Obstet Gynecol* 2008; 31(6): 625- 32.
- [14] Huhta J. Congestive heart failure in the fetus. In *Fetal Cardiology* (2<sup>nd</sup> edition), Yagel S, Silverman NH, Gembruch U (eds.). Informa Healthcare USA, Inc: New York, NY, 2009; 561-78.

- [15] Messing B, Cohen SM, Valsky DV, *et al.* Fetal cardiac ventricle volumetry in the second half of gestation assessed by 4D ultrasound using STIC combined with inversion mode. *Ultrasound Obstet Gynecol* 2007; 30(2):142-51.
- [16] Molina FS, Faro C, Sotiriadis A, Dagklis T, Nicolaides KH. Heart stroke volume and cardiac output by four-dimensional ultrasound in normal fetuses. *Ultrasound Obstet Gynecol* 2008; 32(2):181-7.
- [17] Rizzo G, Capponi A, Cavicchioni O, Vendola M, Arduini D. Fetal cardiac stroke volume determination by four-dimensional ultrasound with spatio-temporal image correlation compared with two-dimensional and Doppler ultrasonography. *Prenat Diagn* 2007; 27(12): 1147-50.
- [18] Uittenbogaard LB, Haak MC, Spreuwenberg MD, VanVugt JMG. Fetal cardiac function assessed with four-dimensional ultrasound imaging using spatiotemporal image correlation. *Ultrasound Obstet Gynecol* 2009; 33(3):272-81.
- [19] DeVore GR, Falkensammer P, Sklansky MS, Platt LD. Spatio-temporal image correlation (STIC): new technology for evaluation of the fetal heart. *Ultrasound Obstet Gynecol* 2003; 22(4):380-7.
- [20] Gonçalves LF, Lee W, Espinoza J, Romero R. Examination of the fetal heart by four-dimensional (4D) ultrasound with spatio-temporal image correlation (STIC). *Ultrasound Obstet Gynecol* 2006; 27(3):336-48.
- [21] Nelson TR, Pretorius DH, Sklansky M, Hagen-Ansert S. Three-dimensional echocardiographic evaluation of fetal heart anatomy and function: acquisition, analysis, and display. *J Ultrasound Med* 1996; 15(1):1-9.
- [22] Gonçalves LF, Espinoza J, Lee W, Mazor M, Romero R. Three- and four-dimensional reconstruction of the aortic and ductal arches using inversion mode: a new rendering algorithm for visualization of fluid-filled anatomical structures. *Ultrasound Obstet Gynecol* 2004; 24(6):696-98.
- [23] National Institute of Standards and Technology. Guidelines for Evaluating and Expressing the Uncertainty of NIST Measurement Results. <http://emtoolbox.nist.gov/Publications/NISTTechnicalNote1297s.pdf> (July 13 2009).
- [24] Bartlett JW, Frost C. Reliability, repeatability and reproducibility: analysis of measurement errors in continuous variables. *Ultrasound Obstet Gynecol* 2008; 31(4): 466-75.
- [25] Hamill N, Romero R, Hassan S, *et al.* The repeatability and reproducibility of fetal cardiac ventricular volume calculations utilizing Spatio-Temporal Image Correlation (STIC) and Virtual Organ Computer-aided AnaLysis (VOCAL™). *J Ultrasound Med*, in press.
- [26] Mielke G, Benda N. Cardiac output and central distribution of blood flow in the human fetus. *Circulation* 2001; 103(12):1662-8.
- [27] Stewart WJ, Jiang L, Mich R, Pandian N, Guerrero JL, Weyman AE. Variable effects of changes in flow rate through the aortic, pulmonary and mitral valves on valve area and flow velocity: impact on quantitative Doppler flow calculations. *J Am Coll Cardiol* 1985; 6(3):653-62.
- [28] Eik-Nes S, Marsal K, Kristofferson K. Methodology and basic problems related to blood flow studies in the human fetus. *Ultrasound Med Biol* 1984; 10(3):329-37.
- [29] Chaoui R, Heling KS, Taddei F, Bollmann R. Doppler echocardiographic analysis of blood flow through the fetal aorta and pulmonary valve in the second half of pregnancy. *Geburt Fraueh* 1995; 55(4): 207-17.
- [30] Rasanen J, Wood DC, Weiner S, Ludomirski A, Huhta JC. Role of the pulmonary circulation in the distribution of human fetal cardiac output during the second half of pregnancy. *Circulation* 1996; 94(5): 1068-1073.
- [31] Thornburg KL, Reller MD. Coronary flow regulation in the fetal sheep. *Am J Physiol* 1999; 277(5 Pt 2): R1249-60.
- [32] Schmidt KG, Silverman NH, Hoffman JIE. Determination of ventricular volumes in human fetal hearts by two-dimensional echocardiography. *Am J Cardiol* 1995; 76(17):1313-16.
- [33] Allan LD, Chita SK, Al-Ghazali W, Crawford DC, Tynan M. Doppler echocardiographic evaluation of the normal human fetal heart. *Br Heart J* 1987; 57(6):528-33.
- [34] De Smedt MC, Visser GH, Meijboom EJ. Fetal cardiac output estimated by Doppler echocardiography during mid- and late gestation. *Am J Cardiol* 1987; 60(4):338-42.
- [35] Kenny JF, Plappert T, Doubilet P, *et al.* Changes in intracardiac blood flow velocities and right and left ventricular stroke volumes with gestational age in the normal human fetus: a prospective Doppler echocardiographic study. *Circulation* 1986; 74(6):1208-16.
- [36] Veille JC, Sivakoff M, Nemeth M. Evaluation of the human fetal cardiac size and function. *Am J Perinatol* 1990; 7(1):54-9.
- [37] Anderson PAW. Myocardial development. In *Fetal and Neonatal Cardiology*, Long W (ed.). W.B. Saunders: Philadelphia, PA, 1990; 17-38.
- [38] Teitel DF. Physiologic Development of the Cardiovascular System in the Fetus. In *Fetal and Neonatal Physiology* (3<sup>rd</sup> edition), Polin RA, Fox WW, Abman H (eds.). W.B. Saunders: Philadelphia, PA, 2003; 609-19.
- [39] Winberg P, Jansson M, Marions L, Lundell BP. Left ventricular output during postnatal circulatory adaptation in healthy infants born at full term. *Arch Dis Child* 1989; 64:1374-78.
- [40] Pemberton J, Li X, Kenny A, Davies CH, Minette MS, Sahn DJ. Real-time 3-dimensional Doppler echocardiography for the assessment of stroke volume: an in vivo human study compared with standard 2-dimensional echocardiography. *J Am Soc Echocardiogr* 2005; 18(10):1030-36.

## 4D Study of Right Heart Anomalies

Giuseppe Rizzo and Domenico Arduini

*Department of Obstetrics and Gynecology, Università Roma "Tor Vergata"*

**Abstract:** In this chapter, the 2D, color Doppler and four dimensional (4D) features of major right heart abnormalities are described. In particular, the echocardiographic views on which the various lesions are present are reported. The diagnostic role of 4D echocardiography in allowing a spatial demonstration of the defects with the possibility of getting new views into the heart is outlined. Videos of major diagnostic features are also provided, to facilitate the understanding of the text.

**Key Words:** 4D Sonography, Fetal Echocardiography, Right Heart Anomalies, Prenatal Diagnosis.

### INTRODUCTION

This chapter will cover the most significant anomalies of the right side of the heart that can be observed prenatally. For each condition after a brief anatomical description, the criteria of echocardiographic diagnosis will be provided. In particular we will focus on the four dimensional (4D) acquisition and postprocessing modalities in fetal hearts with right side anomalies, demonstrating their use through case examples. A classification of right heart anomalies is reported in Table 1

**Table 1:** Fetal right heart anomalies

<b>Anomalies of the inlet</b>
Tricuspid atresia
Tricuspid dysplasia, regurgitation
Ebstein's anomaly
<b>Anomalies of the outlet (without septal defect)</b>
Pulmonary stenosis
Pulmonary atresia
<b>Anomalies of the outlet (with septal defect)</b>
Tetralogy of Fallot
Double outlet right ventricle
Truncus arteriosus

The anomalies of the outlet with associated a ventricular septal defect (the so called conotruncal anomalies) will be described in chapter 15.

### TRICUSPID ATRESIA

Tricuspid atresia is a congenital heart disease (CHD) where there is direct connection between the right atrium and right ventricle. A communication with the right ventricle is usually present and occurs through a ventricular septal defect.

The prevalence of tricuspid atresia has been between 2-3% of infants with CHD and 1-2% prenatally [1,2,3]. Due to the relative hypodevelopment of the right ventricle tricuspid atresia is frequently diagnosed in utero under the hypoplastic right heart syndrome and this may explain the minor incidence reported in prenatal series.

Diagnosis is usually performed by the 4 chamber view of the fetal heart [4] where an asymmetric development of the right ventricle is usually evident and a patent tricuspid valve is not identified (Fig. 1 [video 1](#))

\*Address Correspondence to Giuseppe Rizzo: Department of Obstetrics and Gynecology, Università Roma Tor Vergata Ospedale Fatebenefratelli Isola Tiberina 00186 Rome Italy; Email: giuseppe.rizzo@uniroma2.it

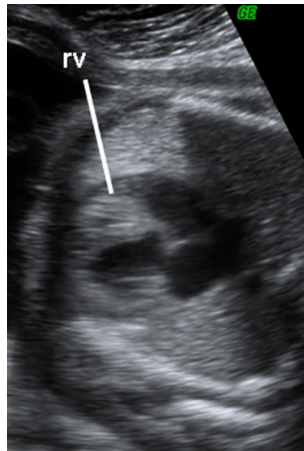


**Figure 1:** ([video 1](#)) A four chamber view of the fetal heart demonstrating tricuspid atresia. The right ventricle (RV) is hypoplastic and there is no opening tricuspid valve.

The associated ventricular septal defect is usually visible, even though it may be of variable size (Fig. 2 [video 2](#)).

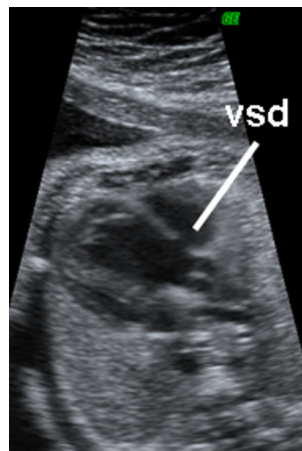


**Figure 2:** ([video 2](#)) Evidence of the ventricular septal defect (VSD) from the 4 chamber view of the fetal heart.

Color Doppler allows to confirm diagnosis by showing the lack of flow velocities across the tricuspid valve, a single ventricular flow inlet across the mitral valve and an unidirectional left to right shunt across the ventricular septal defect (Fig. 3 [video 3](#)).

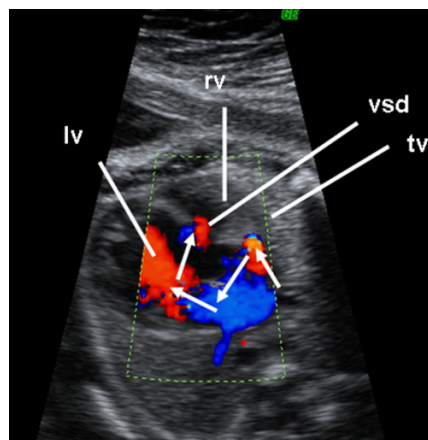


**Figure 3:** ([video 3](#)) Color Doppler shows absence of flow across the tricuspid valve (TV) and unidirectional shunt from the left ventricle (LV) to the right ventricle (RV) across the ventricular septal defect (VSD). Arrows indicate the abnormal blood flow direction due to the cardiac anomaly.

Intracardiac associated anomalies are frequent and in about 50% of the cases an obstructed right outflow is present. Arterial connections are usually concordant but transposed great arteries are present in about 20% of the cases. Less frequently an obstruction to the left ventricle outflow and anomalies of the pulmonary venous connections are present

Echocardiographic diagnostic criteria in tricuspid atresia are reported in Table 2.

**Table 2:** Sonographic features of tricuspid atresia

Small right ventricle
No opening tricuspid valve
Ventricular septal defect
No flow from right atrium to right ventricle
Unidirectional left to right shunt across the ventricular septal defect.

Tricuspid atresia is rarely associated with extracardiac anomalies. However it was reported a 5% incidence of chromosomal anomalies (trisomy 21, 18 deletion of chromosome 8 and 22q11 microdeletions). Unfrequent is also the association with extracardiac anomalies but an association with VATER e VACTEREL syndromes has been reported [1, 3].

Although diagnosis is usually possible by routine screening of fetal heart with the 4 chamber view (4) population-based studies have shown low detection rates, with more than 50% of tricuspid atresia remaining undetected on routine second-trimester fetal ultrasound examination [5-6].

The recent introduction of 4D ultrasonography to clinical practice provided an important advance in imaging technology. With a 4D acquisition of the fetal heart from the 4 chamber view it is possible to obtain several additional informations on the cardiac anatomy in tricuspid atresia.

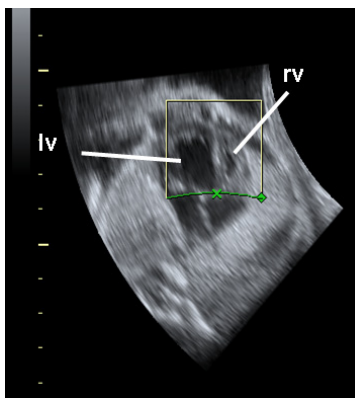


**Figure 4:** (video 4) Apical four chamber view of the fetal heart in a case of tricuspid atresia showing the disproportion between the left (LV) and right (RV) ventricle.

The advantages are:

- a) look at the integrity of the septal wall using tomographic technique (7) (Fig. 5 video 5).

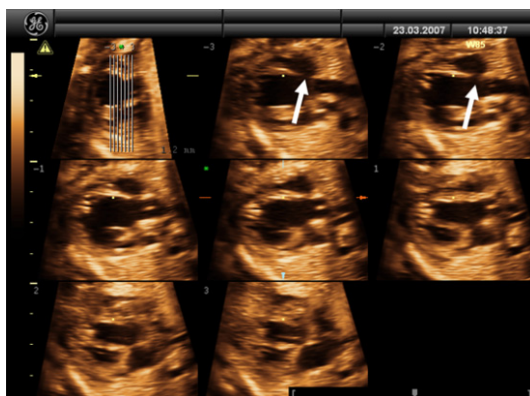


**Figure 5:** (video 5) Tomographic view of a case with tricuspid atresia allowing to evidence a small ventricular septal defect (arrows)

b) rendering the atrioventricular valve showing the tricuspid valve defect (Fig. 6 [video 6](#))

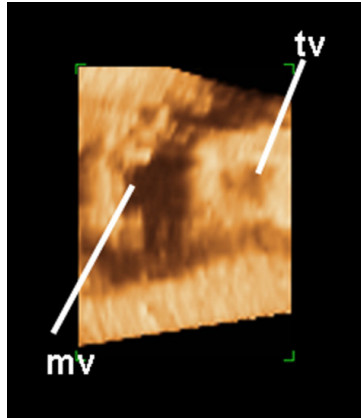


**Figure 6:** ([video 6](#)) From the apical four chamber view of the fetal heart shown in Fig. 4 the rendering function is used. The figure shows a coronal view of the atrioventricular valve during diastole showing the normal opening of the mitral valve (MV) and the “no opening” of the tricuspid valve (TV)

c) rendering the fetal heart to provide a better view of the right ventricle (RV) dimensions and contractility (Fig. 7, [video 7](#))

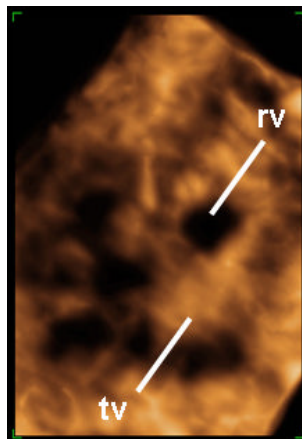


**Figure 7:** ([video 7](#)) Rendering of the 4 chamber view showing the deep size of tricuspid valve and the small right ventricle (RV)

d) providing a “live” view of the abnormal hemodynamic using inversion mode rendering techniques (Fig. 8 [video 8](#)) or rendering with color Doppler or B-flow.

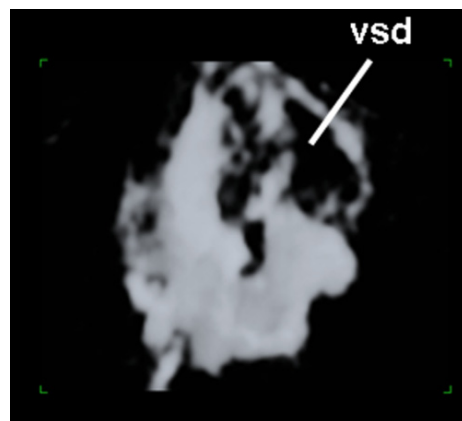


**Figure 8:** ([video 8](#)) Rendering of the 4 chamber view with inversion mode showing the abnormal hemodynamic characterized by the absence of flow across the tricuspid valve and the left to right shunt across the ventricular septal defect (VSD)



## TRICUSPID DYSPLASIA AND REGURGITATION

This anomaly include a wide spectrum of diseases ranging from transient findings to a more severe forms characterized by thickened valve leaflets. Tricuspid regurgitation occurs in about 5% of second trimester fetuses [8] and it is generally induced by a relative immaturity of valve leaflets faced to high value of right ventricular afterload occurring during the first half of pregnancy. With advancing gestation the afterload falls due to reduction in placental impedance to flow, the valvular function improves and as a consequence the tricuspid regurgitation disappears.

Tricuspid dysplasia is distinguished from Ebstein's anomaly on the basis of the normal insertion of the valve leaflets to the ventricular wall.

Diagnosis may be difficult and it is usually performed by the 4 chamber view of the fetal heart were an enlarged right atrium with a tricuspid valve with increased echogenicity may be evidenced. By Color Doppler is possible to document the tricuspid regurgitation (Fig. 9 [video 9](#)).

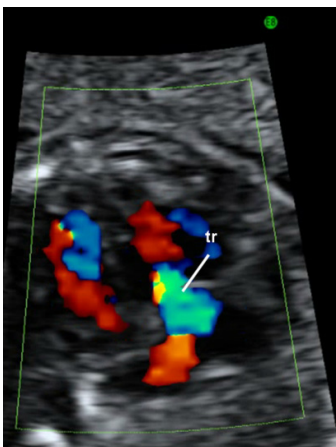


**Figure 9:** ([video 9](#)) Four chamber view of the fetal heart with color Doppler function superimposed showing tricuspid regurgitation (tr) in a second trimester fetus.

Pulsed or continuous Doppler allows to quantificate the severity of regurgitation. It is particularly important to quantify the duration of the regurgitation that may last all the systole (olossystolic) or its initial part (so called trivial) (Fig. 10).

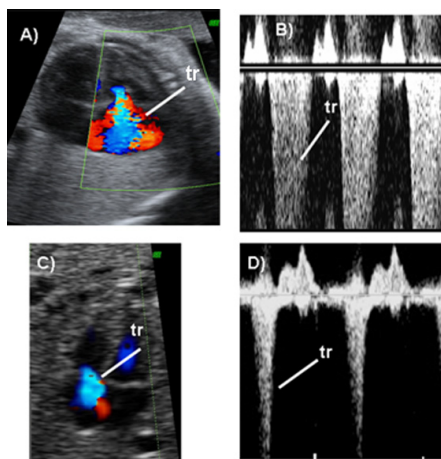


**Figure 10:** Quantification of tricuspid regurgitation (tr) with color and pulsed Doppler techniques. In panel A and B a case with olosystolic regurgitation and C and D a case of "trivial" regurgitation.

In order to avoid a misleading diagnosis of trivial regurgitation instead due to signals generated by physiological valve closure a duration  $> 70$  msec is considered diagnostic [8].



Diagnosis of tricuspid regurgitation at 11+0 to 13+6 weeks of gestation is of clinical interest since 60% of fetuses with trisomy 21 and 30% of fetuses with trisomy 18 have this anomaly [9]. In presence of a normal karyotype (5% of euploid fetuses have this finding) tricuspid regurgitation may be an early marker of more complex CHD (10) (Fig. 11 [video 10](#))



**Figure 11:** ([video 10](#)) Four chamber view of the fetal heart with color Doppler function superimposed showing tricuspid regurgitation (tr) in a fetus at 12 weeks of gestation.

Associated anomalies other than aneuploidies (trisomy 21,18, 13 and 45 X) may include secondary pulmonary stenosis/atresia due to reduced anterograde flow in the right outflow tract-

4D ultrasound provides two major advantages:

a) rendering the tricuspid valve allowing the visualization of the thickened leaflets (Fig. 12 [video 11](#))

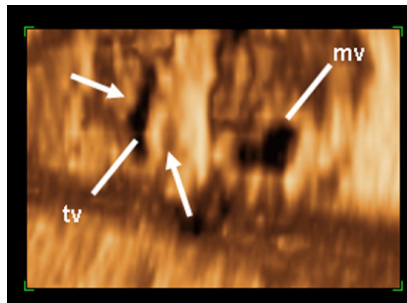


**Figure 12:** ([video 11](#)) Coronal view of the atrioventricular valve showing the normal the mitral valve (MV) and the thickened leaflets (arrows) of the tricuspid valve (TV)

b) exact localization of the color jet of the tricuspid regurgitation by multiplanar navigation of cardiac volume acquired with color Doppler. Indeed as shown in Fig. 13 the jet may be missed in one section (Fig. 13a [video 12](#)) and visualized only after the selection of the proper plane by multiplanar navigation (Fig. 13b [video 13](#)).

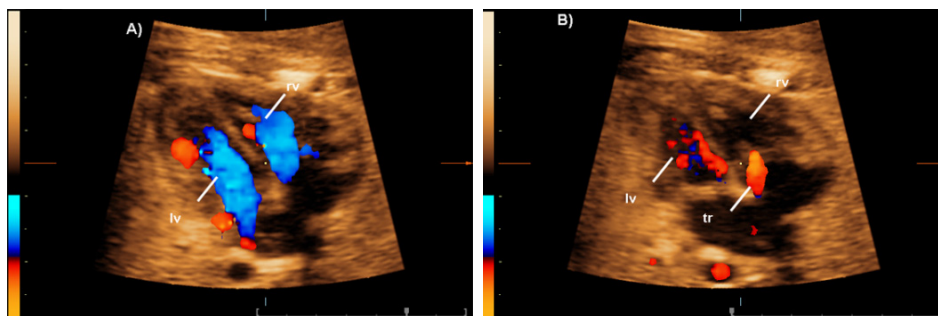


**Figure 13:** A ([video 12](#)) Four chamber view with color Doppler reconstructed from a 4D cardiac volumes showing apparent normal filling of left (LV) and right ventricle (RV). B ([video 13](#)) The plane is slightly scrolled cranially and tricuspid regurgitation (tr) is evidenced.

## EBSTEIN'S ANOMALY

Ebstein's anomaly is a rare entity with a prevalence of 0.3-0.5% of CHD [1, 11]. Ebstein's malformation is a CHD in which the septal and mural (posterior) leaflets of the tricuspid valve are displaced downward into the inlet portion of the right ventricle. Tricuspid valve is always incompetent and there is a right atrium enlargement. The right ventricular size is reduced as its function is inversely related to its dimension [11].

Diagnosis is performed by cardiomegaly with dilatation of right atrium, low insertion of the septal and mural leaflets while the anterior usually appears moving in an abnormal way (spinnaker effect) (Fig. 14 [video 14](#)).

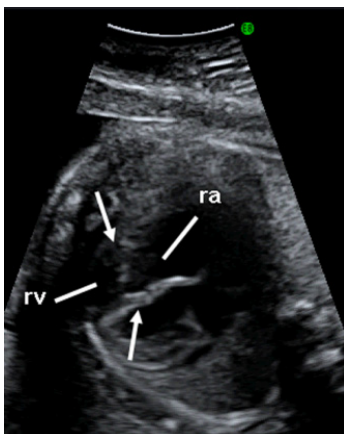


**Figure 14:** ([video 14](#)) Four chamber view of the fetal heart showing an enlarged right atrium (RA), the low insertion (arrows) of the septal and posterior leaflets in the right ventricle (RV) and the “spinnaker effect” ([video 14](#)) and the anterior leaflet.

At color Doppler a massive regurgitant jet is evident (Fig. 15 [video 15](#)).

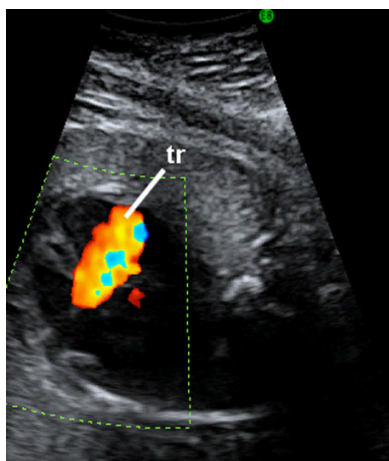


**Figure 15:** ([video 15](#)) Some fetus of Fig. 14 on color Doppler a severe tricuspid regurgitation is shown.

Intracardiac associated anomalies are frequent and include anatomic or functional (due to reduced anterograde flow) pulmonary stenosis-atresia, restrictive foramen ovalis, atrioventricular and ventriculo-arterial discordance [11]. The presence of associated anomalies affects the prognosis.

The presence of chromosomal anomalies is unusual but Ebstein's disease can be associated with Apert's, Noonan's and CHARGE syndromes [11].

4D echocardiography has been shown to be useful in predicting the results of surgical valvuloplasty [12]. Indeed it is possible to:

a) obtain an assessment of the commissures and leaflet surfaces by rendering the tricuspid valve (Fig. 16 [video 16](#)).

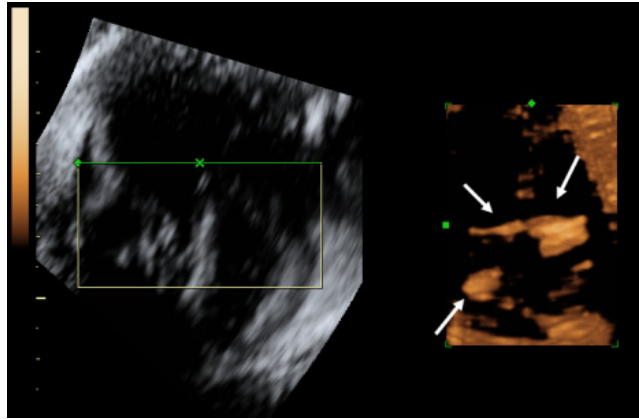


**Figure 16:** ([video 16](#)) Coronal view of the tricuspid valve in Ebstein' disease showing the rendering and the relationship of dysplastic leaflets(arrows)

b) providing a “live” view of the abnormal hemodynamic using rendering with color Doppler by showing the amount of retrograde and anterograde perfusion of the right ventricle (Fig. 17 [video 17](#)).

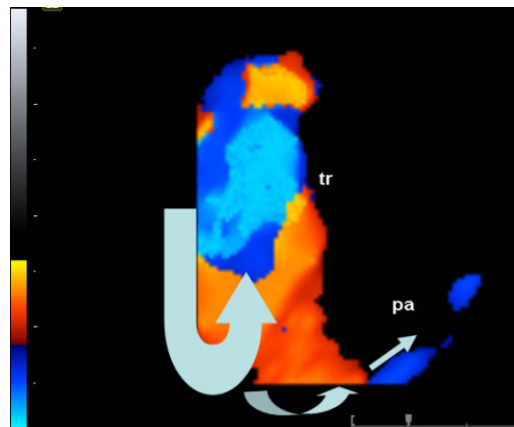


**Figure 17:** ([video 17](#)) Color Rendering of right ventricle hemodynamics in Ebstein's anomaly showing the prevalence of retrograde flow with tricuspid regurgitation (tr) and the marked reduced anterograde flow in pulmonary artery (pa)

c) allowing an absolute volumetric quantification of the functional ventricle and enlarged atrium. This may be obtained manually on acquired cardiac volumes or using an semiautomatic segmentation approach of cardiac cavities (13,14) as shown in Fig. 18.

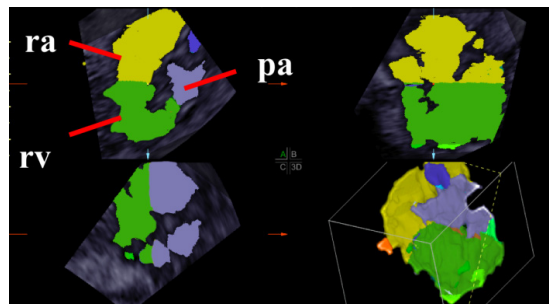


**Figure 18:** Semiautomatic segmentation of the right heart showing the enlarged right atrium (ra yellow), the small right ventricle (rv green ) and pulmonary artery (pa grey) outflow shown in the 3 orthogonal planes and rendered. (3D).

## PULMONARY STENOSIS

Isolated pulmonary stenosis represent 0.8% of CHD [1] and covers a wide spectrum in terms of presentation and severity and must be distinguished from critical stenosis and atresia of the valve.

The 4 chamber view is usually normal and diagnosis is frequently missed in screening program. Right ventricular outflow tract show the sonographic features shown in Table 3.

**Table 3:** Sonographic features of isolated pulmonary stenosis.

Restricted pulmonary valve leaflets
Dilatation after stenosis (occasionally)
Turbulent flow across the PA valve
Increased Doppler velocity

An example of isolated pulmonary stenosis is reported in

Fig. 19 and [video 18](#).

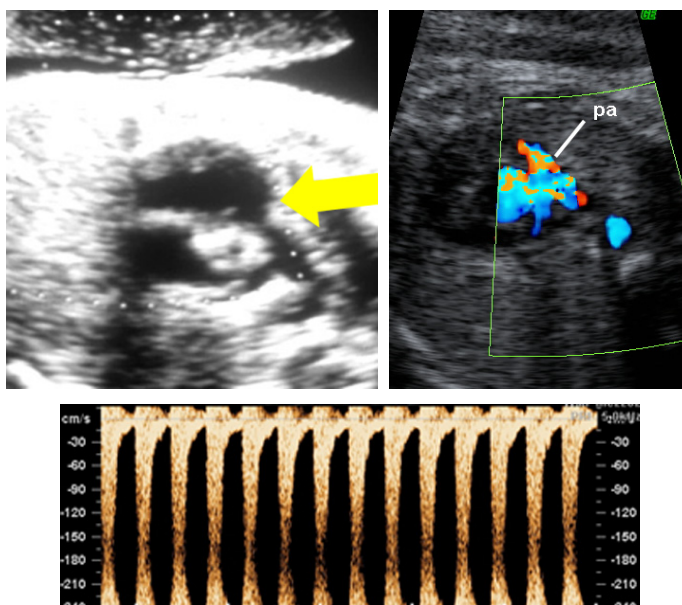


**Figure 19:** ([video 18](#)) Short axis view of the fetal heart showing the narrowing of the pulmonary artery (pa) (arrow upper panel ) and the turbulent flow (middle panel) and the increased flow velocities at pulsed Doppler (lower panel).

Pulmonary stenosis can occur as a part of Noonan's, Alagille's and Williams syndromes and it is unfrequently associated with chromosomal anomalies.

In isolated pulmonary stenosis 4 D echocardiography is useful in evaluating the thickened restricted pulmonary valve leaflets (Fig. 20 [video 19](#)).



**Figure 20:** ([video 19](#)) rendering of the short axis view of the fetal heart showing the thickened pulmonary artery (PA) leaflets.

## PULMONARY ATRESIA

Pulmonary atresia and critical stenosis with intact ventricular has an incidence of about 10%, of all CHD [1]. There is continuity between the two forms and critical stenosis may develop in an atresic valve. According to tricuspid valve there are two different anatomic variants. In absence of tricuspid regurgitation an hypoplastic right ventricle is present while in presence of tricuspid regurgitation the dimension of the right ventricle are normal and the right atrium enlarged. The former situation is more frequent and accounts for about the 70% of cases.

In Fig. 21 ([video 20](#).) an example with hypoplastic right ventricle is reported.

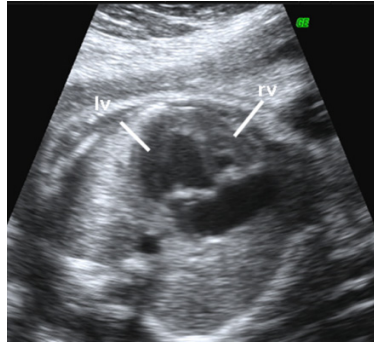


**Figure 21:** ([video 20](#)) Four chamber view showing an hypoplastic right ventricle (rv) when compared to the left ventricle (lv).

Color flow mapping confirms the abnormal filling of the ventricle (Fig. 21 [video 21](#))

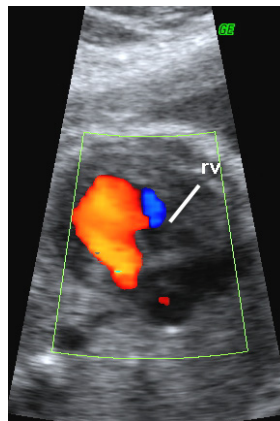


**Figure 22:** ([video 21](#)) Four chamber view with color Doppler function superimposed showing the absent filling of the right ventricle (rv).

The pulmonary artery can vary in size from being near normal to severe hypoplastic and the valve leaflets are thickened and do not disappear during systole (Fig. 23 [video 22](#)).

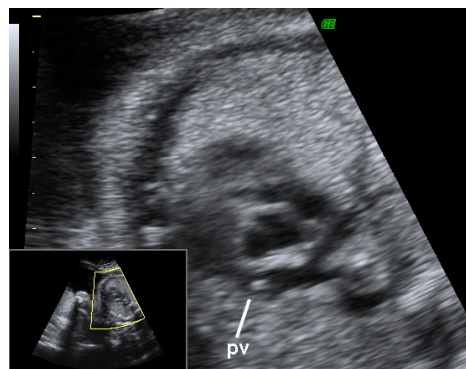


**Figure 23:** ([video 22](#)) A short axis view of the fetal heart showing a pulmonary trunk severely hypoplastic. The pulmonary valve (pv) is also demonstrated and appears to thickened and dysplastic.



Minimal or no forward flow is present across the pulmonary valve or in main pulmonary artery and reverse flow is the ductus arteriosus (ductal dependency).

Ductal dependency may be evidenced from the 3 vessel view of the fetal heart showing flow in the pulmonary trunk in the opposite direction to the flow in the aorta (Fig. 24 [video 23](#))

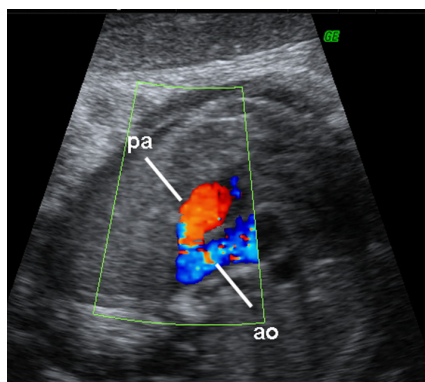


**Figure 24:** ([video 23](#)) 3 vessel view of the fetal heart in a fetus with pulmonary atresia. Color flow mapping shows that in the pulmonary artery (pa) the flow is directed from the spine toward the anterior chest wall, rather than being directed toward the spine as is normal and occurring in aorta (AO).

In presence of a concomitant anomaly of the tricuspid valve (valvular dysplasia or Ebstein's malformation) there is an increase of heart dimension mainly due to an enlargement of the right atrium (Fig. 25 [video 24](#)).

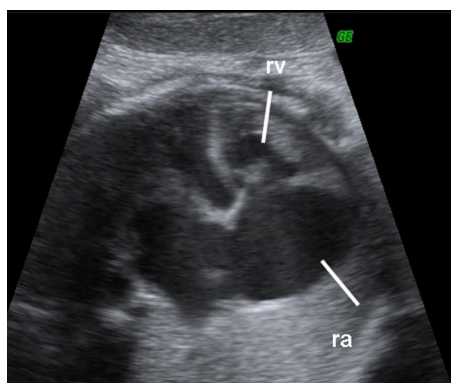


**Figure 25:** ([video 24](#)) Four chamber view of a fetus with pulmonary atresia and associated tricuspid dysplasia. The right atrium (ra) is enlarged and the right ventricle (rv) is hypertrophic and of reduced size.

The dimension of right ventricle can vary from severely hypoplastic to almost normal size. Color flow mapping allows to demonstrated marked tricuspid regurgitation as shown in Fig. 26 ([video 25](#)).

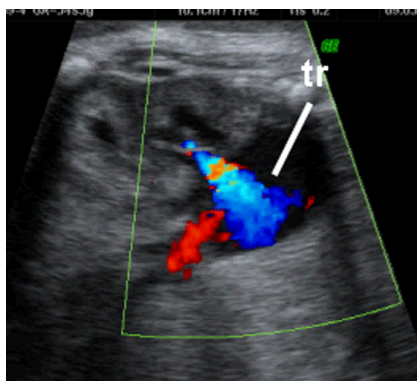


**Figure 26:** ([video 25](#)) Same fetus of Fig. 25 with color flow mapping showing the tricuspid regurgitation (tr).

Pulmonary atresia is not commonly associated with extracardiac anomalies or aneuploidies.

The outcome is affected by the possibility of postnatal treatment with two-ventricle repair that allows a good long term outcome. On the other end those who will end in an univentricular repair face a less optimistic long term prognosis.

Classical criteria of poor prognosis and subsequent univentricular repair are the presence of fibroelastosis in the right ventricle (Fig. 27 [video 26](#)) and the presence of sinusoids (coronary-right ventricle fistulas) (Fig. 28 [video 27](#)) [15, 16].

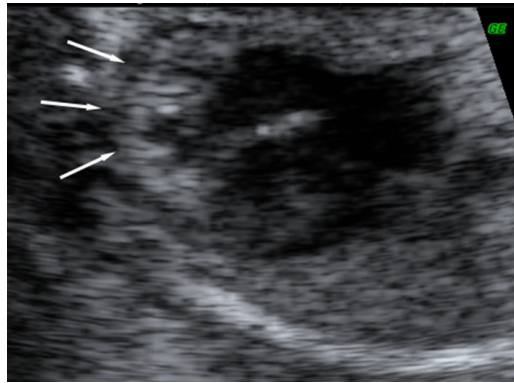


**Figure 27:** ([video 26](#)) Four chamber view of a fetus with pulmonary atresia. The right ventricle size are reduced, the myocardium appears trabeculated and with an increased echogenicity of the free walls (arrows) suggesting the presence of fibroelastosis.

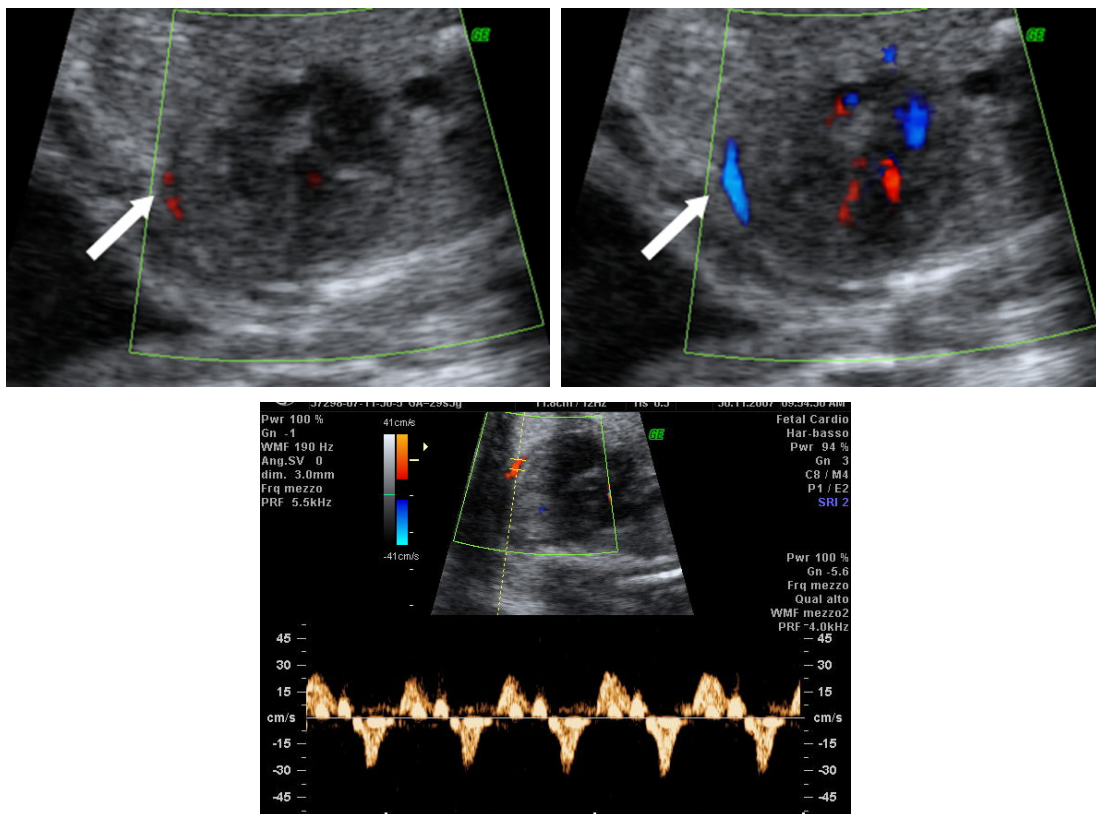


**Figure 28:** ([video 27](#)) Same fetus of Fig. 27 showing the presence of coronary right ventricle fistula (sinusoid). Color flow mapping shows the dilated right coronary artery (arrows) on the surface of right ventricle showing biphasic flow direction (retrograde flow panel A, forward flow panel B) and corresponding spectral Doppler tracing panel C).

More recently further prognostic criteria has been suggested as useful markers to predicts early in gestation the possibility of two-ventricle repairs such as the degree of reduction of ventricular size or changes in the ratios

between left and right ventricle size or atrioventricular valves and the presence absence of tricuspid regurgitation [16, 17]. Their clinical significance remains to be established

In fetuses showing poor prognosis intrauterine treatment has been suggested. The rationale of such approach is that the severity of the disease can further evolve in utero, and an early intervention may improve the outcome by altering the natural history of such conditions by performing fetal cardiac intervention intrauterine by balloon valvuloplastic or radiofrequency perforation [18]. The risk/benefit ratio of this approach is not yet established.

The advantages of 4D fetal echocardiography are similar to those already described for the other right heart diseases and may be summarized as follows:

- a) evaluation of the morphology and dynamics of the pulmonary artery (Fig. 20, [video 19](#)).
- b) evaluation of the tricuspid valve (Fig. 12 [video 11](#)) and its regurgitation.
- c) direct visualization of right ventricle morphology with rendering technique (Fig. 29 [video 28](#)).

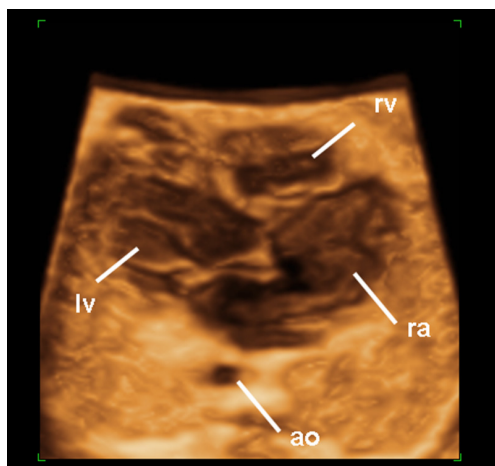


**Figure 29:** ([video 28](#)) Rendering of the fetal heart in a fetus with a hypoplastic right ventricle (RV). LV left ventricle, ra right atrium, ao aorta.

d) providing a “live” view of the abnormal hemodynamic using inversion mode rendering techniques Fig. 30 ([video 29](#)).

e) evaluating ventricular volume, geometry and stroke volume (see also chapter 16). In particular the use of semiautomatic software for volume calculation [14] allows reliable measurements in short time interval compatible with clinical practice (Fig. 31).

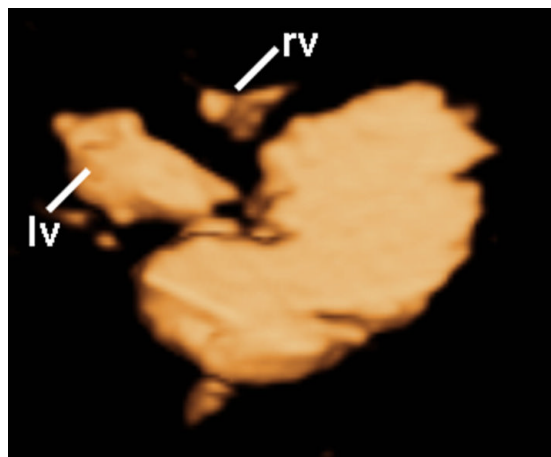


**Figure 30:** ([video 29](#)) Some fetus of Fig. 29, the small right ventricle (rv) is visualized with inversion mode. LV left ventricle.



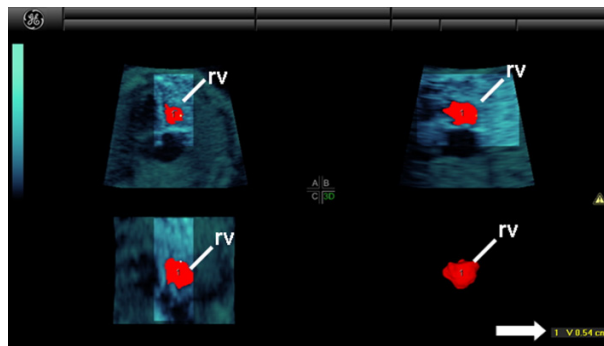


**Figure 31:** Example of quantification of ventricular volume in a fetus with a small right ventricle (rv) during systole using a semiautomatic system (sonoAVC see reference 14). The arrows indicates the absolute ventricular volume during systole.

It is also possible to obtain a simultaneous assessment of both ventricular volumes (Fig. 32 [video 30](#)) allowing to perform ratios between the size of the two ventricles.

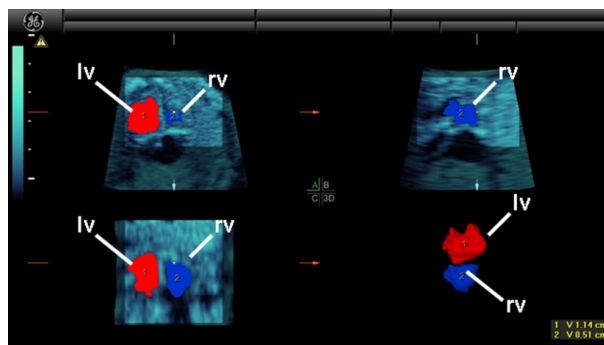


**Figure 32:** ([video 30](#)) Example of simultaneous assessment of right (rv blue) and left (lv red) ventricles using sonoAVC technique.

This approach has the potential to allow an absolute and reliable quantification of ventricular size and function (by assessing the stroke volume) thus allowing serial observations through pregnancy of such fetuses. This may allow to evidence the evolution of the CHD and identify fetuses that may benefit from intrauterine treatment or earlier delivery.

## REFERENCES

- [1] Allan L, Honberger L, Sharland G Textbook of fetal cardiology Greenwich Medical Media London, 2000.
- [2] Fouron JC Anomalies of the right heart. In Fetal cardiology. Yagel S, Silverman NH, Gembruch U 2<sup>nd</sup> Edition, pp 251-268, 2009, Informa Healthcare New York Publisher.
- [3] Wald RM, Tham EB, McCrindle BW, Goff DA, McAuliffe FM, Golding F, Jaeggi ET, Hornberger LK, Tworetzky W, Nield LE. Outcome after prenatal diagnosis of tricuspid atresia: a multicenter experience. *Am Heart J.* 2007;153:772-8.
- [4] International Society of Ultrasound in Obstetrics & Gynecology Cardiac screening of the fetus : guidelines for performing the basic and the extended basic cardiac scan *Ultrasound Obstet Gynecol* 2006; 27: 107-113.
- [5] Grandjean H, Larroque D., Levi S and the eurofetus group- The performance of routine ultrasonographic screening of pregnancies in the Eurofetus study *Am J Obstet Gynecol* 1999 181 446-454.
- [6] Garne E. Stoll C, Clementi M and the Euroscan group. Evaluation of prenatal diagnosis of congenital heart disease by ultrasound experience from 20 European registries. *Ultras Obstet Gynecol* 2001 17 : 386- 391.
- [7] Rizzo G, Capponi A, Vendola M, Pietrolucci ME, Arduini D. Role of tomographic ultrasound imaging with spatiotemporal image correlation for identifying fetal ventricular septal defects. *J Ultrasound Med* 2008;27:1071-1075.
- [8] Messing B, Porat S, Imbar T, Valsky DV, Anteby EY, Yagel S. Mild tricuspid regurgitation: a benign fetal finding at various stages of pregnancy *Ultras Obstet Gynecol* 2005 26: 606-610.
- [9] Falcon O., Faiola S., Huggon I., Allan L., Nicolaidis K. H. Fetal tricuspid regurgitation at the 11 + 0 to 13 + 6-week scan: association with chromosomal defects and reproducibility of the method *Ultras Obstet Gynecol* 2006 27: 609-612
- [10] Huggon IC, Ghi T, Cook AC, Zosmer N, Allan LD, Nicolaidis KH. Fetal cardiac abnormalities identified prior to 14 weeks' gestation. *Ultras Obstet Gynecol* 2002 20: 22-29.

- [11] Paranon S, Acar P. Ebstein's anomaly of the tricuspid valve: from fetus to adult: congenital heart disease. *Heart*. 2008, 94: :237-243.
- [12] Taktak A, Acar P, Dulac Y, Abadir S, Chilon T, Roux D, Glock Y, Fournial G. A new approach to the tricuspid valve in Ebstein's anomaly by real time 3D echocardiography *Arch Mal Coeur Vaiss*. 2005 98:531-537.
- [13] Tutschek B, Sahn DJ. Semi-automatic segmentation of fetal cardiac cavities: progress towards an automated fetal echocardiogram. *Ultrasound Obstet Gynecol* 2008 32:176-180.
- [14] Rizzo G, Capponi A, Pietrolucci ME, Arduini D. The role of sono-Automatic Volume Count (sonoAVC) in measuring fetal cardiac ventricular volumes using four dimensional ultrasound: comparison with Virtual Organ Computer-aided AnaLysis (VOCAL) *J Ultrasound Med* 2010 ;29 :261-270.
- [15] Shinebourne EA, Rigby ML, Carvalho JS. Pulmonary atresia with intact ventricular septum: from fetus to adult: congenital heart disease. *Heart*. 2008; 94:1350-1357.
- [16] Roman KS, Fouron JC, Nii M, Smallhorn JF, Chaturvedi R, Jaeggi ET. Determinants of outcome in fetal pulmonary valve stenosis or atresia with intact ventricular septum. *Am J Cardiol*. 2007, 99:699-703.
- [17] Iacobelli R, Pasquini L, Toscano A, Raimondi F, Michielon G, Tozzi AE, Sanders SP. Role of tricuspid regurgitation in fetal echocardiographic diagnosis of pulmonary atresia with intact ventricular septum. *Ultrasound Obstet Gynecol*. 2008,32:31-35.
- [18] Gardiner HM. In-utero intervention for severe congenital heart disease. *Best Pract Res Clin Obstet Gynaecol*. 2008: 22:49-61.

## 4D Study of Left Heart Anomalies

Giuseppe Rizzo and Domenico Arduini

*Department of Obstetrics and Gynecology, Università Roma "Tor Vergata" Rome Italy*

**Abstract:** In this chapter, the 2D, color Doppler and four dimensional (4D) features of major right heart abnormalities are described. In particular, the echocardiographic views on which the various lesions are present are reported. The diagnostic role of 4D echocardiography in allowing a spatial demonstration of the defects with the possibility of getting new views into the heart is outlined. Videos of major diagnostic features are also provided, to facilitate the understanding of the text.

**Key Words:** 4D Sonography, Fetal Echocardiography, Right Heart Anomalies, Prenatal Diagnosis.

### INTRODUCTION

This chapter will cover the most significant anomalies of the left side of the heart that can be observed prenatally. For each condition after a brief anatomical description, the criteria of echocardiographic diagnosis will be provided. In particular we will focus on the four dimensional (4D) acquisition and postprocessing modalities in fetal hearts with right side anomalies, demonstrating their use through case examples.

### HYPOPLASTIC LEFT HEART SYNDROME

The term Hypoplastic Left Heart Syndrome (HLHS) includes a spectrum of cardiac anomalies characterized by a marked underdevelopment of left ventricle and ascending aorta. This results in a situation where the left side of the heart is completely unable to support the circulation. Its incidence is between 0.1-0.25/1000 newborns and represents about the 10% of the congenital heart disease (CHD) [1,2]. In prenatal diagnosis series the incidence is usually reported higher 12-18% of all CHD and this is due to intrauterine mortality rate.

The "classical" form is characterized by an atresic mitral valve, an atresic aortic valve, an extremely small left ventricle with no inflow from the left atrium (Fig. 1 [video 1](#)).

There is a "minor" form where the mitral valve is small but patent and the left ventricular chamber may be recognized. Other variants of HLHS include critical aortic stenosis, the Shone complex (mitral valve anomaly, aortic coarctation and subaortic stenosis), unbalanced atrioventricular septal defects all associated with severe hypoplasia of the left ventricle and aorta.

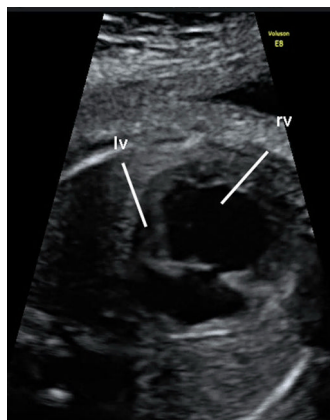


**Figure 1:** ([video 1](#)) The four chamber view of a fetus with the classical form of HLHS. The cavity of the left ventricle is difficult to identify.

\*Address Correspondence to Giuseppe Rizzo: Department of Obstetrics and Gynecology, Università Roma Tor Vergata Ospedale Fatebenefratelli Isola Tiberina 00186 Rome Italy; Email: giuseppe.rizzo@uniroma2.it

Color flow mapping allows to confirm the absence of filling of the left ventricle and the shunt from left to right at the level of foramen ovalis (Fig. 2, [video 2](#))

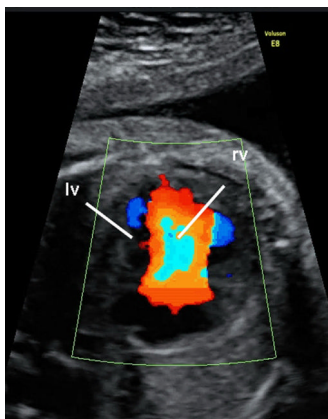


**Figure 2:** ([video 2](#)) Same fetus of Fig. 1. Color flow mapping allows to demonstrate the absence of flow through the mitral valve.

A general characteristic in all the variants of HLHS is that the right ventricle forms the apex of the heart (Fig. 3 [video 3](#))

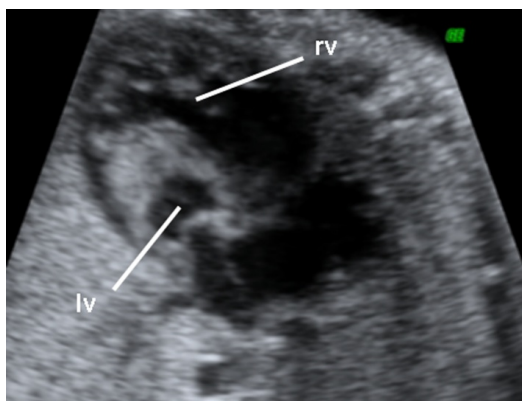


**Figure 3:** ([video 3](#)) Four chamber view in a fetus with HLHS, the left ventricle cavity is small, the walls hyperechogenic. At the apex of the heart the right ventricle (rv) is present

The ascending aorta is hypoplastic and no forward flow is detectable. Color flow mapping allows from the 3 vessel view of the fetal heart to confirm the diagnosis by showing a retrograde flow from the ductus to the aorta (Fig. 4 [video 4](#))

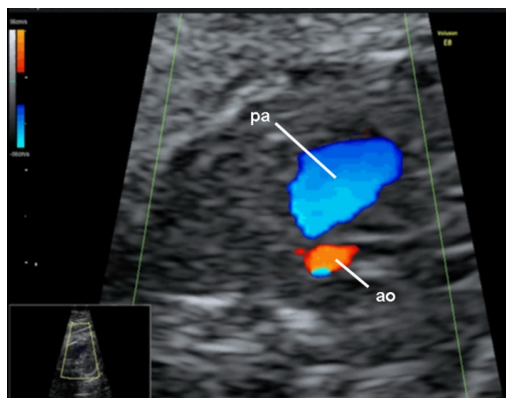


**Figure 4:** ([video 4](#)) 3 vessel view of the fetal heart in a fetus with HLHS. Normal flow direction (blue) in the pulmonary artery (PA), while there is a reverse flow (red) in the aortic trunk (ao).

The HLHS is associated with aneuploidies in about 2% of cases, particularly 45X, but also trisomy 13 and 18. Extracardiac anomalies may be present in up to 18% of cases.

The recent introduction of 4D ultrasonography to clinical practice provided an important advance in imaging technology. With a 4D acquisition of the fetal heart from the 4 chamber view it is possible to obtain few additional informations on the cardiac anatomy in HLHS. The advantages are

a) to render cardiac volume and show in more direct view the severity of the reduction of the left ventricle (Fig. 5 [video 5](#))

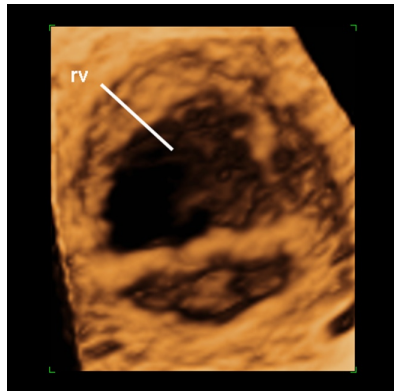


**Figure 5:** ([video 5](#)). Rendering of HLHS (rv right ventricle)

b) to confirm the absent inflow in the left ventricle by using the rendering function with color superimposed (Fig. 6 [video 6](#))

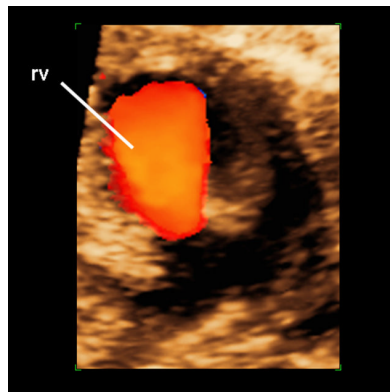


**Figure 6:** ([video 6](#)). Same fetus of Fig. 5 showing no left ventricular filling (rv right ventricle)

c) to evaluate the relative size and position of both ventricles by using render with inversion mode (Fig. 7 [video 7](#)).

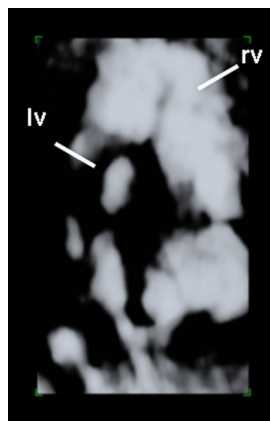


**Figure 7:** ([video 7](#)) Same fetus of Fig. 3 note the small size of the left ventricle (lv) and the right ventricle (rv) forming the apex of the heart.

## AORTIC STENOSIS

Aortic stenosis is an obstruction to the left ventricle outflow tract and the site of obstruction may be subvalvular, valvular or supra-ventricular. The incidence is of 2-3% of all CHD [1,2].

The appearance of the fetal heart will depend on the severity of the obstruction. If aortic stenosis is moderate the left ventricle usually is normal in size, or slightly reduced with a variable degree of hypertrophy of the walls (Fig. 8 [video 8](#))

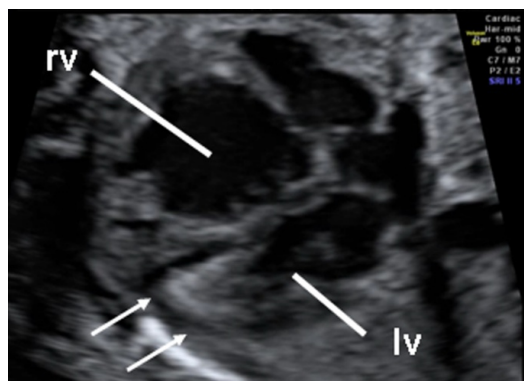


**Figure 8:** ([video 8](#)) The 4 chamber view of a fetus with moderate aortic stenosis. The left ventricle (lv) is smaller than the right ventricle (rv). The LV is hyperechoic (arrows)

The aortic leaflets are abnormal and usually always present during all cardiac cycle (Fig. 9 [video 9](#))

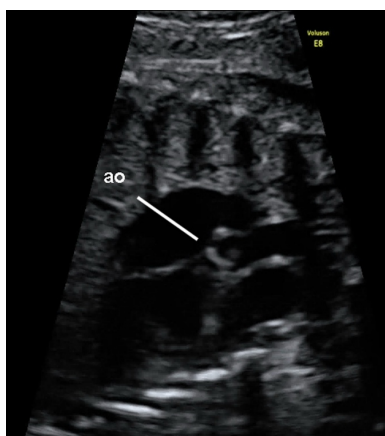


**Figure 9:** ([video 9](#)) Long axis view of the left ventricle showing a thickened aortic valve (ao)

Color flow mapping shows turbulence and increased velocities at the level of aortic valve (Fig. 10 [video 10](#))

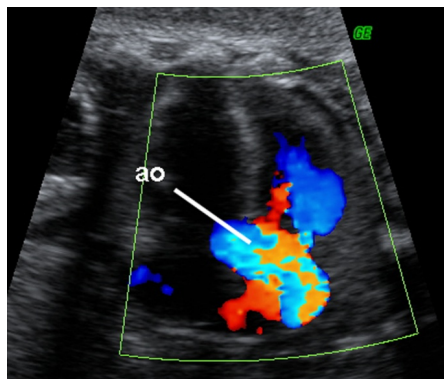


**Figure 10:** ([video 10](#)) Color flow mapping showing increased velocity at the level of ascending aorta.

that can be quantified by using spectral Doppler (Figure 11).

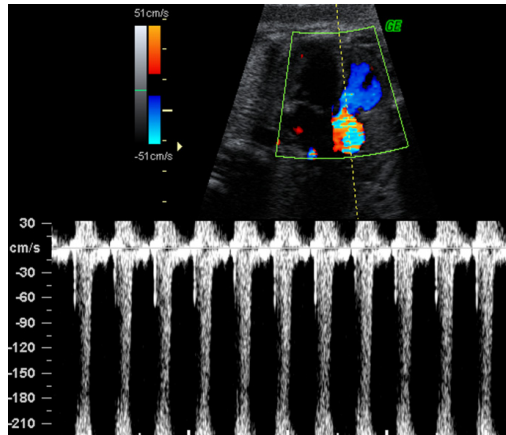


**Figure 11:** The Doppler sample volume is positioned in the ascending aorta just beyond the aortic leaflets and the velocity measured are over 210 cm/sec

Mitral regurgitation is also common due to the high pressure present in the left ventricle (Fig. 12 [video 11](#)).

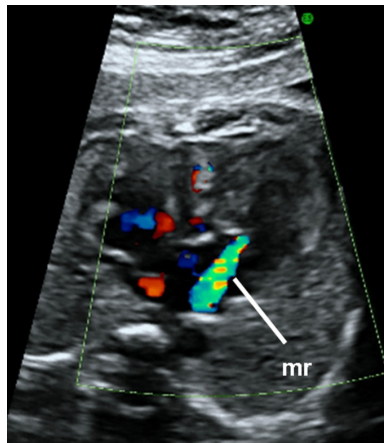


**Figure 12:** ([video 11](#)) Four chamber view of a fetus with aortic stenosis. The left atrium and left ventricles are dilated and an evident mitral regurgitation (mr) is present.

When aortic stenosis is critical the left ventricle is dilated and with poor contractility and increased echogenicity suggesting the presence of fibroelastosis. (Fig. 13 [video 12](#)).

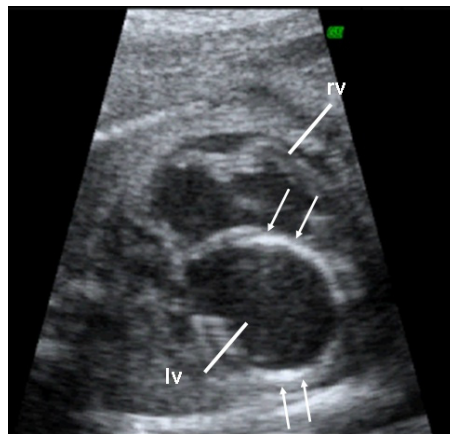


**Figure 13:** ([video 12](#)) Example of critical aortic stenosis. The left ventricle (LV) is increased in size, has poor contractility and its walls have an increased echogenicity (arrows) suggestive of fibroelastosis.



The shape of the ventricle is globular and there is difficult to document flow in the ventricle due to the poor contractility (Fig. 14 [video 13](#)).

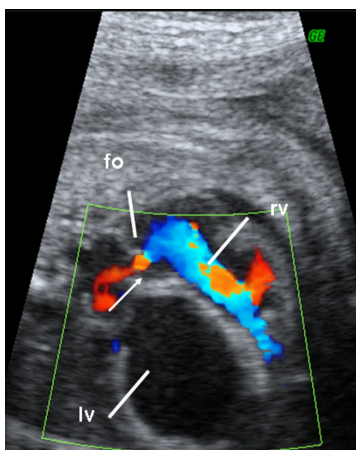


**Figure 14:** ([video 13](#)): Color flow mapping of the same fetus of Fig. 12. Note the absent filling of the left ventricle (LV) and the unidirectional flow (arrow) from the left atrium through the foramen ovale (fo) to the right ventricle

Intracardiac associated anomalies include mitral valve stenosis, ventricular septal defects (Fig. 15 [video 14](#)), restrictive foramen ovale and aortic coarctation. The Shone's Syndrome is a complex left heart disease that include mitral stenosis, aortic stenosis (usually subaortic) and coarctation.

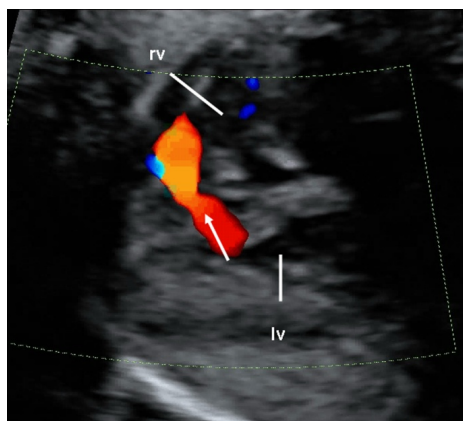


**Figure 15:** ([video 14](#)) Same fetus of figures 8 of 9. Color flow mapping allow the demonstration of a muscular ventricular septal defect. The flow is unidirectional (arrow) from the left ventricle (LV) to the right ventricle (rv) and not bidirectional as usual due to the higher pressure present in the lv for the presence of the aortic stenosis.

Extracardiac anomalies are unusual but aortic stenosis can be associated with Turner syndrome and William's syndrome (supravalvular aortic stenosis).

Aortic stenosis may be a progressive disease that from mild forms may evolve in critical stenosis with fibroelastosis or hypoplastic left heart syndrome [4]. Intrauterine treatment with balloon valvuloplasty has been suggested in the more severe form in the extent to prevent this deterioration but its role remains to be established [5, 6]

4D ultrasound provides the following advantages:

- a) rendering ventricular cavity and provide indirect informations on the proportion of the two ventricles and their contractility, This informations can be obtained both using direct rendering of the fetal heart (Fig. 16, [video 15](#)) or in combination with color Doppler informations (Fig. 17 [video 16](#))
- b) evaluating ventricular volume, geometry and stroke volume This is usually performed by manual methods of calculations by using software such as Organ Computer-aided AnaLysis (VOCAL) [7, 8] (see also chapter 16). (Fig. 18).

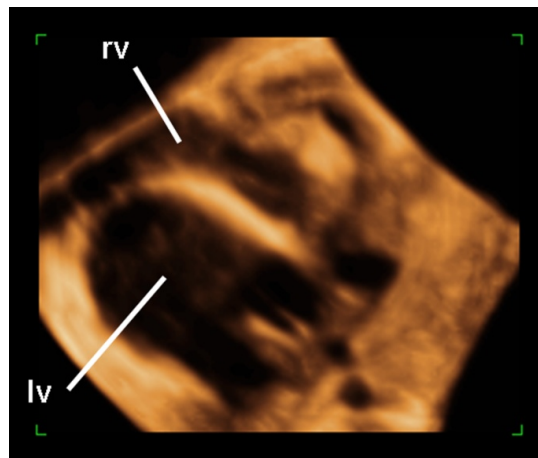


**Figure 16:** ([video 15](#)): Rendering of the four chamber view of a fetus with critical aortic stenosis and fibroelastosis. Note the enlarged left ventricle (lv) and its reduced motility. The right ventricle (rv) forms the apex.

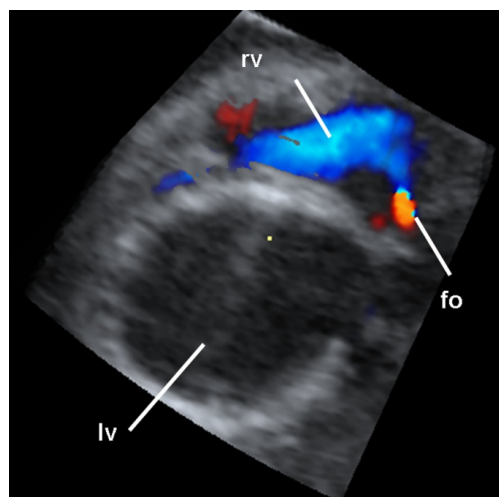


**Figure 17:** ([video 16](#)) Same fetus of Fig. 16. with rendering and color Doppler, Note the absent filling of the left ventricle (lv) and the unidirectional flow across the foramen ovalis (fo) from the left heart to the right ventricle (rv).

The manual method has the disadvantage of the relatively long time of analysis and operator dependency. To overcome these difficulties semiautomatic software for volume calculation [9] has been developed (sono-Automatic Volume Count (sonoAVC)) and these software of analysis allow reliable measurements in short time interval compatible with clinical practice [10] (Fig. 19).

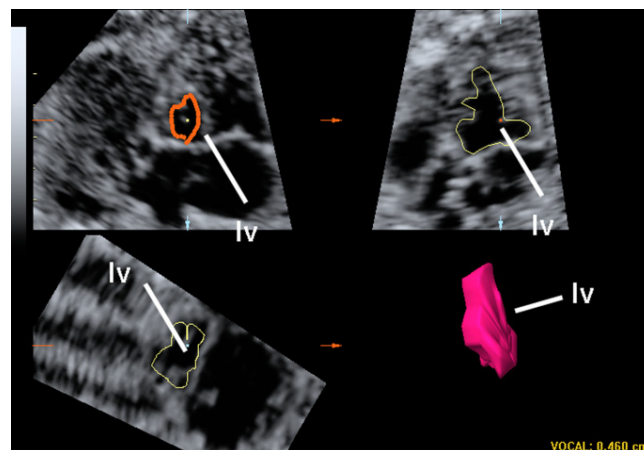


**Figure 18:** Evaluation of left ventricle (LV) with VOCAL software in a fetus with aortic stenosis.



**Figure 19:** Evaluation of left ventricle (LV) with sonoAVC software in the same fetus of Fig. 17

The evaluation of ventricular volume allows longitudinal evaluation of cardiac growth that may be useful in predicting the evolution of the disease in particular when compared to the growth of the right ventricle (Fig. 20 [video 17](#))

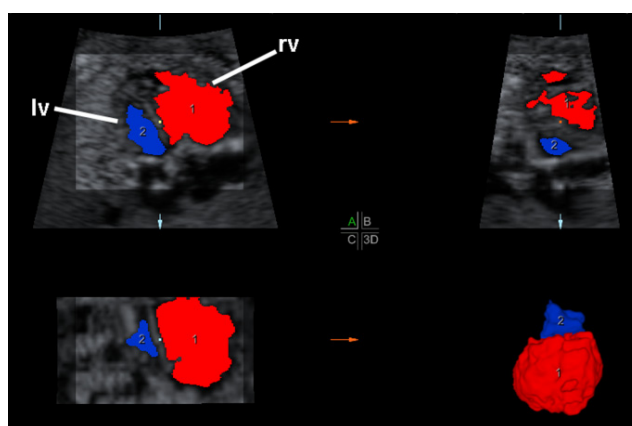


**Figure 20:** ([video 17](#)) Simultaneous assessment of left (lv blue) and right ventricle (rv red) volume by sono AVC

c) improving the diagnosis of associated intracardiac anomalies such as ventricular septal defects that can be overlooked by conventional echocardiography. In particular the application of Tomographic Ultrasound Imaging (TUI) in cardiac volumes acquired with color Doppler allows to obtain a complete view of the septum allowing an easy identification of small defects that can be difficult to evidence with 2D echocardiography [11] (Fig. 20, [video 18](#)).

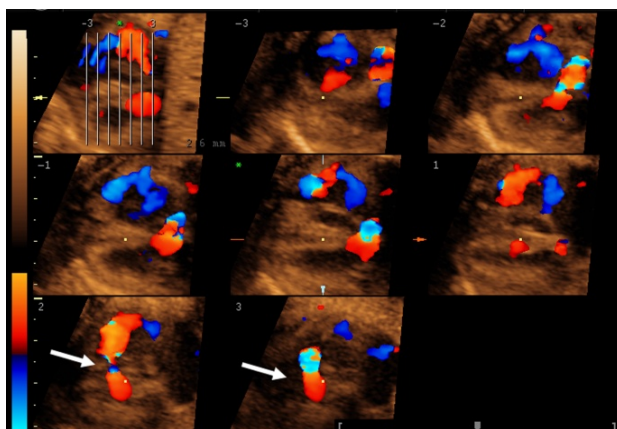


**Figure 21:** ([video 18](#)) Visualization of a muscular septal defect (arrows) with TUI technique in a cardiac volume acquired with color Doppler of a fetus with aortic stenosis.

Further evolution of this technique is the “omniview” function that allows the simultaneous view of the ventricular defect in different planes allowing a better identification and assessment of the amount and direction of the shunt between the two ventricles (Fig. 22, [video 19](#)).

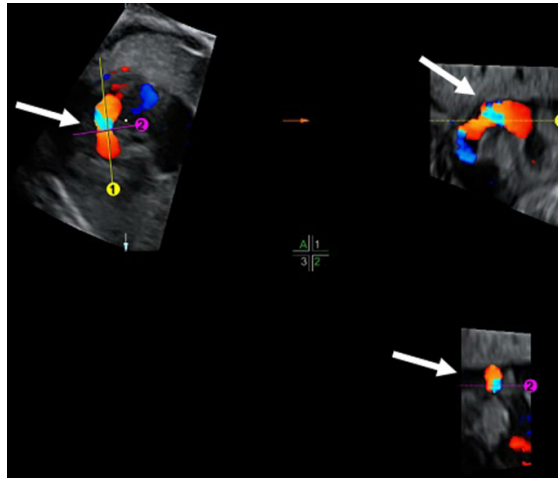


**Figure 22:** ([video 19](#)) Use of the omniview function in the same fetus of Fig. 20. The ventricular septal defect is visualized in two perpendicular planes (yellow and violet lines) allowing to confirm the unidirectional blood direction from the left ventricle to the right.

## AORTIC ARCH ANOMALIES

Aortic arch anomalies consist of several defects with different embryological etiology and the more frequent are aortic coarctation, interrupted aortic arch and right aortic arch.

### Coarctation of Aorta

Coarctation of aorta is characterized by a narrowing of the distal aortic arch (isthmus) and occurs in about 0.2-0.6% of newborns [1, 2]. Prenatal diagnosis is challenging for the difficulties of studying aortic isthmus due to the presence of the patent ductus arteriosus.

In severe case the diagnosis is suspected by the detection of a disproportion of ventricular size from the 4 chamber view [12] (Fig. 23, [video 20](#)).

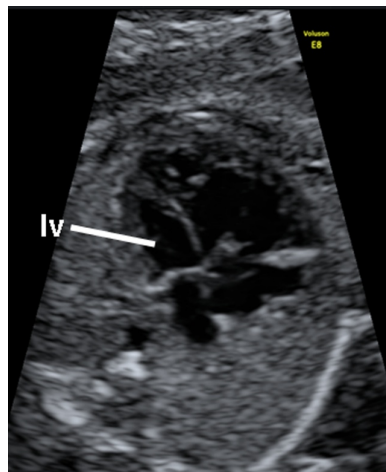


**Figure 23:** ([video 20](#)) Example of 4 chamber view in a fetus with aortic coarctation. The left ventricle (lv) is smaller than the right ventricle.

Discrepancy in the relative size of aorta and pulmonary artery [13] has been also suggested to improve the diagnosis of aortic coarctation

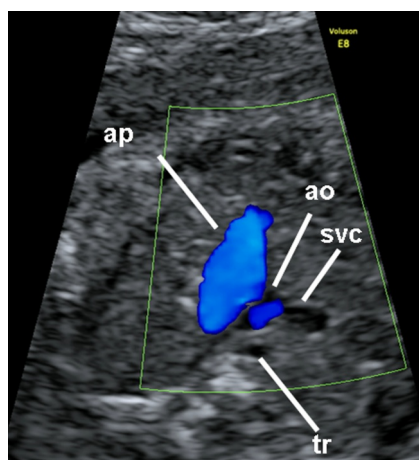


**Figure 24:** ([video 21](#)) 3 vessel and trachea (tr) view in a case of coarctation of aorta. Aorta (ao) is hypoplastic relative to pulmonary artery (pa) and superior vena cava (svc).

Simultaneous visualization of both great vessels can be obtained by the 3 vessel view (Fig. 24, [video 21](#)). In long axis view is also possible to perform comparison between aortic and ductal arch (Fig. 25 [video 22](#)) but this view has been reported as misleading [2] due to the difficulties in correctly visualizing both arches.

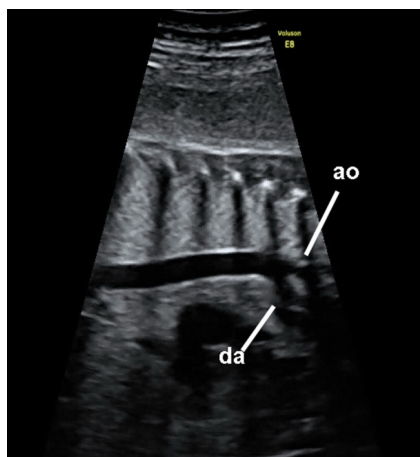


**Figure 25:** ([video 22](#)) Simultaneous visualization of aortic (ao) and ductal (da) arches in a case of coarctation of aorta. Note the reduced size of aorta when compared to ductus arteriosus.

High sensitive Doppler technique such as B flow may

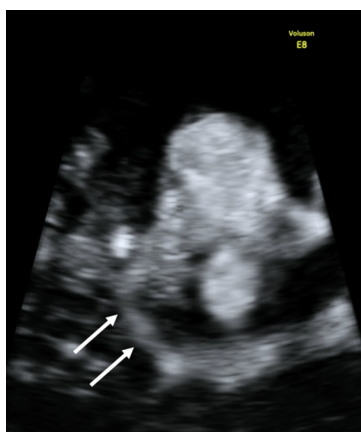


**Figure 26:** ([video 23](#)) Imaging of the aortic arch by B-flow technique. Note the narrowing (arrows) of the arch when compared to descending aorta.

be used to help in delineating the narrow lumen of the aortic arch (Fig. 26 [video 23](#)).

Coarctation of the aorta may worsen with advancing gestation and subtle changes in second trimester may develop in severe forms.

In up to 60% of the cases other intracardiac anomalies are present such as atrial and ventricular defects and obstructive lesions of the left ventricle. There is also an increased incidence of extracardiac malformations and aneuploidies.

The advantages of 4D echocardiography are:

a) rendering the left ventricle cavity providing information on ventricular size and contractility (Fig. 27 [video 24](#)).



**Figure 27:** ([video 24](#)) Rendering of the four chamber view of a fetus with aortic coarctation. Note the small dimension of the left ventricle (lv) despite the normal size of aorta (ao)

b) to obtain an absolute quantification of ventricular volume and stroke volume by using VOCAL or sonoAVC software [7,8,10] as already reported for aortic stenosis.

c) easier identification of atrial and ventricular septal defects by using TUI technique [11] (see aortic stenosis)

d) reconstruction of the aortic arch by using either multiplanar display or B flow technique [14] (Fig. 28 [video 25](#)).

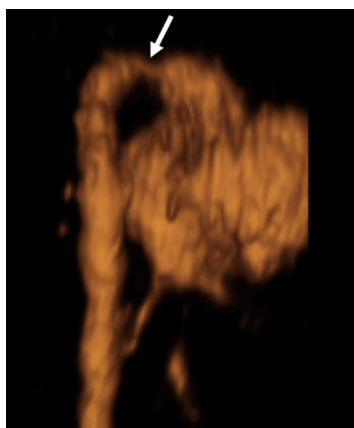


**Figure 28:** ([video 25](#)) Reconstruction of the aortic arch with rendering technique using B-flow technique. Note the narrowing (arrow) of the aortic arch

### Interrupted Aortic Arch

It is a rare anomaly of the aortic arch accounting for < 5% of all arch anomalies and it is divided in 3 types according to the position of the interruption:



1) type A in which the lesion is between the left subclavian artery and descending aorta and it appears as a severe form of aortic coarctation.

2) type B in which there is interruption between the left common carotid artery and the left subclavian artery

3) type C in which the interruption is between the innominate artery and the left common carotid artery and it is an extremely uncommon form

Type B is the most common disease and it is usually characterized by a disproportion of ventricular size (Fig. 29 [video 26](#)). Usually a malalignment ventricular septal defect is present.

The aorta is of reduces size with straight direction and characterized by a V shape bifurcation in the innominate artery (brachiocephalic artery and the left common carotid artery [15] (Fig. 30 [video 27](#)).

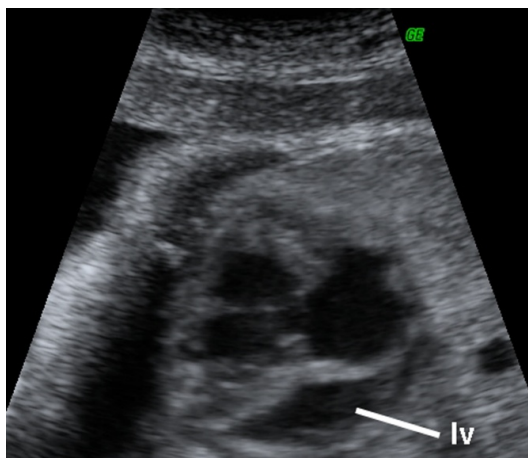


**Figure 29:** ([video 26](#)) Evident disproportion between left (lv) and right ventricle in a case with interrupted aortic arch type B.

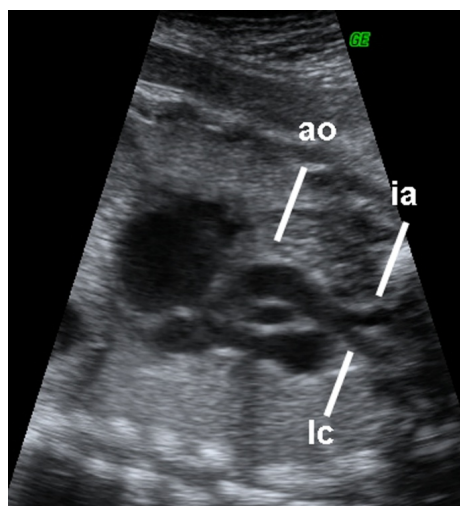


**Figure 30:** ([video 27](#)) Same fetus of figure 29. The aorta (ao) appear straight and branches in the innominate (ia) and left common carotid (lc) arteries.

Microdeletion of chromosome 22q11 is associated up to 75% of cases with type B interrupted aortic arch [16].

The advantages of 4D echoardiography are:

a) rendering the 4 chamber of the fetal heart as already show for aortic stenosis and coarctation

b) providing a topographic visualization of the malalignment ventricular septal defect and of its sizes (Fig. 31 [video 28](#))



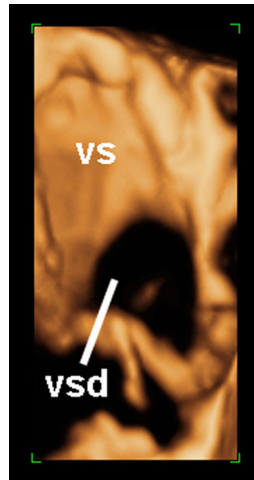


**Figure 31:** ([video 28](#)) “Enface” view of the ventricular septum (vs) in a fetus with interrupted aortic arch type B showing the malalignment ventricular septal defect (vsd).

c) reconstruction of the arch with B-flow technique (Fig. 32 [video 29](#)).

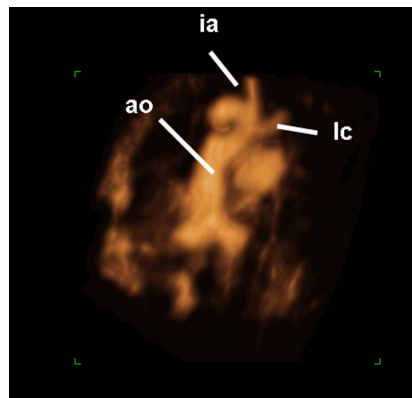


**Figure 32:** ([video 29](#)) Reconstruction of the aortic arch with rendering technique using B-flow technique in the same fetus of Fig. 30. The aorta (ao) appear straight and branches in the innominate (ia) and left common carotid (lc) arteries.

### Right Aortic Arch

It is characterized by an aortic arch that courses to the right side of the trachea and arches around the proximal part of the right main bronchus. It occurs in about 0.1% of newborns [18].

The diagnosis is done from the 3 vessel and trachea view [18] where the trachea appears between the aorta and the pulmonary artery instead of being on the right side of aorta. (Fig. 33 [video 30](#)).

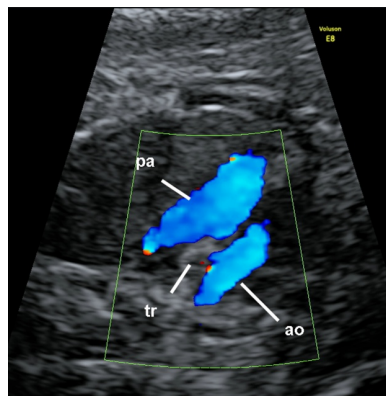


**Figure 33:** [video 30](#) 3 vessel and trachea view of a fetus with right aortic arch. The trachea (tr) is between the pulmonary artery (pa) and aorta (ao)

The right aortic arch is frequently associated with other CHD including tetralogy of Fallot, and truncus arteriosus. Less frequently is associated with tricuspid atresia, transposition of great artery and ventricular septal defects [17].

Chromosome 22q11 microdeletion are frequent and right aortic arch may be the only cardiac sign present. When an aberrant subclavian artery is present there is also an increased risk of trisomy 21 [17].

4D echocardiography provides the following advantages:

- a) allowing a multiplanar display showing the spatial relationship between the trachea and the great vessels (Fig. 34 [video 31](#))
- b) allowing an easier identification of aberrant vessel such as the right subclavian artery by using the TUI technique in volume acquired with color Doppler function (Fig. 35, [video 32](#))
- c) rendering and demonstrating the presence of vascular rings around the trachea (Fig. 36, 37, 38, [video 33](#), [video 34](#), [video 35](#))

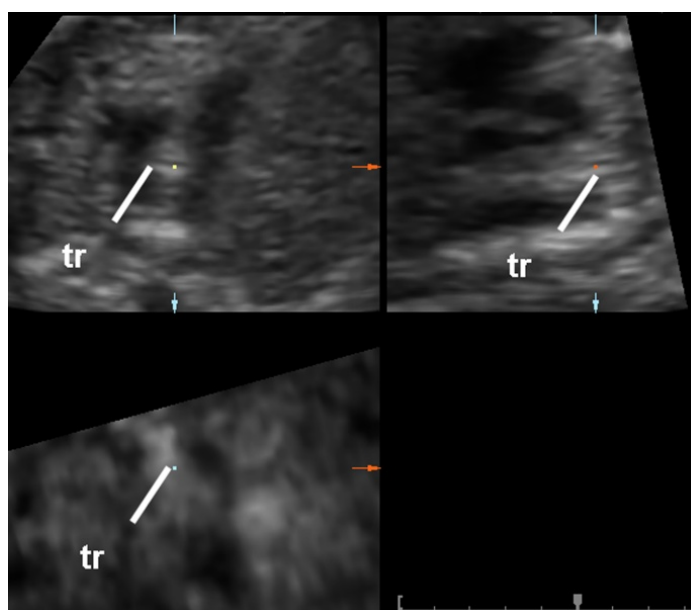


**Figure 34:** ([video 31](#)) Multiplanar display of a fetus with right aortic arch. The dot is placed on the fetal trachea (tr)

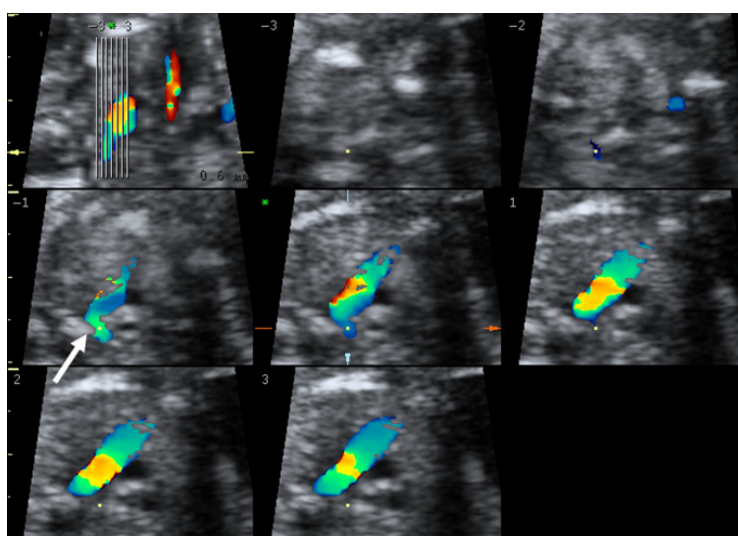


**Figure 35:** ([video 32](#)) Display of aberrant right subclavian artery (arrow) by using the TUI technique

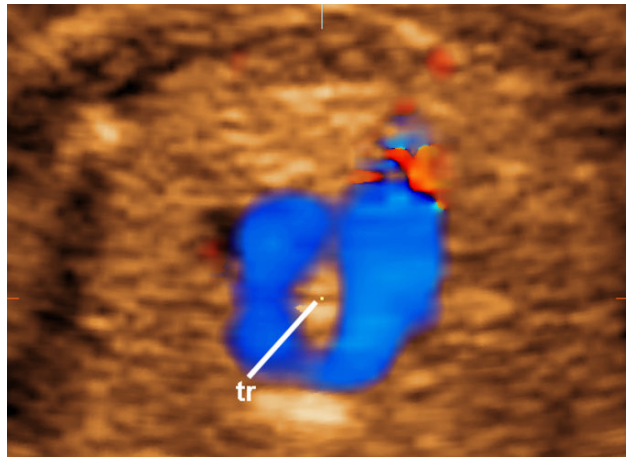


**Figure 36:** ([video 33](#)) Example of vascular ring with the vascular encirclement of the trachea (tr)

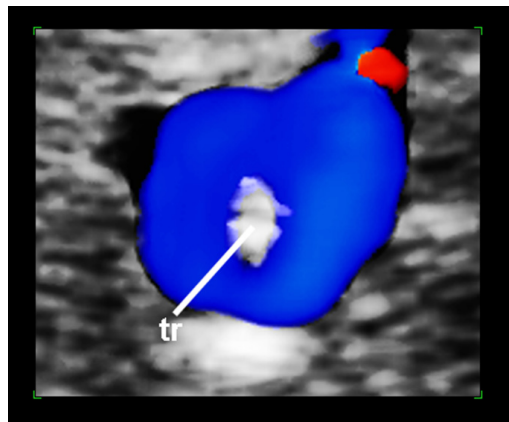


**Figure 37:** ([video 34](#)) Glass body display of the same fetus of Fig. 36

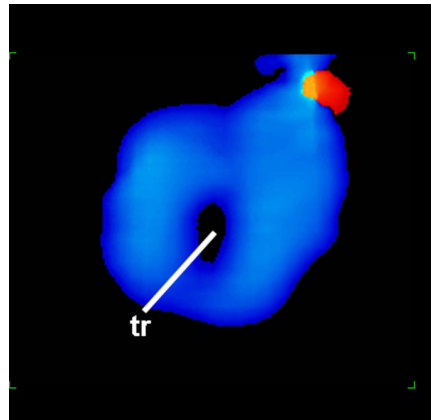


**Figure 38:** ([video 35](#)) Glass body display of the same fetus of Fig. 36

## REFERENCES

- [1] Allan L, Honberger L, Sharland G Textbook of fetal cardiology Greenwich Medical Media London, 2000.
- [2] Allan LD Left heart malformations. In Fetal cardiology. Yagel S, Silverman NH, Gembruch U 2<sup>nd</sup> Edition, pp 291-303, 2009, Informa Healthcare New York Publisher.
- [3] Simpson JM Hypoplastic left heart syndrome. Ultrasound Obstet Gynecol 2000, 15: 271-278.
- [4] Mäkikallio K, McElhinney DB, Levine JC, Marx GR, Colan SD, Marshall AC, Lock JE, Marcus EN, Tworetzky W. Fetal aortic valve stenosis and the evolution of hypoplastic left heart syndrome: patient selection for fetal intervention. Circulation 2006; 113: 1401-1405.

- [5] Kleinman CS. Fetal cardiac intervention: innovative therapy or a technique in search of an indication? *Circulation* 2006 113:1378-1381.
- [6] Gardiner HM. In-utero intervention for severe congenital heart disease. *Best Pract Res Clin Obstet Gynaecol.* 2008; 22:49-61.
- [7] Rizzo G, Capponi A, Cavicchioni O, Vendola M, Arduini D. Fetal cardiac stroke volume determination by four-dimensional ultrasound with spatio-temporal image correlation compared with two-dimensional and Doppler ultrasonography. *Prenat Diagn* 2007; 27: 1147-50.
- [8] Hamill N, Romero R, Hassa S, Lee W, Myers PA, Mitta I, Kusanovi JPC, Chaiworapongs T, Vaisbuc D, Espinoza, J, Gotsch F, Carletti A, Gonçalves LF, Lami Y Repeatability and Reproducibility of Fetal Cardiac Ventricular Volume Calculations Using Spatiotemporal Image Correlation and Virtual Organ Computer-Aided Analysis *J Ultrasound Med* 2009 28: 1301-1311.
- [9] Tutschek B, Sahn DJ. Semi-automatic segmentation of fetal cardiac cavities: progress towards an automated fetal echocardiogram. *Ultrasound Obstet Gynecol* 2008 32:176-180.
- [10] Rizzo G, Capponi A, Pietrolucci ME, Arduini D. The role of sono-Automatic Volume Count (sonoAVC) in measuring fetal cardiac ventricular volumes using four dimensional ultrasound: comparison with Virtual Organ Computer-aided AnaLysis (VOCAL) *J Ultrasound Med* 2010; 29 : 260-70.
- [11] Rizzo G, Capponi A, Vendola M, Pietrolucci ME, Arduini D. Role of tomographic ultrasound imaging with spatiotemporal image correlation for identifying fetal ventricular septal defects. *J Ultrasound Med* 2008; 27:1071-1075.
- [12] Matsui H, Mellander M, Roughton M, Jicinska H, Gardiner HM Morphological and physiological predictors of fetal aortic coarctation. *Circulation.* 2008;118: 1793-1801
- [13] Slodki M, Rychik J, Moszura T, Janiak K, Respondek-Liberska M Measurement of the great vessels in the mediastinum could help distinguish true from false-positive coarctation of the aorta in the third trimester. *J Ultrasound Med.* 2009 28: 1313-1317.
- [14] Espinoza J, Romero R, Kusanovic JP, Gotsch F, Erez O, Hassan S, Yeo L. Prenatal Diagnosis of Coarctation of the Aorta With the Multiplanar Display and B-Flow Imaging Using 4-Dimensional Sonography *J Ultrasound Med* 2009 28: 1375-1378.
- [15] Volpe P, Marasini M, Caruso G, Gentile M. Prenatal diagnosis of interruption of the aortic arch and its association with deletion of chromosome 22q11. *Ultrasound Obstet Gynecol.* 2002 20:327-31
- [16] Volpe P, Marasini M, Caruso G, Marzullo A, Buonadonna AL, Arciprete P, Di Paolo S, Volpe G, Gentile M. 22q11 deletions in fetuses with malformations of the outflow tracts or interruption of the aortic arch: impact of additional ultrasound signs. *Prenat Diagn.* 2003;23:752-7.
- [17] Yoo SJ, Bradley T, Jaeggi E Aortic arch anomalies. In *Fetal cardiology.* Yagel S, Silverman NH, Gembruch U 2<sup>nd</sup> Edition, pp 329-342, 2009, Informa Healthcare New York Publisher.
- [18] Tuo G, Volpe P, Bava GL, Bondanza S, De Robertis V, Pongiglione G, Marasini M. Prenatal diagnosis and outcome of isolated vascular rings. *Am J Cardiol.* 2009 ;103 :416-419.

## Conotruncal Anomalies

Dario Paladini\* and Gabriella Sglavo

*Fetal Medicine & Cardiology Unit, Dept.Obstet.Gynecol. University Federico II of Naples, Italy*

**Abstract:** In the chapter, the 2D, color Doppler and 4D features of major conotruncal abnormalities will be described. In particular, the echocardiographic views on which the various lesions are detected will be described. In addition, the role of color Doppler in the recognition of valve stenosis or insufficiency will be illustrated. Finally, the diagnostic role of 4D echocardiography will be described, only in those cases in which it has additional clinical value. Videos of major diagnostic features are also provided, to facilitate the understanding of the text.

**Key Words:** 4D Ultrasound, Fetal Echocardiography, Conotruncal Anomalies.

### TETRALOGY OF FALLOT (TOF)

**Anatomy.** Tetralogy of Fallot (TOF) is a cardiac malformation characterized by: 1) a malalignment subaortic VSD, 2) an aorta overriding the defect, 2) an obstruction of the right outflow tract, mainly involving the infundibular part, of varying degree; 4) a consequent hypertrophy of the right ventricle which becomes manifest only after birth. In the fetus, the pulmonary stenosis is often late onset and the main diagnostic features become then the malalignment VSD with the overriding aorta. The TOF spectrum comprises a number of variants and subtypes among which TOF with absent pulmonary valve and pulmonary atresia with VSD, which will be addressed separately.

**Ultrasound diagnosis.** As for most conotruncal anomalies, the *4-chamber view* is unremarkable, unless anomalies of the atrioventricular plane are associated, which is rather uncommon. The classic form of TOF is diagnosed on the *outflows' views*, where the malalignment VSD with the overriding aorta can be seen (Fig. 1 - [video 1](#)).

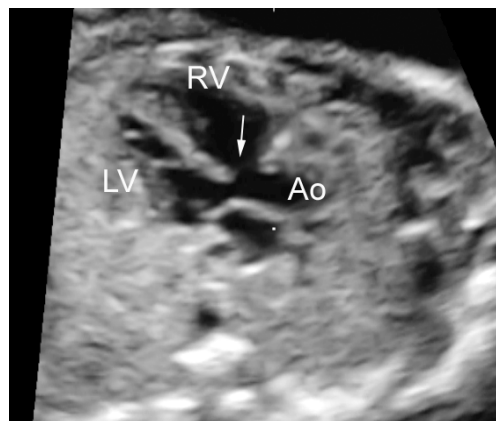


**Figure 1:** Tetralogy of Fallot. On the left outflow tract view, it is possible to detect the malalignment ventricular septal defect (arrow). See also [video 1](#) (Ao: ascending aorta LV: left ventricle; RV: right ventricle)

On the *right outflow tract view*, the smaller pulmonary artery can be detected. As mentioned above, the infundibular stenosis is not a constant finding in the 2nd trimester, but a significant stenosis, sometimes even progressing to atresia, can develop in the 3<sup>rd</sup> trimester [1]. This is why serial ultrasound monitoring is important in order to demonstrate antegrade flow through the pulmonary artery late in gestation to exclude the potential need for prostaglandin therapy after birth. Color Doppler can be used to demonstrate flow through the VSD toward the aorta (Fig. 2 - [video 2](#)) from both ventricles and flow through the smaller pulmonary outflow tract.

\*Address correspondence to Dario Paladini: Fetal Medicine & Cardiology Unit, Dept.Obstet.Gynecol. University Federico II of Naples Napoli Italia E-mail: paladini@unina.it

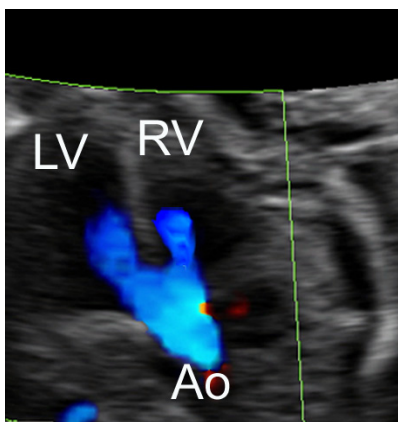


**Figure 2:** Tetralogy of Fallot. Color Doppler investigation of the left outflow tract confirm the malalignment ventricular septal defect with an override of the ascending aorta. See also [video 2](#). (Ao: ascending aorta LV: left ventricle; RV: right ventricle)

Of note that *in utero* it is unusual to detect any significant acceleration of blood across the right outflow tract, even in the presence of an obvious reduction of the vessel size. Spectral Doppler is of limited value, as is 4D echocardiography [2]. The latter may be of help if anomalies of the aortic arch are associated.

From what has been said above, *in utero* TOF cannot be differentiated from a simple malalignment VSD, if evident pulmonary stenosis is absent. Therefore, in the absence of pulmonary outflow obstruction, it is always necessary to consider the possible evolution from malalignment VSD in TOF. Another important concept is that the degree of aortic overriding is variable, and cannot be fully appreciated in the fetus. Therefore, when the aorta emerges about 50% from the right ventricle, differentiation of TOF from a Fallot-like double-outlet right ventricle can be difficult, the two being distinguished only by the degree of aortic overriding. With regard to the differential diagnosis with other conotruncal anomalies, it should be considered that common arterial trunk (CAT) and pulmonary atresia with ventricular septal defect (PAVSD) share with TOF the presence of a malalignment VSD. Hence, if aortic overriding is found, the right outflow tract should be evaluated: if a small pulmonary artery is connected to the right ventricle, the diagnosis is TOF; if this is atretic, it is PAVSD; if the pulmonary artery originates from the single emerging vessel, it is CAT.

Prognosis and survival. The association with extracardiac anomalies is frequent, in particular gastrointestinal and thoracic ones (esophageal and duodenal atresia, and diaphragmatic hernia), even independently of chromosomal anomalies. The aneuploidy risk is high (up to 20% in fetal case series), with equal distribution between trisomies 21 and 18,14,15 [3-5] Consequently, karyotyping is mandatory. There is a lesser association with microdeletion 22q11, except in the variant with absence of the pulmonary valve, where the association is about 25%. [6]. Also the risk of association with non-chromosomal syndromes is relatively high [7].

As for the obstetric management, it is safer to plan the delivery in tertiary referral centers in order to warrant optimal multidisciplinary management of possible associated malformations, notwithstanding the fact that the shunt is significant enough to warrant oxygenation in classic TOF.

The overall prognosis will depend on several factors, including karyotype, associated extracardiac malformations, and cardiac anatomy. This last factor is extremely important as the anatomy of the defect may vary significantly. With regard to survival, case series of patients with isolated TOF report long-term survival rates as high as 80-90%. Hence, if no unfavorable prognostic factors are found *in utero*, and, above all, after birth, TOF is an easily correctable heart defect, with excellent survival and good quality of life [5].

### **ABSENT PULMONARY VALVE SYNDROME (APVS)**

Definition. The absent pulmonary valve syndrome refers to a rare congenital anomaly, namely a severely hypoplastic pulmonary valve with anular stenosis, aneurysmal dilatation of the main pulmonary artery and branches. This anomaly may occur as an isolated lesion, or, more commonly be associated with TOF and ductal agenesis. In the former, the interventricular septum is intact, the pulmonary arteries are less dilated, and the ductus arteriosus is present.

Ultrasound diagnosis. Unlike most conotruncal malformations, APVS can be suspected on the 4-chamber view. The two key features are an evident cardiomegaly and an abnormal cardiac axis [6]. On this view, on some occasions,



the pulmonary trunk may be so dilated to become visible. On the left outflow view, the malalignment VSD with an overriding aorta can be seen. Sweeping further cephalad from this view, a severe dilatation of the pulmonary trunk and branches comes into view (Fig. 3).

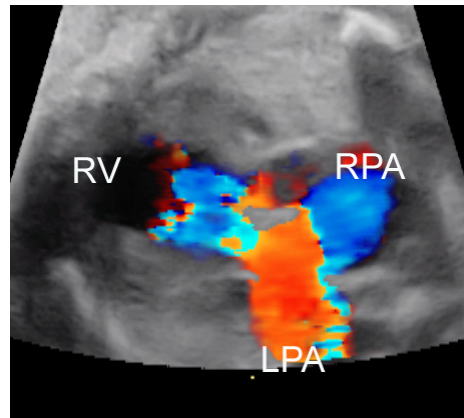


**Figure 3:** Tetralogy of Fallot with absent pulmonary valve. On color Doppler, the right outflow tract view demonstrates the severe dilatation of the main pulmonary trunk and branches, due to the steno-insufficiency of the severely hypoplastic pulmonary valve. Aliasing due to high velocity is also evident on color Doppler. (LPA: left pulmonary artery; RPA: right pulmonary artery; RV: right ventricle)

Color Doppler is used to detect the stenosis and insufficiency of the rudimentary pulmonary valve (Fig. 3). We may apply 4D echocardiography to demonstrate effectively the degree of pulmonary artery dilatation (Fig. 4 - [video 3](#)) and to characterize the severely dysplastic pulmonary valve [2].

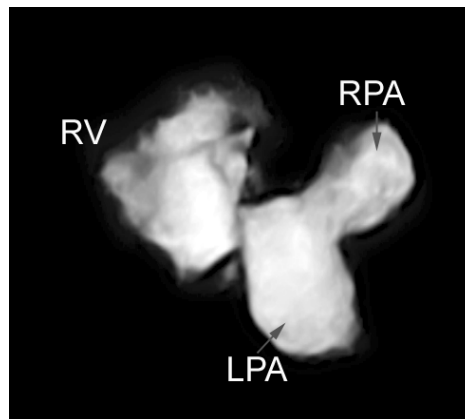


**Figure 4:** Tetralogy of Fallot with absent pulmonary valve. 4D-echocardiography clearly demonstrates the severity of the dilatation of the pulmonary main artery and branches. See also [video 3](#). (LPA: left pulmonary artery; RPA: right pulmonary artery; RV: right ventricle)

**Prognosis and survival.** The risk of association with chromosomal anomalies is extremely high for APVS-TOF, with 25% association rate with the microdeletion 22q11 [6, 8]. On the contrary, the variant with an intact ventricular septum is rarely associated with aneuploidies. Therefore, karyotyping including FISH analysis for the DGCR on chromosome 22 is mandatory in all cases of APVS-TOF [7]. Delivery should take place in a tertiary referral center in order to ensure adequate neonatal management, which may require resuscitation and, in some cases, tracheotomy.

Survival is lower than that reported for TOF, due to the frequent association with the microdeletion 22q11. In addition, severe respiratory distress due to compression of the bronchial tree by massively dilated pulmonary arteries and tracheomalacia may lead to demise after birth.

#### **PULMONARY ATRESIA WITH VENTRICULAR SEPTAL DEFECT (PAVSD)**

**Anatomy.** PAVSD represents an extreme form of TOF. There is a malalignment VSD with an overriding aorta, while the right ventricular outflow tract is, in most cases, similar to that of TOF, with the muscular outlet septum



being anteriorly displaced. In most cases, the muscular outlet septum fuses directly with the parietal musculature of the right ventricle, obliterating the ventriculopulmonary junction. The anatomy of the hypoplastic pulmonary vessel is variable. In the most frequent arrangement, the right and left pulmonary arteries are confluent (communicating with each other) and supplied by the ductus arteriosus. Alternatively, the central pulmonary arteries may be confluent and coexist with Major Aorto-Pulmonary Collateral Arteries (MAPCAs). The third pattern of arterial supply is complete absence of the central pulmonary arteries, the lungs being directly supplied by multiple MAPCAs.

Ultrasound diagnosis. The 4-chamber view is usually normal; in some cases, minor leftward rotation of the cardiac axis and/or cardiomegaly can be appreciated. The malalignment VSD is best visualized on the left outflow tract view (Fig. 5 - [video 4](#)), on which sometimes, as in the case shown, also the hypoplastic pulmonary artery is displayed.

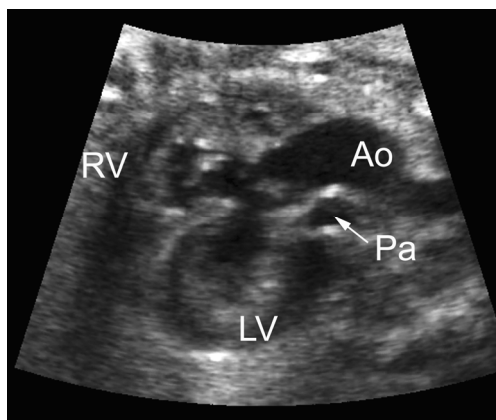


**Figure 5:** Pulmonary Atresia + Ventricular Septal Defect. On the left outflow tract view, it is possible to demonstrate the malalignment ventricular septal defect with the overriding aorta. It is also shown, just behind the aorta, the small, atretic pulmonary artery (arrow) - See also [video 4](#). (Ao: ascending aorta LV: left ventricle; Pa: main pulmonary artery; RV: right ventricle)

When the right and left pulmonary arteries are present, they are commonly smaller than normal and confluent, with the characteristic appearance of a ‘flying seagull’, and their size is usually dependent on the source of arterial supply. The pulmonary vascular bed may be supplied with blood flow from a ductus arteriosus, from MAPCAs, or from a combination of both. Color Doppler can be used to confirm overriding of the aorta (see Fig. 2 and [video 2](#)), and to demonstrate the retrograde blood flow across the ductus arteriosus. The use of color Doppler or power Doppler is also important to demonstrate the presence of MAPCAs branching off the descending thoracic aorta. Spectral Doppler has a limited diagnostic role to play in PAVSD. 4D echocardiography has recently been demonstrated to be very helpful in the definition of the vascularization pattern of the pulmonary arteries [2, 9]. In particular, the use of B-flow imaging and/or the inversion mode can demonstrate the confluent pulmonary arteries and the MAPCAs better than 2D ultrasound. As for the differential diagnosis, it should be underlined that differentiating PAVSD from CAT can be challenging. CAT types II and III and PAVSD share the reduced dimensions of the pulmonary branches and the prevalence of the aortic vessel. When doubts arise, the following anatomic details should be sought to make the final diagnosis: the aortic/truncal valve is always dysplastic (from two to five cusps) and typically stenotic and/or insufficient in CAT, not in PAVSD; the direction of flow within the arterial duct is reversed in PAVSD, anterograde in CAT

Prognosis and survival. The risk of association with chromosomal anomalies is high for PAVSD, which shows a 29% association rate with the 22q11 microdeletion and, to a much lower extent with trisomies 13 and 18 [7]. Therefore, karyotyping with FISH analysis for the DGCR on chromosome 22 is mandatory. Delivery should take place in a tertiary referral center to allow proper neonatal management, being the pulmonary circulation ductus-dependent.

The main prognostic factors for PAVSD are represented by the anatomy of the pulmonary arteries and by the sources of the pulmonary blood supply. The most favorable arrangement, from a surgical point of view, is that in which the two pulmonary branches are confluent and are supplied by the arterial duct. On the contrary, the complete absence of the central pulmonary arteries, with the lungs being directly supplied by multiple MAPCAs, represents the worst scenario, being associated with a significantly worse prognosis; also, it is the most difficult to treat postnatally

## COMMON ARTERIAL TRUNK (CAT)

**Anatomy.** Common arterial trunk (CAT) is characterized by a single arterial trunk arising from the base of the heart, which supplies the systemic, coronary, and pulmonary blood flow. CAT results from a septation failure during development of the ventricular outlets and the proximal arterial segment of the heart tube. The earliest classification, developed by Collett and Edwards [10], includes four different anatomical subtypes with respect to the origin of the pulmonary arteries: in type I, a short main pulmonary trunk arising from the common arterial trunk which gives rise to right and left pulmonary arteries (48-68% of cases); In types II and III, the pulmonary trunk is absent and the two pulmonary branches arise close to one another (29-48% of cases- type II) or distant one from the other (6-10% of cases - type III). Type IV is currently defined as PAVSD.

**Ultrasound diagnosis.** In CAT, the 4-chamber view is usually unremarkable, being a slight increase of the cardiac axis noted in a minority of cases. On the left outflow tract view, the constant malalignment VSD and the usually abnormal truncal valve are seen ([fig.6](#)). Sometimes, the truncus may straddle one ventricle, especially if there is dominance of one ventricle [11]. Visualization of the pulmonary arteries is essential to distinguish CAT from PAVSD and to identify the CAT subtype ([fig 6](#)).

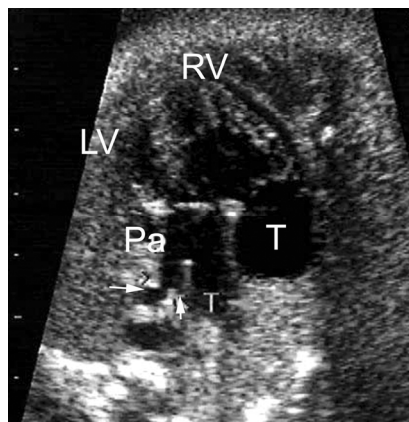


**Figure 6:** Common arterial trunk, type I. The left outflow tract view demonstrates the large truncal root, and the main pulmonary artery branching off the trunk just above the truncal valve. The small, hypoplastic pulmonary branches are also barely visible (arrows). (LV: left ventricle; RV: right ventricle; T: truncus arteriosus)

In the case of PAVSD, the hypoplastic pulmonary arteries are supplied by the ductus arteriosus and/or by the major aorto-pulmonary collateral arteries (MAPCAs). As previously mentioned, in type I CAT, the main pulmonary trunk arises from the posterolateral aspect of the common trunk and bifurcates into two pulmonary arteries ([fig.6](#)). In types II and III, the pulmonary arteries arise separately. The truncal valve is often dysplastic, and may be regurgitant or stenotic. Color Doppler may be used and may help to evaluate the ventriculo-arterial connection ([fig.7](#)), checking for possible stenosis/insufficiency of the truncal valve, and to trace the course and connection of the pulmonary trunk/arteries.

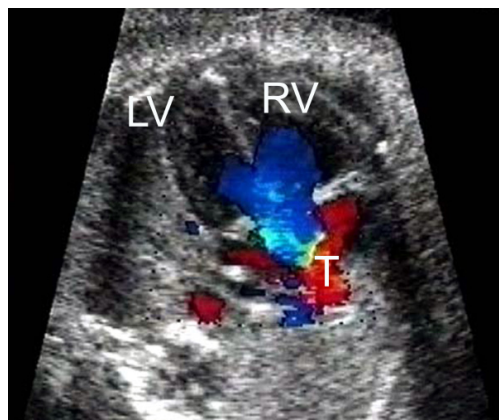


**Figure 7:** Common arterial trunk, type I. On color Doppler, the malalignment ventricular septal defect with overriding of the arterial trunk is confirmed. (LV: left ventricle; RV: right ventricle; T: truncus arteriosus)

The use of 4D echocardiography is extremely useful in the identification of the small pulmonary branches in type II/III CAT (fig.8) and in the characterization of the pulmonary trunk anatomy in PAVSD (especially with inversion mode and B-flow) [2].

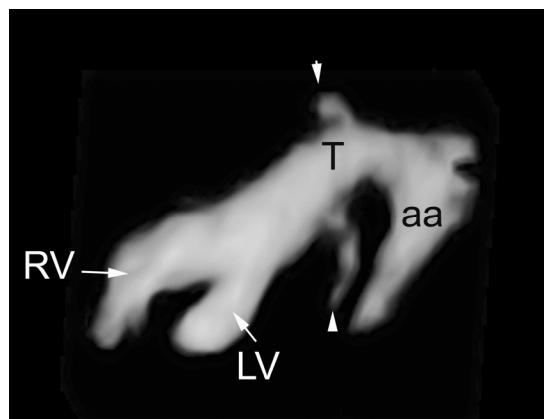


**Figure 8:** Common arterial trunk type II (both pulmonary arteries branching off at the same distance from the valve). On 4D-echocardiography, it is possible to demonstrate the two pulmonary branches directly departing from the arterial trunk (arrowheads). This diagnosis is extremely challenging on two-dimensional echocardiography and is much simpler and straightforward using 4D-echocardiography. (aa: aortic arch; LV: left ventricle; RV: right ventricle; T: truncus arteriosus)

Prognosis and survival. CAT can be associated with cardiac and extracardiac abnormalities in a significant percentage of cases, and some of these may have an impact on management and outcome. Associated cardiac defects, which occur in 20-30% of cases, include absence of ductus arteriosus (50% of cases), interruption of the aortic arch or right aortic arch, and atrioventricular valve atresia [11]. The risk of association with chromosomal anomalies is significant, in the range of 5-10%, but what is extremely high is the risk of association with the microdeletion 22q11, which is present in 30-40% of the cases both in prenatal and in postnatal series [11]. Therefore, karyotyping with FISH analysis for the DGCR is mandatory. Delivery should take place in a tertiary referral center, so that the neonate can be transferred to a pediatric cardiology unit to confirm the diagnosis and receive an adequate management.

The final prognosis depends on the presence of extracardiac and chromosomal anomalies and of unfavorable cardiac anatomy (e.g. severe truncal valve regurgitation, IAA, and straddling with ventricular hypoplasia). Immunodeficiency in case of an underlying DiGeorge syndrome is also an issue.

### DOUBLE-OUTLET RIGHT VENTRICLE (DORV)

Anatomy. DORV encloses a wide range of lesions characterized by a double right ventriculo-arterial connection that may have completely different hemodynamic characteristics. The main feature of DORV is that both great vessels arise for more than 50% from the same ventricle and that the spatial relationship of the two arteries may vary extensively. They can show a normal relationship, with the aorta posterior and the pulmonary artery anterior and to the left, or they can be malposed, with the aorta arising anteriorly, behind the sternum, and the pulmonary trunk posterior above the VSD. The VSD position and commitment is also variable: non-committed, sub-pulmonary, subaortic, doubly committed. Besides, there may be an obstruction of the pulmonary outflow or, much less frequently, the aortic outflow, due to pulmonary stenosis/atresia or aortic coarctation. The most frequent variants are the Fallot type (subaortic VSD, great vessels in normal spatial relationship, and pulmonary artery obstruction), the Taussig-Bing type (subpulmonary VSD and malposed great arteries), and the type with subaortic VSD but without pulmonary stenosis. In many cases, other major cardiac defects such as ventricular hypoplasia (almost always due to straddling and overriding of one of the two atrioventricular valves), aortic coarctation, AVSD, and cardiosplenic syndromes can be associated. Ultrasound diagnosis. It is important to underline that, unless severe anomalies of the atrioventricular junction are associated, the 4-chamber view is unremarkable, as in most conotruncal anomalies. The double right ventriculo-arterial connection is detected on the outflow tract views: the crossover is missing and the great vessels run parallel and arise from the anterior ventricle in normal relationship or malposed (Fig. 9 - [video 5](#)).

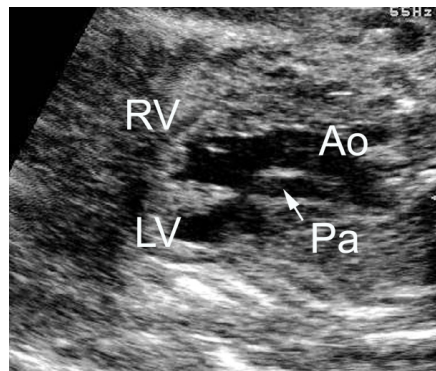


**Figure 9:** Double Outlet Right Ventricle (DORV). On the outflow tracts' view, it is possible to demonstrate the absence of the crossover, with the two great arteries coursing parallel one to the other. The arteries are also malposed, with the aorta anterior and the stenotic pulmonary artery posterior (arrow). The small sub-pulmonary ventricular septal defect is also evident. See also [video 5](#) (Ao: ascending aorta; LV: left ventricle; Pa: main pulmonary artery; RV: right ventricle)

The use of color Doppler may facilitate the assessment of the spatial relationship of the great vessels (Fig. 10).

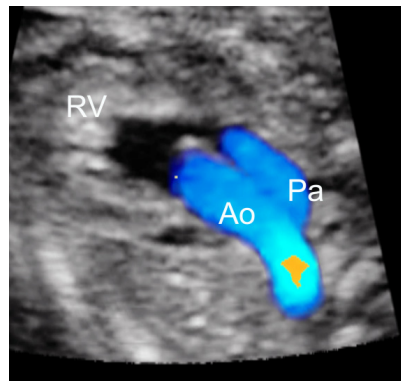


**Figure 10:** Double Outlet Right Ventricle (DORV). On the right outflow tract view, using color Doppler it is possible to demonstrate again the absence of the crossover and the two parallel vessels. In this case, there was no malposition, and the aorta arises normally from the central part of the heart. (Ao: ascending aorta; Pa: main pulmonary artery; RV: right ventricle)

Noteworthy, the diagnosis of outflow obstruction in DORV is based on comparison of the vessel size rather than on increased transvalvular velocity. Very important is the definition of the spatial relationship of the great vessels because it identifies the type of surgical approach required, and therefore the prognosis. Also, DORV may change through the course of pregnancy: the degree of pulmonary outflow obstruction can worsen significantly in the 3rd trimester, and, if one of the atrioventricular valves show straddling or overriding, ventricular hypoplasia can develop. 4D echocardiography may be used to confirm the double ventriculo-arterial connection and the absence of the crossover [2], but these diagnoses can be effectively made on 2D also.

**Prognosis and survival.** From the prognostic standpoint, if DORV is not associated with extracardiac or chromosomal anomalies, the major negative prognostic feature is the presence of other cardiac defects (AVSD, cardiosplenic syndromes, aortic coarctation, and straddling/overriding of the atrioventricular valves with consequent hypoplasia of the underlying ventricle). The general prognosis is very poor if DORV is associated with chromosomal anomalies or syndromic conditions. The risk of association with chromosomal anomalies is very high, in the range of 12-45%, with a prevalence of trisomies 18, 13, and, to a lesser extent, 22q, 11 microdeletion and trisomy 21 [3-5]. Hence, karyotyping is mandatory, especially if extra-cardiac anomalies are found in association. The delivery should take place in a tertiary referral center, so that the neonate can be transferred to a pediatric cardiology unit to confirm the diagnosis and to receive adequate management.

Due to the strong association with aneuploidy and extracardiac anomalies, the overall survival of fetal DORV is 46-50%, if terminations of pregnancy are excluded. However, it is shown that the overall surgical mortality rate for biventricular repair is as low as 13%, with an 86% 10-year survival rate. The mortality is much higher if other major cardiac lesions are associated.

## COMPLETE TRANSPOSITION OF THE GREAT ARTERIES (TGA)

**Anatomy.** Complete transposition of the great arteries (TGA) is determined by the presence of a discordant ventriculo-arterial connection, with the aorta arising from the right ventricle and the pulmonary artery connected to the left ventricle. The pulmonary and systemic circulations function in parallel, rather than in series. This malformation is caused by abnormal formation of the aorto-pulmonary septum. TGA can occur as an isolate anomaly (simple TGA) or be associated with a VSD and/or pulmonary outflow obstruction; less commonly with aortic arch anomalies. It is very rare to find atrioventricular valve abnormalities, including straddling and overriding, associated with TGA. Significant anomalies of the coronary pattern, which are not diagnosable in utero, are associated in two-thirds of the cases. **Ultrasound diagnosis.** The 4-chamber view is unremarkable, as for most conotruncal anomalies, unless major anomalies of the atrioventricular junction are associated. The diagnosis is made on the outflow tract views, where there is no crossover, with the two arteries following a parallel course. The aorta arises from the anterior right ventricle, and the pulmonary artery is connected posteriorly with the left ventricle (fig 11). In order to detect possible (valvular) obstructions of the pulmonary artery and of the aorta (arch coarctation/interruption), it is important to compare the size of the two vessels. On longitudinal views, the anteriorized connection of the ascending aorta gives the aortic arch a wider angle curvature similar to a “hockey club” and not to the classic “umbrella handle” of the normal arch. In case of TGA with an intact ventricular septum, particular attention should be paid in late gestation to signs possibly indicative of a restrictive foramen ovale, such as consistent bulging into the left atrium and/or thickening, or limited movement of a small foramen ovale flap - ref.12).

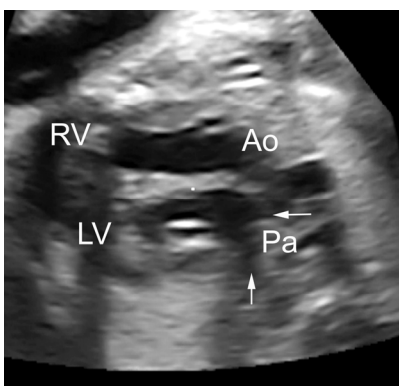


**Figure 11:** Transposition of the Great Arteries (TGA). The left outflow tract view demonstrates also in TGA the absence of the crossover, as in DORV. In this case, however, each vessel is connected with the wrong ventricle: the aorta, anterior, arises from the right ventricle, the pulmonary artery, posterior, from the left ventricle. The type of vessel is identified by showing the two pulmonary branches (arrows) in the pulmonary artery (Ao: ascending aorta; LV: left ventricle; Pa: main pulmonary artery; RV: right ventricle)

Color Doppler may contribute to confirm the ventriculo-arterial discordance, (Fig. 12 - [video 6](#)), to recognise small VSDs not evident on greyscale ultrasound, and to detect possible pulmonary/aortic outflow obstruction. 4D echocardiography has been shown to be useful in the assessment of the spatial relationship of the great arteries, deriving the risk of association with coronary abnormalities ([video 7](#)) [13].

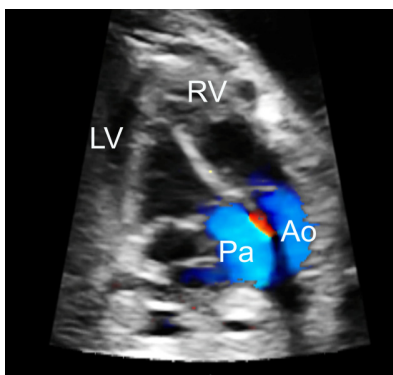


**Figure 12:** Transposition of the Great Arteries (TGA). Color Doppler contributes to the assessment of the ventriculo-arterial connection: each vessel is clearly emerging from a different ventricle. See also [video 6](#) and [video 7](#). (Ao: ascending aorta; LV: left ventricle; Pa: main pulmonary artery; RV: right ventricle)



It can also demonstrate very nicely the parallel course of the great vessels (Fig. 13).

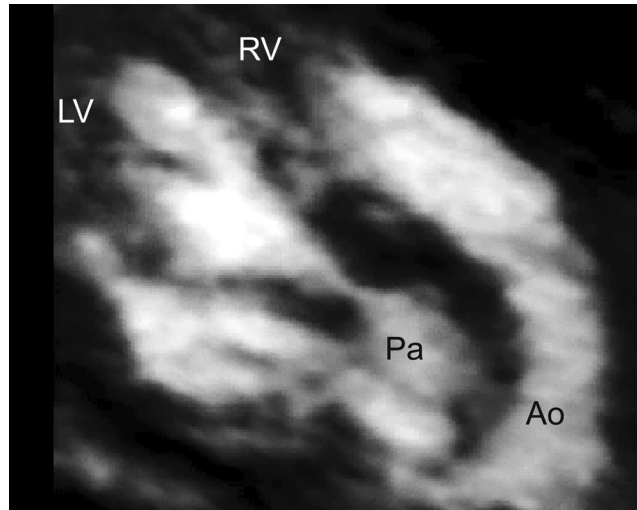


**Figure 13:** Transposition of the Great Arteries (TGA). 4D-echocardiography nicely demonstrates the absence of crossover and the ventriculo-arterial discordance. In this case, inversion mode rendering was used. (Ao: ascending aorta; LV: left ventricle; Pa: main pulmonary artery; RV: right ventricle)

As to the differential diagnosis, TGA can be distinguished from DORV paying attention to the ventriculo-arterial connection. Prognosis and survival. From the cardiological standpoint, the worst prognostic indicator is the occurrence of significant right outflow obstruction, for this represents a contraindication to the classic arterial switch operation. On the other hand, TGA seems to protect from aneuploidy, like cTGA and cardiosplenic syndromes; and is also exceptionally rare the association with other syndromic conditions. Hence, karyotyping can be avoided, unless clear markers of aneuploidy are associated. Serial follow-up scans are indicated, especially in case of TGA with intact ventricular septum, in order to recognize a restrictive foramen ovale, if present. If this is the case, it is necessary to organise the delivery so that the neonate is transferred to the interventional catheterization room within 30 minutes at the latest, in order to perform a life-saving Rashkind atrioseptostomy. As a consequence, delivery should be organized in a tertiary referral center, alerting the cardiac hemodynamist of the imminent delivery [14]. If there is significant shunting across a VSD, together with a non-restrictive foramen ovale, the neonate may be transferred to the pediatric cardiology unit in the first hours of life in order to ensure assessment of oxygen saturation and proper planning of the Rashkind atrioseptostomy. The option of choice for surgical correction of TGA is the arterial switch operation. In some cases, the palliative atrial switch (Senning or Mustard procedure) operation is performed, usually at 3-6 months of life. If early neonatal management is properly planned, this CHD has a long-term survival rate greater than 90% in good functional conditions. What makes the difference is certainly prenatal diagnosis, being responsible for a 7% reduction in surgical mortality [14]. Patients undergoing palliative surgical procedures (Mustard or Senning) have lower survival rates (80%).

### **CORRECTED TRANSPOSITION OF THE GREAT ARTERIES (cTGA)**

**Anatomy.** cTGA is defined by the association of atrio-ventricular and ventriculo-arterial discordance, with the double discordance functionally correcting the circulation. The left atrium is connected via a tricuspid valve to a morphologically right ventricle from which the aorta emerges and, viceversa, the right atrium is connected via the mitral valve to a morphologically left ventricle from which the pulmonary artery emerges. The discordance between cardiac situs and position is very often associated, with dextrocardia in situs solitus and levocardia in situs inversus. Frequently associated are other major cardiac lesions, including VSDs, abnormalities of the left-sided tricuspid valve, pulmonary outflow obstruction and rhythm disturbances.

**Ultrasound diagnosis.** Fundamental for the diagnosis of cTGA is the 4-chamber view, on which the atrioventricular discordance is evident (Fig. 14): the morphologically right ventricle is positioned to the left and is connected to the left atrium; conversely, the left ventricle, forming the apex of the heart, is positioned to the right and is connected to the right atrium.

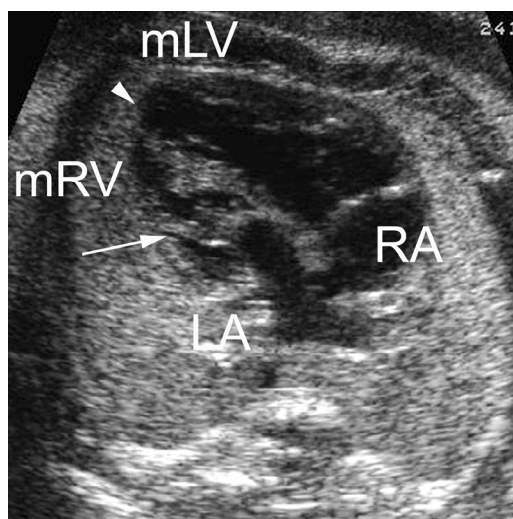


**Figure 14:** Congenitally corrected transposition of the great arteries (cTGA). On the apical 4-chamber view, it is possible to detect the atrio-ventricular discordance. Note the lower insertion of the left-sided abnormal tricuspid valve (arrow) and the fact that the apex of the heart is made by the ventricle positioned on the right side (morphological left ventricle). (LA: left atrium; mLV: *morphological* left ventricle; mRV: *morphological* right ventricle; RA: right atrium)

Other features that may increase the confidence of the diagnosis are the different attachments of the chordae tendinae of the two atrioventricular valves: the left-sided tricuspid valve papillary muscles attach to the ventricular apex, whereas the right-sided mitral valve papillary muscles attach to the lateral free wall (Fig. 15).

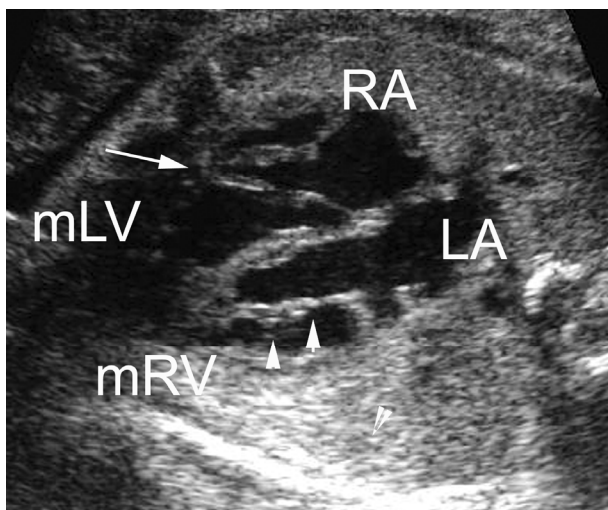


**Figure 15:** Congenitally corrected transposition of the great arteries (cTGA). On the transverse 4-chamber view, it is possible to detect the differential attachments of the chordae tendinae. The left-sided tricuspid ones attach onto the apex of the ventricle (arrowheads), whereas the right-sided mitral ones attach on the lateral myocardial wall (arrow). This is an additional feature supporting the diagnosis of atrio-ventricular discordance. (LA: left atrium; mLV: *morphological* left ventricle; mRV: *morphological* right ventricle; RA: right atrium)

Assessment of the outflows demonstrates the pulmonary artery arising from the right-sided left ventricle and the aorta emerging from the left-sided right ventricle. Recognition of dextrocardia in situs solitus should always prompt assessment of central connections to rule out a cTGA. Anomalies of the tricuspid valve, VSDs, pulmonary and aortic outflow obstruction, and complete heart block are frequently associated [15]. The heart block is progressive, very often appearing only in the 3<sup>rd</sup> trimester or after birth, and is due to the abnormal position of the conduction tissue. Color Doppler may be helpful to distinguish the spatial relationship of the great arteries and in the detection of the VSD. To quantify the transvalvular gradient in the case of pulmonary stenosis it is possible to use spectral Doppler. 4D echocardiography can surely demonstrate the inverted position of the ventricles by inversion-mode or B-flow renderings (Fig. 16, [video 8](#)).



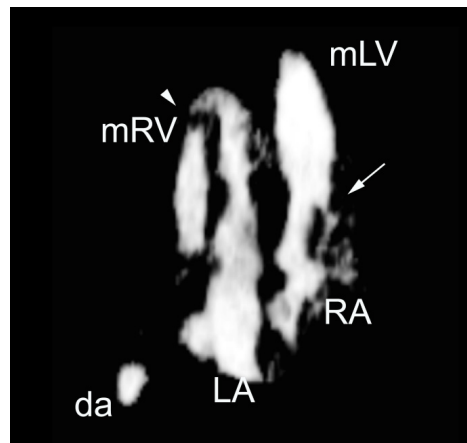


**Figure 16:** Congenitally corrected transposition of the great arteries (cTGA). 4D-Echocardiography confirms both the atrio-ventricular discordance and the differential attachments of the chordae tendinae, with the left-sided tricuspid ones attaching onto the apex of the ventricle (arrowheads) and the right-sided mitral ones attaching on the lateral myocardial wall (arrow). See also [video 8](#). (da: descending aorta; LA: left atrium; mLV: *morphological* left ventricle; mRV: *morphological* right ventricle; RA: right atrium)

Prognosis and survival. Ventricular hypoplasia and outflow atresia represent ominous prognostic signs. Scant is the association with other malformations, with minor renal anomalies having been reported in association with cTGA [15]. The risk of association with chromosomal and non-chromosomal syndromic conditions is virtually non-existent, for cTGA seems to protect from aneuploidy, together with TGA and cardiosplenic syndromes. Therefore, fetal karyotyping is not recommended. It is advisable for delivery to take place in a tertiary referral center, especially if there is evident outflow obstruction, major atrioventricular anomalies or congenital heart block with low cardiac output. Postnatal management of cTGA is controversial. Major surgery can be avoided if there are no outflow obstructions or significant valve abnormalities. The real problem is the long term survival. The frequency and severity of the associated cardiac lesions and the conduction system abnormalities represent the most important determinants of survival and mortality. The main indicators of a poor prognosis are a severe insufficiency of the left-sided tricuspid valve and impaired systolic function of the right (systemic) ventricle. By 45 years of age, 67% of individuals with associated lesions showed heart failure, in comparison with 25% of individuals with isolated cTGA [16].

## REFERENCES

- [1] Hornberger LK, Sanders SP, Sahn DJ, Rice MJ, Spevak PJ, Benacerraf BR, *et al.* In utero pulmonary artery and aortic growth and potential for progression of pulmonary outflow tract obstruction in tetralogy of Fallot. *J Am Coll Cardiol* 1995; 25: 739-45.
- [2] Paladini D, Volpe P. the normal and abnormal fetal heart. A 2D-4D color Atlas. 1<sup>st</sup> edition, 2008. [www.mdmcongress.it/editoria.html](http://www.mdmcongress.it/editoria.html)
- [3] Paladini D, Rustico MA, Todros T, Palmieri S, Gaglioti P, Benettoni A, *et al.* Conotruncal anomalies in prenatal life. *Ultrasound Obstet Gynecol* 1996; 8: 241-6.
- [4] Allan LD, Sharland GK, Milburn A, Lockhart SM, Groves AM, Anderson RH *et al.* Prospective ultrasound diagnosis of 1006 consecutive cases of congenital heart disease in the fetus. *J Am Coll Cardiol* 1994; 23: 1452-8.
- [5] Paladini D, Russo M, Teodoro A, Pacileo G, Capozzi G, Martinelli P, *et al.* Prenatal diagnosis of congenital heart disease in the Naples area during the years 1994-1999 - the experience of a joint fetal-pediatric cardiology unit. *Prenat Diagn* 2002; 22: 545-52.
- [6] Volpe P, Paladini D, Marasini M, Buonadonna AL, Russo MG, Caruso G, *et al.* Characteristics, associations and outcome of absent pulmonary valve syndrome in the fetus. *Ultrasound Obstet Gynecol* 2004; 24: 623-8.
- [7] Paladini D, Volpe P. *Ultrasound of congenital fetal anomalies*. Informa Healthcare, London, 2007.
- [8] Razavi RS, Sharland GK, Simpson JM. Prenatal diagnosis by echocardiogram and outcome of absent pulmonary valve syndrome. *Am J Cardiol* 2003; 91: 429-32.
- [9] Volpe P, Campobasso G, Stanziano A, De Robertis V, Di Paolo S, Caruso G, *et al.* A novel approach to enhance the assessment of sources of pulmonary blood flow and the identification of the anatomy of pulmonary arteries in fetuses with pulmonary atresia with ventricular septal defect: 4D-US with B-flow imaging and spatiotemporal image correlation. *Ultrasound Obstet Gynecol* 2006; 28 (1):40-6.

- [10] Collett RW, Edwards JE. Persistent truncus arteriosus: a classification according to anatomic types. *Surg Clin North Am* 1949;29: 1245-70.
- [11] Volpe P, Paladini D, Marasini M, Buonadonna AL, Russo MG, Caruso G, *et al.* Common arterial trunk in the fetus: characteristics, associations, and outcome in a multicentre series of 23 cases. *Heart* 2003; 89: 1437-41.
- [12] Jouannic JM, Gavard L, Fermont L, Le Bidois J, Parat S, Vouhé PR, *et al.* Sensitivity and specificity of prenatal features of physiological shunts to predict neonatal clinical status in transposition of the great arteries. *Circulation* 2004; 110: 1743-6.
- [13] Paladini D, Volpe P, Sglavo G, Vassallo M, De Robertis V, Marasini M, Russo MG. Transposition of the great arteries in the fetus: assessment of the spatial relationships of the arterial trunks by four-dimensional echocardiography. *Ultrasound Obstet Gynecol.* 2008; 31(3):271-6.
- [14] Bonnet D, Coltri A, Butera G, Fermont L, Le Bidois J, Aggoun Y, *et al.* Detection of transposition of the great arteries reduces neonatal morbidity and mortality. *Circulation* 1999; 99: 916-18.
- [15] Paladini D, Volpe P, Marasini M, Russo MG, Vassallo M, Gentile M, Calabrò R. Diagnosis, characterization and outcome of congenitally-corrected transposition of the great arteries in the fetus. A multicenter series of 30 cases. *Ultrasound Obstet Gynecol* 2006; 27: 281-5.
- [16] Graham TP, Bernard YD, Mellen BG, Celermajer D, Baumgartner H, Cetta F, *et al.* Long-term outcome in congenitally corrected transposition of the great arteries. *J Am Coll Cardiol* 2000; 36: 255-61.

## First Trimester Study of Fetal Heart with 4D Echocardiography

Weissmann-Brenner Alina, Gindes Liat and Achiron Reuven

*Department of Obstetrics and Gynecology, The Chaim Sheba Medical Center, Tel Hashomer, Affiliated with the Sackler Faculty of Medicine, Tel Aviv University, Israel*

**Abstract:** The following chapter discusses the added value of various novel 3- and 4-Dimensional Ultrasound (3D/4D US) applications for assessing fetal cardiac anomalies at the first trimester of pregnancy. Information on the importance of the early diagnosis, the feasibility, the anomalies that can be detected at early stages of pregnancy and the limitation of such early examination are discussed in details.

**Key words:** First Trimester, Fetal Echocardiography, 4D Fetal Echocardiography.

### INTRODUCTION

Congenital heart disease (CHD) is the most common major congenital malformation with a birth incidence of 4-8 per 1000 neonates, and high rates of neonatal mortality (20-30%) [1, 2]. High risk population for CHD includes fetuses with increased NT, family history of CHD, and pre-gestational diabetes (Table 1).

**Table 1:** Common indications for early fetal echocardiography [19, 38, 39]:

1.	Family history	First-degree relative
2.	Pre-existing metabolic disease	Diabetes
3.	Maternal infections	Parvovirus B19, Rubella, Coxsackie
4.	Cardiac teratogen exposure	Retinoids, Phenytoin, Carbamazepine, Lithium, carbonate, Valproic acid
5.	Suspected fetal heart anomaly	
6.	Abnormal fetal karyotype	
7.	Major extracardiac anomaly	
8.	Abnormal nuchal translucency	$\geq 3.5$ mm before 14 weeks' gestation
9.	Fetal cardiac rate or rhythm disturbances	Persistent bradycardia, Persistent tachycardia, Persistent irregular heart rhythm
10.	Reversed end diastolic flow in the umbilical artery	

Prenatal diagnosis of CHD has several purposes: First, patients can be advised about the prognosis and the possible options of treatment and can be referred to tertiary centers for delivery. Second, because there is a strong association between cardiac defects and chromosomal abnormalities [3-5], karyotyping can be offered when CHD are diagnosed. Third, patients can choose termination of pregnancy when severe CHD is diagnosed.

Imaging of the fetal heart in the first trimester of pregnancy is technically more demanding than in mid-gestation because of the relatively smaller size of the fetus and the cardiac structures (the diameter of the heart is about 3 mm at 12 weeks' gestation) (Table 2).

\*Address correspondence to Liat Gindes: MD Department of Obstetrics and Gynecology The Chaim Sheba Medical Center Tel-Hashomer, Ramat Gan, Israel. [52621 E-mail: gindesl@zahav.net.il](mailto:gindesl@zahav.net.il)

**Table 2:** Cardiac anomalies that can be detected at the first trimester of pregnancy.

	No.	Patients	GA	4CV	Complete echo	Anomalies detected	Anomalies missed
<b>Achiron [40]</b>	660	Low risk	13-15	100%	98%	n=3:aortic atresia, TOF, persistent truncus arteriosus	n=3: 2XVSD, rhabdomyoma
<b>Russel [41]</b>	32	Low risk	12-14	100%			
<b>Carvalho [31]</b>	46	Low risk	11-14.6		37-100%		
<b>McAuliffe [3]</b>	160	High risk	11-15.6		95%	n=14: hypoplastic left heart, AV canal, VSD, hypoplastic right heart	n=6:TGA, VSD
<b>Weiner [4]</b>	392	High risk	11-14	100%	88-99%	n=7: hypoplastic left heart, TGA, truncus arteriosus, AV canal, VSD, hypoplastic right heart	n=6: TOF, VSD, ASD
<b>Weiner [5]</b>	200	High risk	11.2-13.5	100%	41-94%	n=12: hypoplastic left heart, AV-canal, truncus arteriosum, hypoplastic right heart, VSD, TGA, TOF	n=6: TOF, pulmonic stenosis, VSDX4, ASD, coarctation of aorta
<b>Gabriel [42]</b>	330	High risk	12-17	100%	94.6%	n=38:VSD, hypoplastic right heartAV canal, TGA, pulmonary atresia, TOF, tricuspid atresia, hypoplastic left heart	n=10:hypoplastic left heart, VSD, ASD, TOF
<b>Carvalho [43]</b>	222	High risk		100%	96%	n=14: AV canal, hypoplastic left heart, VSD, TGA, pulmonary atresia, tricuspid atresia	n=2: VSD, pulmonary stenosis

GA - gestational age 4CV - four chamber view TOF - tetralogy of Fallot. Technological improvements extended the boundaries of the diagnosis of fetal anomalies. The introduction of 3D/4D US opened new era and advanced our capabilities in the demonstration of in-vivo cardiac performance and diagnosis of various fetal malformations. The ultimate goal of 3D and 4D ultrasound is to improve the detection rates of CHD with the ability to navigate the volume and to rotate it, and thus demonstrate additional angles other than the original angle of acquisition. As a result, it has the potential to decrease the dependency on fetal position and sonographer skill because it provides a volume dataset that can be used to display the desired images [6-10].

The objective of this chapter is to review the value of 4DUS examination of the fetal heart during the first trimester.

### 3D/4D VERSUS 2D US EXAMINATION OF THE FETAL HEART

3D/4D US overcomes major limitation of the 2D US: It provides the examiner with an unlimited number of images for review; it allows for correlation between image planes that are perpendicular to the main image acquisition plane; it enables navigation through the volume dataset and examination of the fetal heart in the absence of the patient; it enables the operator to follow abnormal vessels and to find their origin; it has the potential to shorten the evaluation time, especially when complex heart defects are suspected; it enables the reconstruction of a 3D rendered image that contains depth and volume which may provide additional information that is not available from the thin 2D image slices; it provides examination of the fetal heart using a tomographic approach similar to that used to read computerized tomography; the data volume can be stored and reviewed offline by the examiner or it can be viewed by experts at a remote site; it provides the examiner with the ability to review all images in a cine-loop format; and it enables to slow down the heart rate and detect fast details in slow [10-14].

### BASIC PRINCIPLES OF 3D AND 4D ECHOCARDIOGRAPHY:

*Gating:* Gating is the accurate temporal assignment of 3D images within the cardiac cycle, and is essential for the 3D reconstruction of dynamic cardiac structures. Cardiac motion cannot be depicted using non-gated, static reconstructions, which have been shown to be of reduced resolution and suboptimal accuracy. The dynamic changes in the anatomical structures during the cardiac cycle can be displayed using continuously gated, dynamic 3D (i.e. 4D) echocardiography [15-16].

*Spatio-temporal image correlation - STIC:* STIC is a technique that allows examination of the fetal heart within a real time 3D (i.e. 4D) volume, displayed in a cine loop that was developed at University of San Diego California [17,18].

In order to have a good STIC volume the 2D image should be optimized: narrow angle, higher frame rate, avoidance of acoustic shadow and other artifacts. After acquiring the best 2D image the operator has to focus on two points: the window of acquisition and the angle of acquisition. In the window of acquisition it is important to include part of the chest and not to be focused only on the heart. It is important to define the anterior, posterior, right and left sides, and to be able to diagnose enlargement and deviations of the heart. The angle of acquisition should be the minimal angle that includes the information, and by this the acquisition time would be shorter and the movement artifact reduced.

The resultant consecutive volumes are a reconstructed complete heart cycle that displays in an endless loop. This loop may be played in slow motion or stopped at any time for detailed analysis of specific phases of the cardiac cycle. Because there is a volume dataset, each of the scan planes can be moved and rotated while maintaining the synchronized cardiac loop. Thus, the four-chamber view, long axis, short axis, great vessels and all other views can be displayed both in cine loop and as still images (Fig. 1, 2, [video1](#)).

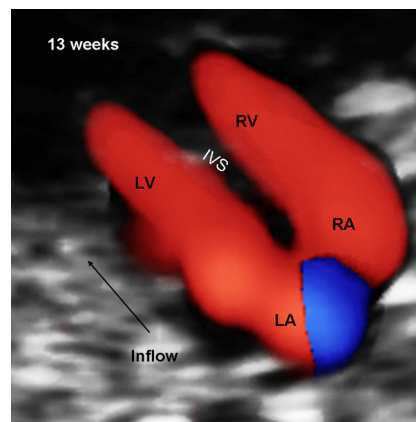


**Figure 1:** Render mode of four chamber view from normal fetus at 13 weeks gestation. The volume acquired with STIC and High Definition Doppler (HDD). Render mode with glass body at the initial acquisition plane was made. RV=right ventricle; LV=left ventricle, IVS=inter ventricular septum; RA=right atrium; LA=left atrium; arrow demonstrate the direction of blood flow from the atria to the ventricles during the diastole.

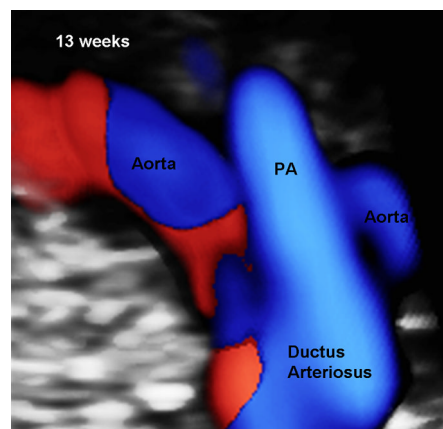


**Figure 2:** The same volume as in figure 1. The volume now is in the upper chest where the PA (pulmonary artery) crosses the aorta.

We can use the volume as 2D images or 3D images. The multiplanar mode demonstrates 2D images that are perpendicular to each other (the axial, sagittal and coronal planes) at the same time. The tomographic ultrasound imaging (TUI) demonstrate 2D images that are parallel to each other and the whole 5 axial views of the heart can be detected at the same time (Fig. 3).

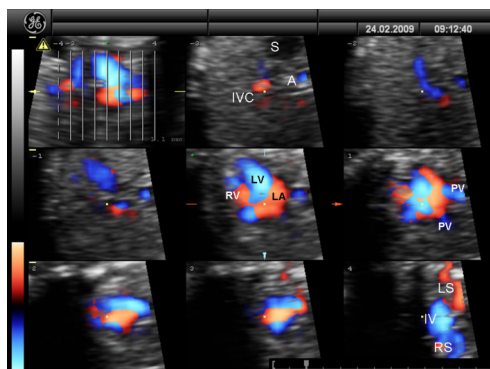


**Figure 3:** Tomographic ultrasound imaging (TUI) of normal fetus at 11 weeks. The volume acquired with STIC and High Definition Doppler (HDD). S=stomach, IVC=inferior vena cava, A=aorta, LA=left atrium, RV=right ventricle, LV=left ventricle, PV=pulmonary vein.

The volume can be demonstrated as a 3D image using rendering tools. The 3D can be manipulated by editing the colors, the image settings, the different modes. Those variable options can extract different information from the same dataset (Fig. 4 [video 2](#), [video 3](#)).

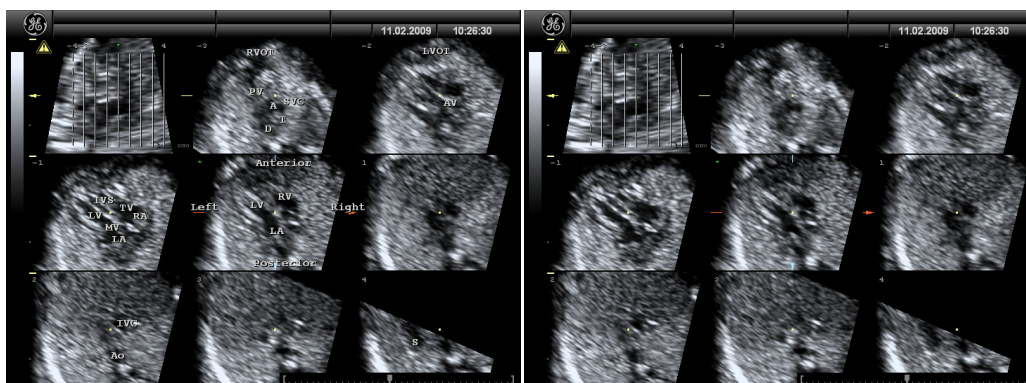


**Figure 4:** Tomographic ultrasound imaging (TUI) of 12w5d normal fetus. The original volume was acquired with STIC on axial plane. Figure A is labeled and figure b is the same but unlabeled. Parallel axial planes of the chest allows whole the axial 2D images that are needed for routine cardiac examination. A=aorta; PV=pulmonic valve; SVC=superior vena cava; D=ductus arteriosus; T=trachea; IVS=interventricular septum; TV=tricuspid valve; LV=left ventricle; MV=mitral valve; RA=right atrium; LA=left atrium; RV=right ventricle; IVC=inferior vena cava; Ao=descending aorta; S=stomach.

In multiplanar reconstruction the screen is divided into four frames, referred to as A (the plane seen at the 2D ultrasound), B (the coronal plane) and C (the sagittal plane); the fourth frame shows the rendered image (Fig. 5, 6,7 [video 4](#)).

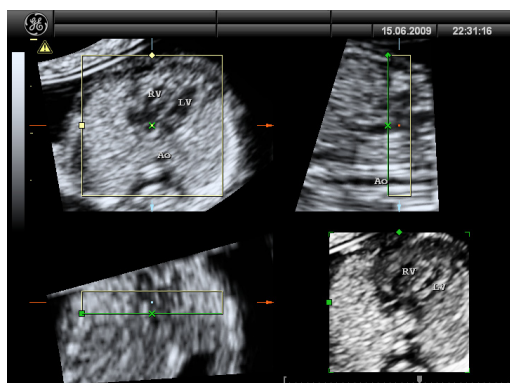


**Figure 5:** 12w3d Normal fetus. The volume was acquired at the level of 4CV in grey scale. Plane A is 2D image of the axial plane of the chest, demonstrate the right ventricle (RV), left ventricle (LV), descending aorta (Ao). Plane B is the calculating plane of the transverse chest view. The ROI (region of interest) dot is on the ascending aorta in all three planes. The descending aorta is clearly visualized in plane B. Plane C demonstrate the aortic, mitral and tricuspid valves. D is the render mode of Plane A.

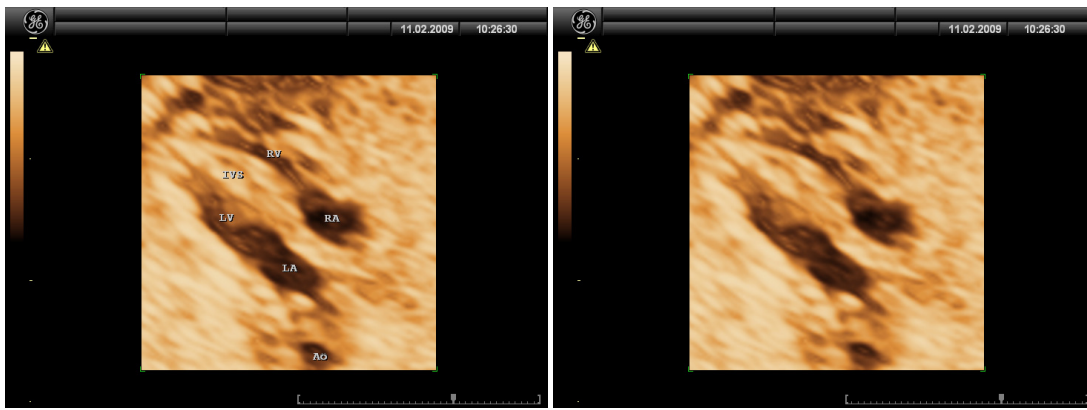


**Figure 6:** The same volume as in figure 5. Render mode with 30% surface and 70% gradient light mode demonstrating the 4CV. Figure 5a is labeled and 5b is not. IVS=interventricular septum; LV=left ventricle; RV=right ventricle; RA=right atrium; LA=left atrium;

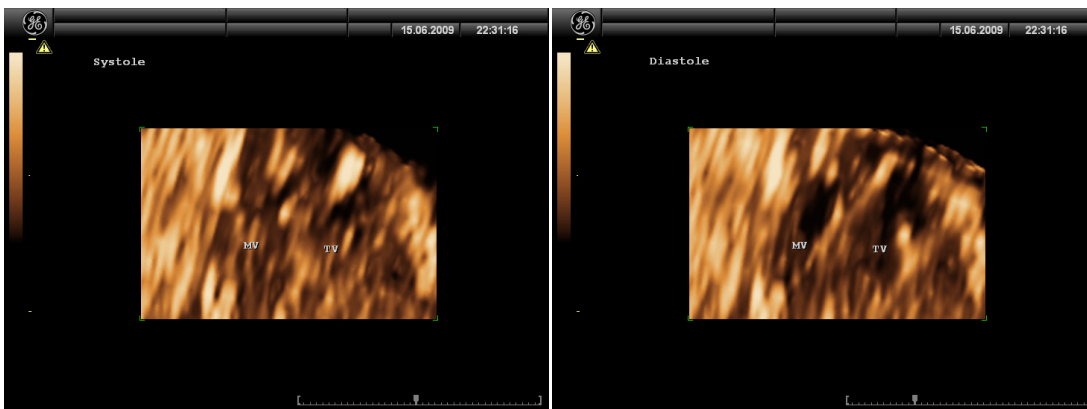


**Figure 7:** Same volume as figure 5. 3D Render of the atrioventricular valves. Figure a the valves are opened. In Figure b the valves are closed

From a good STIC acquisition the operator can scroll through the acquired volume to obtain sequentially each of the classic five axial planes of fetal echocardiography, and any plane may be viewed at any time-point throughout the reconstructed cardiac cycle loop. The cycle can be run or stopped frame-by-frame to allow examination of all phases of the cardiac cycle ([video 5](#)).

Visualization of the intraventricular septum, for example, is possible with the A-frame showing a good four-chamber view, and the bounding box tightly placed around the interventricular septum. The rendered image will show the view of the septum. The operator can determine whether the plane will be displayed from the left or right. Gindes et al demonstrated that the use of render mode with minimal transparency resulted in clearer demonstration of abnormal organs and vessels positions in *situs* abnormalities [21] (Fig. 8).

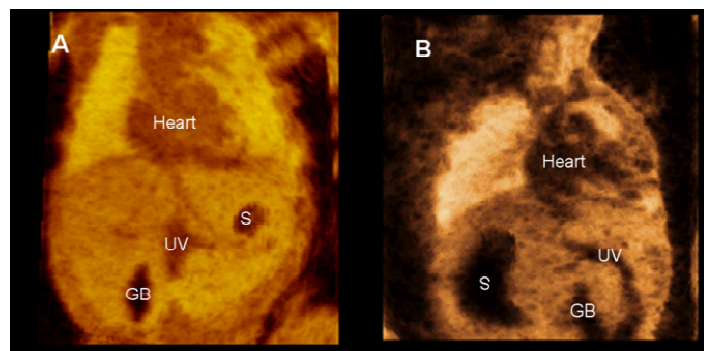


**Figure 8:** The minimal mode rendering allows imaging of hypoechoic structures. In figure a normal situs is demonstrated in fetus of 14 weeks gestation. In figure b another 14 weeks fetus with situs inversus is demonstrated. The heart is on the left side but the stomach is on the right. The gallbladder is on the left and there is persistent right umbilical vein. S=stomach; GB=gallbladder; UV=umbilical vein.



Multislice analysis (such as TUI) in which parallel slices are displayed simultaneously from the plane of interest (the ‘zero’ plane), giving sequential views. The number of slices and their thickness, i.e. the distance between one plane and the next, can be adjusted by the operator. The upper left frame of the display shows the position of each plane within the region of interest, relative to the reference plane. This application has the advantage of displaying sequential parallel planes simultaneously, giving a more complete picture of the fetal heart. The arches and outflow tract anomalies are best visualized with Render mode and TUI [21] (Figs. 3, 4).

Color Doppler may be added to detect the flow through the cardiac cycle ([video 6](#), [video 7](#), [video 8](#), [video 9](#), [video 10](#)).

Inversion mode analyzes the echogenicity of tissue (white) and fluid-filled areas (black) in a volume and inverts their presentation, i.e. fluid-filled spaces such as the cardiac chambers appear white, while the myocardium disappears. In fetal echocardiography it can be applied to create ‘digital casts’ of the cardiac chambers and vessels, and to reconstruct extracardiac vascular tree. Inversion mode shows the stomach and gall bladder as white structures, which can aid the operator in navigating within a complex anomaly scan.

B-flow modality is a direct volume non-gated scanning method able to show blood flow in the heart and great vessels in real-time, without color Doppler flow information [16] ([video 11](#)). The resulting image is a live gray-scale depiction of the blood flow and part of the surrounding lumen. The combination of B-flow with STIC along with the creation of a render image allows very sensitive demonstration of blood vessels and heart chambers (Figs. 9-12 [video 12](#)).

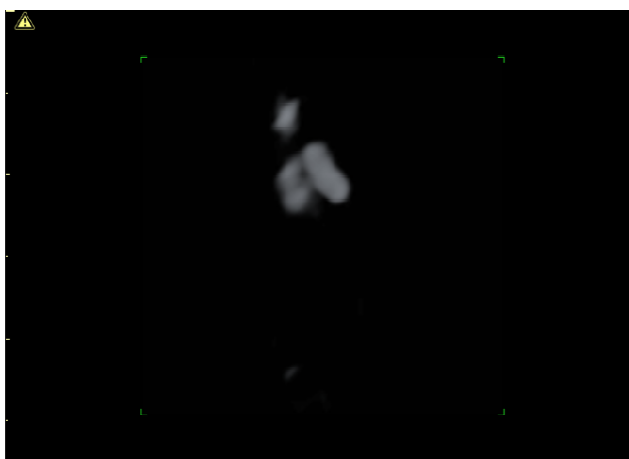


**Figure 9:** B-flow demonstration of the heart at 10.2 weeks.

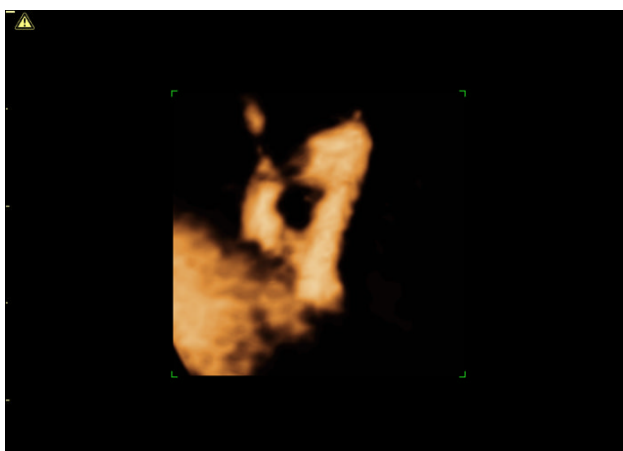


**Figure 10:** B-flow demonstration of the outflow tracts at 13 weeks.

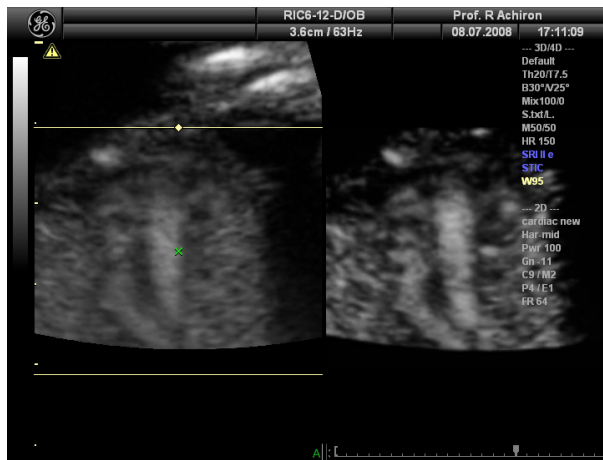


**Figure 11:** Demonstration of the outflow tract at 14 weeks. This volume was acquired with B-mode grey scale, but the transducer received the beam of the blood flow. A is the 2D image and B is the volume of the same image. The blood vessels are much more bolt in the volume. Ao=aorta; PA=pulmonary artery.

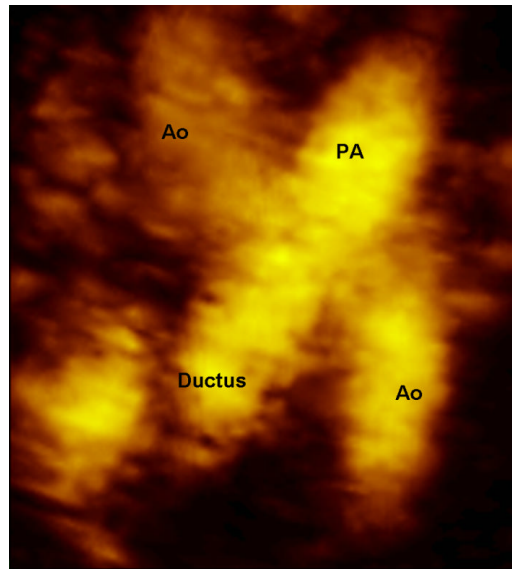


**Figure 12:** B-flow of the outflow tracts at 14 weeks. 23a presents the render mode. Ao=aorta, PA=pulmonary artery.

Gindes et al demonstrated that inversion mode and B-flow were most informative for detecting arches anomalies. Systemic veins were best shown with B-flow [21].

The 3D-4D ultrasound volume presentation tools and their contribution to the diagnosis of fetal cardiac anomalies are presented in Table 3.

**Table 3:** 3D-4D ultrasound volume presentation tools and their contribution to the diagnosis of fetal cardiac anomalies.

	Situs	4 C view	Outflow tract	Arches	Vein
multiplanar	+	+	+	+	+
render	+	++	++	++	+
TUI	+	++	++	++	+

The comparison of the different 3D-4D rendering modes in demonstration cardiac malformations is demonstrated in Table 4.

**Table 4:** Comparison of the different 3D-4D rendering modes in demonstration cardiac malformations.

	Situs	4 C view	Outflow tract	Arches	Vein
<b>Minimal mode</b>	++	-	+	+	+
<b>Surface mode and Gradient light</b>	-	+	+	+	+
<b>Inversion mode</b>	-	+	++	++	+
<b>Glass body</b>	-	++	++	+	+
<b>Color</b>	-	+	++	+	+
<b>B-Flow</b>	-	+	++	++	++

#### **APPROACH TO EARLY 3D/4D FETAL ECHOCARDIOGRAPHY [12-14, 19, 22]:**

The most basic approach for the examination of a volume dataset of the fetal heart acquired with STIC is to scroll through the volume from top to bottom along the original plane of acquisition. This approach allows the examiner to determine quickly the relationship between the apex of the heart and stomach, and to evaluate the four-chamber view, and, in most cases, the five-chamber and three-vessel views [23, 24].

If the examiner wants to review the aortic and ductal arches, or the venous return to the heart, datasets are best acquired using sagittal sweeps through the fetal thorax. These images can be generated by acquiring volume datasets with color Doppler, power Doppler or B-flow imaging, as well as by rendering gray-scale volume datasets with inversion mode.

One of the advantages of the STIC acquisition in the first trimester is the possibility to gain the volume of the entire fetus, resulting in better tracing of the blood vessels. Performed properly, this methodology will provide the examiner with all the necessary planes to conform to the guidelines [7]. A pitfall of this technique is that the heart is small (about 3mm at 12 weeks' gestation), making the observation of small details meticulous.

#### **TIPS FOR BETTER VOLUME ACQUISITION [22, 25]:**

- The ideal fetal position is one in which the fetus is lying on its back.
- Selection of a region of interest (ROI) as narrow as possible maximizes the frame rate during acquisition and improves the temporal resolution of the volume dataset.
- Because of the small size of the fetal heart at the first trimester a relatively narrow acquisition angle can be used. For first and second-trimester fetuses, acquisition angles of between 20° and 25° are usually sufficient to include the stomach, the heart, and the great vessels in the volume dataset.
- The longer the acquisition time, the higher the spatial resolution of the volume dataset. However, for highly active fetuses, faster acquisition time is needed, at the expense of optimal spatial resolution.
- 3D acquisition is preferred in order to obtain higher resolution of the blood vessels.

#### **CARDIAC ANOMALIES THAT CAN BE DETECTED AT THE FIRST TRIMESTER OF PREGNANCY [5, 13, 24, 26-28].**

The cardiovascular system begins to mature in the 3<sup>rd</sup> embryonic week, as the heart is a tubular structure. Formation of the septae, and arterial and venous connections are completed only after 8 weeks gestation. A complete four chambers view may be seen at 10 weeks' gestation [29]. The literature demonstrates that it is possible to perform first trimester echocardiography in both low and high risk population and detect many cardiac anomalies, with higher detection rate from 12 weeks' gestation [4, 5,30, 31].

At the level of 4CV (four chamber view) early detection of ventricular septal defects (VSD), atrial septal defects (ASD), atrioventricular septal defects (AVSD) and tricuspid regurgitation, hypoplastic left heart and truncus arteriosus is possible [5, 13]. At the level of the outflow tract detection of transposition of the great arteries, right and double aortic arch is feasible [5, 26]. Achiron et al also demonstrated anomalies in the fetal central veins and

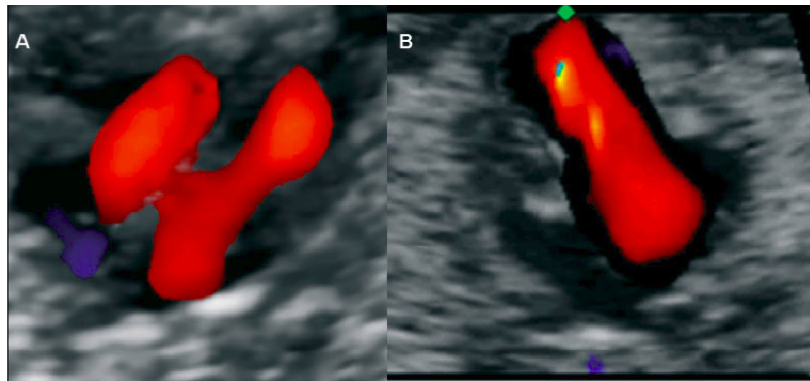
umbilico-portal system including absence of ductus venosus and total anomalous pulmonary venous connection and interrupted inferior vena cava with azygus continuation [27]. In a recent study this group reported on evaluation of thoracic anomalies with 3D and 4D ultrasound, including abnormal situs, diaphragmatic hernia, and lung dysplasia as early as 14 weeks [28].

Table 2 summarizes the cardiac anomalies that can be diagnosed on early echocardiography. According to the literature and in our experience we recommend that full examination of the fetal heart starts at 14 weeks' gestation as a routine. In some cases echocardiography may begin as early as 12 gestational weeks.

#### EXAMPLES:

STIC acquisition with color Doppler demonstrates AVSD. Partial defects may be difficult to diagnose ([video 13](#)).

Color Doppler used in the four-chamber view demonstrates blood flow through the right side of the heart in comparison to the hypoplastic left heart (Fig. 13).



**Figure 13:** Render mode with Color Doppler demonstration of normal four chamber view (A) and hypoplastic left heart at 14 weeks (B).

3D color Doppler reconstruction may demonstrate anomalies of the venous system such as absence of the ductus venosus (Figs. 14-15).

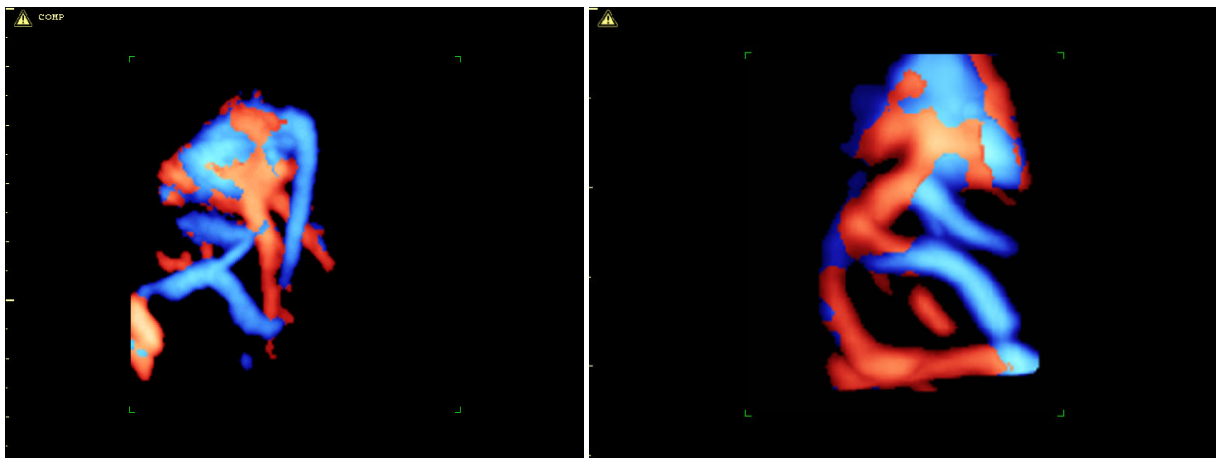


**Figure 14:** Render mode with Color Doppler demonstration of normal blood vessels (A) and absence of ductus venosus at 11+6 weeks (B).

The 3D reconstruction of the fetal venous system was described in detailed by Gindes et al [44].

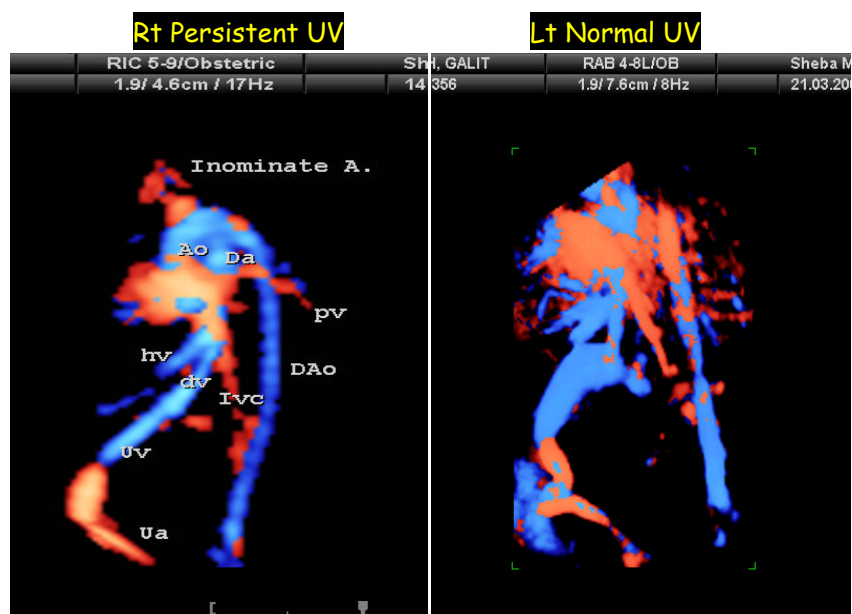


**Figure 15:** Render mode with Color Doppler demonstration of normal blood vessels (A) and right persistent umbilical vein (B). Ao=aorta, Da=ductus arteriosus, hv=hepatic veins, IVC=inferior vena cava, Uv=umbilical vein, Ua=umbilical artery, Pv=pulmonary vein, Dao=descending aorta, Dv=ductus venosum.

#### LIMITATIONS OF EARLY FIRST TRIMESTER 3D/4D ECHOCARDIOGRAPHY [26,27]:

Imaging of the fetal heart in the first trimester of pregnancy is technically more demanding than in mid-gestation because of the relatively smaller size of the fetus and cardiac structures (the semilunar valves are about 1.2mm at 13 weeks).

Advances in ultrasound technology have led to improved visualization of the fetus in the first trimester (high frequency transducers 6-12 MHz, better resolution), yet, special orientation compared with transabdominal sonography is more limited. The exploration is more time-consuming and requires a high level of training of the examiner. Furthermore, in some CHD there are later manifestations of structural and functional changes.

3D/4D fetal echocardiography scanning is prone to artifacts similar to those encountered in 2D ultrasonography (resolution, propagation and attenuation artifacts), and some that are specific to 3D/4D acquisition and post-processing [16, 25]:

1. Movement artifacts: The quality of a STIC acquisition may be adversely affected by fetal body or breathing movements as well as by maternal movements. Quality is improved by scanning with the fetus in a quiet state, and using the shortest scan time possible. When reviewing a STIC acquisition, the B-frame will reveal artifacts introduced by fetal breathing movements.
2. Acoustic shadows: Adjacent structures can produce shadows, but since the orientation has changed it may not be immediately obvious. The consequences for the rendered image may include producing defects in surfaces in which there are no defects. It is essential to review suspected defects with repeated 2D and 3D scanning to confirm their presence in additional scanning planes. One may think that at the first trimester the fetal bones are less calcified and thus allow demonstration of the heart from the back of the fetus, but this is not the case. Bones of young fetuses do create acoustic shadows making the optimal position to view the heart with fetus lying with the back down.
3. Small render box artifacts: Limiting the region-of-interest may result in missing important structures from the rendered image. The render box should include some of the chest structures for orientation.
4. Flow direction interpretation: Rotation of the volume with Doppler directional flow information can be misleading: if the directions are reversed, flow data can be misinterpreted. The operator must confirm any suspected pathological flow patterns by confirming the original direction of scanning, whether flow was toward or away from the transducer during the acquisition scan.

## SAFETY OF FIRST TRIMESTER 3D/4D ECHOCARDIOGRAPHY (6,7,32)?

The use of ultrasound as a diagnostic tool in obstetrics may have biological effects on living tissues. Therefore, safety considerations should be taken into account in order to ensure that first trimester 3D/4D echocardiography remains harmless. Grayscale ultrasound is unlikely hazardous to the fetus because of low thermal index. However, the use of Doppler ultrasound may increase that temperature above 1.5°C. The European Federation for Societies in Medicine and Biology in 1998 concluded that Doppler should be carried out with careful control.

The mechanical index is probably nonexistent because it indicates the potential of the ultrasound to induce tissue cavitation, which involves the occurrence of gaseous bubble formation in an air-water interface (such as lungs and bowel). Fetal lungs and bowel do not contain gas, making the mechanical risk absent [6, 7, 32].

Sheiner *et al* performed 40 examinations consisting of 2D, 3D and 4D ultrasounds. They found that the mean thermal index during the 3D and 4D examinations were comparable with the thermal index during B-mode scanning. The mean mechanical index during the 3D volume acquisition was significantly lower than that in the B-mode [33].

The American Institute of Ultrasound in Medicine, the International Society for Ultrasound in Obstetrics and Gynecology and the World Federation for Ultrasound in Medicine and Biology summarized that 3D sonography did not present more risk than native B-mode imaging [34-36]. Since 3D/4D echocardiography has the ability to shorten the total time of echocardiography in high-risk patients, the ALARA principle is kept: as low as reasonably achievable, i.e. perform the scan for the shortest time possible and with the lowest output possible to permit adequate diagnostic acuity [37]. For flow investigation it is possible to combine the B-flow technique with the STIC. The B-flow has the same TI and MI as the B-mode and it is a non Doppler technique.

In summary, the prenatal detection of fetal heart defects remains challenging. The goal of prenatal echocardiography is to visualize structural and functional anomalies of the fetal heart and great vessels, to optimize diagnostic accuracy and to provide images that will aid both management teams and parents in the understanding of the nature of anomalies. With the technological improvement we can detect part of the cardiac anomalies as early as the first trimester. The application of first trimester 3D/4D ultrasound improves the visualization of both normal and anomalous anatomy and function and offers clearer and better images. Early 3D/4D echocardiography is possible, and should be recommended to high-risk patients as part of the routine sonographic follow-up of their pregnancies.

## REFERENCES

- [1] Hoffman JI, Kaplan S. The incidence of congenital heart disease. *J Am Coll Cardiol* 2002;39:1890-900.
- [2] Hoffman JI. Incidence of congenital heart disease:I. Postnatal incidence. *Pediatr Cardiol* 1995;16:103-113.
- [3] Mc Auliffe FM, Trines J, Nield LE, Chitayat D, Jaeggi E, Hornberger LK. Early fetal echocardiography--a reliable prenatal diagnosis tool. *Am J Obstet Gynecol* 2005;193:1253-9.
- [4] Weiner Z, Lorber A, Shalev E. Diagnosis of congenital cardiac defects between 11 and 14 weeks' gestation in high-risk population. *J Ultrasound med* 2002;21:23-9.
- [5] Weiner Z, Weizman B, Beloosesky R, Goldstein I, Bombard A. Fetal cardiac scanning performed immediately following an abnormal nuchal translucency examination. *Prenat Diagn* 2008;28:934-8.
- [6] DeVore GR, Falkensammer P, Sklansky MS, Platt LD. Spatiotemporal image correlation (STIC): new technology for evaluation of the fetal heart. *Ultrasound Obstet Gynecol* 2003; 22:380-7.
- [7] Garne E, Stoll C, Clementi M. Evaluation of prenatal diagnosis of congenital heart diseases by ultrasound: experience from 20 European registries. *Ultrasound Obstet Gynecol* 2001;17:386-91.
- [8] Tegnander E, Williams W, Johansen OJ, Blaas HG, Eik-Nes SH. Prenatal detection of heart defects in a non-selected population of 30149 fetuses - detection rates and outcome. *Ultrasound Obstet Gynecol* 2006;27:252-65.
- [9] DeVore GR, Polanko B, Sklansky MS, Platt LD. The „spin technique“: a new method for examination of the fetal outflow tracts using three-dimensional ultrasound. *Ultrasound Obstet Gynecol* 2004;24:72-82.
- [10] Sklansky M, Miller D, Devore G, Kung G, Pretorius D, Wong P, Chang RK. Prenatal screening for congenital heart disease using real-time three-dimensional echocardiography and a novel „sweep volume“ acquisition technique. *Ultrasound Obstet Gynecol* 2005;25:435-43.
- [11] Tegnander E, Eik-Nes SH. The examiner's ultrasound experience has a significant impact on the detection rate of congenital heart defects at the second trimester fetal examination. *Ultrasound Obstet Gynecol* 2006;28:8-14.

- [12] Yagel S, Benachi A, Bonnet D, Dumez Y, Hochner-Celnikier D, Cohen SM, Valsky DV, Fermont L. Rendering in fetal cardiac scanning: the intracardiac septa and the coronal atrioventricular valve planes. *Ultrasound Obstet Gynecol* 2006;28:266-74.
- [13] Vinals F, Ascenzo R, Naveas R, Huggons I, Giulliano A. Fetal echocardiography at 11+0 to 13+6 weeks using four-dimensional spatiotemporal image correlation telemedicine via an Internet link: a pilot study. *Ultrasound Obstet Gynecol* 2008;31:633-8.
- [14] Uittenbogaard LB, Haak MC, Spreuwenberg MD, Van Vugt JMG. A systematic analysis of the feasibility of four-dimensional ultrasound imaging using spatiotemporal image correlation in routine fetal echocardiography. *Ultrasound Obstet Gynecol* 2008;31:625-32.
- [15] Hergerg U, Goldberg H, Breuer J. Three- and four-dimensional freehand fetal echocardiography: a feasibility study using a hand-held Doppler probe for cardiac gating. *Ultrasound Obstet Gynecol* 2005;25:362-71.
- [16] Yagel S, Cohen SM, Shapiro I, Valsky DV. 3D and 4D ultrasound in fetal cardiac scanning: a new look at the fetal heart. *Ultrasound Obstet Gynecol* 2007;29:81-95.
- [17] Sklansky MS, Nelson T, Strachan M, Pretorius D. Real-time three-dimensional fetal echocardiography: initial feasibility study. *J Ultrasound Med*. 1999;18:745-52.
- [18] Sklansky MS, Nelson TR, Pretorius DH. Three-dimensional fetal echocardiography: gated versus nongated techniques. *J Ultrasound Med*. 1998;17:451-7.
- [19] Carvalho JS. Fetal heart scanning in the first trimester. *Prenat Diagn* 2004;24:1060-7.
- [20] Vinals F, Poblete P, Giuliano A. Spatio-temporal image correlation (STIC): a new tool for the prenatal screening of congenital heart defects. *Ultrasound Obstet Gynecol* 2003;22:388-94.
- [21] Gindes L, Hegesh J, Weisz B, Gilboa Y, Achiron R. Three and four dimensional ultrasound: a novel method for evaluating fetal cardiac anomalies. *Prenat Diagn* 2009.
- [22] Goncalves LF, Lee W, Espinoza J, Romero R. Examination of the fetal heart by four-dimensional (4D) ultrasound with spatio-temporal image correlation (STIC). *Ultrasound Obstet Gynecol* 2006;27:336-48.
- [23] Yoo SJ, Lee YH, Kim SH. Three vessel view of the fetal upper mediastinum: an easy means of detecting abnormalities of the ventricular outflow tracts and great arteries during obstetric screening. *Ultrasound Obstet Gynecol* 1997;9:173-82.
- [24] Yagel S, Cohen SM, Achiron R. Examination of the fetal heart by five short-axis views: a proposed screening method for comprehensive cardiac evaluation. *Ultrasound Obstet Gynecol* 2001;17:367-9.
- [25] Nelson TR, Pretorius DH, Hull A, Sklansky MS, James G. Sources and impacts of artifacts on clinical three-dimensional ultrasound imaging. *Ultrasound Obstet Gynecol* 2000;16:374-83.
- [26] Achiron R, Rotstein Z, Hegesh J, Bronshtein M, Zimand S, Lipitz S, Yagel S. Anomalies of the fetal aortic arch: a novel sonographic approach to in-utero diagnosis. *Ultrasound Obstet Gynecol*. 2002;20:553-7.
- [27] Achiron R, Hegesh J, Yagel S, Lipitz S, Cohen SB, Rotstein Z. Abnormalities of the fetal central veins and umbilico-portal system: prenatal ultrasonographic diagnosis and proposed classification. *Ultrasound Obstet Gynecol* .2000;16:539-48.
- [28] Achiron R, Gindes L, Zalel Y, Lipitz S, Weisz B. Three- and four-dimensional ultrasound: new methods for evaluating fetal thoracic anomalies. *Ultrasound Obstet Gynecol* 2008;32:36-43.
- [29] Dolkart LA, Reimers FT. Transvaginal fetal echocardiography in early pregnancy: normative data. *Am J Obstet Gynecol* 1991;165(3):688-91.
- [30] Haak MC, Twisk JW, Van Vugt JM. How successful is fetal echocardiographic examination in the first trimester of pregnancy? *Ultrasound Obstet Gynecol* 2002;20:9-13.
- [31] Carvalho SRM, Mendes MC, Neto OBP, Berezowski AT. First trimester fetal echocardiography. *Gynecol Obstet Invest* 2008;65:162-8.
- [32] Abramowicz JS. Prenatal exposure to ultrasound waves: is there a risk? *Ultrasound Obstet Gynecol* 2007;29:363-7.
- [33] Sheiner E, Hackmon R, Shoham-Vardi I, Pombar X, Hussey MJ, Strasser HT, Abramowicz JS. A comparison between acoustic output indices in 2D and 3D/4D ultrasound in obstetrics. *Ultrasound Obstet Gynecol* 2007;29:326-8.
- [34] Abramowicz JS, Kossof G, Marsal K, ter Haar G. International Society of Ultrasound in Obstetrics and Gynecology (ISUOG) Safety and Bioeffects Committee: safety statement. *Ultrasound Obstet Gynecol* 2000;16:594-6.
- [35] Barnett SB. WFUMB Symposium on Safety of Ultrasound in Medicine: conclusions and recommendations on thermal and mechanical mechanisms for biological effects of ultrasound. *Ultrasound Med Biol* 1998;24:S1-58.
- [36] American Institute of Ultrasound in Medicine. Mechanical bioeffects from diagnostic ultrasound: AIUM consensus statements. *J Ultrasound Med* 2000;19:69-168.
- [37] Abramowicz JS. Ultrasound in obstetrics and gynecology: Is this hot technology too hot? *J Ultrasound Med* 2002;21:1327-33.
- [38] The international society of ultrasound in obstetrics and gynecology. Cardiac screening examination of the fetus: guidelines for performing the basic and extended cardiac scan. *Ultrasound Obstet Gynecol* 2006;27:107-13.
- [39] Berg C, Thomsen Y, Geipel A, Gembruch U. Reversed end-diastolic flow in the umbilical artery at 10-14 weeks of gestation is associated with absent pulmonary valve syndrome. *Ultrasound Obstet Gynecol* 2007;30:254-8.



- [40] Achiron R, Weissman A, Rotstein Z, Lipitz S, Mashiach S, Hegesh J. Transvaginal echocardiographic examination of the fetal heart between 13 and 15 weeks' gestation in a low-risk population. *J Ultrasound Med* 1994;13:783-9.
- [41] Russell NE, McAuliffe FM. First-trimester fetal cardiac function. *J Ultrasound Med*. 2008;27:379-83.
- [42] Gabriel CC, Galindo A, Martinez JM, Carrera JM, Gutierrez-Larraya F, de la Fuente P, Puerto B, Borrell A. Early prenatal diagnosis of major cardiac anomalies in a high-risk population. *Prenat Diag* 2002;22:586-93.
- [43] Carvalho JS, Moscoso G, Tekay A, Campbell S, Thilaganathan B, Shinebourne EA. Clinical impact of first and early second trimester fetal echocardiography on high risk pregnancies. *Heart* 2004;90:921-6.
- [44] Gindes L, Pretorius DH, Romine LE, Kfir M, D'Agostini D, Hull A, Achiron R. 3-Dimensional Ultrasound Demonstration of Fetal Abdominal Blood Vessels. *JUM* 2009; 977-88.

## Assessment of Cardiac Geometry and Stroke Volumes by 4D Fetal Echocardiography

Lami Yeo\*, Roberto Romero and Wesley Lee

*Department of Obstetrics and Gynecology, Wayne State University School of Medicine, Perinatology Research Branch, Intramural Division, NICHD, NIH, DHHS, Hutzel Women's Hospital Detroit, Michigan, USA, \* Division of Fetal Imaging, William Beaumont Hospital, Royal Oak, Michigan, USA*

**Abstract:** Accurate and reliable methods to assess fetal cardiac function would be useful in evaluating fetuses with cardiac disease (structural or otherwise). Traditionally, two-dimensional echocardiography has been used to estimate fetal ventricular volume, and assess cardiac function. However, the unique and complex geometry of the fetal ventricles makes analysis of cardiac function using this modality a challenge, and hence, the interest in using three- and four-dimensional ultrasound. Although theoretically appealing, three-dimensional echocardiography had to overcome several difficulties, including: gating, suboptimal image quality, and lack of real-time observation. Four-dimensional fetal echocardiography is a method to assess ventricular volume and cardiac function, and can overcome many of the pitfalls of conventional methods. Thus, this modality offers an important method for the assessment of fetal cardiac function.

**Key Words:** 4D Ultrasound, Fetal Echocardiography, Cardiac Volumes, Stroke Volume.

### INTRODUCTION

The cardiovascular system is the first to functionally develop in the human embryo (Esh-Broder UOG 2004) [1]. Fetal disease (structural congenital heart disease, or systemic disorders affecting the heart) may change the anatomy and physiology of the cardiac chambers. Examples include hydrops, diabetic cardiomyopathy, intrauterine growth restriction, and twin to twin transfusion syndrome. Therefore, quantifying ventricular volume and calculating cardiac function parameters (e.g. stroke volume, cardiac output, ejection fraction, etc.) contributes to the evaluation of congenital heart disease (Figs. 1 and 2).

Several methods to obtain ventricular volume measurements through four-dimensional (4D) echocardiography and STIC (Spatio-Temporal Image Correlation) are available. These methods allow calculation of stroke volume, cardiac output, and ejection fraction. We will review the methodology and normal values to assess cardiac function in this chapter. Additionally, we will briefly discuss the roles and limitations of two- and three-dimensional fetal echocardiography in estimating ventricular volumes.

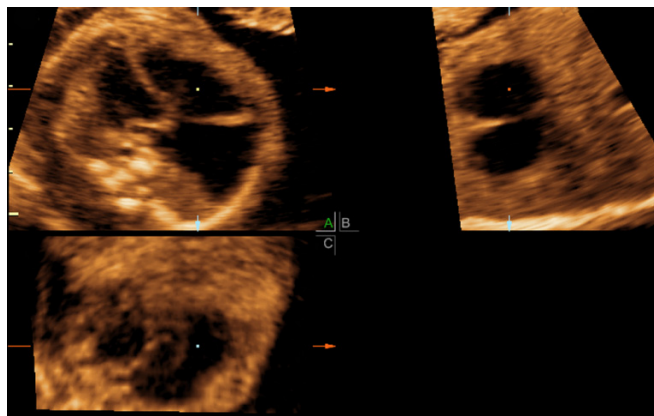


**Figure 1:** Multiplanar examination of a fetal heart showing the four-chamber view (A-plane) from a spatio-temporal image correlation (STIC) acquisition in a 24-week fetus at end-diastole. In this multiplanar reconstruction, the navigation point is placed in the right ventricle in the A-plane. The fetus has pulmonary atresia and a dysplastic tricuspid valve with severe regurgitation. The right atrium is severely enlarged, and the right ventricle is moderately/severely dilated.

\*Address correspondence to Lami Yeo: Hutzel Women's Hospital 3990 John R. 4 Brush North, Detroit, Michigan, 48201 USA E-mail: lyeo@med.wayne.edu

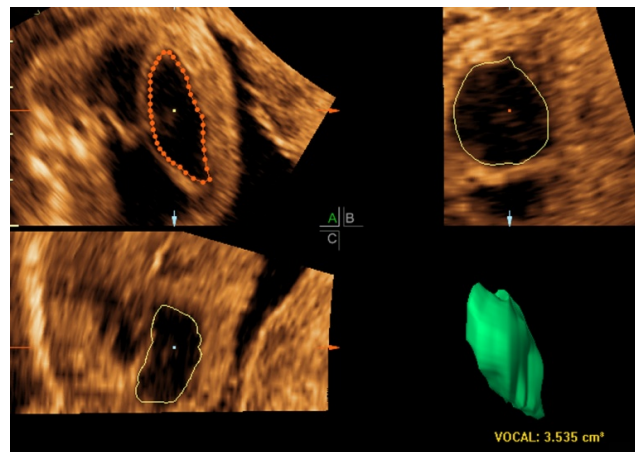


**Figure 2:** Same fetus as Figure 1. Quantification of fetal right ventricular volume during end-diastole, using the VOCAL™ (Virtual Organ Computer-aided AnaLysis) tool and manual trace. The right ventricular end-diastolic volume (3.5 mL) is above the 95<sup>th</sup> centile for gestational age.

### FETAL VENTRICULAR VOLUME (TWO-DIMENSIONAL AND THREE-DIMENSIONAL ECHOCARDIOGRAPHY)

Traditionally, two-dimensional (2D) echocardiography has been used to estimate fetal ventricular volume; however, this technology has limitations. Simpson and Cook reported a prospective study of normal human fetuses (measurement of 32 different variables) to determine the repeatability of: 1) 2D ultrasound measurements in real-time B-mode; 2) M-mode; and 3) Doppler measurements (Simpson UOG 2002) [2]. The formula employed to estimate the left ventricular (LV) volume was the method of discs (Simpson's rule), which divides this ventricle into 20 equal thickness discs, where each disc is assumed to be circular. The technique involves tracing the LV endocardial border at end-diastole and at end-systole. However, this formula can not be applied to the right ventricle (RV) due to its complex geometric shape. For M-mode measurements, all volumetric data were computed using the Teichholz formula (Teichholz AJC 1976) [3]. Simpson and Cook found that the repeatability of most echocardiographic measurements was poor, and this applied particularly to ventricular volumes and volume flow estimations (Simpson UOG 2002) [2]. Using Simpson's rule, the coefficient of variation exceeded 10% in the estimation of both LV end-diastolic volume (13%) and stroke volume (14%). Moreover, inter-observer errors were consistently higher than intra-observer errors, suggesting that for sequential measurements, the same observer should conduct the assessment. Computing ventricular volumes using the Teichholz formula also did not appear to be very repeatable; the coefficient of variation was over 30% for both the estimation of LV end-diastolic volume (32%) and stroke volume (36%). Observer errors reported in estimation of LV end-diastolic volume, stroke volume, and ejection fraction were lower for 2D techniques than for equivalent measurements made by M-mode echocardiography.

The reasons for these limitations are several. First, Simpson's rule is restricted to monoplanes and assumes a prolate (elongated) ellipsoid shape of the LV, with a ratio of long axis to short axis of 2:1 (Bhat Circulation 2004) [4]. However, this assumption may not apply to the developing fetal heart. Second, when using Simpson's rule, it may be impossible to achieve two orthogonal planes of the ventricle, in the absence of reliable scanning plane landmarks (Esh-Broder UOG 2004) [1]. Third, quantitative echocardiographic methods perform poorly in distorted ventricles, in which standard geometric assumptions become tenuous (Wyatt AHJ 1980) [5]. Fourth, performing cross-sectional measurements of the ventricles assumes that the endocardium is smooth, which is not accurate (Sedmera Anat Rec 2000) [6]. Finally, in the rapidly contracting fetal heart, it may be difficult to identify the precise points of end-diastolic and end-systolic frames. For these reasons, it is generally accepted that 2D echocardiography has some limitations in assessing fetal cardiac function (Simpson UOG 2002) [2] (Simpson Prenat Diagn 2004) [7].

It is generally agreed upon that three-dimensional (3D) volume quantitation is more accurate than 2D-derived methods, because it avoids geometric assumptions and magnification of small errors (inherent in the latter modality) (Bhat JUM 2004) [8]. We have shown that there are changes in cardiac geometry with advancing gestational age (Espinoza JUM 2007) [9]. Therefore, three-dimensional (3D) echocardiography has been utilized to evaluate cardiac

volume and function. However, some investigators have noted the assessment of ventricular volume and ejection fraction to be arduous, with processing of acquired data to be time-consuming (Esh-Broder UOG 2004) [1]. Levental *et al.* found that non-gated 3D volume acquisition of the fetal heart and the subsequent planar reformatting generated suboptimal image quality (Levental 1998 JUM) [10]. Moreover, the inability to observe the heart in real-time was a limitation. Other investigators have noted gating difficulties in using 3D echocardiography (Meyer-Wittkopf JUM 2001) [11]. Meyer-Wittkopf *et al.* found that both the quantitative 3D analysis and endocardial tracing were time-consuming and required considerable expertise (Meyer-Wittkopf JUM 2001) [11]. Therefore, the applicability and reproducibility of this technique might be limited in a clinical setting. Meyer-Wittkopf *et al.* also noted problems with the anatomic accuracy of tracing the endocardium, which can influence the accuracy of quantitative 3D echocardiography. Therefore, while 3D echocardiography can overcome some of the limitations of 2D echocardiography, there are still challenges in utilizing this modality to evaluate fetal ventricular volume and cardiac function.

Recently, a novel approach involving semi-automatic segmentation of fetal cardiac cavities to assess ventricular volume was presented (Tutschek and Sahn UOG 2008) [12]. Tutschek and Sahn retrospectively analyzed STIC cardiac volumes off-line using a commercially available segmentation algorithm designed for ovarian folliculometry (SonoAVC, or Sonography-based Automatic Volume Count). Individual “cavities” in a static volume were selected and assigned individual colors, and diameters and volumes were calculated. For two normal fetuses (21 and 29 weeks of gestation), end-diastolic (0.45-1.35 mL) and end-systolic (0.20-0.57 mL) ventricular volumes were determined, and ejection fraction was calculated (49% and 58%). Tutschek and Sahn proposed that their technique was an important step towards an automated fetal volume echocardiogram. However, the authors acknowledged that because this technique required manual editing (introducing operator-dependency), it was not yet suited for routine fetal echocardiography, and its quantitative aspects still needed to be validated (Tutschek and Sahn UOG 2008) [12].

#### **FETAL VENTRICULAR VOLUME (FOUR-DIMENSIONAL ECHOCARDIOGRAPHY)**

Four-dimensional (4D) fetal echocardiography minimizes the effect of several technical factors. When STIC datasets are acquired, examination times are dramatically reduced since acquisitions generally take no more than 12.5 seconds to complete (Uittenbogaard UOG 2008) [13]. Moreover, when computing ventricular volumes, no geometric assumptions are made and measurements are not angle-dependent. This is important, because RV geometry *in-utero* differs from that of the LV. The RV is tripartite, and has inflow, apical, and outflow portions. Because of its complex shape, calculating RV volume is difficult and must be measured using non-geometric techniques (Huhta 2009) [14]. Several investigators have evaluated the utility of fetal cardiac datasets obtained with 4D echocardiography in calculating cardiovascular parameters (Messing UOG 2007) [15] (Molina UOG 2008) [16] (Rizzo Prenat Diagn 2007) [17] (Uittenbogaard UOG 2009) [18].

Four-dimensional STIC is a novel approach to clinically assess the fetal heart (DeVore 2003 UOG) [19] (Gonçalves 2006 UOG) [20]. The technology uses a slow regular sweep of high line density 3D data, with the data realigned into its correct temporal domain in 3D space, to yield a 4D cine sequence (Bhat 2004 JUM) [8]. Therefore, it acquires a cardiac volume dataset and displays a cine loop of a complete single cardiac cycle in motion. The volume set can be manipulated both spatially and temporally. The principles used by the STIC algorithm to synchronize spatial and temporal information (3D images plus motion) in cardiac volume datasets are similar to the non-ECG motion Fourier analysis gating method proposed by Nelson *et al.* in 1996 (Nelson JUM 1996) [21]. STIC avoids the need for gated acquisition, making it ideal for fetal echocardiography. From the cine loop, a specific cardiac phase can be identified and analyzed by observing the opening and closing of the atrioventricular and semilunar valves. Because STIC captures end-diastolic and end-systolic time points in the cardiac cycle, it allows volume measurements at these specific points. From this, fetal cardiac parameters such as stroke volume and ejection fraction can be calculated.

In 2004, Bhat *et al.* investigated the ability of 4D STIC to produce quantitatively accurate dynamic fetal heart images using an *in vitro* pulsatile balloon model and apparatus (Bhat 2004 JUM) [8]. Volume determination was undertaken to correspond to systolic and end-diastolic volumes within the inner balloon, as well as stroke volume.

Volume data was analyzed by customized radial summation techniques using 4D data analysis software, and was compared with known volumes (2.5 to 10 mL) and masses. 4D STIC was found to be feasible, practical, and an acceptably accurate method for volume and mass estimations in the ranges comparable with the mid- and late-gestation fetal heart. Good correlation was found between observed and actual systolic volumes ( $R^2 = 0.92$ ), diastolic volumes ( $R^2 = 0.90$ ), and stroke volumes ( $R^2 = 0.92$ ), and there was good overall correlation across all volumes ( $R^2 = 0.91$ ). However, there was a wider range of percentage error in the lowest volumes tested (2.5 mL), attributed to difficulties in spatial resolution or from distortions within the model apparatus itself. 4D STIC was found to be particularly accurate for diastolic estimations, and at volumes of greater than 2.5 mL.

Using 4D fetal echocardiography and STIC, different methods have been used to obtain ventricular volume measurements (Messing UOG 2007) [15] (Molina UOG 2008) [16] (Rizzo Prenat Diagn 2007) [17] (Uittenbogaard UOG 2009) [18]. Messing et al. used inversion mode (Messing UOG 2007) [15], Rizzo et al. and Molina et al. used VOCAL™ (Virtual Organ Computer-aided ANALysis) (Rizzo Prenat Diagn 2007) [17] (Molina UOG 2008) [16], and Uittenbogaard et al. used the 3D Slice method (Uittenbogaard UOG 2009) [18]. VOCAL™ is the most frequently used method to obtain volume measurements from 3D datasets. Inversion mode is a rendering algorithm which transforms echolucent structures into solid voxels, thus “inverting” their presentation. Thus, anechoic structures such as cardiac chambers, lumen of the great vessels, stomach, and bladder appear echogenic on the rendered image, while structures that are normally echogenic prior to gray-scale inversion (e.g. bones) become anechoic (Gonçalves UOG 2004) [22]. By adjusting the thresholding level within the inversion mode, this allows fine-tuning to eliminate speckle within the volume. Messing et al. reported nomograms for fetal ventricular volume by using inversion mode and STIC (Messing UOG 2007) [15]. Inversion mode was used because it allowed superior demonstration of fluid-filled fetal anatomical structures and much better segmentation based on thresholding within the region of interest. VOCAL™ was then used to perform rotational measurements of the volume. By combining the VOCAL™ volume with inversion mode thresholding, only the fluid-filled portion of the ventricle was ultimately measured, and a new intraventricular model created (Fig. 3).

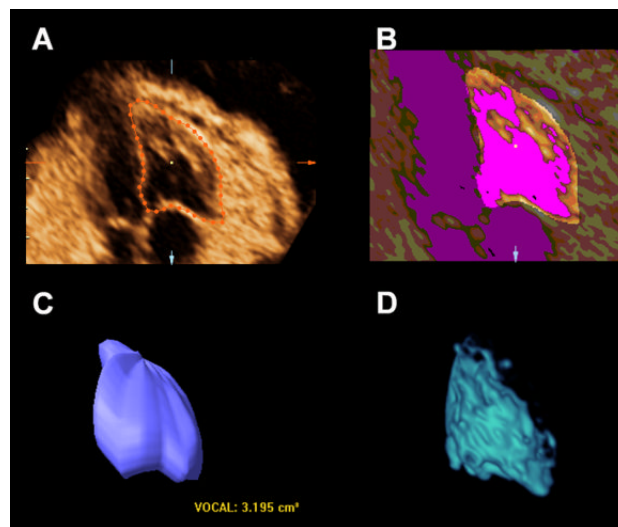


**Figure 3:** Post-processing quantification of right ventricular volume in end-diastole. (A) The VOCAL™ trace (drawn including the myocardium) in the A frame at the level of the four-chamber view; (B) the same frame with the inversion mode activated; (C) the three-dimensional model created by the VOCAL™ tool, which includes the entire traced volume; and (D) the final intraventricular volume model based only on the fluid-filled portion of the ventricle.

In this cross-sectional study of 100 normal fetuses (20.5-40 weeks of gestation), nomograms were created for right end diastolic volume (EDV), right end systolic volume (ESV), left EDV, left ESV, and total stroke volume vs. gestational age and estimated fetal weight. Table 1 shows various fetal cardiac parameters and their mean volumes (95% CI) (cm<sup>3</sup>) at midgestation, and at term.

Fetal cardiac parameters and their mean volumes (95% CI) (cm<sup>3</sup>) at midgestation and term, as determined by 4D sonography (STIC combined with inversion mode).

Table 1

Fetal cardiac parameter	Mean volume (95% CI) (cm <sup>3</sup> )	
	Midgestation	Term
LEDV	0.53 (0.39-0.66)	3.96(3.41-4.51)
LESV	0.17 (0.12-0.22)	1.56 (1.2-1.8)
REDV	0.68 (0.56-0.79)	5.44 (4.69-6.18)
RESV	0.26 (0.19-0.31)	2.29 (1.88-2.71)

LEDV, left end-diastolic volume; LESV, left end-systolic volume; REDV, right end-diastolic volume; RESV, right end-systolic volume Table based upon the report from Messing et al. UOG 2007 [15]

The mean right EDV:left EDV ratio was 1.4 (95% CI: 1.3-1.5), and was relatively stable throughout pregnancy. The EDV and ESV of both ventricles were found to correlate strongly with gestational age and average estimated fetal weight; however, the correlation was slightly stronger with estimated fetal weight (Messing UOG 2007) [15]. Messing et al. also observed similarity between their data for near-term infants, and those derived from neonatal echocardiographic studies. Volume measurements were both reliable and reproducible (inter- and intraobserver variations <10% and <5%, respectively).

In 2008, Molina et al. established cross-sectional reference intervals (12-34 weeks of gestation) for fetal heart stroke volume and cardiac output in 140 normal singleton pregnancies (Molina UOG 2008) [16]. This was accomplished by initially measuring ventricular volumes (systole and diastole) using 4D STIC and the VOCAL™ technique (Fig. 4), and demonstrated its feasibility.

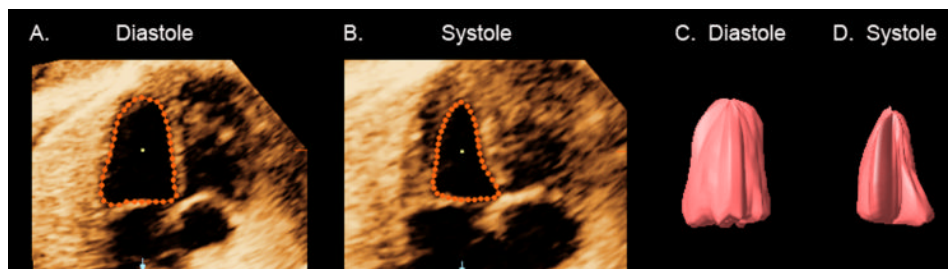


**Figure 4:** Three-dimensional ultrasound images of the left ventricle in diastole (A) and systole (B), and the cardiac volumes obtained from them using VOCAL™ (Virtual Organ Computer-aided AnaLysis) (C and D, respectively).

Factors that could affect the acquisition of 4D volumes included maternal obesity and breathing movements, fetal movements, and fetal position. Advantages of the VOCAL™ technique included: 1) when drawing the contours of the ventricle, the entire ventricle is visualized simultaneously in all planes; and 2) after the initial calculation of ventricular volume, it is possible to modify the contour in each plane. However, various limitations were noted when using the VOCAL™ technique: 1) its reproducibility in the first trimester was poor, due to small ventricular volume; 2) in the third trimester, factors obscured the accurate definition of the limits of the ventricles (fetal spine-up position, fetal breathing movements, shadows from ossified ribs); and 3) with advancing gestation, the anatomic accuracy of endocardial tracing became progressively worse because the myocardium and atrioventricular septa appear thicker, and have lower resolution in the orthogonal plane (vs. original data acquisition) (Molina UOG 2008) [16]. This finding may be related to spatial volume artifacts, slower frame rates, or erroneous rendering algorithms, as described by others (Meyer-Wittkopf JUM 2001) [11].

Uittenbogaard et al. performed a prospective, longitudinal study (12-30 weeks of gestation) using 4D STIC to provide reference values for left and right ventricular volumes, and cardiac function indices (stroke volume, ejection fraction, cardiac output) (Uittenbogaard UOG 2009) [18]. The relationships of ventricular volume and cardiac function indices with gestational age and estimated fetal weight were also determined. All volumetric data were obtained using the 3D Slice method (Fig. 5), which is based on Simpson's rule. Multiple slices of the four-chamber view were manually traced, and the areas multiplied by the slice thickness and summed (Uittenbogaard UOG 2009) [18].



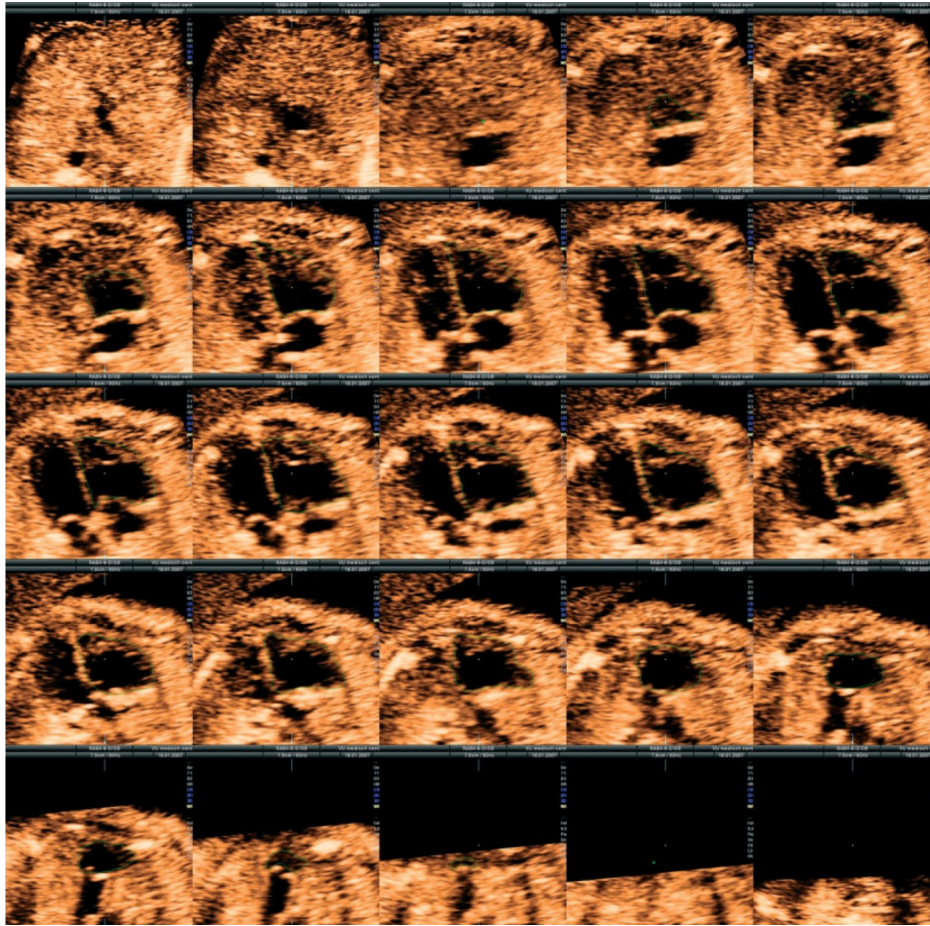


**Figure 5:** Compilation of images 1 mm apart obtained by multiplanar imaging of a spatiotemporal image correlation volume (3D Slice method) frozen in end-diastole. The outlines of the right ventricle have been traced as indicated by a thin green line. The figure demonstrates the complex geometric shape of the right ventricle. Reproduced with permission from Uittenbogaard *et al.* UOG 2009 [18]

From 63 fetuses, 202 STIC volumes were included in the analysis. Volumes were acquired longitudinally from 12 weeks of gestation onwards (with an interval of 3-4 weeks), as long as high-quality acquisition was possible. Volumes were acquired from 12-30 weeks of gestation only, because beyond 29 weeks of gestation, the failure rate of STIC acquisition increased remarkably. There were only three technically acceptable STIC volumes beyond 30 weeks of gestation. Tables 2 and 3 show the mean, 5<sup>th</sup>, and 95<sup>th</sup> centiles of left and right systolic and diastolic ventricular volumes in relation to gestational age. The RV/LV ratio remained constant at around 1.12, for both end-systole and end-diastole.

**Table 2:** Mean, 5<sup>th</sup>, and 95<sup>th</sup> centiles of left systolic and diastolic ventricle volumes in relation to gestational age

Gestational Age (weeks)	Left ventricle ESV (mL)			Left ventricle EDV (mL)		
	Mean	5 <sup>th</sup>	95 <sup>th</sup>	Mean	5 <sup>th</sup>	95 <sup>th</sup>
12	0.03	0.02	0.04	0.04	0.03	0.06
13	0.04	0.03	0.05	0.07	0.05	0.09
14	0.06	0.04	0.08	0.10	0.07	0.13
15	0.08	0.04	0.13	0.15	0.09	0.20
16	0.12	0.05	0.18	0.21	0.12	0.30
17	0.16	0.07	0.26	0.30	0.17	0.43
18	0.22	0.09	0.35	0.41	0.23	0.59
19	0.29	0.12	0.45	0.55	0.31	0.78
20	0.37	0.16	0.58	0.72	0.42	1.02



**Table 2: cont...**

21	0.48	0.21	0.74	0.93	0.55	1.30
22	0.60	0.28	0.91	1.17	0.71	1.62
23	0.73	0.36	1.11	1.44	0.89	1.98
24	0.89	0.45	1.33	1.73	1.08	2.37
25	1.06	0.55	1.57	2.03	1.28	2.79
26	1.24	0.66	1.82	2.34	1.47	3.21
27	1.43	0.76	2.09	2.63	1.64	3.62
28	1.61	0.87	2.35	2.89	1.77	4.02
29	1.79	0.95	2.62	3.11	1.85	4.38
30	1.95	1.02	2.88	3.27	1.86	4.69

Data based on regression equations.

EDV, end-diastolic volume; ESV, end-systolic volume

Slightly modified and reproduced with permission from Uittenbogaard *et al.* UOG 2009 [18]

**Table 3: Mean, 5<sup>th</sup>, and 95<sup>th</sup> centiles of right systolic and diastolic ventricle volumes in relation to gestational age.**

Gestational Age (weeks)	Right ventricle ESV (mL)			Right ventricle EDV (mL)		
	Mean	5 <sup>th</sup>	95 <sup>th</sup>	Mean	5 <sup>th</sup>	95 <sup>th</sup>
12	0.03	0.02	0.03	0.05	0.03	0.06
13	0.04	0.03	0.05	0.07	0.04	0.10
14	0.06	0.04	0.08	0.11	0.06	0.15
15	0.09	0.05	0.13	0.16	0.09	0.23
16	0.13	0.07	0.18	0.23	0.13	0.34
17	0.17	0.09	0.26	0.33	0.18	0.47
18	0.20	0.12	0.35	0.45	0.26	0.64
19	0.32	0.17	0.47	0.61	0.36	0.86
20	0.41	0.22	0.60	0.80	0.49	1.11
21	0.53	0.29	0.76	1.03	0.64	1.41
22	0.66	0.37	0.95	1.29	0.83	1.75
23	0.81	0.47	1.16	1.59	1.04	2.13
24	0.98	0.57	1.38	1.90	1.26	2.54
25	1.16	0.68	1.63	2.22	1.48	2.97
26	1.34	0.80	1.88	2.54	1.69	3.39
27	1.52	0.90	2.14	2.84	1.87	3.80
28	1.69	0.99	2.39	3.09	2.00	4.18
29	1.85	1.06	2.63	3.29	2.08	4.51
30	1.98	1.10	2.85	3.43	2.07	4.78

Data based on regression equations. EDV, end-diastolic volume; ESV, end-systolic volume Slightly modified and reproduced with permission from Uittenbogaard *et al.* UOG 2009 [18]

Uittenbogaard *et al.* felt that the 3D Slice method was preferable and advantageous in obtaining volume measurements. From an *in-vitro* validation study using a balloon model (performed by the same group), the 3D Slice method was proven to be less time-consuming than the use of VOCAL™ or inversion mode. Moreover, manual adjustment of threshold settings when using inversion mode is operator dependent, and this is not the case in the 3D Slice method. Uittenbogaard *et al.* found significantly larger values for end-systolic and end-diastolic ventricular volume (compared to that of Messing *et al.*), and proposed that these differences could be explained by using inversion mode, since it is more dependent on B-mode gain, gray-scale curve, and dynamic range settings. (Uittenbogaard UOG 2009) [18].

Uittenbogaard *et al.* observed the following limitations in performing STIC acquisitions: 1) low image resolution at young gestational ages; 2) numerous acoustic shadows at advanced gestational ages; 3) high failure rate late in gestation; 4) abundant fetal movement; and 5) a persistent unfavorable fetal position (Uittenbogaard UOG 2009) [19].

An important concept when performing quantitative measurements is the potential for measurement error, which can have important consequences when applied clinically. This concept applies to measuring fetal ventricular volumes as well. *Repeatability* of measurements refers to the variation in repeat measurements made on the same subject under identical conditions, while *reproducibility* refers to the variation in measurements made on a subject under changing conditions (National Institute of Standards and Technology) [23]. A comprehensive understanding of fetal ventricular volume repeatability is limited, because previous work has not included assessments of both agreement and reliability, as recommended by Bartlett and Frost (Bartlett UOG 2008) [24]. Moreover, the reproducibility of fetal ventricular volume measurements (obtained by STIC and VOCAL™) is a subject that requires further investigation. Therefore, our group recently quantified both repeatability and reproducibility in the calculation of fetal ventricular volumes (systole and diastole) obtained using the STIC and VOCAL™ technique (Hamill JUM 2009) [25]. From the VOCAL™ application, the sub-feature “Contour Finder/Trace” was utilized (Figs. 6 and 7). This feature employs a sophisticated algorithm which helps to find the contour of the ventricle as the mouse is moved along the ventricular wall.

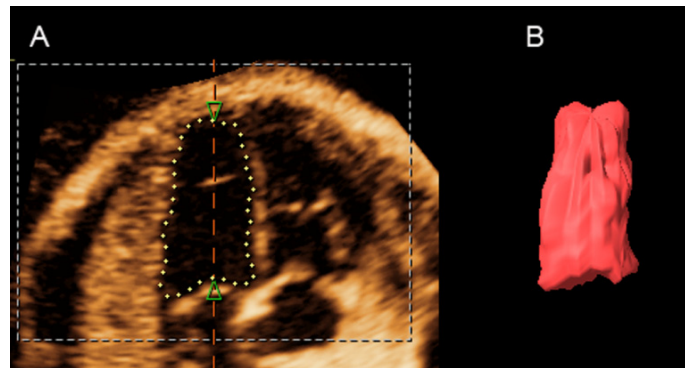


**Figure 6:** Quantification of left ventricular volume in end-diastole. (A) The VOCAL™ trace (using sub-feature “Contour Finder/Trace”) in the A frame at the level of the four-chamber view; (B) the three-dimensional model created by the VOCAL™ tool, which includes the entire traced volume.

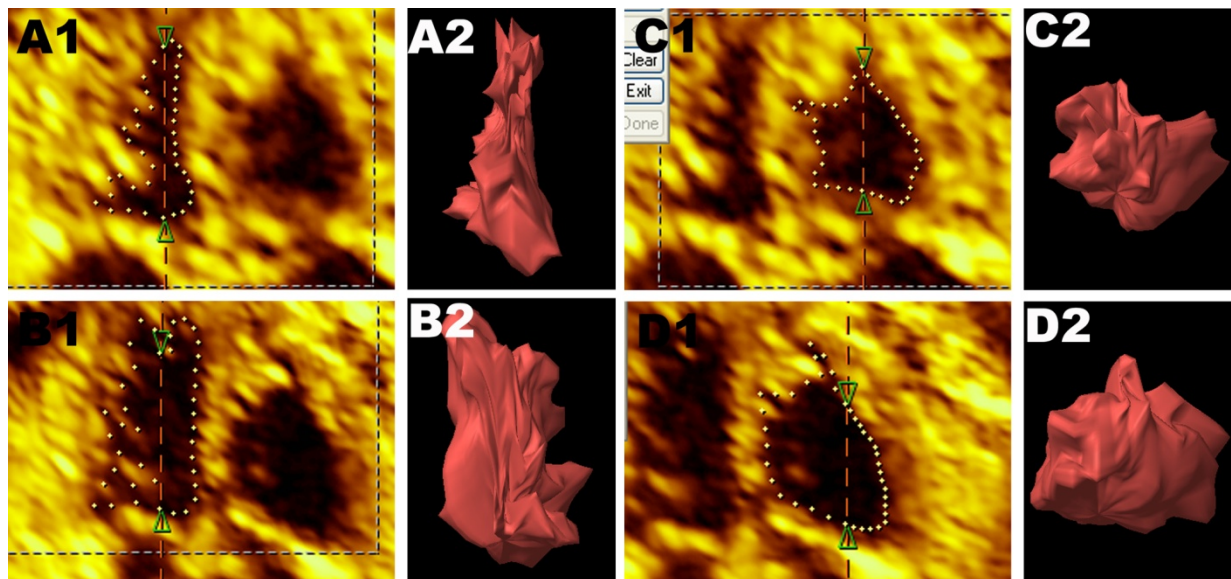


**Figure 7:** Selected VOCAL™ rotational steps utilizing “Contour Finder/Trace” for each ventricle in end systole and end diastole (A: Left ventricle in systole; B: Left ventricle in diastole; C: Right ventricle in systole; D: Right ventricle in diastole) at the level of the four chamber view (image 1: A, B, C, D) and the rendered image (image 2: A, B, C, D). Reproduced with permission from Hamill *et al.* JUM 2009 [25]

Twenty-five normal pregnancies were evaluated for the following: 1) to compare the coefficient of variation (CV) in the calculation of ventricular volumes, when the number of rotational steps is varied from 15° to 30°; 2) to compare the CV in volume calculations between 3 methods of quantifying ventricular volumes from STIC and VOCAL™ (manual trace, inversion mode, and “Contour Finder/Trace”); and 3) to determine *repeatability* (ventricular volumes

were measured twice by each of three observers). *Reproducibility* was assessed by obtaining two STIC datasets from each of 44 normal pregnancies; for each STIC dataset, 2 ventricular volume calculations were performed. Agreement and reliability were evaluated by computing CV and intraclass correlation (ICC), respectively, and the technique was considered *repeatable* if there was good agreement (CV < 10%), as well as good reliability (ICC > 0.90). The technique was considered *reproducible* if there was a negligible difference (<1%) in agreement between datasets, as well as good reliability (ICC > 0.90). Measurement error introduced into STIC acquisitions was examined by constructing a Bland-Altman plot.

The following results were observed: 1) ventricular volume calculations obtained with “Contour Finder/Trace” had better agreement (3.6%, 95% CI 3.0-4.2) than either inversion mode (6.0%, 95% CI 4.9-7.2;  $p < 0.001$ ), or manual trace (10.5%, 95% CI 8.7-12.5;  $p < 0.001$ ); 2) agreement in ventricular volume measurements using STIC and VOCAL™ (“Contour Finder/Trace”) was better with 15° than 30° rotation (3.6%, 95% CI 3.0-4.2 vs. 7.1%, 95% CI 5.8-8.6;  $p < 0.001$ ) (an effect likely due to the complicated geometry of the fetal ventricles) 3) ventricular volume measurements were *repeatable* with good agreement (CV < 10%) and excellent reliability (ICC > 0.95) for both intra-observer and inter-observer measurements (Table 4); and 4) ventricular volume calculations were *reproducible* with a negligible difference in agreement (CV < 1%), and good reliability (ICC > 0.90) (Table 5).

**Table 4:** Repeatability of ventricular volumes utilizing VOCAL™ with the sub-feature “Contour Finder/Trace”

	Observer 1 (n=25)	Observer 2 (n=25)	Observer 3 (n=25)
<b>Agreement*</b>	2.8% (2.3 – 3.3)	3.6% (3.0 – 4.3)	6.3% (5.2 – 7.6)
<b>Intra-observer reliability#</b>	0.998 (0.996– 0.998)	0.996 (0.994– 0.997)	0.990 (0.985– 0.993)
<b>Inter-observer reliability#</b>	0.96 (0.94 – 0.97)		

\*Agreement expressed as mean percent coefficient of variation (95% CI) #Reliability expressed as intraclass correlation (95% CI) Reproduced with permission from Hamill *et al.* JUM 2009 [25]

**Table 5:** Reproducibility of ventricular volumes utilizing VOCAL™ with the sub-feature “Contour Finder/Trace.”

	STIC Dataset A	STIC Dataset B
<b>Agreement*</b>	4.0% (3.5 – 4.7)	3.8% (3.2 – 4.6) <sup>†</sup>
<b>Intra-observer reliability#</b>	0.998 (0.997– 0.998)	0.997 (0.996 – 0.998)
<b>Inter-observer reliability#</b>	0.94 (0.92 – 0.96)	

\*Agreement expressed as mean percent coefficient of variation (95% CI) <sup>†</sup>Paired t-test not significant ( $t = 0.47$ ;  $p = ns$ ) #Reliability expressed as intraclass correlation (95% CI) Reproduced with permission from Hamill *et al.* JUM 2009 [25]

The Bland-Altman plot comparing the percent difference between volume calculations from each STIC acquisition indicated that minimal bias was introduced between acquisitions (<1%; mean percent difference -0.4%, 95% limits of agreement -5.4 – 5.9). Therefore, we found that fetal echocardiography using STIC and VOCAL™ allowed both *repeatable* and *reproducible* calculations of ventricular volumes, when using the sub-feature “Contour Finder/Trace” (Hamill JUM 2009) [25]. It is noteworthy that ventricular volume calculations obtained using VOCAL™ and manual trace achieved CVs greater than 10%, suggesting this may not be the most optimal method to quantify ventricular volumes.

Obtaining fetal ventricular volume measurements using 4D STIC technology, however, is not without limitations. STIC produces a computer-generated cine loop of a single cardiac cycle that is an assemblage of 20 to 30 real cardiac cycles. It is possible that some degree of smoothing, or averaging of the ventricular borders could occur, introducing a degree of error into the calculations performed. STIC volume datasets may also be limited by acoustic shadowing (signal loss in the sound path secondary to echogenic structures), dropout (signal loss in the sound path without intervening structures), motion artifact, fetal positioning, and respirations. Moreover, regardless of the method used in conjunction with STIC to determine ventricular volumes, (e.g. inversion mode, VOCAL™, etc), there is still a significant learning curve and time commitment required to orient, process, and analyze the data.

These factors have hindered the widespread adoption of multi-dimensional sonographic techniques. Nevertheless, we anticipate that this practice will change in the future as sonologists become more accustomed to these tools. Importantly, the use of 4D sonographic technology to obtain fetal ventricular volumes has advantages over 2D and 3D sonography, and it has been demonstrated that ventricular volumes obtained through STIC and VOCAL™

provide both repeatable and reproducible calculations. Therefore, the available literature supports the continued practice of this technique. Once ventricular volumes have been determined, cardiac function parameters (e.g. stroke volume, cardiac output, ejection fraction) can be subsequently calculated.

### **FETAL STROKE VOLUME AND CARDIAC OUTPUT (USING TWO-DIMENSIONAL AND DOPPLER ECHOCARDIOGRAPHY)**

Cardiac output (CO) is the volume of blood that is pumped over a unit of time. The formula for calculating cardiac output is: *stroke volume (SV) x heart rate*. Traditionally, 2D and Doppler echocardiography have been used to calculate fetal SV and CO (Mielke Circulation 2001) [26]. SV is calculated by multiplying the time velocity integral (TVI) of the Doppler tracing, with the flow cross-sectional area. TVI is the area measured under the Doppler velocity envelope for one heartbeat. The cross-sectional area is calculated from  $\pi d^2/4$ , where  $d$  is the valve diameter. Therefore, the formulas for calculating SV and CO are:

$$SV = TVI \times \pi d^2/4$$

$$CO = SV \times \text{fetal heart rate}$$

Animal experimentation has demonstrated that Doppler echocardiography can be used to accurately quantify volumetric flow through the aortic and pulmonary valves (Stewart JACC 1985) [27]. However, it is important to consider methodological problems with this technique. Rizzo *et al.* assessed the agreement of fetal SV (measured with 2D and Doppler sonography) with 4D STIC sonography (Rizzo Prenat Diagn 2007) [17]. Both techniques were found to measure SV reliably and with good reproducibility. However, Rizzo *et al.* noted that the performance of 2D Doppler echocardiography was operator-dependent, and required various views of the fetal heart in order to measure Doppler velocity waveforms of the outflow tracts and valve diameter. Based on the formulas described above, errors in SV (and therefore, CO) may arise from inaccuracies in vessel diameter and Doppler recordings (Mielke Circulation 2001) [26]. Moreover, errors in measuring the TVI and valve area (even if small) will greatly influence volume flow measurements, particularly because the area of the valve is related to the square of the radius, thus accentuating any errors (Eik-Nes UMB 1984) [28]. Even by including just one vessel wall thickness (measuring vessel diameter from outer surface to inner surface), this will overestimate the diameter and consequently, the volume of blood flow. Indeed, vessel areas represent the most important source of error in flow calculations, and particularly in vessels with a small diameter, the error will be substantial (Mielke Circulation 2001) [26]. Simpson and Cook determined the repeatability of Doppler echocardiographic measurements in the human fetus (Simpson UOG 2002) [2]. They found that intra- and inter-observer errors were high for Doppler variables, such as vessel dimension, SV, and CO. For aortic Doppler measurements, the CV was greater than 10% for both the calculated SV (16%), and CO (16%). Performing Doppler echocardiography is also time-consuming, and requires both a favorable position of the fetus and an experienced sonologist. Therefore, these factors have limited its application in clinical practice, and measures of absolute volume flow using this modality have largely fallen out of favor.

### **FETAL STROKE VOLUME, CARDIAC OUTPUT, EJECTION FRACTION (FOUR-DIMENSIONAL ECHOCARDIOGRAPHY)**

In adults and children, cardiac function is commonly expressed as SV and ejection fraction (EF). Both indices can be calculated from end-systolic and end-diastolic ventricular volumes. SV is the volume of blood pumped from one ventricle of the heart with each contraction, and SV applies equally to both ventricles. Its value is obtained by subtracting end-systolic volume (ESV) from end-diastolic volume (EDV) (or preload) for a given ventricle. Hence, the formula for calculating SV is:

$$SV = EDV - ESV$$

SV depends on various factors, such as heart size, contractility, duration of the contraction, preload, and afterload. The most commonly used index of LV function is the EF. This is the amount of blood pumped per contraction (SV), compared to the maximum left ventricular volume prior to contraction (EDV), and as the term states, it is calculated as a *fraction*. Even in healthy hearts, some blood always remains in the ventricles after each contraction. Therefore,

EF is the percentage of the blood within the ventricles that is ejected during systole, and is a measure of the effectiveness of the heart as a pump. EF is often used as a clinical index to evaluate the inotropic status of the heart. The formula for calculating EF is:

$$EF = SV \times 100\% / EDV$$

In the fetus, both ventricles pump blood to the systemic arterial circulation. Since pulmonary vascular resistance is higher in the fetus (vs. postnatally), most of the RV output enters the systemic arterial circulation via the ductus arteriosus. Because the pulmonary and systemic circulations are separate in fetal life, each ventricle has a SV which is determined by the preload, contractility, and afterload of that chamber. However, because of the large volume and pressure work required from the RV, it is a large contributor to the work output of the fetal heart (Huhta 2009) [14]. Indeed, it has been shown that the RV volume that is ejected is greater than that of the LV by echocardiography measurements throughout gestation (Chaoui Geburtshilfe Frauenheilkd 1995) [29]. Chaoui *et al.* found that the SV and CO of the RV had a higher ratio (1.3:1) than that of the LV, thus expressing RV dominance in the fetus (Chaoui Geburtshilfe Frauenheilkd 1995) [29]. This distribution of CO is maintained, in spite of significant changes in the pulmonary vascular resistance and flow between 20-37 weeks of gestation (Rasanen Circulation 1996) [30]. Further evidence that the RV performs more work than the LV is shown by data in fetal lambs, that measured the coronary blood flow of both ventricles (Thornburg AJP 1999) [31]. The RV coronary flow was found to be consistently one-third greater than that of the LV.

Prior studies (not utilizing 4D echocardiography) that evaluated fetal SV, EF, or CO either: 1) could not overcome the limitations of differentiating ventricular volume from the myocardium (due to the non-uniform shape of the endocardium); or 2) relied on sophisticated and time-consuming mathematical calculations (Meyer-Wittkopf JUM 2001 [11] Schmidt AJC 1995 [32] Mielke Circulation 2001) [26] that could not be applied in routine clinical settings.

After first establishing ventricle volumetry (using 4D STIC and inversion mode) in fetuses ranging from 20.5-40 gestational weeks, EF and SV were also calculated (Messing UOG 2007) [15]. Right, left, and total SV were found to correlate strongly with estimated fetal weight and gestational age: 1) total SV and EFW,  $r^2 = 0.809$ ; and 2) total SV and gestational age,  $r^2 = 0.766$ . Left EF ranged from 42.5 to 86% in these fetuses. However, EF was found to have no correlation with estimated fetal weight or gestational age, but instead, remained fairly stable throughout gestation (Messing UOG 2007) [15].

Rizzo *et al.* assessed the agreement of fetal SV measured with 2D and Doppler sonography vs. 4D ultrasound with STIC (Rizzo Prenat Diagn 2007) [17]. Stroke volumes were cross-sectionally measured in a population of normal and growth-restricted fetuses (n=56) in the second half of pregnancy. The VOCAL™ technique was used to evaluate end-systolic and end-diastolic volumes of each ventricle, and the contour was traced manually (Figs. 8 and 9).

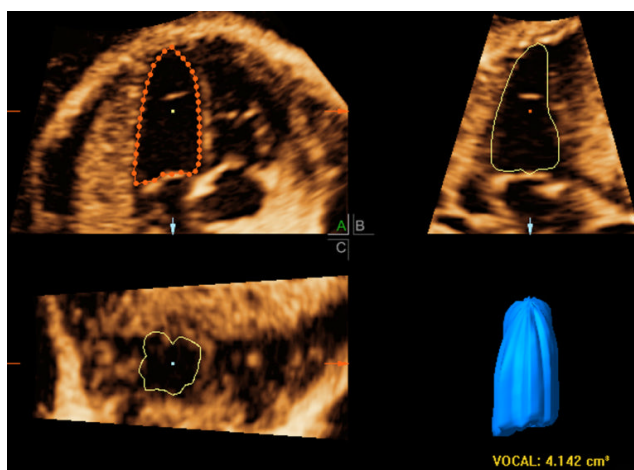


**Figure 8:** Example of quantification of the fetal left ventricular volume during end-diastole, using the VOCAL™ (Virtual Organ Computer-aided AnaLysis) tool and manual trace.

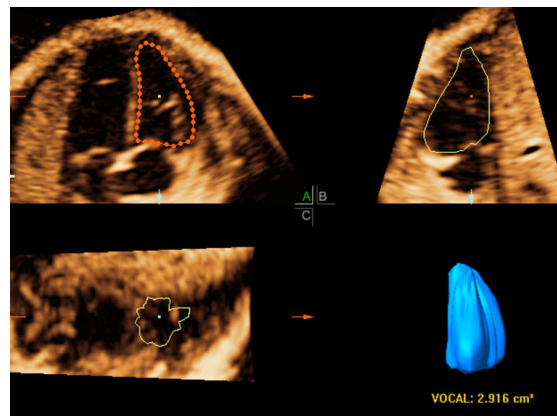


**Figure 9:** Example of quantification of the fetal right ventricular volume during end-diastole, using the VOCAL™ (Virtual Organ Computer-aided ANALysis) tool and manual trace.

The SV from both ventricles was calculated by taking the difference between the end-diastolic and end-systolic volumes. Doppler velocity waveforms were recorded from the outflow tracts, and the aortic and pulmonary valve diameters were measured. Intraclass correlation was used to evaluate the agreement between left and right SV obtained by the two techniques, and proportionate Bland-Altman plots were constructed. The amount of time necessary to obtain SV using both techniques was also analyzed.

For the left ventricle SV (measured by 4D STIC), intraobserver and interobserver correlation coefficients were 0.98 (95% CI 0.92-0.99) and 0.95 (95% CI 0.88-0.97), respectively. For the right ventricle SV (measured by 4D STIC), intraobserver and interobserver correlation coefficients were 0.97 (95% CI 0.91-0.98) and 0.93 (95% CI 0.87-0.95), respectively. There was good agreement found between SV measured either by 2D Doppler or 4D STIC. The intraclass correlation coefficient between 2D Doppler and 4D STIC measurements were 0.977 (95% CI 0.963-0.986) and 0.980 (95% CI 0.968-0.988), for the LV and RV, respectively. The proportionate limits of agreement between the two methods were 18.7 to 23.9% and -20.9 to 21.7%, for the LV and RV, respectively. Importantly, the average time necessary to acquire a 4D STIC volume and analyze both left and right SV was  $3.1 \pm 0.84$  minutes, which was significantly lower than the time necessary to obtain the same measurements using 2D Doppler ( $7.9 \pm 2.3$  minutes;  $p < 0.0001$ ).

Rizzo *et al.* noted several advantages in using 4D STIC (vs. 2D Doppler): 1) SV can be measured by only obtaining the four-chamber view, and then automatically acquiring a cardiac volume dataset; 2) STIC avoids the “operator dependency” of the measurements necessary when using 2D Doppler, which also requires various cardiac views in order to measure valve diameter and Doppler velocity waveforms; and 3) it dramatically reduces the time necessary to measure SV. Therefore, 4D STIC was a simple and rapid technique to estimate fetal SV, and is likely to become the method of choice (Rizzo Prenat Diagn 2007) [17].

Molina *et al.* reported cross-sectional reference intervals (12-34 weeks of gestation) for fetal SV and CO in 140 normal singleton pregnancies (Molina UOG 2008) [16]. This was accomplished by initially measuring ventricular volumes (systole and diastole) using 4D STIC and the VOCAL™ technique (30° rotation), and demonstrated its feasibility. In 50 cases, SV were measured by the same sonologist twice, and intraobserver agreement of measurements was calculated. Mean left and right SV and CO increased exponentially with gestation (Table 6).

**Table 6:** Mean (5<sup>th</sup>, 95<sup>th</sup> centiles) of left and right stroke volume and left and right cardiac output with gestation.

Gestational age(weeks)	Left stroke volume (mL)	Right stroke volume (mL)	Left cardiac output (mL/min)	Right cardiac output (mL/min)
12	0.02 (0.01, 0.03)	0.01 (0.01, 0.02)	2.39 (1.45, 3.92)	1.80 (1.01, 3.21)
13	0.02 (0.02, 0.04)	0.02 (0.01, 0.03)	3.80 (2.31, 6.25)	3.15 (1.78, 5.58)
14	0.04 (0.02, 0.06)	0.03 (0.02, 0.06)	5.86 (3.57, 9.64)	5.24 (2.98, 9.22)
15	0.06 (0.04, 0.09)	0.05 (0.03, 0.09)	8.78 (5.34, 14.43)	8.33 (4.76, 14.56)

Table 6: cont...

16	0.08 (0.05, 0.14)	0.08 (0.05, 0.14)	12.75 (7.76, 20.97)	12.68 (7.30, 22.02)
17	0.12 (0.07, 0.20)	0.12 (0.07, 0.21)	18.02 (10.96, 29.62)	18.54 (10.75, 31.98)
18	0.17 (0.10, 0.27)	0.18 (0.10, 0.30)	24.78 (15.08, 40.73)	26.10 (15.23, 44.72)
19	0.22 (0.14, 0.37)	0.24 (0.14, 0.40)	33.22 (20.21, 54.60)	35.48 (20.84, 60.41)
20	0.30 (0.18, 0.48)	0.32 (0.19, 0.54)	43.45 (26.44, 71.42)	46.72 (27.63, 79.02)
21	0.38 (0.23, 0.62)	0.41 (0.24, 0.69)	55.54 (33.79, 91.28)	59.75 (35.57, 100.38)
22	0.48 (0.29, 0.78)	0.51 (0.31, 0.87)	69.44 (42.25, 114.13)	74.42 (44.59, 124.19)
23	0.59 (0.36, 0.97)	0.63 (0.37, 1.06)	85.04 (51.74, 139.77)	90.52 (54.60, 150.06)
24	0.72 (0.44, 1.17)	0.76 (0.45, 1.27)	102.12 (62.13, 167.85)	107.83 (65.48, 177.59)
25	0.85 (0.52, 1.39)	0.89 (0.53, 1.50)	120.41 (73.26, 197.91)	126.16 (77.12, 206.40)
26	0.99 (0.61, 1.62)	1.03 (0.61, 1.74)	139.58 (84.92, 229.41)	145.38 (89.45, 236.27)
27	1.14 (0.69, 1.86)	1.18 (0.70, 1.99)	159.24 (96.89, 261.73)	165.46 (102.49, 267.13)
28	1.28 (0.79, 2.10)	1.34 (0.79, 2.25)	179.04(108.93,294.26)	186.51 (116.29, 299.13)
29	1.43 (0.88, 2.34)	1.50 (0.89, 2.53)	198.61(120.84,326.43)	208.82 (131.07, 332.69)
30	1.58 (0.96, 2.58)	1.69 (1.00, 2.84)	217.65(132.42,357.72)	232.86 (147.13, 368.55)
31	1.71 (1.05, 2.80)	1.88 (1.12, 3.17)	235.91(143.53,387.73)	259.37 (164.97, 407.79)
32	1.84 (1.13, 3.01)	2.11 (1.25, 3.55)	253.21(154.06,416.18)	289.36 (185.27, 451.93)
33	1.97 (1.20, 3.21)	2.37 (1.41, 3.98)	269.48(163.96,442.91)	324.25 (208.99, 503.08)
34	2.08 (1.27, 3.40)	2.67 (1.59, 4.50)	284.70(173.22,467.93)	365.98 (237.45, 564.09)

Reproduced with permission from Molina *et al.* UOG 2008 [16]

Moreover, the ratio of right to left SV increased significantly with gestation, from about 0.97 (12 weeks) to 1.13 (34 weeks). In the Bland-Altman plot, the mean percentage difference and 95% limits of intraobserver agreement for left SV and right SV were -2.1% (-18.4, 14.2) and -0.8% (-16.4, 18.0), respectively.

It is noteworthy that right and left CO values from this study are smaller than those in prior reports, which estimated CO from either 2D sonographic assessment of ventricular dimensions or from cross-sectional area measurements and Doppler velocity waveforms of the outflow tracts (Table 7).

**Table 7:** Fetal cardiac output in previous studies using two-dimensional ultrasound in comparison with the results of the present study.

Reference	Method of measurement	Left cardiac output (mL/min)			Right cardiac output (mL/min)		
		16 weeks	24 weeks	34 weeks	16 weeks	24 weeks	34 weeks
Mielke and Benda [26]	Vessel area and TVI	20	125	380	30	175	575
Allan <i>et al.</i> [33]	Vessel area and TVI	33	127	409	44	171	547
De Smedt <i>et al.</i> [34]	AVV area and TVI	50	150	550	75	175	625
Kenny <i>et al.</i> [35]	Vessel area and TVI	83	167	400	116	226	518
Veille <i>et al.</i> [36]	M-mode echocardiography	48	142	362	55	166	433
Schmidt <i>et al.</i> [32]	Method of discs	23	102	367	34	133	423
Molina <i>et al.</i> [16]	4D ultrasound and VOCAL	13	102	285	13	108	366



4D, four-dimensional; AVV, atrioventricular valve; TVI, time velocity integral; VOCAL, Virtual Organ Computer-aided AnaLysis Slightly modified and reproduced with permission from Molina *et al.* UOG 2008 [16]

Molina *et al.* suggested that the results of the Doppler studies may be inaccurate, because fetal myocardium is greatly limited in its ability to contract when compared to the postnatal period; therefore, the Frank-Starling law (on which the Doppler technique relies) applies in a different manner (Molina UOG 2008) [16].

Molina *et al.* also point out that the findings of fetal CO are not comparable with postnatal Doppler study results because: 1) myocardial contractility is better and ventricular compliance greater in the neonatal period than in fetal life (Anderson 1990) [37] (Teitel 2003) [38]; and 2) in the first hours after birth (following closure of the ductus arteriosus and the foramen ovale), there is a decrease in CO. Indeed, Winberg *et al.* measured CO in normal newborns using Doppler sonography, and demonstrated a decrease from about 240 mL/min/kg (in the first 2 hours), to 190 mL/min/kg (at 24 hours) (Winberg ADC 1989) [39].

Uittenbogaard *et al.* performed a prospective, longitudinal study (12-30 weeks of gestation) using 4D STIC to provide reference values for left and right ventricular volumes and cardiac function indices (SV, CO, EF) (Uittenbogaard UOG 2009) [18]. Additionally, the relationships of cardiac function indices with gestational age and estimated fetal weight were determined. All volumetric data were obtained using the 3D Slice method (Fig. 5), which is based on Simpson's rule. Table 8 shows the mean, 5<sup>th</sup>, and 95<sup>th</sup> centiles of left and right ventricular SV in relation to gestational age. The mean right to left SV ratio showed right dominance, remaining fairly constant (around 1.2) throughout gestation. Bland-Altman analysis showed a coefficient of variation for measured SV of 13.7% (intraobserver agreement).

**Table 8** Mean, 5<sup>th</sup>, and 95<sup>th</sup> centiles of left and right ventricle stroke volume, in relation to gestational age

Gestational Age (weeks)	Left ventricle SV (mL)			Right ventricle SV (mL)		
	Mean	5 <sup>th</sup>	95 <sup>th</sup>	Mean	5 <sup>th</sup>	95 <sup>th</sup>
12	0.02	0.00	0.03	0.02	0.00	0.04
13	0.03	0.00	0.05	0.03	0.00	0.06
14	0.04	0.01	0.07	0.04	0.00	0.08
15	0.06	0.01	0.11	0.07	0.01	0.12
16	0.09	0.02	0.15	0.10	0.02	0.18
17	0.13	0.04	0.22	0.14	0.04	0.24
18	0.18	0.06	0.29	0.20	0.08	0.33
19	0.24	0.10	0.39	0.28	0.12	0.44
20	0.33	0.15	0.51	0.37	0.18	0.56
21	0.42	0.21	0.64	0.48	0.25	0.71
22	0.54	0.28	0.80	0.61	0.34	0.88
23	0.66	0.36	0.97	0.75	0.44	1.06
24	0.80	0.45	1.15	0.90	0.54	1.26
25	0.94	0.53	1.34	1.04	0.63	1.45
26	1.07	0.61	1.54	1.18	0.71	1.64
27	1.19	0.67	1.72	1.30	0.77	1.82
28	1.30	0.71	1.88	1.39	0.80	1.97
29	1.37	0.71	2.03	1.44	0.79	2.09
30	1.41	0.68	2.14	1.46	0.74	2.18

Data based on regression equations. SV, stroke volume. Slightly modified and reproduced with permission from Uittenbogaard *et al.* UOG 2009 [18]

Table 9 compares the results of combined SV determined from this study to that of prior studies, which used either 2D sonography and Doppler or 4D sonographic techniques, demonstrating varying results (Allan BHJ 1987) [33] (Kenny Circulation 1986) [35] (Rasanen Circulation 1996) [30] (Mielke Circulation 2001) [26] (Messing UOG 2007) [15] (Molina UOG 2008) [16] (<sup>a</sup>Uittenbogaard UOG 2009) [18]. Regardless of the method used, all studies using 4D echocardiography reported relatively small SV values, as compared with the larger values found in studies that used 2D sonography and Doppler (Table 9).

**Table 9** Combined left and right stroke volumes in previous studies using both two-dimensional and four-dimensional ultrasound imaging in comparison with the results of the present study

Reference	Method of measurement	20 weeks	24 weeks	30 weeks
Allan (1987) [33]	Vessel area and TVI	1.16	2.13	4.49
Kenny (1986) [35]	Vessel area and TVI	1.93	2.74	4.63
Rasanen (1996) [30]	Vessel area and TVI	1.18	2.89	6.28
Mielke and Benda (2001) [26]	Vessel area and TVI	0.85*	2.06*	4.56*
Messing (2007) [15]	STIC and inversion mode	0.41	1.26	2.95
Molina (2008) [16]	STIC and VOCAL	0.55	1.27	2.69
Uittenbogaard (2009) [18]	STIC and 3D Slice Method	0.72	1.72	2.63

\*Obtained from figures. 3D, three dimensional; STIC, spatiotemporal image correlation; TVI, time velocity integral; VOCAL, Virtual Organ Computer-aided AnaLysis. \*Slightly modified and reproduced with permission from Uittenbogaard

Uittenbogaard *et al.* suggested that this could be due to: 1) inaccuracies in Doppler calculations based on prenatal and postnatal differences in myocardial contractility (Molina UOG 2008 [16]; and 2) errors in measurement of the vessel cross-sectional area in Doppler studies, where the lumen is assumed to be round but instead, could be slightly oval. Therefore, Uittenbogaard *et al.* has proposed that the Doppler studies may have been erroneous, and led to overestimation of fetal SV (and subsequently CO) (Uittenbogaard UOG 2009) [18]. Since 4D echocardiographic estimations avoid geometric assumptions and are less susceptible to measurement errors, these results may provide a more accurate reflection of fetal cardiac volumes and function.

Table 10 shows the mean, 5<sup>th</sup>, and 95<sup>th</sup> centiles of left and right CO in relation to gestational age. To calculate left and right CO, SVs were multiplied by the fetal heart rate, as recorded within each STIC volume. The mean left CO increased from 2.40 (95% CI, 0.63-4.18) mL/min at 12 weeks, to 197.74 (95% CI, 98.40-297.08) mL/min at 30 weeks. The mean right CO increased from 2.60 (95% CI, 0.00-5.22) mL/min at 12 weeks to 204.81 (95% CI, 105.01-304.61) mL/min at 30 weeks.

**Table 10:** Mean, 5<sup>th</sup>, and 95<sup>th</sup> centiles of left and right cardiac output, in relation to gestational age.

Gestational Age (weeks)	Left cardiac output (mL/min)			Right cardiac output (mL/min)		
	Mean	5 <sup>th</sup>	95 <sup>th</sup>	Mean	5 <sup>th</sup>	95 <sup>th</sup>
12	2.40	0.63	4.18	2.60	0.00	5.22
13	3.81	0.78	6.83	4.17	0.17	8.16
14	5.88	1.10	10.65	6.51	0.67	12.34
15	8.84	1.84	15.85	9.88	1.73	18.04
16	12.98	3.25	22.71	14.61	3.67	25.56
17	18.58	5.64	31.52	21.03	6.82	35.24
18	25.93	9.28	42.58	29.46	11.51	47.41
19	35.29	14.45	56.13	40.18	18.01	62.34
20	46.82	21.29	72.34	53.32	26.47	80.18
21	60.58	29.88	91.28	68.89	36.87	100.90
22	76.42	40.06	112.79	86.62	48.97	124.27
23	94.01	51.49	136.53	106.02	62.26	149.78
24	112.77	63.60	161.94	126.31	75.96	176.65
25	131.90	75.59	188.20	146.47	89.07	203.87
26	150.43	86.50	214.36	165.32	100.38	230.25
27	167.28	95.24	239.33	181.62	108.68	254.56
28	181.40	100.74	262.05	194.22	112.80	275.64
29	191.80	102.05	281.55	202.16	111.78	292.53
30	197.74	98.40	297.08	204.81	105.01	304.61

Data based on regression equations. CO, cardiac output.

Slightly modified and reproduced with permission from Uittenbogaard *et al.* UOG 2009 [18]

Mean left and right ventricular EF remained constant with advancing gestational age. The mean left ventricle EF was 0.45 (95% CI, 0.23-0.67), and the mean right ventricle EF was 0.46 (95% CI 0.26-0.66).

Recently, \*our group determined fetal CO from datasets acquired with 4D echocardiography, using STIC and VOCAL™ technology. From VOCAL™, the sub-feature “Contour Finder/Trace” was utilized, which employs a sophisticated algorithm that helps to find the contour of the ventricle as the mouse is moved along the ventricular wall. There were 102 fetuses evaluated cross-sectionally between 19-39 weeks of gestation, and results were grouped according to gestational age quartiles (19-24, 25-28, 29-32, and 33-39 weeks). Ventricular volumes were determined from both ventricles in systole and diastole. Left and right ventricular SV were calculated, and then used to compute CO (ml/min). CO was also expressed as a function of estimated fetal weight (ml/min/kg) (Table 11).

**Table 11:** Mean ( $\pm$  SD) left and right cardiac output (also expressed as a function of estimated fetal weight) in relation to gestational age

Gestational age (weeks)	Left ventricle CO (ml/min)	Left ventricle CO (ml/min/kg)	Right ventricle CO (ml/min)	Right ventricle CO (ml/min/kg)
19-24 (n=26)	47 $\pm$ 12	98 $\pm$ 21	46 $\pm$ 11	96 $\pm$ 19
25-28 (n=26)	81 $\pm$ 22	89 $\pm$ 25	97 $\pm$ 16	96 $\pm$ 16
29-32 (n=26)	133 $\pm$ 28	89 $\pm$ 17	126 $\pm$ 35	84 $\pm$ 22
33-39 (n=25)	210 $\pm$ 39	85 $\pm$ 16	236 $\pm$ 41	95 $\pm$ 14

\*Oral communication abstract OC004. Hamill N, Romero R, Myers SA, *et al.* Fetal cardiac output determination by four-dimensional fetal echocardiography using spatiotemporal image correlation (STIC) and VOCAL™. *Ultrasound Obstet Gynecol* 2008; 32(3): 244

The following observations were made: 1) left and right ventricular CO increased with gestational age (Spearman rho = 0.8, P < 0.001); 2) however, CO expressed as a function of estimated fetal weight did not change with advancing gestational age (LV CO:  $r_s = -0.06$ , P = 0.5; RV CO:  $r_s = -0.03$ ; P = 0.8); and 3) intra- and inter-observer coefficients of variation were 2.3% and 4.0%, respectively. Therefore, we found that fetal CO can be reproducibly estimated with 4D echocardiography, using STIC and VOCAL™ techniques.

An area of future investigation that may be applicable to the fetus was studied by Pemberton *et al.* in 50 pediatric/adult patients (Pemberton JASE 2005) [40]. Pemberton *et al.* investigated the use of real-time color Doppler 3D echocardiography (xMatrix™ probe) to calculate SV, and compared this to 2D pulsed Doppler measurements. Using 3D Doppler data, flow volumes were calculated using specially designed computer software. There was excellent correlation between the SV obtained from live 3D echocardiography and 2D Doppler ( $r^2 = 0.90$ ; p < 0.001, standard error of the estimate = 6.98 mL).

## CONCLUSIONS

Quantifying ventricular volume and calculating cardiac function parameters reliably is important in assessing cardiac function, as well as the severity and prognosis of cardiac disease. Both two- and three-dimensional echocardiography have been used for these purposes, but have limitations. Four-dimensional echocardiography appears to overcome most of the pitfalls of traditional methods. It avoids geometric assumptions, is less susceptible to measurement errors, and has proven to be a feasible method to assess fetal cardiac function. Moreover, the performance of 4D STIC is uncomplicated and rapid. Using this technology, normal reference ranges of ventricular volume (end-diastolic and end-systolic), stroke volume, cardiac output, and ejection fraction throughout gestation have been generated. STIC promises to be part of the methodology used to assess fetal cardiac function. Further studies, however, are needed to determine the behavior of fetuses with abnormal cardiac function, and to correlate this with adverse perinatal outcome.

## REFERENCES

- [1] Esh-Broder E, Ushakov FB, Imbar T, Yagel S. Application of free-hand three-dimensional echocardiography in the evaluation of fetal cardiac ejection fraction: a preliminary study. *Ultrasound Obstet Gynecol* 2004; 23(6): 546-51.
- [2] Simpson JM, Cook A. Repeatability of echocardiographic measurements in the human fetus. *Ultrasound Obstet Gynecol* 2002; 20(4):332-9.
- [3] Teichholz LE, Kreulen T, Herman MV, Gorlin R. Problems in echocardiographic volume determinations: echocardiographic-angiographic correlations in the presence or absence of asynergy. *Am J Cardiol* 1976; 37(1):7-11.
- [4] Bhat AH, Corbett V, Carpenter N, *et al.* Fetal ventricular mass determination on three-dimensional echocardiography: studies in normal fetuses and validation experiments. *Circulation* 2004; 110(9):1054-60.

- [5] Wyatt HL, Meerbaum S, Heng MK, Gueret P, Corday E. Cross-sectional echocardiography. III. Analysis of mathematic models for quantifying volume of symmetric and asymmetric left ventricles. *Am Heart J* 1980; 100(6 Pt 1):821-8.
- [6] Sedmera D, Pexieder T, Vuillemin M, Thompson RP, Anderson RH. Developmental patterning of the myocardium. *Anat Rec* 2000; 258(4): 319-337.
- [7] Simpson J. Echocardiographic evaluation of cardiac function in the fetus. *Prenat Diagn* 2004; 24 (13): 1081-91.
- [8] Bhat AH, Corbett VN, Liu R, *et al.* Validation of volume and mass assessments for human fetal heart imaging by 4-dimensional spatiotemporal image correlation echocardiography: in vitro balloon model experiments. *J Ultrasound Med* 2004; 23(9):1151-
- [9] Espinoza J, Gotsch F, Kusanovic, JP, *et al.* Changes in fetal cardiac geometry with gestation: implications for 3- and 4-dimensional fetal echocardiography. *J Ultrasound Med* 2007; 26(4): 427-43.
- [10] Levental M, Pretorius DH, Sklansky MS, Budorick NE, Nelson TR, Lou K. Three-dimensional ultrasonography of normal fetal heart: comparison with two-dimensional imaging. *J Ultrasound Med* 1998; 17(6):341-8.
- [11] Meyer-Wittkopf M, Cole A, Cooper SG, Schmidt S, Sholler GF. Three-dimensional quantitative echocardiographic assessment of ventricular volume in healthy human fetuses and in fetuses with congenital heart disease. *J Ultrasound Med* 2001; 20(4):317-27.
- [12] Tutschek B, Sahn DJ. Semi-automatic segmentation of fetal cardiac cavities: progress towards an automated fetal echocardiogram. *Ultrasound Obstet Gynecol* 2008; 32(2):176-80.
- [13] Uittenbogaard LB, Haak MC, Spreeuwenberg MD, VanVugt JMG. A systematic analysis of the feasibility of four-dimensional ultrasound imaging using spatiotemporal image correlation in routine fetal echocardiography. *Ultrasound Obstet Gynecol* 2008; 31(6): 625- 32.
- [14] Huhta J. Congestive heart failure in the fetus. In *Fetal Cardiology* (2<sup>nd</sup> edition), Yagel S, Silverman NH, Gembruch U (eds.). Informa Healthcare USA, Inc: New York, NY, 2009; 561-78.
- [15] Messing B, Cohen SM, Valsky DV, *et al.* Fetal cardiac ventricle volumetry in the second half of gestation assessed by 4D ultrasound using STIC combined with inversion mode. *Ultrasound Obstet Gynecol* 2007; 30(2):142-51.
- [16] Molina FS, Faro C, Sotiriadis A, Dagklis T, Nicolaidis KH. Heart stroke volume and cardiac output by four-dimensional ultrasound in normal fetuses. *Ultrasound Obstet Gynecol* 2008; 32(2):181-7.
- [17] Rizzo G, Capponi A, Cavicchioni O, Vendola M, Arduini D. Fetal cardiac stroke volume determination by four-dimensional ultrasound with spatio-temporal image correlation compared with two-dimensional and Doppler ultrasonography. *Prenat Diagn* 2007; 27(12): 1147-50.
- [18] Uittenbogaard LB, Haak MC, Spreeuwenberg MD, VanVugt JMG. Fetal cardiac function assessed with four-dimensional ultrasound imaging using spatiotemporal image correlation. *Ultrasound Obstet Gynecol* 2009; 33(3):272-81.
- [19] DeVore GR, Falkensammer P, Sklansky MS, Platt LD. Spatio-temporal image correlation (STIC): new technology for evaluation of the fetal heart. *Ultrasound Obstet Gynecol* 2003; 22(4):380-7.
- [20] Gonçalves LF, Lee W, Espinoza J, Romero R. Examination of the fetal heart by four-dimensional (4D) ultrasound with spatio-temporal image correlation (STIC). *Ultrasound Obstet Gynecol* 2006; 27(3):336-48.
- [21] Nelson TR, Pretorius DH, Sklansky M, Hagen-Ansert S. Three-dimensional echocardiographic evaluation of fetal heart anatomy and function: acquisition, analysis, and display. *J Ultrasound Med* 1996; 15(1):1-9.
- [22] Gonçalves LF, Espinoza J, Lee W, Mazor M, Romero R. Three- and four-dimensional reconstruction of the aortic and ductal arches using inversion mode: a new rendering algorithm for visualization of fluid-filled anatomical structures. *Ultrasound Obstet Gynecol* 2004; 24(6):696-98.
- [23] National Institute of Standards and Technology. Guidelines for Evaluating and Expressing the Uncertainty of NIST Measurement Results. <http://emtoolbox.nist.gov/Publications/NISTTechnicalNote1297s.pdf> (July 13 2009).
- [24] Bartlett JW, Frost C. Reliability, repeatability and reproducibility: analysis of measurement errors in continuous variables. *Ultrasound Obstet Gynecol* 2008; 31(4): 466-75.
- [25] Hamill N, Romero R, Hassan S, *et al.* The repeatability and reproducibility of fetal cardiac ventricular volume calculations utilizing Spatio-Temporal Image Correlation (STIC) and Virtual Organ Computer-aided AnaLysis (VOCAL™). *J Ultrasound Med*, 2009; 28:1301-1311.
- [26] Mielke G, Benda N. Cardiac output and central distribution of blood flow in the human fetus. *Circulation* 2001; 103(12):1662-8.
- [27] Stewart WJ, Jiang L, Mich R, Pandian N, Guerrero JL, Weyman AE. Variable effects of changes in flow rate through the aortic, pulmonary and mitral valves on valve area and flow velocity: impact on quantitative Doppler flow calculations. *J Am Coll Cardiol* 1985; 6(3):653-62.
- [28] Eik-Nes S, Marsal K, Kristofferson K. Methodology and basic problems related to blood flow studies in the human fetus. *Ultrasound Med Biol* 1984; 10(3):329-37.
- [29] Chaoui R, Heling KS, Taddei F, Bollmann R. Doppler echocardiographic analysis of blood flow through the fetal aorta and pulmonary valve in the second half of pregnancy. *Geburtshilfe Fraunheilkd* 1995; 55(4): 207-17.

- [30] Rasanen J, Wood DC, Weiner S, Ludomirski A, Huhta JC. Role of the pulmonary circulation in the distribution of human fetal cardiac output during the second half of pregnancy. *Circulation* 1996; 94(5): 1068-1073.
- [31] Thornburg KL, Reller MD. Coronary flow regulation in the fetal sheep. *Am J Physiol* 1999; 277(5 Pt 2): R1249-60.
- [32] Schmidt KG, Silverman NH, Hoffman JIE. Determination of ventricular volumes in human fetal hearts by two-dimensional echocardiography. *Am J Cardiol* 1995; 76(17):1313-16.
- [33] Allan LD, Chita SK, Al-Ghazali W, Crawford DC, Tynan M. Doppler echocardiographic evaluation of the normal human fetal heart. *Br Heart J* 1987; 57(6):528-33.
- [34] De Smedt MC, Visser GH, Meijboom EJ. Fetal cardiac output estimated by Doppler echocardiography during mid- and late gestation. *Am J Cardiol* 1987; 60(4):338-42.
- [35] Kenny JF, Plappert T, Doubilet P, *et al.* Changes in intracardiac blood flow velocities and right and left ventricular stroke volumes with gestational age in the normal human fetus: a prospective Doppler echocardiographic study. *Circulation* 1986; 74(6):1208-16.
- [36] Veille JC, Sivakoff M, Nemeth M. Evaluation of the human fetal cardiac size and function. *Am J Perinatol* 1990; 7(1):54-9.
- [37] Anderson PAW. Myocardial development. In *Fetal and Neonatal Cardiology*, Long W (ed.). W.B. Saunders: Philadelphia, PA, 1990; 17-38.
- [38] Teitel DF. Physiologic Development of the Cardiovascular System in the Fetus. In *Fetal and Neonatal Physiology* (3<sup>rd</sup> edition), Polin RA, Fox WW, Abman H (eds.). W.B. Saunders: Philadelphia, PA, 2003; 609-19.
- [39] Winberg P, Jansson M, Marions L, Lundell BP. Left ventricular output during postnatal circulatory adaptation in healthy infants born at full term. *Arch Dis Child* 1989; 64:1374-78.
- [40] Pemberton J, Li X, Kenny A, Davies CH, Minette MS, Sahn DJ. Real-time 3-dimensional Doppler echocardiography for the assessment of stroke volume: an in vivo human study compared with standard 2-dimensional echocardiography. *J Am Soc Echocardiogr* 2005; 18(10):1030-36.

---

## **Feasibility, Technique and Potential Role of Fetal Cardiovascular MRI: Evaluation of Normal Anatomical Structures and Assessment of Congenital Heart Disease**

**Lucia Manganaro\*, MD, Marco Di Maurizio, MD and Sara Savelli, MD**

*Dept of Radiology, Università di Roma "La Sapienza" Rome and \*Ospedale Meyer Florence Italy*

**Abstract** Fetal magnetic resonance imaging (MRI) is a third-level diagnostic tool for the study of fetal malformations and has been applied in the diagnosis and definition of fetal central nervous system (CNS) and other fetal, placental and uterine diseases. Recent developments of new realtime sequences during free breathing without cardiac triggering have established a potential role of MRI in the study of fetal heart: MRI can study the morphology using steady-state free precession (TrueFISP) sequences on sagittal, coronal and axial planes, orthogonally oriented to the fetal diaphragm and allows to identify the viscero-atrial situs, the heart and its axis. It is also possible to perform a dynamic study, through the acquisition of cine-MR sequences with real-time steady-state free precession (SSFP) oriented according to the standard projections used in fetal echocardiographic scannings. At the moment, there is no evidence that short-term exposure to electromagnetic fields of 1.5 T or less harms the fetus. MRI can analyze the normal anatomy by transverse, long axis and angulated views to visualize the principal cardiac planes. There are recent evidences of a useful role of MRI in the definition of congenital heart disease (CHD). The study of fetal CHD can be made by direct signs such as volumetric abnormalities of the heart and of the cardiac chambers, abnormalities of the structure, thickness and signal intensity of the myocardial walls, anomalies of the cardiac axis orientation, defects of the ventricular and atrial septa and anomalies of the origin, size and course of the great arteries. The difficulty to recognize a "normal" anatomical structure in the reference projections, the increase of the vascular size before a vascular stenosis and the presence of cardiomegaly and pericardial effusion are instead considered as indirect signs of CHD are considered as suspect for fetal CHD. Despite current limitations, fetal MRI seems to be a promising diagnostic method for the assessment of the fetal heart.

**Key Words:** Fetal MRI, Fetal Heart, Congenital Heart Disease.

### **INTRODUCTION**

Fetal echocardiography is at present the most commonly used diagnostic technique to detect congenital heart diseases (CHD). The application of echocardiography has completely modified diagnosis, counselling, management and least but not last prognosis of CHD, thanks to early characterization of these diseases in the prenatal period [1-3].

The main limitations of fetal echocardiography are well known and classifiable as intrinsic, like the direct operator experience and ability-dependence and ultrasonography equipment-dependence, and extrinsic, related to mother or fetus, like maternal habitus, oligohydramnios, gestational age and fetal position[4,5].

Thanks to recent technologic development and to the availability of the ultrafast sequences, it is now possible to use Magnetic Resonance Imaging (MRI) as III level method in the definition of fetal malformative diseases, after obstetrical screening and specialized ultrasonography performed in II level centres.

MRI examination allows a global evaluation of a case, through the analysis of both anatomy of the district of interest and its possible disruption expressed by modifications in signal intensity of parenchyma and affected organs.

In particular MRI may be useful in case of complex fetal anomalies or uncertain pathological conditions, ultrasonography (US) may not always allow to obtain adequate diagnostic information for therapeutic management of pregnant patient [6,7].

Thanks to high spatial resolution and the multiplanar imaging, MRI turns out to be suitable for documenting fetal diseases, particularly useful to study central nervous district and fetal body, as it has been recently reported in many

---

\*Address correspondence to Lucia Manganaro: Dept of Radiology, Università "La Sapienza" Rome Italia E-mail: lucia.manganaro@uniroma1.it

papers of medical literature [8].

For a very long time, heart has represented an exception to the diagnostic possibilities of MRI above described, behaving like a real “black hole” [9]. This technical lack of fetal MRI (FMR) in representing fetal cardiovascular structures is due to three typologies of factors, concerning MRI method:

Small size of fetal heart and big vessels, which make the use of high spatial resolution sequences necessary; High heart rate, which requires high temporal resolution sequences; High blood flow, which requires high-quality sequences, not susceptible to moving fluids. Sequences usually used in FMR, single shot T2-weighted, cannot sample the signal coming from moving blood through heart and vessels and represent these structures as black, due to the absence of signal caught at that level.

On the other hand in adult patients MRI has become the gold standard for the characterization of anatomy, functionality and cardiac volumetry. On this basis some authors has recently begun to evaluate the potential role of MRI in the study of fetal cardiac diseases thanks to the use of new real-time free-breathing sequences without cardiac triggering and with good temporal and blood- myocardial contrast resolution, able to offer a representation of the cardiac dynamics and morphology [10].

## **SAFETY**

MRI does not use ionizing radiations and up to now no detrimental effects have been shown for the fetus with exposition fields of 1.5 Tesla (T) or less. According to the last guidelines (Safety Committee of the Society for Magnetic Resonance Imaging), fetal MRI is recommended to be performed after the II trimester of pregnancy when other methods based on non-ionizing radiations are inadequate or inconclusive for the diagnostic characterization of the disease or if MRI is believed to provide critical information about therapeutic management and planning of pregnancy[11].

The main factors that can determine problems to the fetus are to be linked with three components of MRI equipment: magnetic field, radiofrequency and gradients. Queasiness, metallic taste and dizziness are the only side effects described for static magnetic fields up to 1.5 T.

More important are, instead, problems as amniotic liquid and fetus warming, noise and peripheral nervous stimulation caused by radiofrequency and gradients.

A rise of 2 °C or more in temperature has theratogenic effects to fetal central nervous system. However in vivo and in vitro studies on pregnant animals and human fetal samples do not show a meaningful temperature rise either on the maternal surface nor at fetal level, with a maximum rise value of 0.5 °C in 15 minutes and 1.5 T magnet studies. [12].

Neither a meaningful noise increase or auditory damages to children exposed to MRI in utero has been demonstrated, while amniotic liquid in fetal auditory canal has been indicated as protective factor against auditory damages [13].

Finally, turning on and off gradients during the acquisition of sequences determines mainly maternal skin surface warming, while the temperature decreases gradually when the distance from body margin increases.

The only general recommendation among fetal MRI operators is to alternate high SAR sequences with low SAR sequences during the examination, in order to let disperse, during this gap, warm that may had been created by high SAR sequences[14].

## **RESONANCE IMAGING AND STUDY TECNIQUE**

Before performing every MRI examination an interview with the pregnant women is necessary, to ensure there are not common contraindications to MRI (cardiac pacemaker, metallic clips) and to collect clinical-



anamnesic data and to visualize ultrasound sonography and echocardiographic documentation where the pathological suspect originated. It is also important that medical staff obtains an informed consent; during this explanation a first approach have to be assessed with the patient, in order to obtain her active collaboration during sequences involving breathing and to explain fetal MRI performing procedures (duration, safety, diagnostic value).

MRI study has to be performed at least with an 1 T magnet, but the examination will be more diagnostic using a 1.5 T magnet. Different typologies of coils can be used depending also on the gestational age and sac length: phased-array or cardio multicanal surface coils are surely higher-quality because they allow to get higher signal also for limited longitudinal length (50-60 cm); you can also use integrated spine coils to study the body, since they allow to get a larger view during later gestational ages[15].

Pregnant patient lays comfortably and usually positioned supine or, if this position is not comfortable (compression of inferior vena cava, hydramnios, multiple pregnancies especially during later gestational ages), on the left side and she has to relax for a moment in this position in order to reduce spontaneous fetal movements.

In some cases, in order to minimize claustrophobic feeling, the patient can be positioned in the gantry in feet-first position. No sedatives or contrast agents are used either for fetus or for the mother.

If possible, it is recommendable to perform the examination in the morning, after a 4 hours fasting at least, since it has been proved that hypoglycemia reduces fetal movements; or, if ultrasound examination can be performed before MRI to assert fetal sleep or wakefulness stage, you can wait the sleep stage, taking into account that a regular fetal sleep-wakefulness cycle implies an alternation of this stages every 30 minutes.

Study protocol includes the acquisition of many sequences, some of them are necessary, others can be added optionally according to clinical request.

Images of each series are used as scout for the following sequences to minimize orientation problems owing to fetal position changes [16,17].

The main basic sequences used in standard fetal MRI are:

- A localizer sequence;
- A Single Shot (SSh) Half Fourier or FSE acquired T2-weighted sequence with maternal coronal plane for identification of fetal head, rachis and stomach and localization of placenta (anterior/posterior);
- A thin-slab (3-4 mm) SSh T2-weighted multiplanar-oriented sequence on axial, sagittal and coronal planes, orthogonal to the organ/district concerned, for a detailed evaluation of fetal anatomy.

The excellent compromise among spatial and contrast resolution and signal to noise ratio (SNR) of these sequences, as well as their execution speed, enable an outstanding visualization of fetal anatomy during every stage of pregnancy and, in particular, they allow to detect static fluids and structures featured by high fluid composition, like hyperintense structures, allowing then the study of fetal brain, of cavities containing fluid (nasal and oral cavity, pharynx, trachea, stomach and proximal intestine, urinary system, gall bladder), of lungs, placenta and amniotic fluid (AF). gradient-echo(GRE), 2D or 3D, breath-holding T1-weighted sequences, with and without adipose tissue signal saturation.

These sequences allow to recognize some organs and tissues thanks to the presence of blood, adipose tissue, meconium or other structures with high signal intensity on T1, enabling, in particular, to detect: thyroid or goitre or thyroidal ectopy; liver; intestinal meconium-filled loops (distal bowel), allowing differential diagnosis between urethral dilatation and megacolon; ischemic-hemorrhagic methemoglobin-filled areas and some encephalic structures like cortex, cerebellum and basal ganglia after the 24<sup>th</sup> week; placental vascular

stasis, haematoma or thromboses. Nevertheless, because of a longer acquisition time these sequences are more susceptible of artefacts caused by fetal motions [10,18].

Fetal cardiovascular study implies the use of the abovementioned thin-slab SS<sub>H</sub> T<sub>2</sub>-weighted sequences, as preliminary and anatomical sequences on three spatial planes and the acquisition of gradient-echo (GRE) steady-state free precession (SSFP) sequences on three spatial planes, to evaluate cardiac district and big vessels, according to the main views used in fetal echocardiography.

In fact, these sequences show an intermediate T<sub>1</sub> and T<sub>2</sub> contrast by using ultrashort TR (< 3ms), that is not susceptible of motions and allow to detect moving fluids as high signal intensity structures.

Cine-MR steady-state free precession (SSFP) with k-space sampling, radial and cartesian (2DFT) sequences, oriented according to standard views is also used in fetal echocardiography.

These sequences allow to detect heart and big vessels, thus obtaining the visualization of cardiac axis, evaluation of regular visceral-cardiac situs, localization of cardiac chambers and simultaneous atrial and ventricular contraction.

Combining SSFP with real-time technique has allowed the visualization of cardiac movement without triggering or synchronization with fetal heart or mother's breath-holding.

Usually an MRI study lasts from a minimum of 15 to a maximum of 20- 45 minutes.

## **ANATOMY AND ACQUISITION TECHNIQUE**

The study of fetal heart with MRI technique is now possible by acquiring morphologic and dynamic sequences with multiplanar scans, using, in particular, two different techniques of anatomical planes acquisition [4,5].

The first technique is based on the acquisition of orthogonal view on three corporal axes (axial, coronal and sagittal) and multiple axial, sagittal and oblique scans, reproducing the main echocardiographic views, in particular [19,20]:

- Transverse views (four chamber view, origin of aorta (five chambers), pulmonary outflow tract (three vessels), aortic arch);
- Sagittal views (short-axis views of the left ventricle, tricuspid-aorta, long-axis of the ductus arteriosus, long-axis of the aortic arch);
- Oblique view (simultaneous visualization of long-axis view of the left ventricle, aortic arch and aortic duct).

The second acquisition method implies the use of views orthogonal to three corporal axes (axial, coronal, sagittal) and orthogonal to cardiac axes (long and short) following the technique usually performed in adult cardiac MRI [21]: in particular

- Orthogonal to cardiac long-axis (long horizontal and vertical axis of the heart, four chamber view);
- Orthogonal to cardiac short-axis (medium and basal short cardiac axis).

Both these techniques allow to determine heart position, its size, cardiac axis orientation, evaluation of location, position and size of cardiac chambers, main inflow vessels (SVC, IVC and pulmonary veins) and outflow vessels (Aorta, Ao, and Pulmonary Artery, PA), the concordance between ventricles and outflow vessels, aortic arch course and calibre.

Anatomical study of the heart implies systematic evaluation of cardiac orientation and volumetry, morphology and volumetry of cardiac chambers and the structure of myocardial walls, as well as the study of integrity of interventricular (IVS) and interatrial septum (IAS) with foramen ovalis (FO).

Anatomical study of big vessels, instead, implies evaluation of origin, calibre and course of cardiac outflow vessels (aorta, Ao, pulmonary artery, PA) and arterial duct (AD) and evaluation of calibre and course of inflow vessels (superior vena cava, SVC, inferior vena cava, IVC, pulmonary veins, PV).

In this study, we will refer to MRI views based on main echocardiographic views and a short MRI iconographic gallery will be shown, with anatomical structures that have to be visualized and analyzed on different acquisition planes.

## TRANSVERSE VIEWS

### Four Chambers (Figure 1)

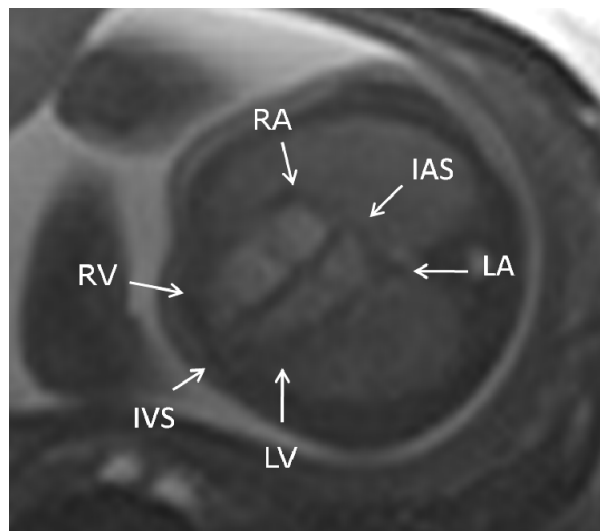


**Figure 1:** Showing the transverse view of the fetal thorax (RA right atrium, RV right ventricle, LA left atrium, LV left ventricle, IVS ventricular septum, IVA atrial septum)

Through this view we can analyse:

- Heart size compared to thorax (heart-thorax ratio)
- Position of cardiac apex
- Cardiac axis
- Structure of cardiac chambers
- Atrio-ventricular valvular plane (AVP)
- Ventricular and atrial septa

Four chamber plane evaluates first of all atrial and ventricular chambers sizes, apex orientation, cardiac axis angle (about 44°) and myocardial thickness. At the moment we cannot evaluate the difference of thickness relating to systole and diastole.

Myocardium shows a typical hypointense signal. In particular, myocardial wall of the left ventricle is thicker, more uniform and hypointense, while it appears thinner, jagged, porous in the right ventricle. It is not always possible to document the moderator band of right ventricle apex. There are many opposing opinions about it in literature. Its bad visualisation is an MRI limitation in assessing viscera-atrial situs. Ventricular septum is well visible and its thickness and signal intensity are equal to ventricular walls.

Ventricles appear basically symmetric, triangle-shaped, more strengthened the left one, more enlarged the right one. Papillary muscles can be detected especially when they are hypertrophic in a condition of myocardial hypertrophy.

Atrioventricular valves are only indirectly detectable and they appear like a thin hypointense line, called atrioventricular plane. Atrial myometrium is thin and symmetric and atrial septum appears as a hypointense line, better visible only after the II trimester of pregnancy.

### Aortic Origin (Figure 2)

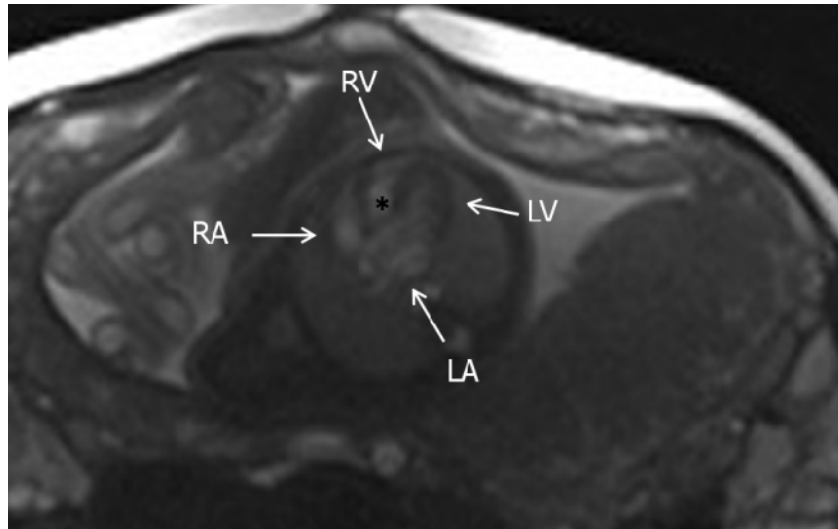


**Figure 2:** Five chambers; black asterisk Aorta origin

By this view, we can analyse the origin of the aorta from left ventricle, in the middle of the heart, as well as the structures of above-mentioned views.

### Pulmonary Outflow Tract (Figure 3)

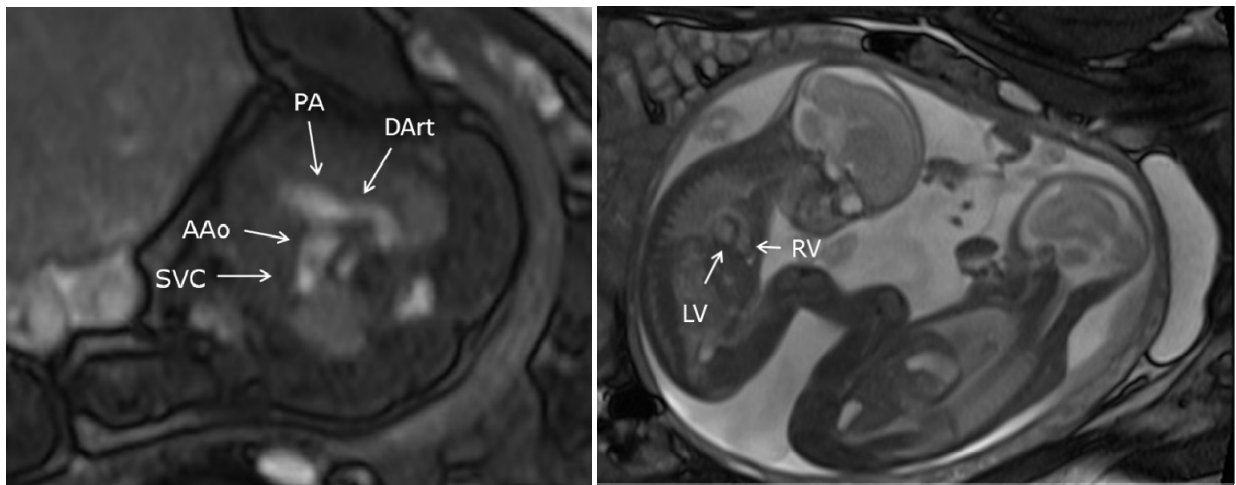


**Figure 3:** Three Vessels; SVC superior vena cava, AAo ascending Aorta, PA pulmonary artery-common tract, DArt Ductus Arteriosus)

It allows the evaluation, from right to left, of superior vena cava, aorta and pulmonary artery and the part of aortic duct that links PA to descending Ao.

## SAGITTAL VIEWS

### Long-axis of the aortic arch (Figure 4)

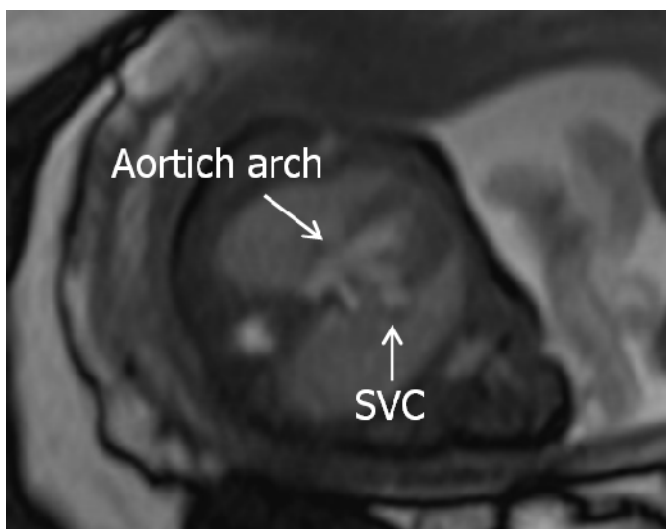


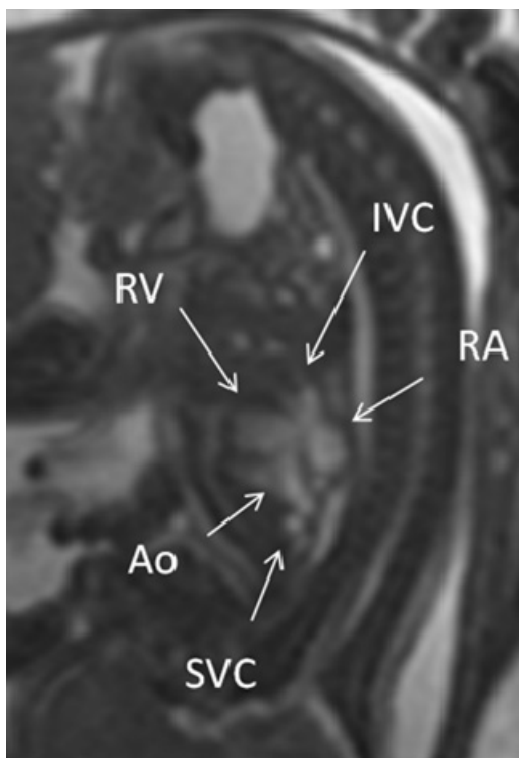
**Figure 4:** Long axis view of the aortic arch (superior vena cava SVC). This view shows both aorta arch and superior vena cava.

#### Short-axis view of the left ventricle (Figure 5)

**Figure 5:** Short axis view of the left ventricle

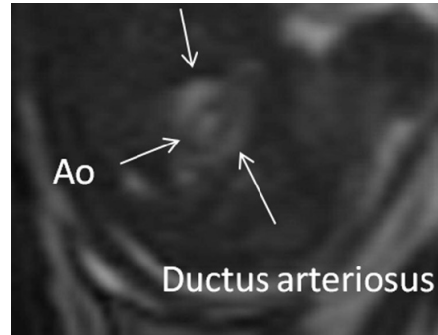
This view of the left ventricle allows a good evaluation of myocardial thickness, of the outflow tract of pulmonary artery and ventricles position.

#### Tricuspid-Aorta View (Figure 6)

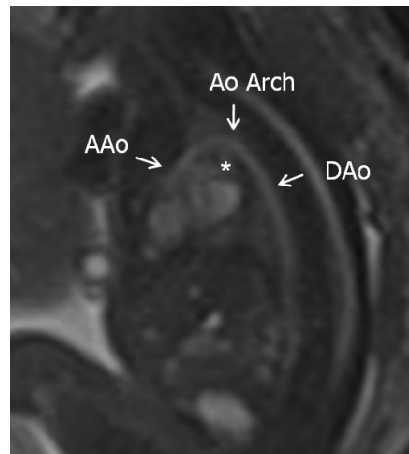


**Figure 6:** Tricuspid-aorta view (IVC inferior vena cava).

It allows to evaluate the position of right cardiac chambers and IVC and SVC inflow tract

**Aorta Outflow Tract (Figure 7)****Figure 7:** Long-axis view of aortic duct

This view allows the visualization of PA that connects with Ao through aortic duct. This forms an arch that links the descending aorta.

**Long-Axis View of the Aortic Arch (Figure 8)****Figure 8:** Long axis view of the aortic arch (white asterisk Pulmonary Artery)

This view shows the aortic arch on long axis with the origin of three epi-aortic vessels.

**OBLIQUE VIEWS****Long-Axis View of Left Ventricle (Figure 9)****Figure 9:** Long axis view of the left ventricle

This view visualizes outflow tract and the aorta at the origin and in its ascending tract.

### Arch and Aortic Duct View (Figure 10)

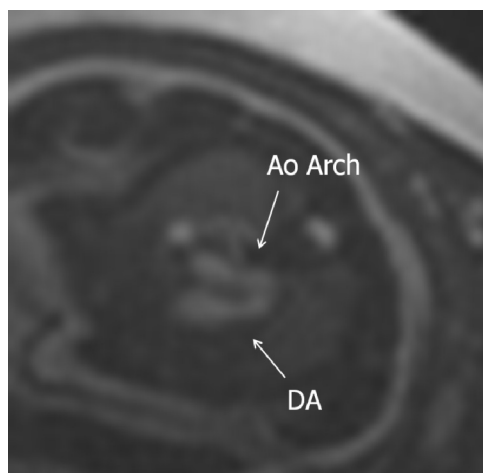


**Figure 10:** Arch and aortic duct view (DA ductus arteriosus)

It allows to visualize simultaneously arch and aortic duct and to compare their calibre and course.

Obviously, anatomical evaluation of heart and big vessels has to imply a simultaneous detecting of thoracic structures (thymus, lungs, trachea and oesophagus) and well detectable epiaortic vascular

### STRUCTURES

Auxologic data about the evaluation of cardiac structures are not yet available, being the MRI study of fetal heart quite recent. Nevertheless, first results show that data are equivalent to echocardiographic biometry data. A summary of the main views is reported in Tab 1.

**Table 1.** Summarizing table of main MRI/echocardiographic views

MRI/ECHOCARDIOGRAPHY VIEWS		VISUALIZED ANATOMICAL STRUCTURES
Transverse	4 chambers	Heart size compared to thorax Position of cardiac apex Cardiac axis Cardiac chambers structure AV valvular plane Ventricular and atrial septum
	5 chambers	4 chambers + position and connection of the aorta at the origin with the heart Superior vena cava
	3 vessels	Aorta Pulmonary artery PA that connects to the Ao via the ductus, forming a ductal arch
	Long-axis of aortic arch	Ao arch and SVC myocardial thickness
	Short-axis of left ventricle	PA outflow tract Position of ventricles
Sagittal	Tricuspid-aorta	Position of right cardiac chambers IVC and SVC outflow tract Aorta outflow tract
	Long-axis of aortic duct	PA connects to descending Ao via aortic ductus
	Long-axis of aortic arch	Aortic arch on long axis with the origin of three epiaortic vessels Left atrium
Oblique	Long axis of left ventricle	Inflow tract and aorta at the origin and in its ascendant tract
	Arterial arch and aortic duct	Simultaneous view of Ao arch and AD arch



## **PATHOLOGY**

According to the last studies published in literature, the fetal MRI of cardiovascular district and congenital cardiac diseases in utero is feasible and it is likely to be successful in the future, even though several technical limitations, only partially solved, still exist.

One of the first meaningful data about MRI study concerns its improved diagnostic accuracy during later ages of pregnancy compared to echocardiography, which is well known to be affected by limitations concerning the reduction of acoustic window (physiologic oligohydramnios) and gradual calcification in fetal ribs that impairs US propagation.

MRI study in cases of complex cardiac anomalies is certainly more difficult to arrange and understand: serious malrotation anomalies or severe ventricular hypertrophy may change normal heart geometry, thus requiring sequences oriented on new anatomical planes to be obtained during the examination itself. As a consequence longer acquisition time and sometimes sequences repetition until the correct standard anatomical view is obtained are necessary.

In MRI studies detailed knowledge of fetal cardiovascular district is fundamental and a training to learn how to perform and report an examination is necessary [22].

Some of the main limitations concern the impossibility to study by MRI cardiac rate alterations and to make hemodynamic evaluations of valve-based diseases (ex. incontinence, reflux), which can be only assumed once they have determined an anatomical alteration.

Cardiac contractility and valvular functionality, in fact, cannot be reliably evaluated by MRI. Technical impossibility of triggering fetal heart beat and still limited temporal resolution of current cine-MR sequences (2-3 frames per second) do not allow to analyse real-time cardiac functionality. The acquisition of cardiac movements is artificial, and their speed depends on the duration of acquisition of slices and not on the real velocity of atrioventricular movements.

In this research, we have tried to highlight the possibility to identify the main pathological aspects of congenital cardiovascular malformations and to create, starting from the experience and dictates of echocardiography, a new MRI semeiotics for the main congenital heart diseases.

### **MRI: Direct and Indirect Signs**

The approach to the study of congenital heart diseases in echocardiography is usually based on sequential evaluation of anatomical structures and, in particular, it consists in building, during the examination, an anatomical sequence formed by atria, ventricles and great heart vessels, thus defining atrial situs, atrioventricular and ventricular-arterial concordances [23,24].

Classification of congenital heart diseases is based on anatomical-clinical aspects. According to these we can generically classify diseases in 4 main groups:

- With pulmonary hypoinflow (Pulmonary Stenosis, Tetralogy of Fallot, Tricuspid Atresia, Tricuspid Ebstein's Anomaly)
- With pulmonary hyperinflow (interatrial septal defects, IAD, interventricular septal defects, IVD, atrioventricular septal defects, truncus arteriosus, TA, and Aorto-Pulmonary septal defects)
- With pulmonary normal inflow (anomalous systemic and pulmonary venous returns, Ao coarctation, correct Transposition of the Great Arteries, aortic Stenosis)
- Duct-dependent (pulmonary atresia of ventricular septum (VS), Transposition of great arteries, mitral-aortic Atresia, Interruption of the aortic arch)

The correct approach to identify CHD requires first a screening examination, performed through routine obstetric ultrasonography, where 4 chamber view and outflow vessels view are visualized. In case of abnormal heart

visualization or in presence of specific risk factors for congenital heart diseases, depending on familiar, personal or fetal history, a II level examination such as echocardiography considered the gold standard for congenital heart disease diagnosis, is necessary. Echocardiography have to be performed in specialist centres by paediatric heart specialists or obstetric gynaecologists with specific training.

MRI methods can be defined as a III level method that only patients with echocardiographic suspect of cardiovascular disease can undergo [25].

MRI diagnosis of simple and complex malformative diseases of fetal heart is based on a integrated evaluation of direct and indirect signs of cardiac anatomy alteration.

We consider **direct** signs of cardiovascular disease the following aspects: morpho-volumetric anomalies of cardiac chambers and myocardium, malrotations, septal defects and anomalies of the origin, course and calibre of great vessels; while we consider **indirect** signs the absence of anatomical structures in the preliminary view, the prevascular calibre increase due to stenosis, the presence of cardiomegaly or pericardial effusion.

On the basis of these preliminary considerations we can classify MRI congenital heart diseases in three groups: diagnosable by the identification of direct signs, diagnosable by the identification of indirect signs or more often diagnosable by the identification of both typologies of signs [26].

#### Direct signs:

Ventricular septum defects both isolated and associated like in tetralogy of Fallot or truncus arteriosus are directly visualized as a solution of continuity of septum into infundibular, membranous or muscular part (Fig. 11), in particular by the acquisition of 4 chambers views and short-axis sagittal view of left ventricles. It is not always easy to distinguish an isolated IVD from other multiple and contiguous IVDs, especially in case of complex pathologic conditions.

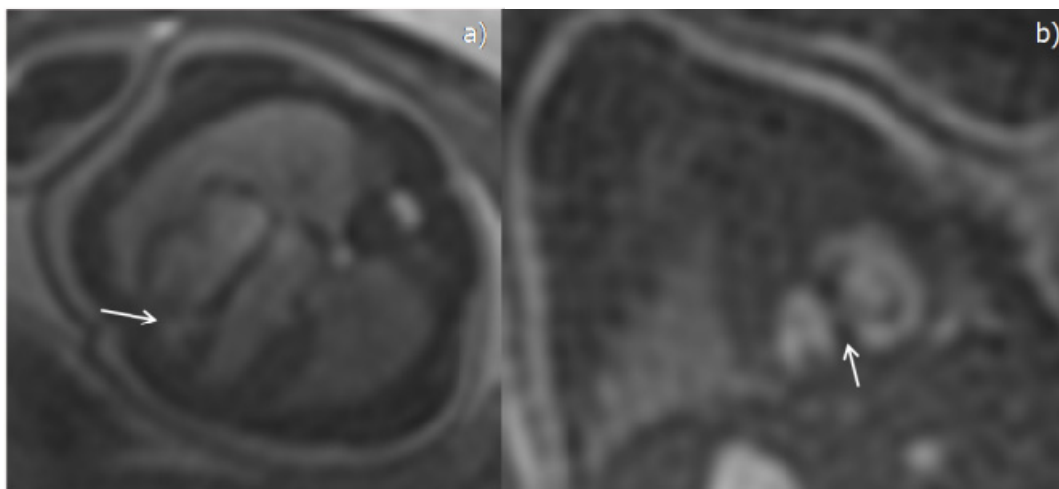


**Figure 11:** A millimetric solution of continuity of ventricular septum into muscular part, well showed by the acquisition of 4 chambers views (a) and short-axis sagittal view of left ventricle (b).

In complete atrioventricular canal, a great defect of IVS and IAS, for example, crux septum-primum, with disappearance or anomalous representation of atrioventricular plane, are considered direct diagnostic elements, even though valves cannot be visualized. Defining defect balancing or misbalancing depends on morpho-volumetric evaluation of two ventricular chambers and on the analysis of signal and myocardial thickness.

Hypoplastic left heart syndrome (Fig. 12) is detected also by MRI as a volumetric reduction of both cardiac left chambers till they become virtual volumes, with right ventricle forming the cardiac apex; there are also other direct signs concerning the calibre of Aorta, which appears particularly reduced at the arch level, and of the aortic duct, which appears increased in oblique view of the arch and aortic duct (in cases of duct-dependence of systemic circulation). Particularly useful are dynamic sequences that allow to detect small cavity of hypoplastic ventricle, that, due to its stuck walls, is sometimes undetectable with static sequences.

In situs inversus the position of heart and stomach on the right side is easily detectable, first of all by the position of fetus compared to the mother, thus defining right and left sides of fetus itself. In case of heterotaxic syndromes, instead, making differential diagnosis might be more complex.

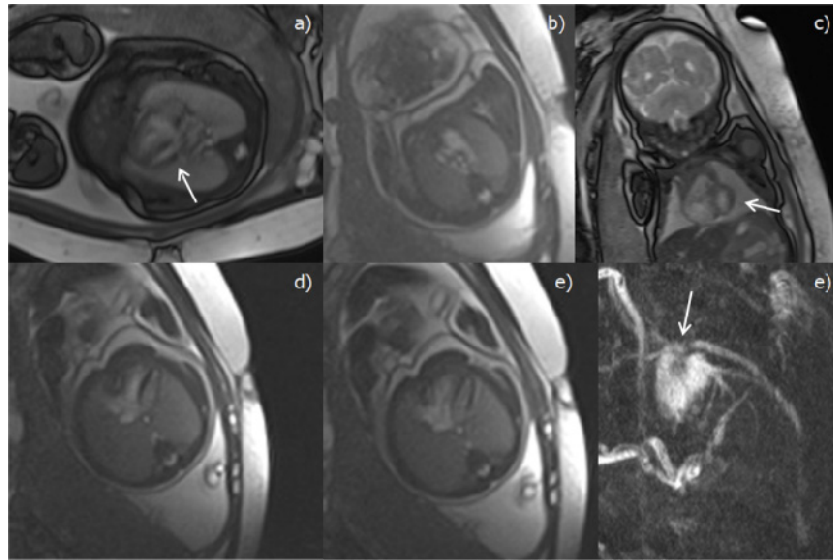


**Figure 12:** Hypoplastic left heart syndrome. Volumetric reduction of both cardiac left chambers till they become virtual volumes, with right ventricle forming the cardiac apex, on 4 chambers view (a) and coronal plane (c), in diastolic (d) and systolic phases (e); there are also other direct signs concerning the calibre of Aorta, which appears particularly reduced at the arch level (f) and of the aortic duct, which appears increased in oblique view of the arch and aortic duct (in cases of duct-dependence of systemic circulation) (b).

Anomalies of the origin (transposition of great vessels, overriding aorta, balanced truncus arteriosus) and course of great vessels (right-sided aortic arch) are all visualized by direct characterization of the vessel/s with anomalous origin or course. (Table 2, Figs. 13 and 14)

**Table 2.** Direct signs of morpho-volumetric anomalies

### MORPHO-VOLUMETRIC ANOMALIES

Cardiomegaly

Left heart hypoplastic syndrome

VS defects (isolated and associated)

Tricameral biventricular heart

Situs ambiguous with right isomerism

Complete atrioventricular canal

Myocardial anomalies

(ex. Spungious cardiomyopathy, myocardial hypertrophies)

Left-malrotation

Right-malrotation

Tuberous sclerosis

(Multiple rhabdomyomas)

Pericardial effusion

### DIRECT MRI SIGN

Cardiac- thoracic perimeters ratio inferior to 1/3

Volumetric reduction of both left cardiac chambers till they become virtual volumes and right ventricle forming cardiac apex

Solution of continuity of septum in infundibular, membranous and muscular part

One large atrial chamber and two ventricles

Stomach on the right side, transversalized medium liver, medium heart with apex on the left side and normal ventricles localization

Large VS and AS defect (crux septum primum) with disappearance of atrioventricular plane

Myocardial walls thickening compared to expected value considering gestational age according to normograms, acute signal hypointensity, more compact structure of myocardial wall, hypertrophic papillary muscles

Inclination angle of cardiac axis superior than 55° or inferior to 35° to meridian sagittal line

Multiple hypointense nodularities spread through myocardial walls

Hyperintense fluid pericardial > 2 mm thickness

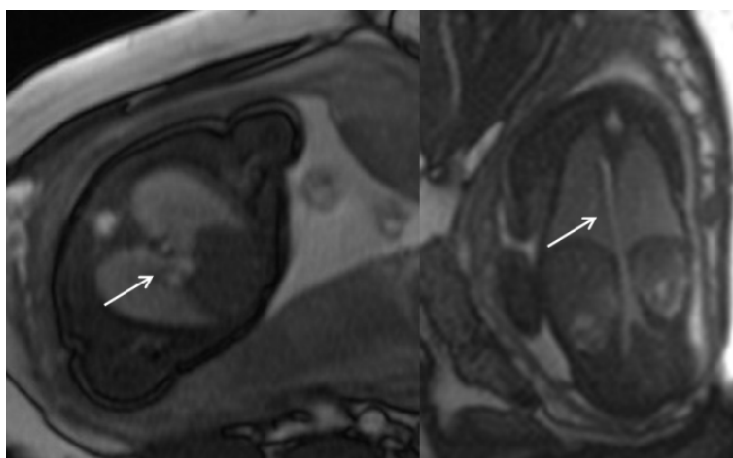


**Figure 13:** Right-sided aortic arch. The arch coursed from right to right directly posteriorly to join the descending Ao on the axial and coronal planes detected a right-sided aortic arch;

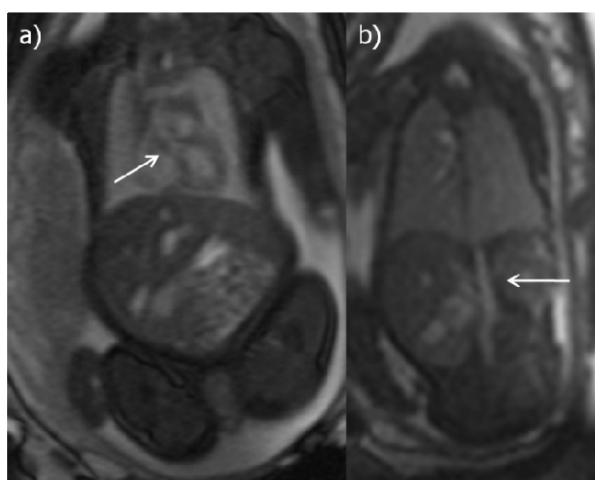


**Figure 14:** Right-sided aortic arch. Ascending Ao shows a normal origin and the descending tract crossed the midline at the level of diaphragmatic hiatus and lied just to the left of the abdominal spine.

In the transposition of the great arteries (TGA) (Fig. 15, 16 and 17) MRI allows to evaluate, by integrating dynamic and static sequences, the origin and the course of PA and Ao and ventricle-arterial discordance.

Defining a condition of correct transposition of great arteries (CTGA) might be more complex, especially during earlier gestational ages since it is more difficult to find the moderator band and consequently RV; through direct and indirect signs, instead, frequent associated anomalies, as, for example, large IVD and VA plane anomalies (direct) and right outflow tract obstruction (indirect), can be documented better.

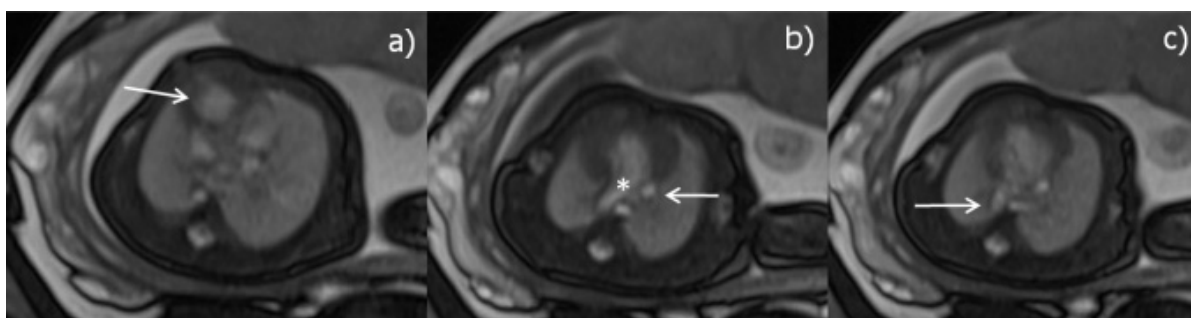


**Figure 15:** Complete transposition of the great vessels (TGA) with left ventricle hypoplasia and PA atresia. Transverse planes show the Ao (white arrow) arising from the RV (a), continuing into the arch (b, white asterisk Aortic arch, white arrow superior vena cava) and the descending tract that lies on the correct left side of the spine (white arrow in c), direct signs of TGA;

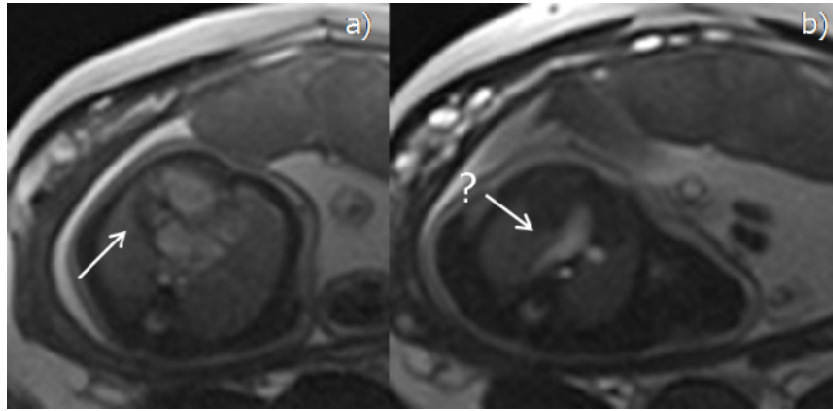


**Figure 16:** Complete transposition of the great vessels (TGA) with left ventricle hypoplasia and PA atresia.) Left ventricle appears particularly reduced of volume (white arrow in a) and on the three vessels view is not visualized PA and ductus arteriosus, indirect signs of PA atresia (white arrow in b)

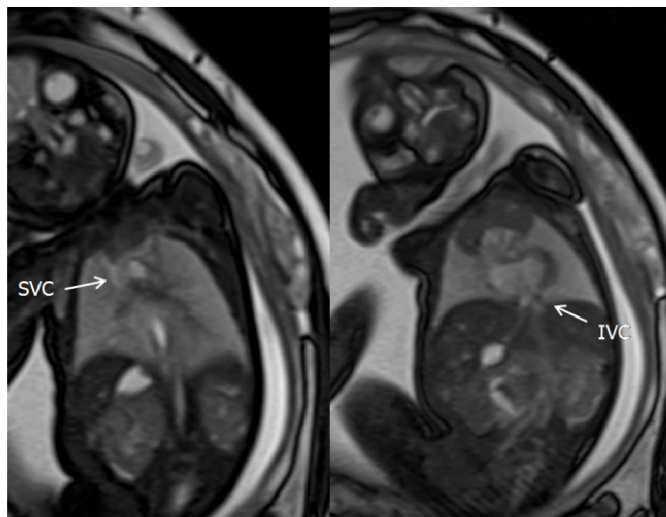


**Figure 17:** Complete transposition of the great vessels (TGA) with left ventricle hypoplasia and PA atresia.) Normal inflow in the right atrium of SVC and IVC with increased calibre

Also in Truncus arteriosus, through the integration of direct and indirect signs, we can define better direct visualization of a single cardiac outflow vessel (Fig 18 and 19) as well as the general pathological condition, by characterizing, in particular, the right position of the aortic arch and its potential interruption, its agenesis or AD dilatation, potential IVD (direct) and truncal valve stenosis that determines dilatation of ventricular chambers (indirect).

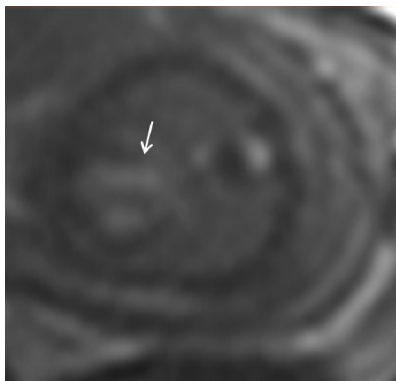


**Figure. 18:** Truncus Arteriosus type 2. The image on axial planes shows: a unique efflux vessel overriding the ventricles (truncus arteriosus, TA, white arrow).

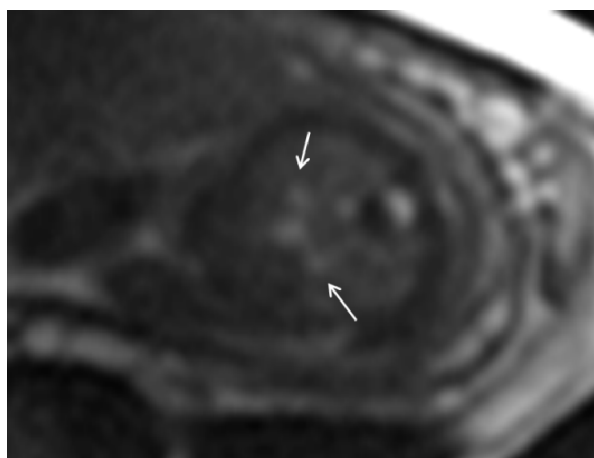


**Figure. 19:** Truncus Arteriosus type 2. The image on axial planes shows: a unique efflux providing both the lungs (right and left pulmonary artery) (white arrows) and continues the same way of the aorta.

The main direct signs of hypertrophic cardiomyopathy are: increase of myocardial walls thickness compared to expected value, considering gestational age (measured from endocardiac surface to epicardiac surface), acute signal hypointensity and more compact structure of myocardial wall, together with hypertrophic papillary muscle; the diagnosis of this primitive disorder of cardiac muscle is proved by echocardiography, which excludes mechanic and valvular causes.

The anomaly of origin and course of PA and Ao together with morpho-volumetric alteration of ventricles allows to recognize a condition of double-exit right ventricle (Fig. 20) and in particular: both outflow vessels origins mainly from right ventricles, showing an anomalous course, basically parallel, which is often associated with discontinuity of atrioventricular plane and IVD.

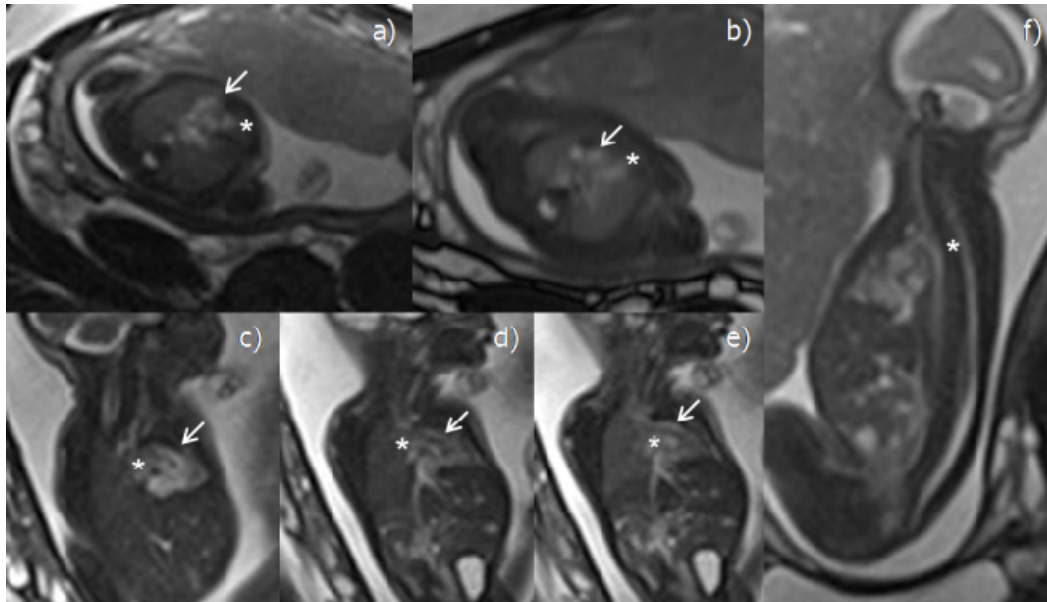


**Figure. 20:** Double-exit right ventricle. and in particular: both outflow vessels (white asterisk Aorta, white arrows PA) origins mainly from right ventricles, showing an anomalous course, basically parallel, which is often associated with discontinuity of atrioventricular plane and IVD.

In case of tuberous sclerosis, identification of common cardiac hamartomas (Fig. 21 and 22) by RMI is direct. They are spread more frequently in left ventricle or along IVS and with movable cardiac walls, as you can see in dynamic MR-cine sequences, and appear acutely hypointense in T2-weighted sequences and EGR sequences and hyperintense in T1-weighted sequences; moreover, thanks to multiplanarity and multiparametricity of the method, also subependymal nodules along cerebral ventricles and in Monro's foramen are easily detectable and identifiable.



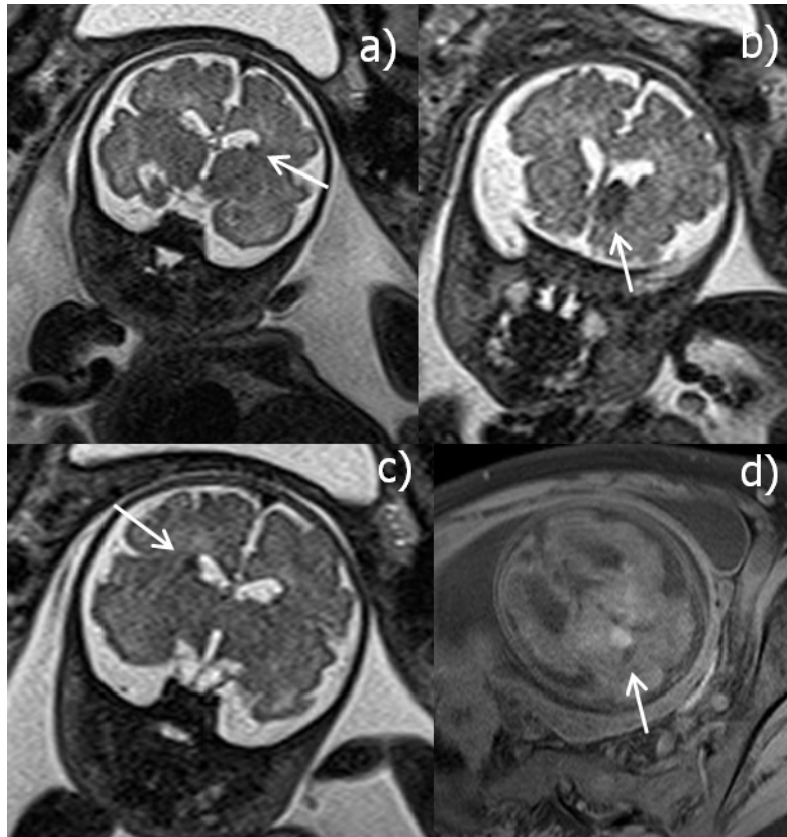


**Figure. 21:** Tuberous sclerosis. The SS T2 weighted images on the coronal plane (a,b,c) and T1 weighted with Fat Saturation image (d) on axial plane of the fetal head detect small subependymal nodules;

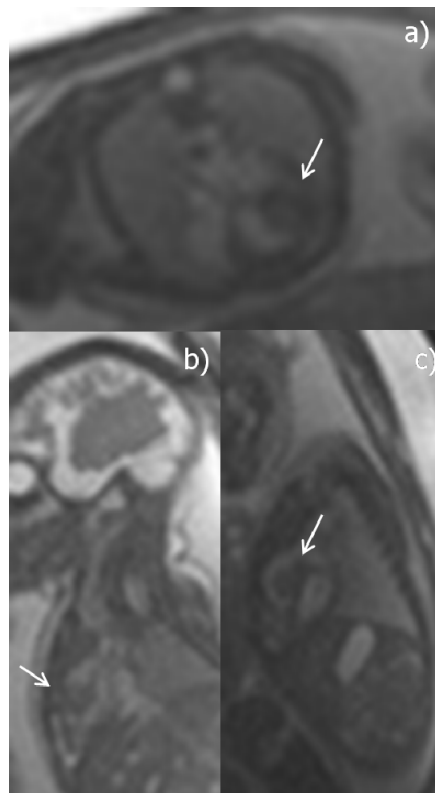


**Figure 22:** Tuberous sclerosis The gradient-echo (GRE) steady-state free precession images on the transverse (a) and long-axis (b,c) planes show a big nodular hypointense lesion localized on the right Atrioventricular valvular plane (white arrows).



## Indirect Signs

Vessels calibre anomalies and valves anomalies (Ao coarctation, pulmonary atresia/stenosis, mitral-aortal disease, tricuspid atresia) are basically revealed by indirect signs, in particular dilatation of cardiac chambers caused by vessel stenosis and post-stenotic dilatation. (Tables 3, 4)

**Table 3.** Indirect signs of valvular and great vessels anomalies

<b>VESSELS CALIBRE ANOMALIES / VALVULAR ANOMALIES</b>	<b>INDIRECT SIGN</b>
Pulmonary stenosis	RV dilatation and hypertrophy + lack of visualization of right outflow tract and PA
Tetralogy of Fallot Pulmonary Artery hypoplasia	RV dilatation + direct signs + reduction or lack of visualization of right outflow tract and PA
Coarctation of the Aorta	LV dilatation and bad visualization of ascendant Ao and Ao arch
Tricuspid atresia	RA dilatation
Mitral-aortal disease	LV volumetric reduction with myocardial hypertrophy and episodes of slowing and turbulence of blood flow

**Table 4.** Indirect signs of anomalies of the origin and course of great vessels

<b>ANOMALIES OF THE ORIGIN AND COURSE OF GREAT VESSELS</b>	<b>MRI DIRECT SIGN</b>
Balanced truncus arteriosus	One single arterial outflow vessel that overrides VS
Complete transposition of great arteries	Ao originates from RV and PA originates from LV in heart with normal atrio-ventricular concordance
Overriding aorta (Tetralogy of Fallot, IVD)	middle-placed origin of Ao, overriding VS and two ventricles
Right-positioned aortic arch	Aortic arch with right- to-left course

Aortic arch and PA hypoplasia are directly visualized by detecting with standard views corresponding vessels, characterized by small sizes compared to surrounding vessels, even though differential diagnosis excludes an outflow obstructive disease of corresponding ventricles.

Since we cannot rely on a correct MRI evaluation about blood flow direction and characteristics, characterizing correctly this homogeneous group of heart diseases is more difficult.

In aortic coarctation it is possible to determine different typologies of obstruction related to the origin of epiaortic vessels (distally to left subclavian artery, between common left carotid artery and subclavian artery and between left common carotid and right truncus arteriosus) especially associated to indirect calibre increase or decrease.

The main indirect signs of diagnosis of aortic stenosis are volumetric alteration of left ventricle, potential dilatation of right ventricle, myocardial wall thickening, generalised hydrops and growth retardation.

In pulmonary atresia/stenosis conditions the main MRI signs are volumetric alteration of right ventricle (mainly increase), together with right atrium widening and myocardial hypertrophy, reduction or lack of visualization in preliminary views of right outflow tract and PA. (Fig. 23, [video 1](#))

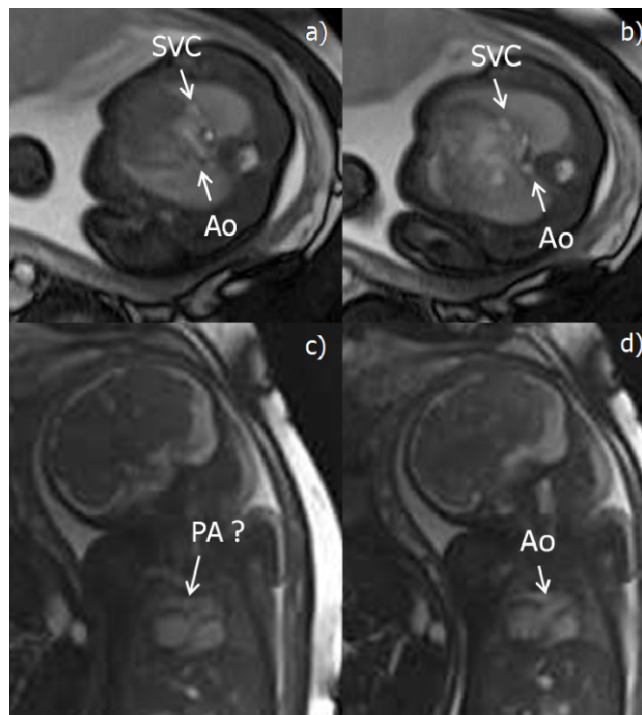


**Figure. 23:** Volumetric widening of right ventricle and atrium with lack of visualization on axial and coronal views of right outflow tract and PA (indirect signs)

It is important to notice that in every gestational age the evaluation of smaller vascular structures, like pulmonary veins, is more difficult, probably because of limited spatial resolution, and it is also more difficult to detect cardiac outflow vessels during earlier gestational weeks, probably because of their small sizes and because of increased fetal motion during MRI acquisition noticed during these gestational ages.

## CONCLUSIONS

The use MRI in evaluating fetal heart still reveals some diagnostic limitations secondary to two typologies of factors: intrinsic and extrinsic.

The first intrinsic limitation concerns technical problems: it is still necessary to develop the equipment in order to overcome some lacks such as the low spatial and temporal resolution. Because of these limitations it is not possible to reproduce or give direct information about valvular or rate diseases.

The second extrinsic limitation is the still limited experience that is based on the few data still available in the literature. Multicentric studies are therefore necessary to acquire more experience, to construct biometric reference limits and generate diagnostic guidelines.

In the immediate future the use of dedicated sequences, with potential pseudo-angiographic study, might open new horizons. Similarly the application of new 3T magnet field equipments might increase spatial resolution. New possibilities of therapeutic treatments during prenatal period will undoubtedly require further efforts to reach higher image quality.

These will be our future challenges.

At the moment MRI can be performed in accurately selected cases, for unsure or multi-organ disease, where accurate counselling is necessary to plan clinic therapeutic iter of baby patient.

## REFERENCES

- [1] Carvalho JS. Fetal echocardiography. A sophisticated tool in obstetrics. *Minerva Cardioangiol* 2005;53:129–38.

- [2] Allan L. Technique of fetal echocardiography. *Pediatr Cardiol* 2004;25:223–33.
- [3] Cooper MJ, Enderlein MA, Dyson DC, Rog'e CL, Tarnoff H. Fetal echocardiography:retrospective review of clinical experience and an evaluation of indications. *Obstet Gynecol* 1995;86:577–82.
- [4] Jeanty P, Chaoui R, Tihonenko I, Grochal F. A review of findings in fetalcardiac section drawings. Part 1: The 4-chamber view. *J Ultrasound Med* 2007;26:1601–10.
- [5] Jeanty P, Chaoui R, Grochal F, Tihonenko I. A review of findings in fetal cardiac section drawings. Part 2: High abdominal views. *J Ultrasound Med* 2007;26:1743–6.
- [6] DeVore GR. Influence of prenatal diagnosis on congenital heart defects. *Ann N Y Acad Sci* 1998;847:46–52.
- [7] Deng J, Rodeck CH. New fetal cardiac imaging techniques. *Prenat Diagn* 2004;24:1092–103.
- [8] Chiappa E. The impact of prenatal diagnosis of congenital heart disease on pediatric cardiology and cardiac surgery. *J Cardiovasc Med* 2007;8:12–6.
- [9] Yang PC, Kerr AB, Liu AC, *et al.* New real-time interactive cardiac magnetic resonance imaging system complements echocardiography. *JamColl Cardiol* 1998;32:2049–56.
- [10] Manganaro L, Savelli S, Di Maurizio M, *et al.* Potential role of fetal cardiac evaluation with magnetic resonance imaging: preliminary experience. *Prenat Diagn* 2008;28:148–56.
- [11] De Wilde JP, Rivers AW, Price DL A review of the current use of magnetic resonance imaging in pregnancy and safety implications for the fetus. *Prog Biophys Mol Biol* 2005; 87: 335-353.
- [12] Hand JW, Li Y, Thomas EL, Rutherford MA, Hajnal JV Prediction of specific absorption rate in mother and fetus associated with MRI examinations during pregnancy. *Magn Reson Med* 2006; 55: 883-893.
- [13] Levine D, Zuo C, Faro CB, Chen Q Potential heating effect in the gravid uterus during MR HASTE imaging. *J Magn Reson Imaging* 2001; 13: 856-861.
- [14] Dimbylow P (2007) SAR in the mother and foetus for RF plane wave irradiation. *Phys Med Biol* 2007; 52: 3791-3802.
- [15] Muthupillai R, Cheong B, Pereyra M, Flamm SD Fast 3D cine steady-state free precession imaging with sensitivity encoding for assessment of left ventricular function in a single breath-hold. *Am J Roentgenol* 2006; 187: 1235-1239.
- [16] Shankaranarayanan A, Simonetti O P, Laub G, Lewin J S, Duerk JL (2001) Segmented k-Space and Real-Time Cardiac Cine MR Imaging with Radial Trajectories. *Radiology* 2001; 221: 827-836.
- [17] Deng J, Rodeck CH New fetal cardiac imaging techniques. *Prenat Diagn* 2004; 24: 1092–1103.
- [18] Gorincour G, Bourli'e Re-Najean B, Bonello B, *et al.* Feasibility of fetalcardiac magnetic resonance imaging: preliminary experience. *UltrasoundObstet Gynecol* 2007;29:105–10.
- [19] Carvalho JS Fetal echocardiography. A sophisticated tool in obstetrics. *Minerva Cardioangiol* 2005; 53: 129–138.
- [20] Allan L (2004) Technique of fetal echocardiography. *Pediatr Cardiol* 2004; 25: 223–233.
- [21] Saleem SN Feasibility of MRI of the fetal heart with balanced steady-state free precession sequence along fetal body and cardiac planes. *Am J Roentgenol* 2008; 191: 1208-1215.
- [22] Chung T Assessment of cardiovascular anatomy in patients with congenital heart disease by magnetic resonance imaging. *Pediatr Cardiol* 2000; 21: 18–26.
- [23] Cook AC, Yates RW, Anderson RH Normal and abnormal fetal cardiac anatomy. *Prenat Diagn* 2004; 24: 1032-1048.
- [24] Tanner K, Sabine N, Wren C Cardiovascular malformations among preterm infants. *Pediatrics* 2005; 116: e833-e838.
- [25] Earing MG, Webb GD Congenital heart disease and pregnancy: maternal and fetal risks. *Clin Perinatol* 2005; 32: 913–919.
- [26] Manganaro L, Savelli S, Di Maurizio M *et al* Assessment of congenital heart disease (CHD): Is there a role for fetal magnetic resonance imaging (MRI)? *Eur J Radiol* 2009; 72: 172-80.

## Conclusions and Future Developments

**Giuseppe Rizzo and Domenico Arduini**

*Department of Obstetrics and Gynecology, Università Roma "Tor Vergata", Italy*

**Abstract** Despite the dramatic improvement in the quality of diagnostic ultrasound Congenital Heart Disease (CHD) are the most common and less frequently diagnosed prenatally anomalies. This is mainly secondary to the difficulties in training expert and dedicated sonographer in the study of fetal heart. Four dimensional (4D) sonography may overcome operator dependency allowing offline 4D examination of the fetal heart. This approach opens the possibility of performing a virtual echocardiography in fetuses at high risk or suspected to be affected by a CHD through networking capabilities. As a consequence virtual echocardiography may allow to extend the benefit of advanced of cardiac examination in patients followed in peripheral centers thus reducing the number of unnecessary referral to tertiary centers.

**Key Words:** Congenital Heart Disease, Screening, 4D Echocardiography, Spatiotemporal Image Correlation (stic), virtual Echocardiography. Virtual Reality.

Congenital heart disease (CHD) are the most common structural anomalies, commonly estimated to be 8/1000 live births (chapter 1). Despite their high prevalence and the clinical importance of their identification during pregnancy, thus allowing to evidence associated structural and genetic and to improve the perinatal outcome, the results of the screening programs up to now reported are far from to reach acceptable levels of diagnostic efficiency (chapter 2).

A detailed study of fetal cardiac anatomy (chapter 3) improve the possibility of diagnosing CHD, but the degree of experience of the sonographer has a significant impact on the quality of the examination of the fetal heart and as a consequence of the rate of detection of major CHD. Indeed, it has been shown that the learning curve of a sonographer already confident in obtaining the four chamber view to properly visualize also the outflow tracts requires a training time of up to 3 years [1].

The revolution in diagnostic ultrasound occurred with the advent of four dimensional (4D) applications may overcome these problems of operator dependency allowing offline 4D examination of the fetal heart. The use of the SpatioTemporal Image Correlation (STIC) algorithm allows examination of the fetal heart within a real-time 4D volume, displaying the cardiac cycle in a cine loop. With this technique it is possible to acquire a volume starting from the standard four chamber view of the fetal heart and then off line navigating inside the volume in a multiplanar way obtaining all the diagnostic planes necessary. We recently described a technique of analysis, the "3 steps technique" (Fig. 1), that makes it possible to obtain in less than 1 minute the four chambers view and the outflow tract views. (2).

In video 1 the three simple steps of scrolling and rotation on Y axis are shown (in this example the total amount necessary to complete the heart study was 25 seconds)

In this way every examiner able to obtain a four chamber view of the fetal heart may acquire a volume cardiac datasets. Once acquired, the "digital heart" can be examined by searching the conventional planes (e.g. outflow tracts) or to obtain offline any other virtual cardiac plane (e.g. en face view of the ventricular septum), views of the fetal heart that are difficult or impossible to obtain with conventional 2D ultrasound.

\*Address correspondence to **Giuseppe Rizzo**: Department of Obstetrics and Gynecology, Università Roma Tor Vergata Ospedale Fatebenefratelli Isola Tiberina 00186 Rome Italy; Email: giuseppe.rizzo@uniroma2.it

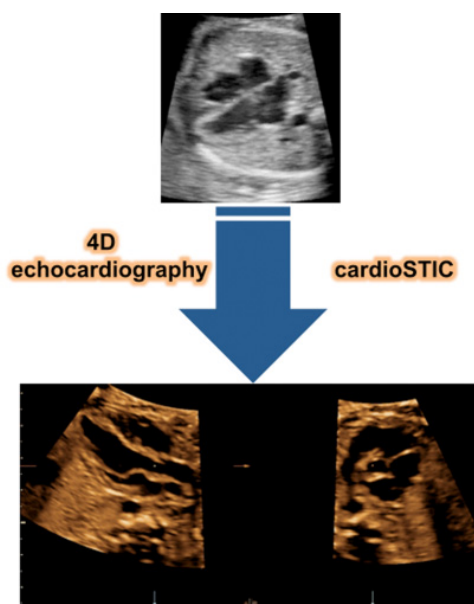


**Figure 1:** ([video 1](#)) Possibility of obtaining the outflow tracts from the 4 chamber view using the “3 steps technique” [2] from acquired 4D cardioSTIC volume data sets.

This approach can be also used to avoid unnecessary referrals for echocardiography to tertiary centers. Indeed the prevalence of CHD in pregnant women with traditional risk factors is extremely low and as shown in Fig. 2.

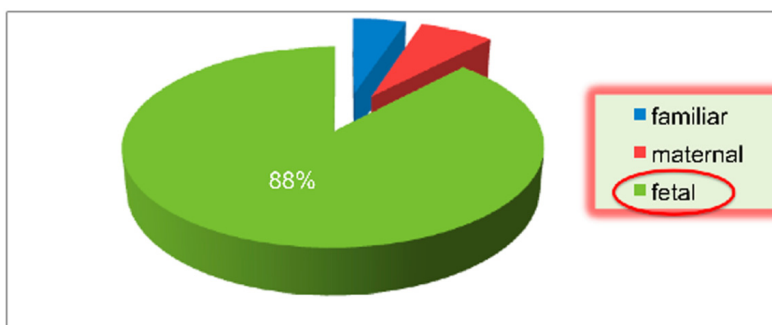


**Figure 2:** Prevalence of CHD in the population referred to the Department of Obstetrics and Gynecology Università di Roma Tor Vergata according to the risk factor

In our experience 88% of CHD diagnosed were found when a fetal risk factor was present while the prevalence is extremely low when maternal or familiar risk factors are the indication of referral. Of interest is that among fetal risk factor the two most effective risk subcategories were the abnormalities in second and first trimester (nuchal translucency NT) screenings (Fig. 3).

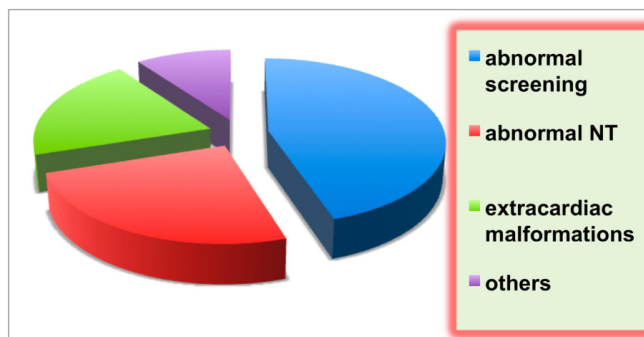


**Figure 3:** Prevalence of CHD in the population referred to the Department of Obstetrics and Gynecology Università di Roma Tor Vergata among fetal risk factors. The most frequent subgroups were abnormal second trimester screening (blue) and increased nuchal translucency (red)

The availability of a cardiac volume datasets acquired properly may allow to perform a virtual echocardiography. This may be performed off-line after the end of the examination of the patents directly by the sonographer or supervised by an observer with more detailed experience. In fetuses suspected to be affected by a CHD or with “classical” risk factor (i.e. familiar, maternal) the cardiac volume can be sent using internet networking capabilities to a referral center [3]. This approach has been already proved particularly efficient in countries in which patients are screened far from referral centers [4, 5].

Virtual echocardiography allows to extend the possibility of having an advanced cardiac examination to pregnancies followed in peripheral unit and avoid unnecessary referral. This approach allows also the identification of patients in which the referral is indicated for performing a conventional echocardiography in tertiary unit. (Fig. 4).

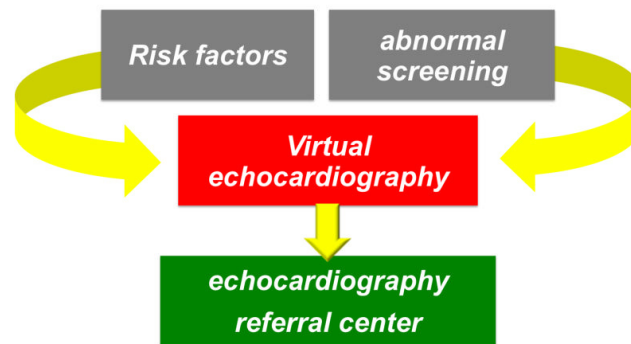


**Figure 4:** Flow chart of the admission criteria to conventional echocardiography in presence of the possibility of performing a virtual fetal heart examination using internet networking capabilities to a referral center.

In the near future, by using the new diagnostic advances allowed by 4D ultrasonography, it will become possible to refer only selected patients to experts team in fetal cardiology where a detailed antenatal diagnosis can be obtained and a multidisciplinary discussion done with the parents regarding the risks, surgical intervention required and long-term outcome (Fig. 5).

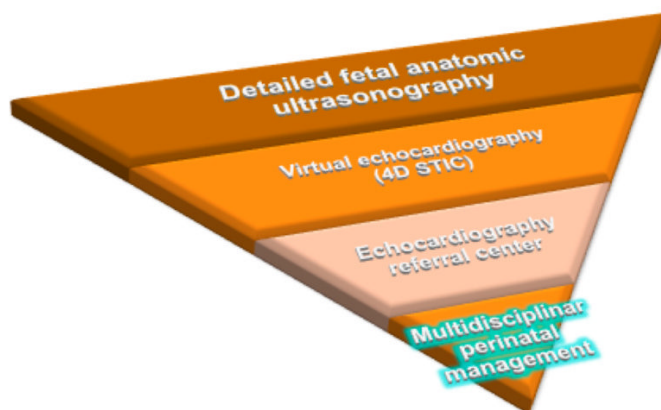


**Figure 5:** Diagnostic steps to be followed in the management of a fetus with CHD

Further future developments will be dependent by the technology available but there are already some evidences of the possibility to generate non-linear virtual reality object movies of volume images acquired prenatally [6]. Virtual

reality have been currently applied to assist in complex surgical procedure in medical imaging and education and there is no doubt that will be applied in the near future also to the study of the fetal heart.

## REFERENCES

- [1] Tegnander E, Eik-Nes SH. The examiner's ultrasound experience has a significant impact on the detection rate of congenital heart defects at the second-trimester fetal examination. *Ultrasound Obstet Gynecol.* 2006, 28: 8-14.
- [2] Rizzo G, Capponi A, Muscatello A, Cavicchioni O, Vendola M, Arduini D. Examination of the fetal heart by four-dimensional ultrasound with spatiotemporal image correlation during routine second-trimester examination: the 'three-steps technique'. *Fetal Diagn Ther* 2008; 24: 126-131.
- [3] Roberts D. How best to improve antenatal detection of congenital heart defects *Ultrasound Obstet Gynecol* 2008; 32: 846-848.
- [4] Viñals F, Mandujano L, Vargas G, Giuliano A. Prenatal diagnosis of congenital heart disease using four-dimensional spatio-temporal image correlation (STIC) telemedicine via an Internet link: a pilot study. *Ultrasound Obstet Gynecol* 2005; 25: 25-31.
- [5] Viñals F, Ascenzo R, Naveas R, Huggon I, Giuliano A. Fetal echocardiography at 11 + 0 to 13 + 6 weeks using four-dimensional spatiotemporal image correlation telemedicine via an Internet link: a pilot study. *Ultrasound Obstet Gynecol* 2008; 31: 633-638.
- [6] Tutschek B. Simple virtual reality display of fetal volume ultrasound. *Ultrasound Obstet Gynecol* 2008; 32: 906-909.



## INDEX

### A

aberrant subclavian artery, 48, 131  
 absent pulmonary valve syndrome 134, 135, 136, 144, 157  
 abdomen (fetal), 10, 3, 9, 78, 84, 96  
 abnormal systemic venous connections, 84, 87, 90, 93  
 alcohol, 2, 4, 7, 9  
 aneuploidies, 34, 96, 108, 114, 120, 128, 135, 136, 140, 142, 144  
 anomalous pulmonary venous connection, 66, 84, 88, 89, 154  
 aortic arch, 13, 20, 24, 25, 41, 44, 45, 46, 56, 57, 58, 59, 63, 64, 81, 83, 92, 126, 127, 128, 130, 133, 135, 139, 153, 180, 185  
 aortic atresia, 147, 196  
 aortic coarctation, 13, 14, 41, 118, 123, 116, 126, 128, 139, 140, 193  
 aortic stenosis, 2, 13, 14, 118, 121, 122, 123, 124, 125, 128, 129, 186, 193  
 aortic valve 23, 24, 44, 65, 118, 121, 132  
 Apert syndrome 109  
 arrhythmia (fetal) 8, 9, 28, 50  
 atrioventricular septal defect, 1, 5, 13, 34, 35, 36, 94, 96, 99, 100, 118, 153, 154, 186  
 atrioventricular valve, 9, 10, 20, 22, 74, 95, 101, 106, 115, 139, 140, 141, 143, 150, 157, 172, 182  
 azygos continuation, 45, 66, 84, 90, 91

### B

B Flow, 38, 44, 45, 46, 49, 50, 52, 58, 59, 62, 63, 64, 65, 67, 84, 85, 87, 88, 101, 127, 128, 137, 139, 143, 151, 153, 156  
 balloon valvuloplastic, 115, 123  
 blood flow, 20, 22, 26, 28, 45, 46, 50, 59, 62, 63, 95, 99, 100, 104, 137, 148, 151, 144, 168, 178, 193

### C

cardiac function, 3, 15, 26, 32, 159, 160, 163, 168, 172, 174, 186  
 cardiac output, 26, 60, 61, 102, 134, 159, 163, 168, 174  
 cardiomegaly, 109, 135, 137, 177, 188  
 CATCH 22 (Di George Syndrome), 2, 139  
 CHARGE syndrome, 109  
 coarctation aorta, 13, 14, 41, 118, 123, 116, 126, 128, 139, 140, 193  
 color Doppler, 34, 38, 44, 46, 50, 52, 55, 58, 59, 70, 72, 77, 88, 90, 94, 95, 97, 100, 101, 103, 104, 106, 109, 112, 131, 134, 136, 137, 141, 144, 154, 174  
 common arterial Trunk, 97, 135, 138, 139  
 complete transposition of great artery 2, 3, 65, 76, 141, 142, 144, 147, 189  
 correct transposition of great artery 81, 186, 189  
 conotruncal anomalies, 1, 2, 3, 4, 6, 15, 40, 41, 134, 139  
 coronary artery 114, 124, 138, 141, 169  
 coronary sinus 90, 92, 94

### D

Di George Syndrome 2, 139  
 Double outlet right ventricle, 2, 15, 23, 75, 76, 103, 139  
 ductus arteriosus, 1, 3, 4, 10, 24, 25, 40, 56, 58, 59, 63, 113, 119, 126, 135, 149, 180, 190  
 ductus venosus, 46, 62, 63, 67, 76, 154

### E

Early gestation 146  
 Endocardial fibroelastosis 114, 122, 123, 124  
 Ebstein's anomaly, 2, 13, 103, 109  
 Epidemiology, 1

**F**

Folic Acid, 2  
Foramen ovalis 9, 11, 14, 22, 94, 109, 123, 124, 172, 180  
Four chamber view , 8, 9, 10, 13, 14, 15, 20, 32, 38, 42, 52, 57, 80, 95, 105, 118, 153, 159, 162, 180, 196  
Frank –Starling mechanism 26, 172

**G**

genetic syndrome 2, 11, 186  
glass body mode 99, 100

**H**

Hepatic veins 66, 90, 155  
Heterotaxia 2, 21, 142, 150, 188  
High Definition Power Flow Doppler, 62, 148  
Hypoplastic left heart syndrome, 2, 8, 9, 13, 75, 118, 147, 154, 188  
hypoplastic right heart, 13, 103, 112

**I**

inferior vena cava, 10, 26, 46, 62, 67, 84, 92, 155, 183, 190  
interrupted aortic arch 127, 128, 129, 130  
interrupted vena cava 39, 44, 45, 56  
inversion Mode, 38, 44, 57, 74, 84, 87, 88, 91, 92, 106, 115, 120, 139, 151, 153, 162

**K**

karyotype 9, 108, 135, 146

**L**

Left atrium 9, 10, 11, 20, 21, 22, 25, 45, 80, 141, 185  
left heart disease 118  
left superior vena cava (persistent) 84, 90, 92, 95  
left ventricle 8, 12, 20, 21, 22, 104, 118, 121, 124, 142, 143, 190, 193  
left ventricle outflow tract 1, 3, 12, 15, 20, 23, 44, 62, 105, 121  
lithium 3, 9, 146  
long axis view 12, 13, 23, 24, 41, 180, 184  
lung (fetal) 21, 137, 154, 156, 185, 191

**M**

Magnetic Resonance imaging 177  
Matrix probe, 29, 34, 50, 64, 70, 174  
Microdeletion chromosome 22q1 (DiGeorge syndrome) 2, 139  
mitral valve, 10, 12, 91, 106, 118, 143  
multiplanar 33, 39, 78, 118, 128, 131, 152, 191, 196  
multivitamins, 2

**N**

Noonan Syndrome, 109, 111  
nuchal translucency, 9, 14, 146, 197

**O**

Obesity (maternal) 173

**P**

power Doppler, 38, 52, 62, 70, 99, 137, 153  
processing volumes , 15, 38, 50, 161  
pulmonary atresia, 2, 13, 14, 103, 112, 114, 136, 193  
pulmonary stenosis, 2, 8, 13, 14, 108, 110, 111, 139, 147, 193

pulmonary veins, 10, 20, 57, 84, 88, 181, 194  
pulmonary valve 12, 13, 23, 24, 112, 113, 135, 136, 170

## R

radiofrequency perforation, 115, 178, 188  
render, 30, 32, 38, 44, 50, 58, 70, 74, 87, 92, 98, 101, 106, 123, 148, 152, 155  
right aortic arch, 63, 126, 130, 131, 139  
right atrium 10, 20, 21, 25, 44, 57, 81, 90, 91, 107, 109, 113, 152, 159 181, 193  
right heart anomalies, 103  
right ventricle 2, 11, 12, 15, 21, 22, 23, 105, 109, 110, 112, 125, 134, 141, 142, 144, 159, 191  
right ventricle outflow tract 11, 13, 15, 18, 20, 24, 44, 52, 76, 82, 108, 139, 141, 153, 191

## S

screening congenital heart disease 1, 2, 8, 14, 177, 197  
Shone complex 118, 123  
short axis view 12, 41, 111, 112, 180, 183  
situs, 9, 14, 20, 21, 97, 150, 177  
sonoAVC, 116, 124, 125, 128, 161  
spatio-temporal image correlation (STIC), 15, 50, 81, 84, 85, 97, 103, 118, 148  
spectral Doppler 25, 90, 114, 122, 135, 137, 143  
spin technique 39, 50, 56  
stroke volume, 26, 116, 123, 159, 168  
superior vena cava, 13, 15, 45, 84, 90 92, 95, 127, 149, 183

## T

tetralogy of Fallot, 2, 14, 23, 76, 103, 121, 144, 147, 193  
three vessel view, 20, 24, 39, 42, 45, 74, 91, 163  
thymus 13, 185  
tomographic ultrasound imaging (TUI) 41, 57, 81, 125, 131, 148, 151  
trachea (fetal) 13, 42, 55, 63, 130, 131, 132, 179, 185  
transposition of the great arteries, 2, 3, 65, 76, 141, 142, 144, 147, 189  
tricuspid atresia, 103, 147, 186, 193  
tricuspid dysplasia, 107  
tricuspid regurgitation, 107, 108, 112, 113, 153  
tricuspid valve, 10, 12, 22, 23, 81, 103, 104, 106, 109, 142, 143, 149  
trisomy, 105, 106, 120, 131, 140  
truncus arteriosus, 2, 4, 23, 100, 131, 138, 147, 190

## U

Umbilical artery 46, 146, 155  
Umbilical vein 10, 62, 65, 76, 150, 165

## V

Vein of Galen aneurysm 68  
Ventricular coronary arterial communication (fistola) 114  
ventricular septal defects, 1,2,3,13, 14, 94, 95, 96, 97, 98, 135, 139, 141  
ventricular septum 9,10, 20, 23, 34, 58, 77, 94, 135, 142, 149, 181  
ventricular volume 32, 115, 116, 123, 159  
VOCAL, 116, 124, 128, 159, 160  
Volume acquisition, 31, 38, 51, 57, 80, 143, 161

## W

William's Syndrome 111, 123